PYRYLIUM SALTS FOR BIOIMAGING, SENSING AND SOLID-STATE EMISSION

IGNACIO MUÑOZ RESTA

Director:

Francisco Galindo Honrubia.

UNIVERSITAT
JAUME·I

June 2021

Programa de doctorado en Ciencias

Escuela de Doctorado de la Universitat Jaume I

PYRYLIUM SALTS FOR BIOIMAGING, SENSING AND SOLID-STATE EMISSION

Memoria presentada por Ignacio Muñoz Resta para optar al grado de doctor por la Universitat Jaume I

IGNACIO MUÑOZ RESTA – NIF:Y6627090E

Firmado digitalmente por IGNACIO MUÑOZ RESTA - NIF:Y6627090E
Fecha: 2021.09.02 13:28:05 +02'00'

Doctorando
Ignacio Muñoz Resta

GALINDO HONRUBIA FRANCISCO - 20154900T

Firmado digitalmente por GALINDO HONRUBIA FRANCISCO - 20154900T
Nombre de reconocimiento (DN): c=ES, serialNumber=IDCES-20154900T, givenName=FRANCISCO, sn=GALINDO HONRUBIA, cn=GALINDO HONRUBIA FRANCISCO - 20154900T
Fecha: 2021.09.02 16:52:21 +02'00'

Director
Francisco Galindo Honrubia

Castellón de la Plana, Junio 2021

FINANCIACIÓN RECIBIDA

- Ayuda Santiago Grisolía (GRIOSLIAP/2018/071) para el personal investigador en formación de carácter predoctoral.
- Proyecto concedido por el Ministerio de Ciencia, Innovación y Universidades (RT20128-101675-B-100).
- Proyecto concedido por la Universitat Jaume I (UJI-B2018-30).
- Proyecto concedido por la Generalitat Valenciana (AICO/2020/322).

The main part of this work has been published up to the date in the following papers directly related to this thesis:

Solid-state white-light emission from a pyrylium dye obtained in one synthetic step. Muñoz Resta, I.; Miravet, J. F.; Yamaji, M.; Galindo, F. *J. Mater. Chem. C* **2020**, 8, 14348.

Fluorescent styrylpyrylium probes for the imaging of mitochondria in live cells. Muñoz Resta, I.; Lucantoni, F.; Miravet, J. F.; Apostolova, N.; Galindo, F. **2021**. *Submitted*.

Detection of subcellular nitric oxide in the mitochondria by a pyrylium probe: assays in cell cultures and peripheral blood. Muñoz Resta, I.; Bedrina, B.; Martínez-Planes, E.; Minguela, A.; Galindo, F. **2021**. *Submitted*.

Phenol-based styrylpyrylium dyes for trace water detection via chromogenic and fluorogenic responses. Muñoz Resta, I.; Galindo, F. **2021**. *Submitted*.

Papers published as collateral work and collaborations:

A cost-effective combination of Rose Bengal and off-the-shelf cationic polystyrene for the photodynamic inactivation of *Pseudomonas aeruginosa*. Arnau del Valle, C.; Pérez-Laguna, V.; Muñoz Resta, I.; Gavara, R.; Felip-León, C.; Miravet, J. F.; Rezusta, A.; Galindo, F. *Materials Science & Engineering C* **2020,** 117, 111302.

Photodynamic Inactivation of *Staphylococcus aureus* Biofilms Using a Hexanuclear Molybdenum Complex Embedded in Transparent polyHEMA Hydrogels. López-López, N.; Muñoz Resta, I.; De Llanos, R.; Miravet, J. F.; Mikhaylov, M.; Sokolov, M. N.; Ballesta, S.; García-Luque, I.; Galindo, F. *ACS Biomater. Sci. Eng.* **2020**, 6, 6995-7003.

Photodynamic inactivation of *Pseudomonas aeruginosa* by PHEMA films loaded with Rose Bengal: potentiation effect of potassium iodide. López-Fernández, A. M.; Muñoz Resta, I.; De Llanos, R.; Galindo, F. *Polymers*, **2021**, 13, 2227.

AGRADECIMIENTOS

En primer lugar, quiero agradecer al director de esta tesis, Paco, por haberme dado la oportunidad de realizar el doctorado en su grupo. Gracias por haber apostado por mí sin siquiera conocerme, fue algo arriesgado para ambos que finalmente salió muy bien. Aprendí mucho de vos en este tiempo, pero me quedo principalmente con tu dedicación al trabajo y tu capacidad organizativa. Como doctorando siempre me sentí muy bien guiado y acompañado.

A Nadezda y Federico, por su ayuda en la obtención de imágenes por microscopía confocal. A Begoña, Alfredo y Elena, por su colaboración en los ensayos biológicos relativos al óxido nítrico. A Minoru, por su asistencia en las medidas de emisión en estado sólido y en los cálculos computacionales.

A Juan, César, Begoña, Raquel, Diego, Ana T. y Ana B. Creo que no hubiese podido elegir un mejor grupo de trabajo para desarrollar esta tesis. Me hicieron sentir como en casa desde el primer día y eso no es decir poco, cuando nos separan de Argentina más de 11000 kilómetros. A Bárbara, Rosa, Cota, Gemma, Laura, no puedo decir que fuimos todos parte de un gran grupo de laboratorio, pero casi. De esta experiencia me llevo grandes compañeros de trabajo, pero sobre todo grandes amigos.

A los alumnos de fin de grado y máster que pasaron por el laboratorio y trabajaron conmigo (Noelia, Judit, Rubén, Carmen, Marina, Ana, Andrés, Sheila, Stefany). Creo que la mejor forma de aprender aparece cuando uno intenta explicar lo que sabe a otras personas. Espero que se hayan llevado una buena experiencia del mundo de la investigación.

A la Universidad de Buenos Aires por la formación recibida. Como un convencido defensor de la educación pública, no puedo estar más orgulloso de las herramientas que adquirí

durante mi paso por la licenciatura. Y, como no, a los profesores que tuve. Quiero mencionar especialmente a Sole, con quien di los primeros pasos dentro de un laboratorio (como alumno y como investigador). Un gran ejemplo de la calidad, tanto personal como académica, que me ofreció la universidad.

A mis amigos, del colegio y de la universidad, por haberme bancado durante todo este tiempo. Siempre fueron un gran apoyo. El claro ejemplo de que cuando las relaciones son genuinas, no hay kilómetros ni virtualidad que las debilite. A Christian, por nuestras charlas casi diarias que hicieron que la distancia se acortara considerablemente. Feliz de tenerte como amigo.

A Raquel, Hugo y Pedro, mis papás y mi hermano, por su constante apoyo. Desde el día que les dije "me voy a presentar a una beca para hacer el doctorado en España", fueron un pilar fundamental en cada paso de esta etapa (y de las anteriores, y seguramente de las que vendrán). En una época en la que sentirse acompañado se volvió más importante que nunca para contrarrestar el aislamiento que nos impuso la pandemia, siempre pude contar con ustedes para cualquier cosa que necesité. A Pau, Javi y Oli, tener un pedacito de la familia tan cerca hizo todo más fácil. Gracias por recibirme siempre en su casa.

Y, finalmente, a Gaby. Nos conocimos unos meses antes de mi viaje y apostamos todo a pesar de la distancia. Estos tres años hubieran sido muy distintos si no te hubiera tenido a mi lado. Gracias por enseñarme que el hogar no es necesariamente un lugar físico, muchas veces un mensaje, una llamada, una sonrisa o un brazo sobre el hombro alcanzan para sentirse en casa. Porque, como está escrito en *El palacio de la luna*, "que lo quieran a uno de esa forma lo cambia todo".

ABSTRACT

This thesis, entitled "Pyrylium salts for bioimaging, sensing and solid-state emission" is structured in 7 chapters that cover different aspects related to several applications and reactivity of pyrylium salts.

In Chapter 1, a general introduction of the application field and versatility of pyrylium salts is presented, trying to highlight the key aspects of their reactivity that are exploited in the experimental development of the thesis.

In Chapter 2, the general objectives of the thesis are introduced.

In Chapter 3, the synthesis of 2 families of 4 styrylpyrylium salts each with different substituents on the aromatic rings is presented. It includes their characterization by nuclear magnetic resonance and mass spectrometry techniques and through measurements of their photophysical properties in solution (absorption and emission spectra, quantum yields and fluorescence lifetimes). The internalization of 4 of them in liver cancer cells (Hep3b) is explored by confocal microscopy, and colocalization and membrane potential variation analyses are also performed. Additionally, their cytotoxicity against this cell line is studied.

In Chapter 4, structural modifications on one of the probes reported in Chapter 3 are performed, to obtain a compound sensitive to nitric oxide (NO) with mitochondrial internalization. For this, the -NH_2 functionality is added to an electronically activated aromatic ring with a -OCH_3 group and its response to NO is analysed in different matrices. In aqueous medium, reaction kinetics are obtained, and the sensitivity and selectivity of the synthesized probe are studied. Model compounds to assess the necessity of using an electronically activated ring and the influence on the position of the substituents are synthesized. Colocalization assays

are carried out and its reaction against nitric oxide generated both exogenously (in HT29 cells) and endogenously (in RAW 264.7 macrophages) is studied. Finally, a more complex matrix (peripheral blood) is used and the response of the probe to an inflammatory stimulus is analysed.

In Chapter 5, the synthesis of pyrylium salts with the hydroxy nitro functionality is discussed. The acid-base equilibrium between the pyrylium and quinone methide forms of these compounds is studied, by means of absorbance and fluorescence. Based on the results obtained from the physicochemical study, an application for the compounds as moisture sensors in organic solvents (acetone and acetonitrile) is tested.

In Chapter 6, a library of 7 compounds (methyl-4,6-diphenylpyrylium salts) with different substituents on the aromatic rings is introduced, all solid-state emitters and one emitting white light (first report of a pyrylium salt with this property). A complete characterisation is carried out, structural and photochemical, complemented with stability studies against thermal decomposition and computational calculations.

Finally, in Chapter 7 the general conclusions of the thesis are described, emphasizing on the expansion of the application field of pyrylium salts as mitochondrial probes, sensors (for nitric oxide and water traces in organic solvents) and solid-state emitters.

RESUMEN

La presente tesis, titulada "Pyrylium salts for bioimaging, sensing and solid-state emission" se encuentra estructurada en 7 capítulos que abarcan distintos aspectos relacionados con aplicaciones y reactividad de las sales de pirilio.

En el Capítulo 1, se plantea una introducción general que intenta poner de manifiesto el amplio campo de aplicación y la versatilidad de las sales de pirilio, además de hacer hincapié en los aspectos clave de su reactividad que son aprovechados en el desarrollo experimental de la tesis.

En el Capítulo 2, se introducen los objetivos generales de la tesis.

En el Capítulo 3, se presenta la síntesis de 2 familias de 4 sales de estiril-pirilio cada una, con diferentes sustituyentes sobre los anillos aromáticos. Incluye una caracterización de éstos por técnicas de resonancia magnética nuclear y de espectrometría de masas, y a través de medidas de sus propiedades fotofísicas en solución (espectros de absorción y emisión, rendimientos cuánticos y tiempos de vida de fluorescencia). Mediante microscopía confocal, se explora la internalización de 4 de ellos en células hepáticas cancerosas (Hep3b), y se realizan ensayos de colocalización y de variación del potencial de membrana. También, se estudia su citotoxicidad frente a dicha línea celular.

En el Capítulo 4, se encaran modificaciones estructurales sobre una de las sondas reportadas en el Capítulo 3, con el fin de obtener un compuesto sensible a óxido nítrico (NO) y de internalización mitocondrial. Para ello, se agrega la funcionalidad $-NH_2$ sobre un anillo aromático activado con un grupo dador ($-OCH_3$), y se analiza su respuesta frente a NO en distintas matrices. En medio acuoso, se obtienen cinéticas de reacción y se estudia la sensibilidad

y la selectividad de la sonda sintetizada. Se sintetizan compuestos modelo para evaluar la necesidad de utilizar un anillo activado electrónicamente y la influencia en la posición de los sustituyentes. Se llevan a cabo ensayos de colocalización y se estudia su reacción frente a óxido nítrico generado tanto exógena (en células HT29) como endógenamente (en macrófagos RAW 264.7). Finalmente, se trabaja con una matriz más compleja (sangre periférica) y se analiza la respuesta de la sonda frente a un estímulo inflamatorio.

En el Capítulo 5, se aborda la síntesis de sales de pirilio con la funcionalidad hidroxi nitro. Se estudia el equilibrio ácido-base entre las formas pirilio y quinoidal de dichos compuestos, tanto por absorbancia como por fluorescencia. En función de los resultados obtenidos del estudio fisicoquímico, se ensaya una aplicación para los compuestos como sensores de humedad en solventes orgánicos (acetona y acetonitrilo).

En el Capítulo 6, se introduce una biblioteca de 7 compuestos (metil-4,6-difenil pirilios) con distintos sustituyentes sobre los anillos aromáticos, todos emisores en estado sólido y uno en particular emisor de luz blanca (primer reporte de una sal de pirilio con esta propiedad). Se lleva a cabo una caracterización completa de los mismos, tanto estructural como fotoquímica, complementada con estudios de estabilidad frente a la descomposición térmica y cálculos computacionales.

Finalmente, en el Capítulo 7 se describen las conclusiones generales de la tesis, destacando la ampliación del campo de aplicación de las sales de pirilio como sondas mitocondriales, sensores (de óxido nítrico y de trazas de agua en solventes orgánicos) y emisores en estado sólido.

ABBREVIATIONS

AA: ascorbic acid

Abs.: absorption

ACN: acetonitrile

ACQ: aggregation-caused quenching

ANOVA: analysis of variance

ATP: adenosine triphosphate

a.u.: arbitrary units

BODIPY: boron-dipyrromethene

ca.: circa

CACT: carnitine-acylcarnitine translocase

CCCP: carbonyl cyanide m-chlorophenyl hydrazone

CIE: *Commission Internationale de l'Eclairage*

CLSM: confocal laser scanning microscopy

Compd.: compound

CT: charge transfer

CTCF: corrected total cell fluorescence

D: delocalized

DCM: dichloromethane

DEA NONOate: Diethylammonium (Z)-1-(N,N-diethylamino)diazen-1-ium-1,2-diolate

DFT: density functional theory

DHA: dehydroascorbic acid

DLC: delocalized lipophilic cation

DMEM: Dulbecco's Modified Eagle Medium

DMF: dimethylformamide

DMSO: dimethyl sulfoxide

DSC: differential scanning calorimetry

Em.: emission

ESI: electrospray ionization

Exc.: excitation

F: fluorescence

FRET: Förster Resonance Energy Transfer

FSC: forward side scatter

FWHM: Full Width at Half Maximum

GSH: glutathione

h.: hour

HCC: hepatocellular carcinoma

HOMO: Highest energy Occupied Molecular Orbital

HRMS: high-resolution mass spectrometry

i.e: *id est*

IQR: inter-quartile range

L: localized

L-NMMA: L-N^{G}-monomethyl arginine acetate

LOD: limit of detection

LOQ: limit of quantification

LPS: lipopolysaccharide

LUMO: Lowest energy Unoccupied Molecular Orbital

MFI: mean fluorescence intensity

min.: minute

MTT: 3-(4,5-dimethylthiazol-2-yl)-2,5-diphenyl tetrazolium bromide

NK: natural killer

NMR: nuclear magnetic resonance

NO: nitric oxide

NOS: nitric oxide synthase

Nu: nucleophile

OLED: organic light-emitting diode

OLEFET: organic light-emitting field-effect transistor

PBS: phosphate-buffered saline

PDT: photodynamic therapy

PMMA: poly (methyl methacrylate)

Q-TOF: quadrupole-time of flight

RNS: reactive nitrogen species

ROI: region of interest

ROS: reactive oxygen species

RPMI: Roswell Park Memorial Institute

S: shoulder

SD: standard deviation

SNAP: S-nitroso-N-acetylpenicillamine

SS: Stokes shift

Sv.: solvent

TCSPC: time-correlated single-photon counting

TD-DFT: time-dependent density functional theory

TGA: thermogravimetric analysis

THF: tetrahydrofuran

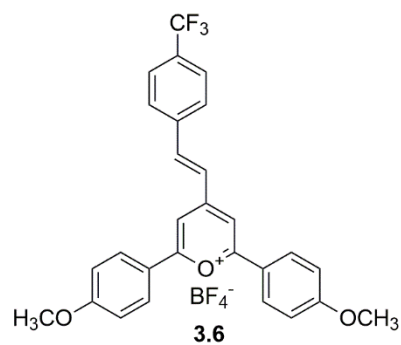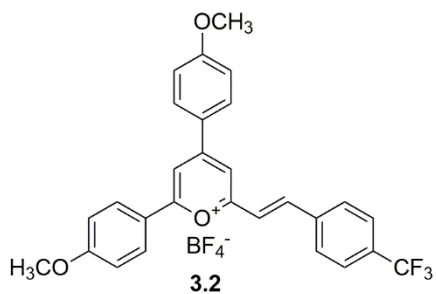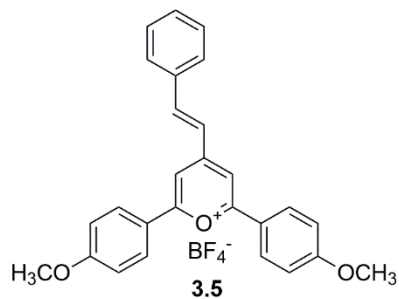TICT: twisted intramolecular charge transfer
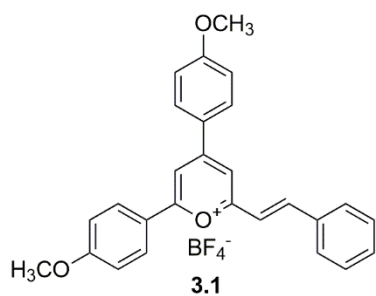
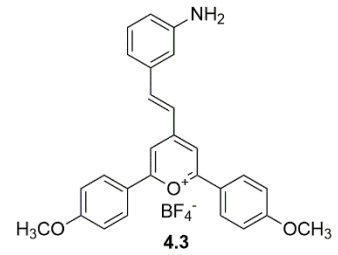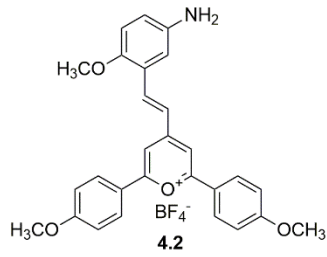TMRM: tetramethyl rhodamine methyl ester
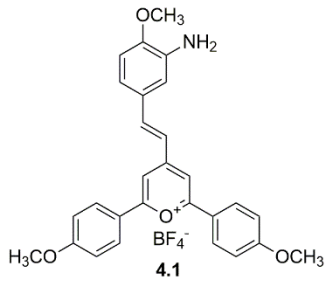
TPP: triphenyl phosphonium
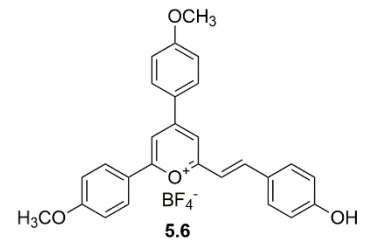
UV-vis: ultraviolet visible

vol.: volume

COMPOUND CHART

MITOCHONDRIAL IMAGING

3.1

3.5

3.2

3.6

3.3

3.7

3.4

3.8

NITRIC OXIDE SENSING

4.1

4.2

4.3

WATER SENSING

5.1

5.2

5.3

5.4

5.5

5.6

SOLID-STATE EMISSION

6.1

6.2

6.3

6.4

6.5

6.6

6.7
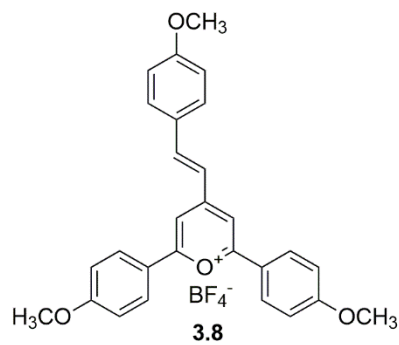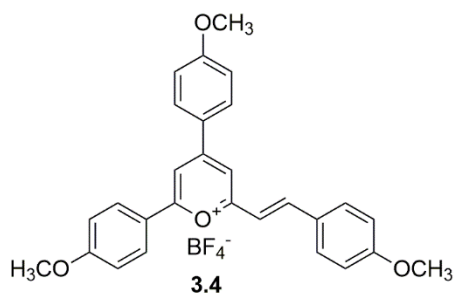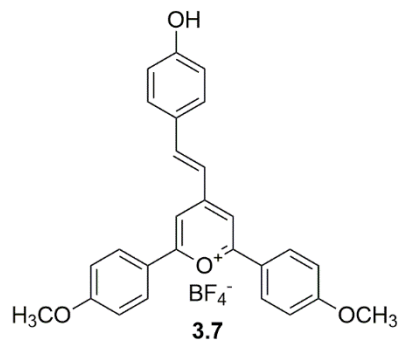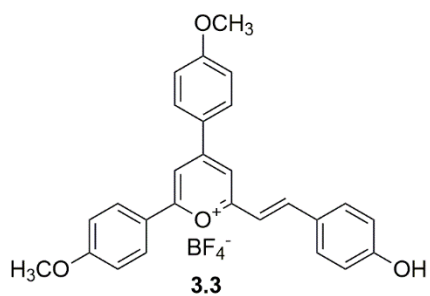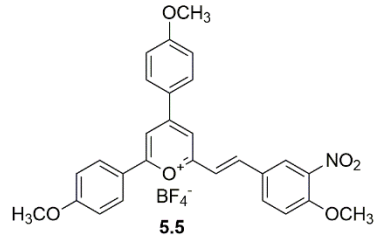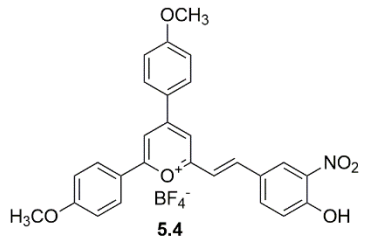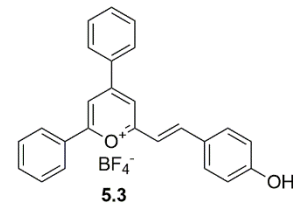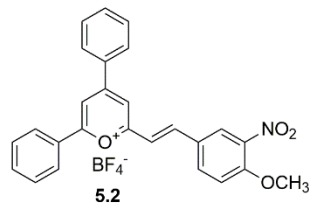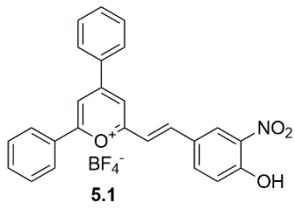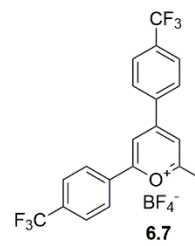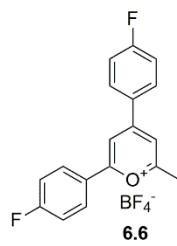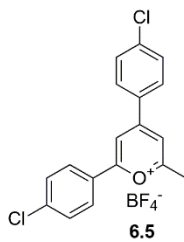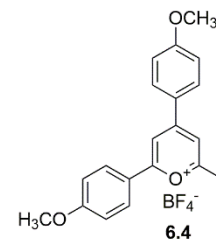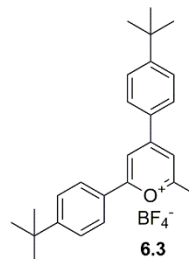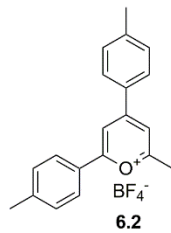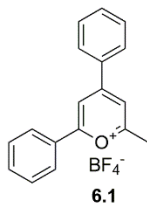
TABLE OF CONTENTS

Chapter 1

General Introduction

1.1. ¿WHY PYRYLIUM COMPOUNDS?

The application field of pyrylium compounds is widely extended. It is easy to find these salts as intermediates in medicinal, synthetic, and material chemistry. As shown in **Figure 1**, a quick search of the number of published works shows that the interest in pyrylium compounds remains high and with constant growth over the last 70 years.
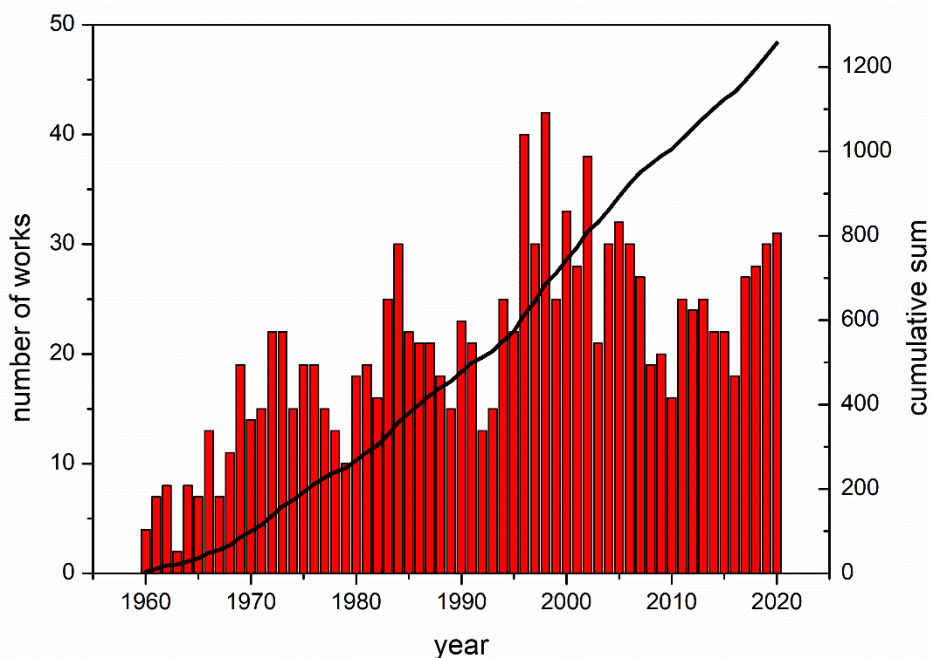
Figure 1. Number of published papers related to pyrylium compounds over the last 70 years (Scopus).

Because of their easily tunable properties, pyrylium cations have been used as photosensitizers in photodynamic therapy (PDT),[1–3] lasers,[4,5] fluorescent probes,[6,7] chemosensors,[8,9] polarity probes,[10] photocatalysts,[11–13] ionic liquids,[14] charge transporters[15] and intermediates in organic synthesis,[16,17] just to mention some applications. Despite all the research related to these compounds, the frontiers of their knowledge can still be expanded. And that is the motivation of this thesis.

1.2. THE PYRYLIUM CATION

The pyrylium cation is the oxygenated analogue of the benzene, in which a -CH is replaced by a positively charged oxygen atom.[18] Due to the high electronegativity of this last one, the six-membered ring is very perturbed. For this, pyrylium salts are stable but reactive. The counter-anion depends on the synthesis method: it is mainly a multi-atomic anion, such as BF_4^-, ClO_4^-, HSO_4^-, but it also can be a halogen like Br^- or I^-. Because of their easy synthesis and purification (their solubility in organic solvents is usually low, so they can be purified just by precipitation or recrystallization), pyrylium salts were used over the years as intermediates in the obtaining for other heterocycles (with stronger aromaticity) or carbocycles[19–21], as can be seen in **Figure 2**.
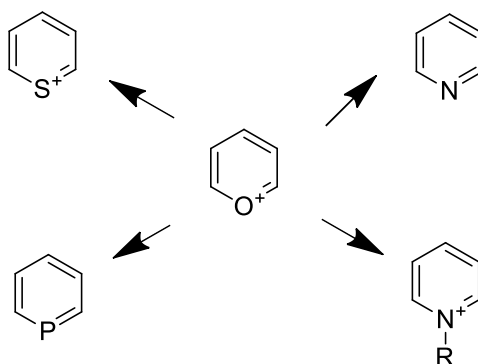
Figure 2. Pyrylium cation is an intermediate in the obtaining of other heterocycles.

1.3. SYNTHESIS OF PYRYLIUM SALTS

Pyrylium compounds are synthesized mostly from 1,5-dicarbonyl compounds (**Figure 3**).[18] The different methods vary in the way to obtain such compounds.[22–24]
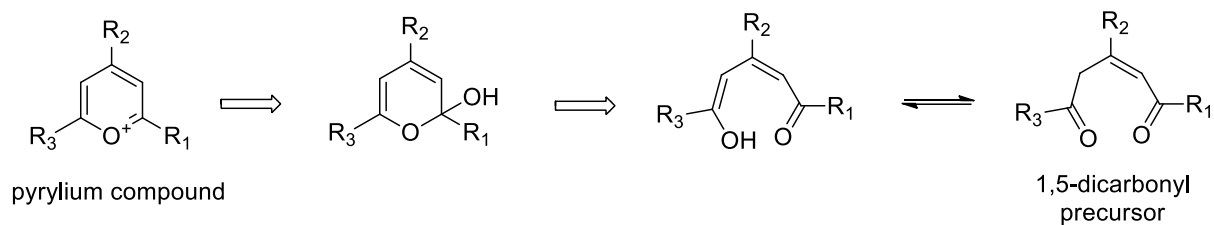
Figure 3. Retrosynthetic analysis for the obtaining of pyrylium compounds from 1,5-dicarbonyl precursors.

An example can be seen in **Figure 4** for the synthesis of the 2,4,6-triphenylpyrylium tetrafluoroborate from benzaldehyde and 2 molecules of acetophenone mediated by BF_3-etherate:
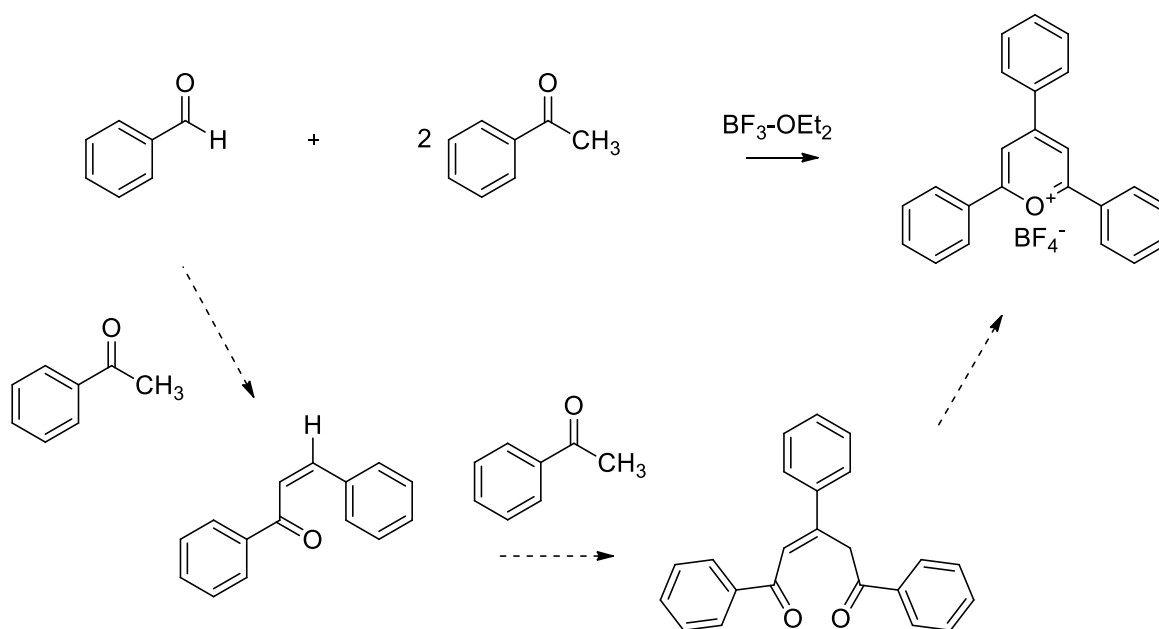
Figure 4. Steps involved in the synthesis of 2,4,6-triphenylpyrylium tetrafluoroborate from benzaldehyde and acetophenone.

The first step involves an aldol condensation between the benzaldehyde and one molecule of acetophenone. Next, a Michael addition of the second molecule of the acetophenone to the intermediate chalcone gives the pentane-1,5-dione, followed by a cyclodehydratation,

catalysed by the Lewis acid (BF$_3$), that provides the triarylpyrylium salt. Chalcones are usually commercial products, so the synthesis can be even more simplified. As well, Diels-Alder reactions are widely used for the obtaining of symmetrical and unsymmetrical pyrylium compounds (**Figure 5**).[25]

R = aryl, heteroaryl
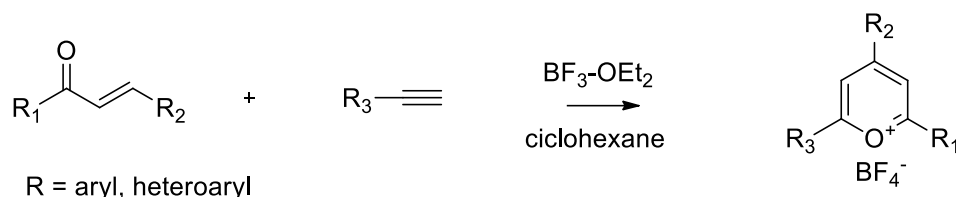
Figure 5. Synthesis of symmetrical and unsymmetrical pyrylium compounds by means of Diels-Alder reaction from chalcones and terminal alkynes.

1.4. REACTIVITY OF PYRYLIUM SALTS

As a π-deficient heterocycle, the pyrylium ring is highly susceptible to attack from nucleophiles.[18] It is stable in acidic and neutral conditions, but not in basic medium. Their reactivity can be compared to that of the protonated carbonyl compounds, being addition reactions the more frequent ones. As can be seen in **Figure 6**, the favoured positions for the nucleophilic attack can be rationalized from the resonance structures of the ring (and confirmed by DFT calculations):[26]
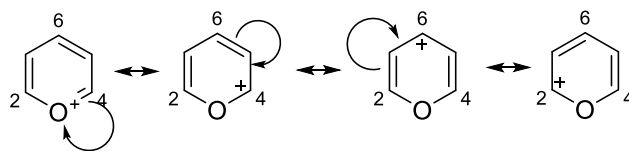
Figure 6. Resonance structures of pyrylium cation.

Basically, after the attack, there are different possibilities (**Figure 7**): a pyran ring is formed,[27] the pyrylium ring opens to give stable products or it's transformed into another species.[28] For this, pyrylium compounds are very attractive intermediates in organic chemistry.
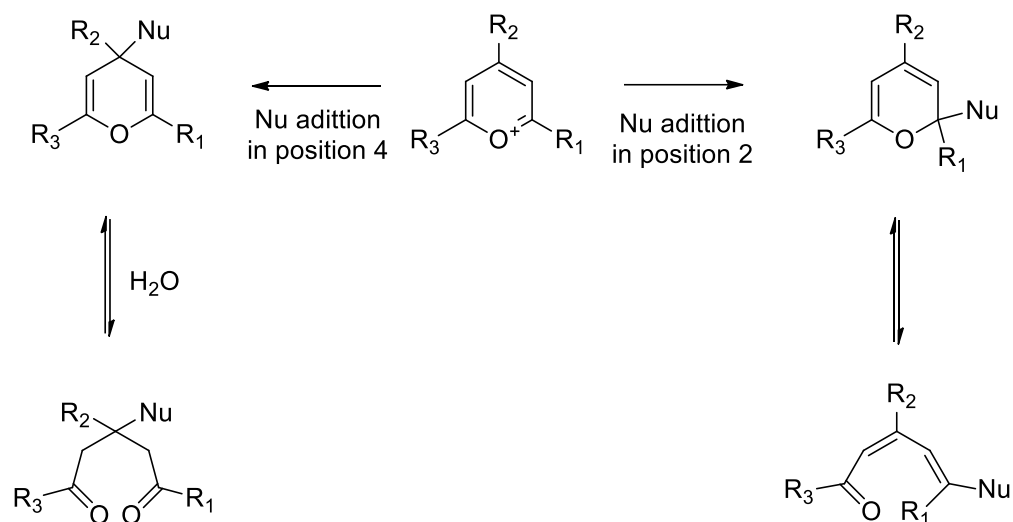
Figure 7. Nucleophilic addition to the pyrylium cation in positions 2 or 4.

Thus, introducing electron-donating groups at the 2/6 positions (and in position 4, but less effectively) leads to an improvement of the chemical stability of the ring.

1.5. PHOTOPHYSICAL PROPERTIES OF PYRYLIUM COMPOUNDS

From an optical point of view, 2,4,6- trisubstituted pyrylium salts can be considered as two-dimensional chromophores (**Figure 8**), with absorption bands along the *x* and the *y* axis, depending on the direction of the transition dipole moment:[29–31]
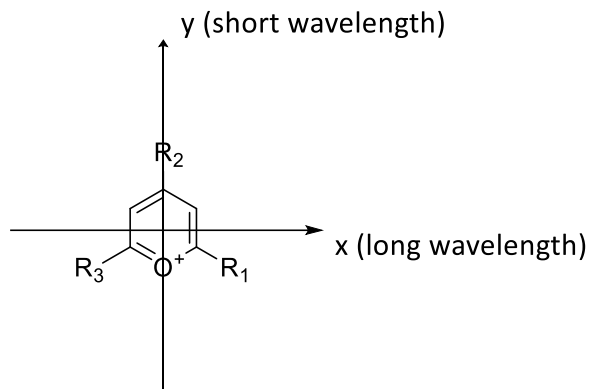
Figure 8. 2,4,6-trisubstituted pyrylium compounds as two-dimensional chromophores.

Typically, the long-wavelength absorption band could be ascribed to the *x*-chromophore (450-600 nm), while the short-wavelength one to the *y*-chromophore (350-450 nm). A third band, located around 300 nm (the carbonyl absorption region) and less intense, is commonly present. This band could indicate the existence of a balance between the open and close forms,[32] largely displaced to the close one. Naturally, substituents in positions 2 and 6 affect mainly the *x*-band, while substituents in position 4 the *y*-band. In general, when the substitution pattern is similar, the molar extinction coefficient (and, consequently, the absorption intensity) is larger for the *y* than for the *x*-band. Due to the electronic deficiency of the pyrylium core, increasing the donor strength of the substituents generally leads to a bathochromic shift of the bands.[30]

Regarding fluorescence, pyrylium salts usually have high emission quantum yields, especially when the pyrylium core is stabilized with substituents of medium donor strength.[30] In most cases, only one emission band is observed, but depending on the substitution it is possible to achieve dual fluorescence, with one band localized in the pyrylium ring and the other delocalized throughout the whole dye.[33,34] In some cases, fluorescence is quenched because of the formation of a nonradiative twisted intramolecular charge transfer -TICT- state (polar

solvents with low viscosity and a high acceptor strength of the pyrylium ring facilitates twisting).[30] Since the pyrylium core is a stronger acceptor within the *y*-chromophore, this one is more likely to twist than the *x*-chromophore. Additionally, strong donating groups (like dimethyl amino) stimulate the charge separation and, thus, the formation of a TICT state.[35]

Specific considerations about absorption and emission spectra regarding the synthesized pyrylium compounds will be discussed deeply in the following chapters.

1.6. APPLICATIONS OF PYRYLIUM SALTS

As mentioned before, the applications of these compounds are extended over a large diversity of fields. Here, some of them will be mentioned and briefly examined, especially the ones closely related to the present thesis.

1.6.1. Pyrylium compounds as fluorescent probes

Imaging in biological systems is a great tool for understanding metabolic processes, chemical reactions inside the cells, disease diagnosis and so on. Because of its high spatiotemporal resolution and sensitivity, fluorescence stands out within the techniques available to achieve such objectives.[36,37]

Pyrylium compounds have been used as fluorescent probes for cell imaging for years. For example, in 2013, Molnar et al have reported a library of new fluorochromes for cell staining, in which a pyrylium dye (**Figure 9**) was found to localize in mitochondria or nucleus, depending on the power of the laser used during image acquisition by confocal microscopy.[38]
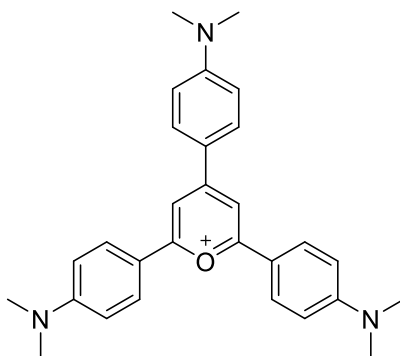
Figure 9. Pyrylium dye that localizes alternatively in mitochondria or nucleus.

One year later, Beltrán et al have described a family of pyrylium probes with the hydroxy amino functionality (**Figure 10**), for nitric oxide sensing in cuvette and murine macrophages, with high sensitivity and selectivity.[7]

R = -H, -CH$_3$, -OCH$_3$, -Ph
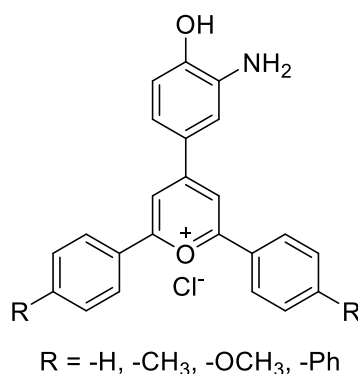
Figure 10. Pyrylium compounds for nitric oxide sensing in murine macrophages.

Taking as a model one of the compounds synthesized previously by Beltrán, in 2018 Ma et al have described the preparation of a pH-dependent pyridinium compound (**Figure 11**) for cancer cell imaging in living cells. This probe was able to distinguish between normal and cancerous cells using two-photon fluorescence microscopy.[6]
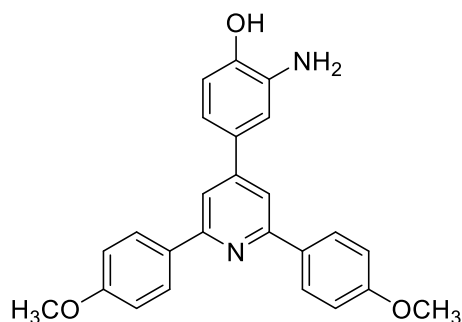
Figure 11. Pyridinium probe for cancer cell imaging.

Wen et al have studied systematically a family of pyrylium probes for imaging and sensing. They have found that certain compounds, with long-emission wavelengths, high quantum yields, large Stokes shifts and enhanced photostability were adequate for bioimaging applications and stained selectively the mitochondria of the cells, like the one shown in **Figure 12**.[26]
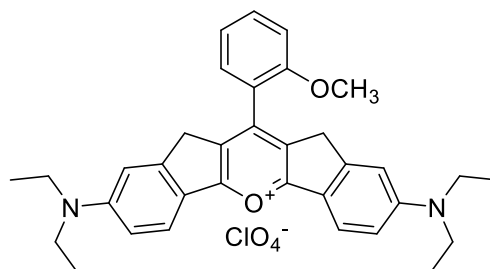
Figure 12. Pyrylium dye for mitochondria staining.

Chakraborty et al have synthesized a rigid pentacyclic pyrylium fluorophore (**Figure 13**), used to monitor intracellular pH changes during apoptosis. This turn-on sensor was able to respond quickly to the pH variations, with good reversibility and photostability.[39]
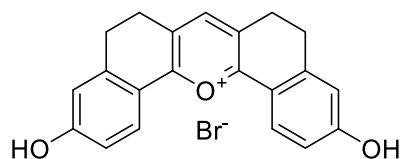
Figure 13. Pyrylium compound as a pH probe.

In 2020, Chen et al have reported a library of polycyclic pyrylium and pyridinium fluorophores, two of them which found to be specific mitochondria-labelling reagents (**Figure 14**), with outstanding photophysical properties, low cytotoxicity and enhanced photostability.[40]
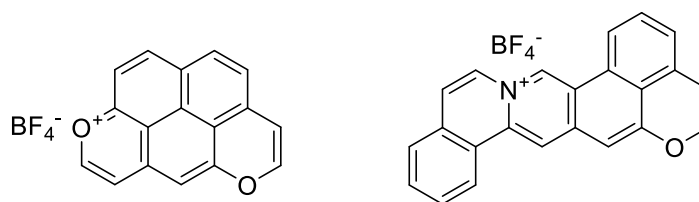
Figure 14. Mitochondria-targeting probes.

1.6.2. *Pyrylium compounds as chemosensors*

A chemosensor is a species that interacts with a specific analyte to produce a detectable change. In the case of pyrylium salts, the group of Martínez-Máñez was pioneering to investigate these compounds' properties for chemosensing purposes.[41]

During the last 20 years, this group has reported a large variety of pyrylium salts for the detection of different anions such as sulphide,[42] cyanide[8], and hydrogen carbonate[43]. Two of them can be seen in **Figure 15**. In all cases, chromogenic sensors suitable for naked-eye detection were described, with high sensitivity and rapid response to the analytes.
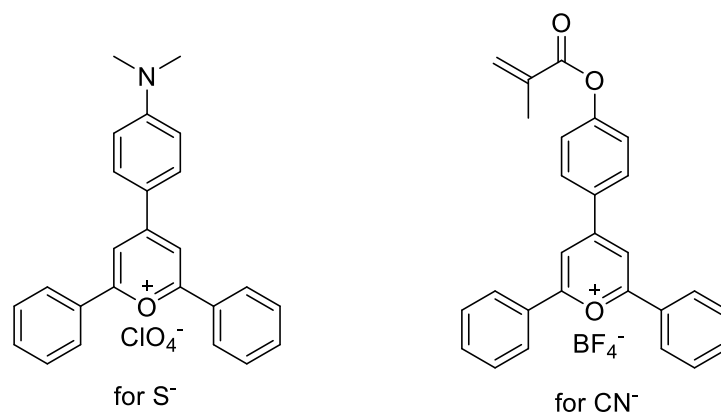
Figure 15. Pyrylium probes for the chemosensing of anions.

Also, pyrylium-based chemosensors for amines and proteins were investigated deeply over the past 15 years. In 2004, Wetzl et al have described a study on the reactivity of a family of pyrylium dyes (one of them shown in **Figure 16A**) for gel electrophoresis and protein quantification.[44] In 2010, Scaramuzzo et al have reported a new monolayer platform based on the pyrylium scaffold reactive to amine-terminated molecules (**Figure 16B**).[45] In 2017, Yurova et al have reported the fabrication of functional electrospun nanofibers for the detection of biogenic amines in food samples, based on one of the dyes that Wetzl had studied many years before.[46]
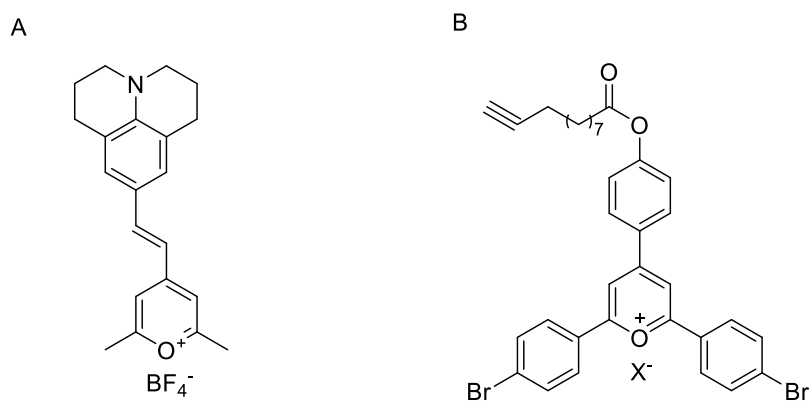
Figure 16. Pyrylium compounds reactive towards amines.

Due to the intrinsic importance of amino acids in the regulation of homeostasis, pyrylium compounds for sensing these species were also described. In 2014, Agostini et al have designed a surfactant-assisted probe for the recognition of glutathione -GSH- in water (**Figure 17A**).[47] One year later, Qian et al have reported a chemosensor capable of the selective detection (colorimetric and fluorometric) of lysine in an aqueous environment between 20 amino acids (**Figure 17B**).[48]
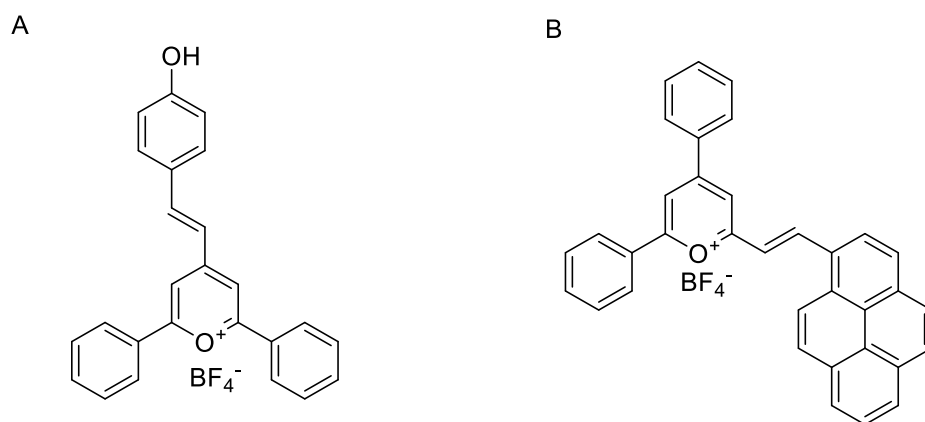
Figure 17. Pyrylium compounds for the recognition of amino acids or their derivates.

1.6.3. Pyrylium compounds in optics

The application of pyrylium compounds as optic devices dates from at least 30 years ago. In 1987, Tripathi et al have reported the synthesis of 47 substituted pyrylium and 6 thiopyrylium salts,[49] and they have found that several compounds have an important response as laser dyes, especially the ones shown in **Figure 18**. These two compounds stand out because of the wide wavelength range where the laser effect can be observed (2200 cm^{-1} / 2800 cm^{-1}).
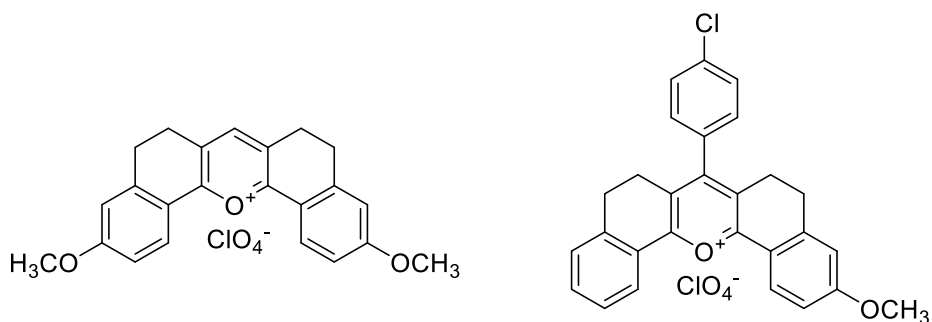
Figure 18. Pyrylium compounds with lasing properties.

In 2000, Fakis et al have described the synthesis of three pyrylium dyes with high efficiency lasing properties in solution or thin films, suitable for two-photon absorption fluorescence (**Figure 19**).[5]
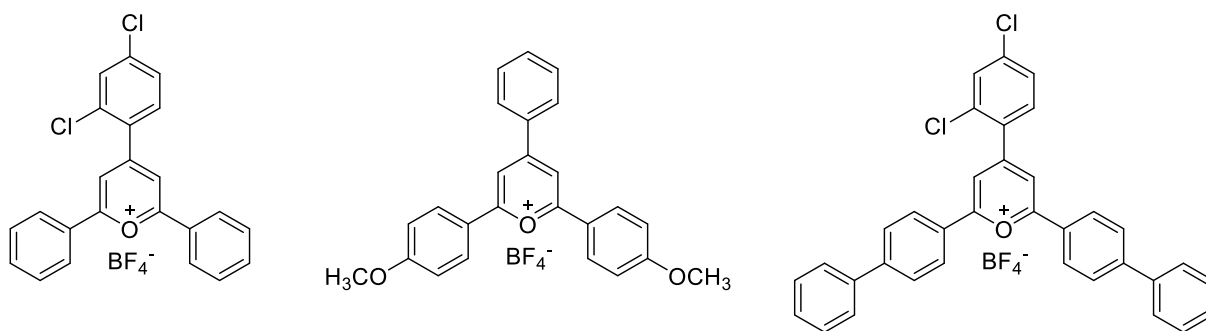
Figure 19. Pyrylium compounds as laser dyes.

As solid-state emitters, some examples of pyrylium dyes have been described. In 2005, Li et al have reported a mesoporous silica-based composite, in which a pyrylium compound (**Figure 20**) have been encapsulated. The resulting material showed a broad emission spectrum in the solid-state.[50]
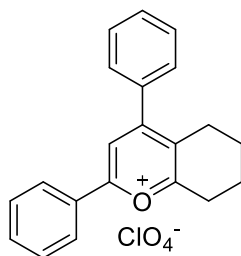
Figure 20. Pyrylium salt encapsulated in mesoporous silica displaying solid-state emission.

In 2013, Gong et al have described a new family of bispyrylium compounds (**Figure 21**), with tunable fluorescence emission depending on the connecting π bridges and potential applications as organic emissive materials.[51]
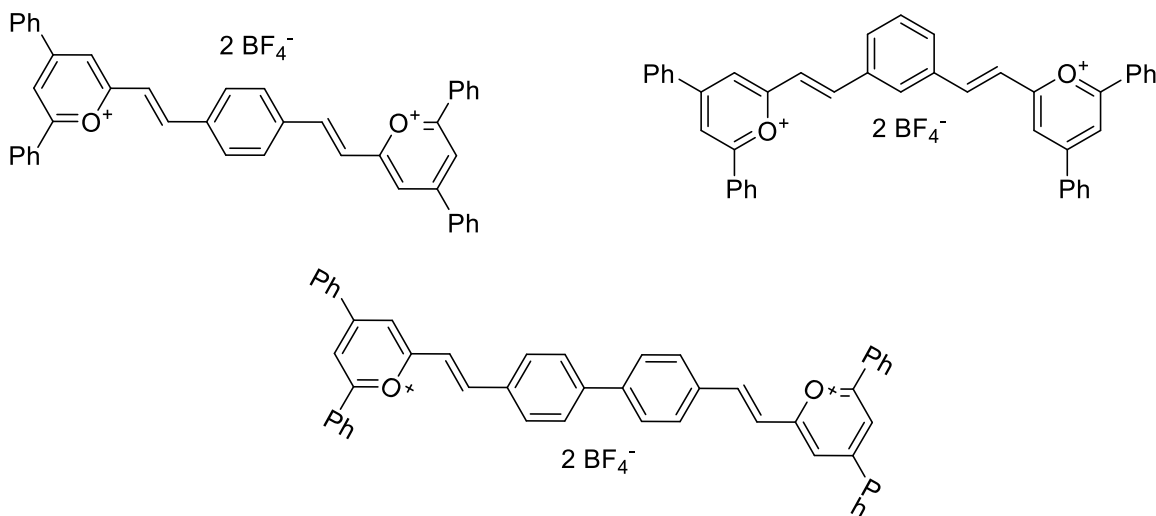
Figure 21. Highly conjugated bispyrylium compounds with solid-state emission properties.

In the same year, Yang et al have informed the synthesis of a family of α-free pyrylium perchlorates (**Figure 22**), with tunable fluorescence in solution and the solid-state, easily accessible by changing the aryl substituents in positions 2 and 4.[52] By x-ray diffraction, they have found that the increase of (C-H)-π interactions, leads to higher fluorescence quantum yields in solid-state.
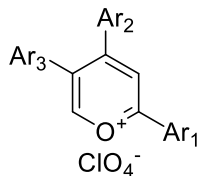
Figure 22. Pyrylium perchlorates with tunable fluorescence emission.

1.7. FINAL CONSIDERATIONS

Despite the widely extended applications of pyrylium compounds in fields like optics, photocatalysis and chemosensing, their use in other areas, like bioanalysis, is not fully exploited. Considering the previously described items regarding different aspects of the synthesis and reactivity of these compounds, pyrylium salts are great candidates as probes for the visualization and quantification of different analytes of biological interest. It is worth mentioning that, even though there is a great number of dyes based on xanthenic, cyanines, coumarins or bodipys scaffolds already available for these purposes, their production usually implies great synthetic efforts and the use of chromatographic techniques for obtaining pure compounds. Taking all this into account, in the next chapters novel uses of pyrylium salts will be developed, with special emphasis on the synthetic ease, photophysical properties, and biological applications.

1.8. REFERENCES

1   T. Y. Ohulchanskyy, M. K. Gannon, Y. Mao, A. Skripchenko, S. J. Wagner, P. N. Prasad and M. R. Detty, 'Switched-on' flexible chalcogenopyrylium photosensitizers. Changes in photophysical properties upon binding to DNA, *J. Phys. Chem. B*, 2007, **111**, 9686–9692.

2   N. K. Brennan, J. P. Hall, S. R. Davies, S. O. Gollnick, A. R. Oseroff, S. L. Gibson, R. Hilf and M. R. Detty, In vitro photodynamic properties of chalcogenopyrylium analogues of the thiopyrylium antitumor agent AA1, *J. Med. Chem.*, 2002, **45**, 5123–5135.

3   H. Wang, X. Qian, K. Wang, M. Su, W. W. Haoyang, X. Jiang, R. Brzozowski, M. Wang, X. Gao, Y. Li, B. Xu, P. Eswara, X. Q. Hao, W. Gong, J. L. Hou, J. Cai and X. Li, Supramolecular Kandinsky circles with high antibacterial activity, *Nat. Commun.*, 2018, **9**, 1815.

4   T. Kotowski, W. Skubiszak, J. A. Soroka, K. B. Soroka and T. Stacewicz, Pyrylium and thiopyrylium high efficiency laser dyes, *J. Lumin.*, 1991, **50**, 39–45.

5   M. Fakis, J. Polyzos, G. Tsigaridas, J. Parthenios, A. Fragos, V. Giannetas, P. Persephonis and J. Mikroyannidis, Novel class of pyrylium dyes with high efficiency in lasing and two-photon absorption fluorescence, *Chem. Phys. Lett.*, 2000, **323**, 111–116.

6   J. Ma, W. Li, J. Li, R. Shi, G. Yin and R. Wang, A small molecular pH-dependent fluorescent probe for cancer cell imaging in living cell, *Talanta*, 2018, **182**, 464–469.

7   A. Beltrán, M. Isabel Burguete, D. R. Abánades, D. Pérez-Sala, S. V. Luis and F. Galindo, Turn-on fluorescent probes for nitric oxide sensing based on the ortho-hydroxyamino

structure showing no interference with dehydroascorbic acid, *Chem. Commun.*, 2014, **50**, 3579–3581.

8   F. García, J. M. García, B. García-Acosta, R. Martínez-Máñez, F. Sancenón and J. Soto, Pyrylium-containing polymers as sensory materials for the colorimetric sensing of cyanide in water, *Chem. Commun.*, 2005, 2790–2792.

9   M. Comes, M. Dolores Marcos, R. Martínez-Máñez, F. Sancenón, J. Soto, L. A. Villaescusa, P. Amorós and D. Beltrán, Chromogenic discrimination of primary aliphatic amines in water with functionalized mesoporous silica, *Adv. Mater.*, 2004, **16**, 1783–1786.

10   A. Beltrán, M. I. Burguete, S. V. Luis and F. Galindo, Styrylpyrylium Dyes as Solvent-Sensitive Molecules Displaying Dual Fluorescence, *European J. Org. Chem.*, 2017, 4864–4870.

11   M. A. Miranda, M. A. Izquierdo and F. Galindo, Steady-State and Time-Resolved Studies on Oxetane Cycloreversion Using (Thia)pyrylium Salts as Electron-Transfer Photosensitizers, *Org. Lett.*, 2001, **3**, 1965–1966.

12   N. A. Romero and D. A. Nicewicz, Organic Photoredox Catalysis, *Chem. Rev.*, 2016, **116**, 10075–10166.

13   M. A. Miranda and H. García, 2,4,6-Triphenylpyrylium Tetrafluoroborate as an Electron-Transfer Photosensitizer, *Chem. Rev.*, 1994, **94**, 1063–1089.

14   J. Pernak, A. Świerczyńska, M. Kot, F. Walkiewicz and H. MacIejewski, Pyrylium sulfonate based ionic liquids, *Tetrahedron Lett.*, 2011, **52**, 4342–4345.

15   R. F. Khairutdinov and J. K. Hurst, Cyclic transmembrane charge transport mediated by pyrylium and thiopyrylium ions, *J. Am. Chem. Soc.*, 2001, **123**, 7352–7359.

16   D. Moser, Y. Duan, F. Wang, Y. Ma, M. J. O'Neill and J. Cornella, Selective Functionalization of Aminoheterocycles by a Pyrylium Salt, *Angew. Chemie - Int. Ed.*, 2018, **57**, 11035–11039.

17   S. Che, Z. Yang, I. Popovs, H. Luo, Y. Luo, W. Guo, H. Chen, T. Wang, K. Jie, C. Wang and S. Dai, A succinct strategy for construction of nanoporous ionic organic networks from a pyrylium intermediate, *Chem. Commun.*, 2019, **55**, 13450–13453.

18   J. Santamaría and C. Valdés, Six-Membered Rings with One Oxygen: Pyrylium Ion, Related Systems and Benzo-Derivatives, *Mod. Heterocycl. Chem.*, 2011, **3**, 1631–1682.

19   A. R. Katritzky, R. C. Patel and E. Anglia, The Preparation of Pyridiniums from Pyryliums, *J. Cemical Soc. Perkin I*.

20   J. D. Tovar and T. M. Swager, Pyrylium salts via electrophilic cyclization: Applications for novel 3- arylisoquinoline syntheses, *J. Org. Chem.*, 1999, **64**, 6499–6504.

21   C. Müller, D. Wasserberg, J. J. M. Weemers, E. A. Pidko, S. Hoffmann, M. Lutz, A. L. Spek, S. C. J. Meskers, R. A. J. Janssen, R. A. Van Santen and D. Vogt, Donor-functionalized polydentate pyrylium salts and phosphinines: Synthesis, structural characterization, and photophysical properties, *Chem. - A Eur. J.*, 2007, **13**, 4548–4559.

22   A. Dinculescu, T. S. Balaban, C. Popescu, D. Toader and A. T. Balaban, Synthesis of Pyrylium Salts with Various Anions, *Bull. des Sociétés Chim. Belges*, 1991, **100**, 665–672.

23   N. . Markina, T.A.; Boiko, Synthesis of 2-methyl-4,6-diarylpyrylium tetrafluoroborates, *Chem. Heterocycl. Compd.*, 1985, 138–139.

24   A. M. Bello and L. P. Kotra, Improved synthesis of pyrylium salts leading to 2,4-disubstituted diarylfurans via novel mechanism, *Tetrahedron Lett.*, 2003, **44**, 9271–9274.

25   C. T. Fathimath Salfeena, Basavaraja, K. T. Ashitha, V. P. Kumar, S. Varughese, C. H. Suresh and B. S. Sasidhar, Synthesis of symmetrical and unsymmetrical triarylpyrylium ions via an inverse electron demand Diels-Alder reaction, *Chem. Commun.*, 2018, **54**, 12463–12466.

26   S. Y. Wen, W. Zhang, T. B. Ren, Q. L. Zhang, Y. P. Liu, L. Shi, R. Hu, X. B. Zhang and L. Yuan, Donor and Ring-Fusing Engineering for Far-Red to Near-Infrared Triphenylpyrylium Fluorophores with Enhanced Fluorescence Performance for Sensing and Imaging, *Chem. - A Eur. J.*, 2019, **25**, 6973–6979.

27   C. Patchanee, K. Hemming;, D. McKerrecher; and R. J. K. Taylor, The Preparation of 4-Substituted Pyrylium Salts and their Use in Dienal Synthesis, *J. Heterocycle Chem.*, 1996, 1083–1089.

28   F. Heidarizadeh and F. Abadast, Reactions of some nucleophiles with pyrylium salts, *Orient. J. Chem.*, 2011, **27**, 1421–1436.

29   A. T. Balaban, V. E. Sahini and E. Keplinger, Electronic absorption spectra of alkyl- and phenyl-substituted pyrylium salts, *Tetrahedron*, 1960, **9**, 163–174.

30   F. Haucke, Gunter; Czerney, Peter; Cebulla, Absorption and fluorescence of pyrilium salts, *Berichte der Bunsengesellschaft für Phys. Chemie*, 1992, **96**, 880–886.

31   N. Manoj, G. Ajayakumar, K. R. Gopidas and C. H. Suresh, Structure absorption spectra correlation in a series of 2,6-dimethyl-4-arylpyrylium salts, *J. Phys. Chem. A*, 2006, **110**, 11338–11345.

32   A. Franconetti, L. Contreras-Bernal, S. Jatunov, M. Gómez-Guillén, M. Angulo, R. Prado-Gotor and F. Cabrera-Escribano, Electronically tunable anion-π interactions in pyrylium complexes: Experimental and theoretical studies, *Phys. Chem. Chem. Phys.*, 2014, **16**, 18442–18453.

33   A. Pigliucci, P. Nikolov, A. Rehaman, L. Gagliardi, C. J. Cramer and E. Vauthey, Early excited state dynamics of 6-styryl-substituted pyrylium salts exhibiting dual fluorescence, *J. Phys. Chem. A*, 2006, **110**, 9988–9994.

34   P. Nikolov and S. Metzov, Peculiarities in the photophysical properties of some 6-styryl-2,4-disubstituted pyrylium salts, *J. Photochem. Photobiol. A Chem.*, 2000, **135**, 13–25.

35   A. Loibl, W. Oschmann, M. Vogler, E. A. Pidko, M. Weber, J. Wiecko and C. Müller, Substituent effects in pyridyl-functionalized pyrylium salts, pyridines and λ3,σ2-phosphinines: a fundamental and systematic study, *Dalt. Trans.*, 2018, **47**, 9355–9366.

36   M. J. Ruedas-Rama, J. D. Walters, A. Orte and E. A. H. Hall, Fluorescent nanoparticles for intracellular sensing: A review, *Anal. Chim. Acta*, 2012, **751**, 1–23.

37   X. Huang, J. Song, B. C. Yung, X. Huang, Y. Xiong and X. Chen, Ratiometric optical nanoprobes enable accurate molecular detection and imaging, *Chem. Soc. Rev.*, 2018, **47**, 2873–2920.

38   E. Molnár, S. Kuntam, P. K. R. Cingaram, B. Peksel, B. Suresh, G. Fábián, L. Z. Fehér,

A. Bokros, Á. Medgyesi, F. Ayaydin and L. G. Puskás, Combination of small molecule microarray and confocal microscopy techniques for live cell staining fluorescent dye discovery, *Molecules*, 2013, **18**, 9999–10013.

39 S. Chakraborty, M. M. Joseph, S. Varughese, S. Ghosh, K. K. Maiti, A. Samanta and A. Ajayaghosh, A new pentacyclic pyrylium fluorescent probe that responds to pH imbalance during apoptosis, *Chem. Sci.*, 2020, 12695–12700.

40 X. Chen, L. Yan, Y. Liu, Y. Yang and J. You, Switchable cascade C–H annulation to polycyclic pyryliums and pyridiniums: discovering mitochondria-targeting fluorescent probes, *Chem. Commun.*, 2020, 15080–15083.

41 R. Martínez-Máñez and F. Sancenón, Chemodosimeters and 3D inorganic functionalised hosts for the fluoro-chromogenic sensing of anions, *Coord. Chem. Rev.*, 2006, **250**, 3081–3093.

42 D. Jiménez, R. Martínez-Máñez, F. Sancenón, J. V. Ros-Lis, A. Benito and J. Soto, A new chromo-chemodosimeter selective for sulfide anion, *J. Am. Chem. Soc.*, 2003, **125**, 9000–9001.

43 B. García-Acosta, F. García, J. M. García, R. Martínez-Méñez, F. Sancenón, N. San-José and J. Soto, Chromogenic signaling of hydrogen carbonate anion with pyrylium-containing polymers, *Org. Lett.*, 2007, **9**, 2429–2432.

44 B. K. Wetzl, S. M. Yarmoluk, D. B. Craig and O. S. Wolfbeis, Chameleon labels for staining and quantifying proteins, *Angew. Chemie - Int. Ed.*, 2004, **43**, 5400–5402.

45 F. A. Scaramuzzo, A. González-Campo, C. C. Wu, A. H. Velders, V. Subramaniam, G.

Doddi, P. Mencarelli, M. Barteri, P. Jonkheijm and J. Huskens, Pyrylium monolayers as amino-reactive platform, *Chem. Commun.*, 2010, **46**, 4193–4195.

46   N. S. Yurova, A. Danchuk, S. N. Mobarez, N. Wongkaew, T. Rusanova, A. J. Baeumner and A. Duerkop, Functional electrospun nanofibers for multimodal sensitive detection of biogenic amines in food via a simple dipstick assay, *Anal. Bioanal. Chem.*, 2018, **410**, 1111–1121.

47   A. Agostini, I. Campos, M. Milani, S. Elsayed, L. Pascual, R. Martínez-Máñez, M. Licchelli and F. Sancenón, A surfactant-assisted probe for the chromo-fluorogenic selective recognition of GSH in water, *Org. Biomol. Chem.*, 2014, **12**, 1871–1874.

48   X. Qian, W. Gong, F. Wang, Y. Lin and G. Ning, A pyrylium-based colorimetric and fluorimetric chemosensor for the selective detection of lysine in aqueous environment and real sample, *Tetrahedron Lett.*, 2015, **56**, 2764–2767.

49   S. Tripathi, V. Wintgens, P. Valat, V. Toscano, J. Kossanyi and F. Bos, Laser effect of a series of variously substituted pyrylium and thiopyrylium salts, *J. Lumin.*, 1987, **37**, 149–157.

50   D. Li, J. Zhang and M. Anpo, Preparation of organic-inorganic material from MCM-48 and pyrylium salt, *Opt. Mater. (Amst).*, 2005, **27**, 671–673.

51   G.-L. Gong, Wei-Tao; Qian, Xiao-min; Wang, Fu-Rui; Lin, Yuan; Ning, Synthesis and Photophysical Properties of New Highly Conjugated Bispyrylium Compounds, *Heteroat. Chem.*, 2013, **24**, 66–71.

52   L. Yang, J. Ye, Y. Gao, D. Deng, W. Gong, Y. Lin and G. Ning, Highly efficient one-pot

synthesis of α-free pyrylium salts with tunable fluorescence emission via ring-expanding

reaction of triarylcyclopentadienes, *Tetrahedron Lett.*, 2013, **54**, 2967–2971.

Chapter 2

Objectives

The general objective of this thesis is the development of pyrylium salts **to expand their application fields to new frontiers**, in areas as diverse as **cellular bioimaging**, **analyte sensing** and **solid-state emission**.

Specific objectives are faced in each chapter as follows:

1. Synthesis and characterisation of styrylpyrylium dyes and their evaluation as **intracellular fluorescent probes** in live cells by confocal microscopy.

2. Development of new **fluorescent sensors for nitric oxide** based on pyrylium probes, and their assay in different biological environments such as **cell cultures** and **peripheral blood samples**.

3. Study of the acid-base behaviour of pyrylium salts with hydroxy groups, and, based on this property, design of **fluorescent sensors for moisture** in organic solvents.

4. Preparation of a library of pyrylium salts displaying **solid-state emission features**, with fine-tuning of their photophysical properties by introducing different substituents on the structure.
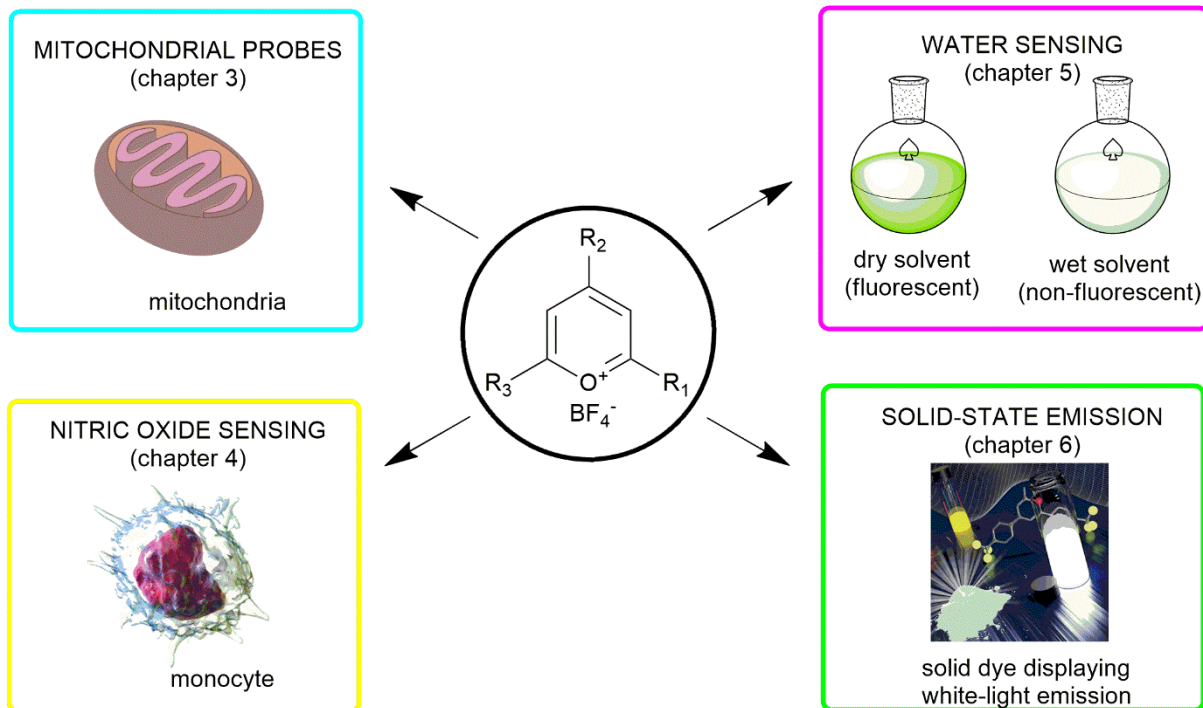
Figure 1. Graphical abstract of the objectives.

Chapter 3

Styrylpyrylium dyes as mitochondrial probes

The results presented in this chapter are based on the following article:

Fluorescent styrylpyrylium probes for the imaging of mitochondria in live cells. Muñoz Resta, I.; Lucantoni, F.; Miravet, J. F.; Apostolova, N.; Galindo, F. **2021**. *Submitted*.

Confocal microscopy and toxicity assays were performed in collaboration with Dr. Nadezda Apostolova and Dr. Federico Lucantoni from the Department of Pharmacology, University of Valencia (Valencia, Spain).

3.1. INTRODUCTION

Mitochondria are one of the most versatile cellular organelles because they are involved in multiple biologically relevant processes taking place in eukaryotic organisms. Commonly known as *powerhouses of the cell*, their functions vary from energy production to important roles in metabolism, innate immunity, and intrinsic apoptosis, just to mention a few.[1] Morphologically, mitochondria are the only organelles in animal cells with two membranes: an outer one, porous and permeable, and an inner one with very restricted transport properties.[2] Is onto this latter one, and in the isolated space that it encircles, the mitochondrial matrix, that the key function of mitochondria takes place: the oxidative phosphorylation. This metabolic process couples the energy released from a series of redox reactions to the translocation of protons from the matrix to the external side of the inner membrane. So, a proton gradient that acts as the driving force for the synthesis of ATP - the universal intermediate that serves as the energy source for most of the chemical reactions that occur within the cells - is generated.[3]

Because of the highly negative potential that is produced due to the proton flux through the inner membrane, delocalized lipophilic cations, DLCs, accumulate efficiently within mitochondria.[1,4] This class of molecules are species with positive charge and a π-conjugated system, with the possibility of fine-tuning the charge distribution and polarity by the introduction of different substituents.[5] As fluorescence microscopy is a well-established technique for cell imaging, a great number of reported emissive DLCs has expanded the library of small-molecule fluorescent probes for visualizing mitochondria.[1,2,4,6–9]

Some examples of DLCs as mitochondrial fluorescent markers comprise molecules as diverse as rhodamines,[10–12] bisamidines,[13,14] coumarin-based fluorophores,[15–19] indole-ring substituted derivates,[5] pentamethinium salts,[20] quaternized imidazole [1,2-a]-pyridines[21], boron

dipyrromethenes (BODIPYs)[22], tetraphenylethylene derivates[23,24] and cyanine dyes.[25,26] Notably, exceptions are described and certain probes targeting mitochondria are neutral compounds, such as the recently developed acridone derivates, described by the group of A. Orte.[27] An innovative novel approach for the generation of mitochondrial markers utilizes a completely different mechanism, mediated by the enzyme carnitine-acylcarnitine translocase (CACT) to deliver the probe inside the organelle (regardless of the transmembrane potential).[28] However, one common problem of most reported mitochondrial probes based on xanthenic, cyanine and BODIPY architectures is their small Stokes shift (SS). For instance, the SS of paradigmatic examples of mitochondrial probes like rhodamine 123, tetramethyl rhodamine methyl ester (TMRM) and DiOC6(3) is scarcely a few nanometers.

Alterations in mitochondrial physiology are associated with a vast number of human conditions such as neurological, cardiovascular, metabolic, and neoplastic diseases. It is well known that DLCs can be toxic to the organelle at high concentrations.[3] So, besides acting as fluorescent markers, they could also be used as therapeutic agents in the treatment of mitochondrial disorders.[29,30] Although all DLCs share the same mechanism for accumulation in the mitochondria, i.e., response to negative inside transmembrane potential, their mechanisms of toxicity are relatively diverse and points to different targets, such as the electron transport chain, the mitochondrial permeability or specific enzymes of the organelle.[31]

Mitochondrial staining using pyrylium dyes has been reported only in few cases during the last years.[32–34] Additionally, although not used for bioimaging, several pyrylium salts have been studied as potential anticancer drugs[35,36] pointing to mitochondria as the site of action. However, their easy synthesis and purification,[37] in addition to high emission quantum yields,[38] make them very attractive for bioimaging applications. Another benefit of pyrylium dyes is that

they do not tend to participate in type I or II photosensitization processes, thus preventing photodamage during image acquisition by generated reactive oxygen species (ROS).

In this chapter, the synthesis and characterisation of eight styrylpyrylium dyes (**Chart 1**) are reported. Four of them have been tested and found useful for mitochondrial fluorescence bioimaging in cultured hepatocarcinoma cells (Hep3B). Notably, the described pyrylium dyes display large SS depending on the substitution and the solvent (more than 100 nm in some cases).

3.1 R = -H	**3.5** R = -H
3.2 R = -CF$_3$	**3.6** R = -CF$_3$
3.3 R = -OH	**3.7** R = -OH
3.4 R = -OCH$_3$	**3.8** R = -OCH$_3$
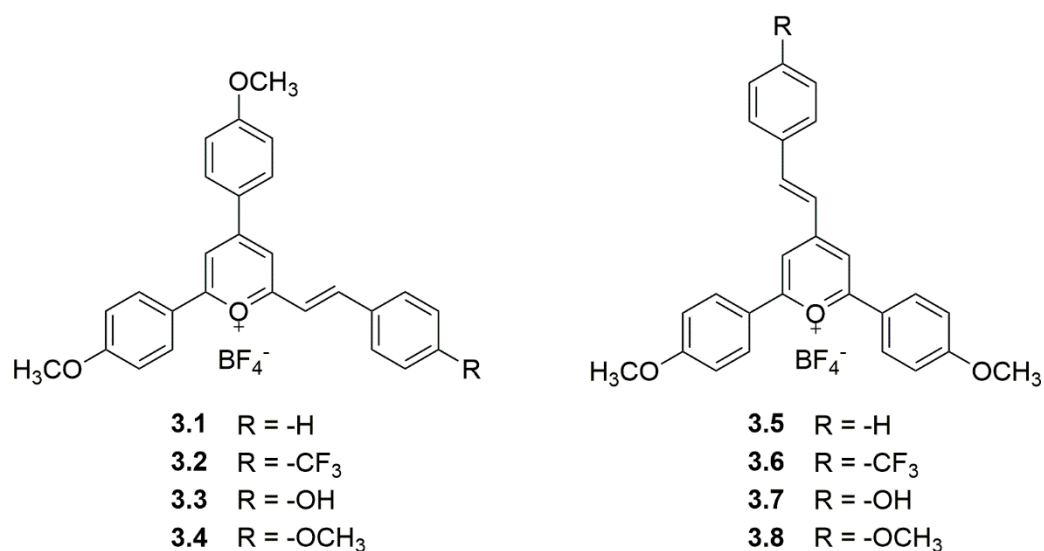
Chart 1. Styrylpyrylium dyes synthesized and studied as mitochondrial probes.

3.2. RESULTS AND DISCUSSION

3.2.1. SYNTHESIS AND CHARACTERISATION

Following procedures used previously for the preparation of similar compounds,[39,40] dyes **3.1-3.4** were prepared in a two-step process as shown in **Scheme 1**. A condensation between *p*-metoxyacetophenone and acetic anhydride catalysed by BF$_3$-etherate led to the intermediate 2,4-bis(4-methoxyphenyl)-6-methylpyrylium tetrafluoroborate. The reaction between this intermediate and the corresponding *p*-substituted benzaldehydes in acetic acid

resulted in the desired products, all of them easily purified by precipitation in diethyl ether and obtained in moderate to high yields (74 – 87%).
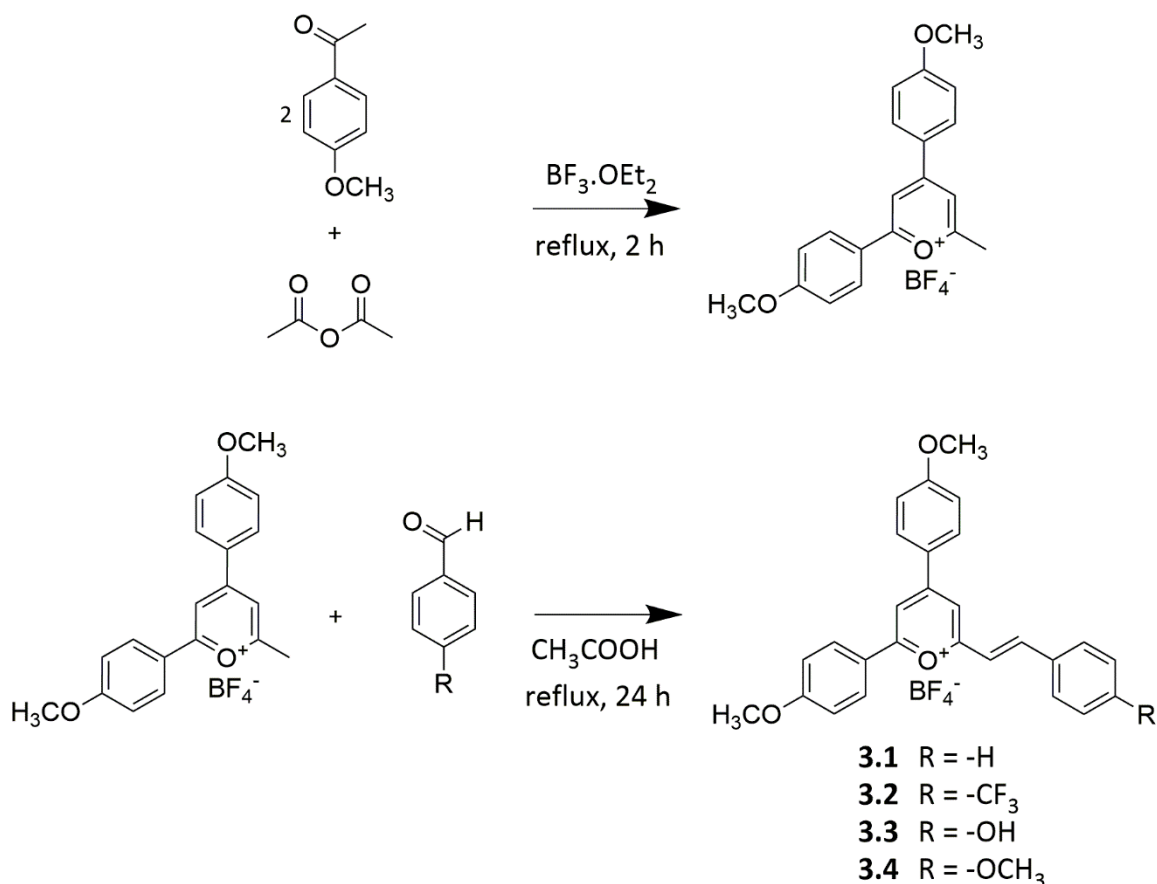
Scheme 1. Synthesis of compounds **3.1-3.4**.

A related family of compounds with the same substituents but a different position of the styryl chain were synthesized, as can be seen in **Scheme 2**, adapting a previously reported procedure.[41] The synthesis of the intermediate 2,6-bis(4-methoxyphenyl)-4-methylpyrylium tetrafluoroborate was carried out in three consecutive steps, following by the reaction with the corresponding *p*-substituted benzaldehydes to yield the required products **3.5-3.8**. The obtained compounds were isolated simply by precipitation in diethyl ether (yields 58-86 %), avoiding chromatographic techniques, thus providing a comparative advantage over other probes.
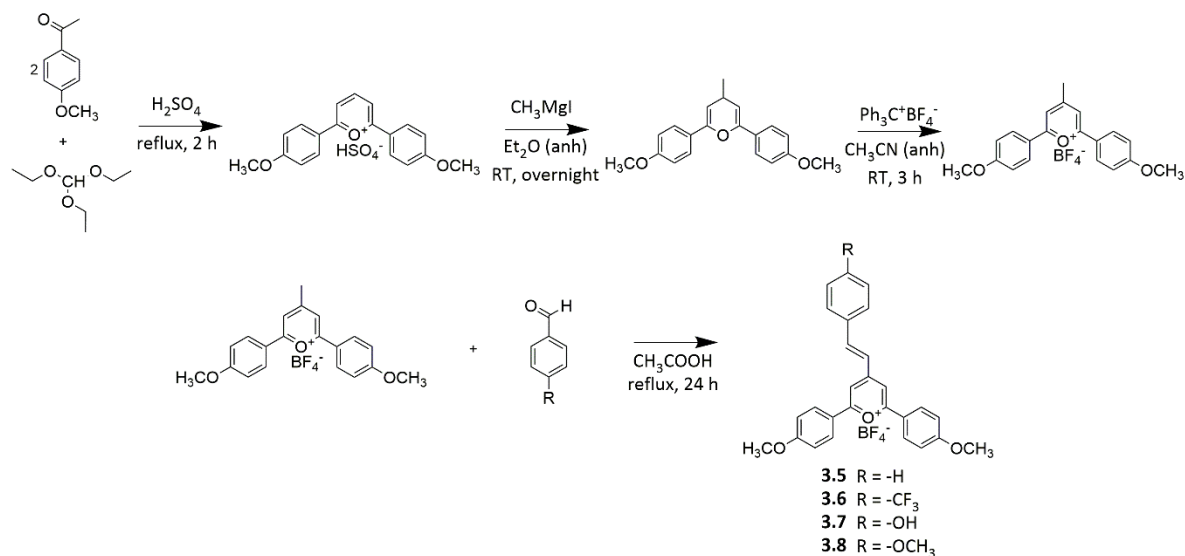
Scheme 2. Synthesis of compounds **3.5-3.8**.

All eight compounds are strongly coloured, with emissions within the yellow and the orange (**Figures 1-4**). Their photophysical properties were determined in three solvents of different polarities: dichloromethane (DCM), acetonitrile (ACN), and phosphate-buffered saline (PBS) 10 mM, pH 7.4. The data for all the compounds are collected in **Table 1**.
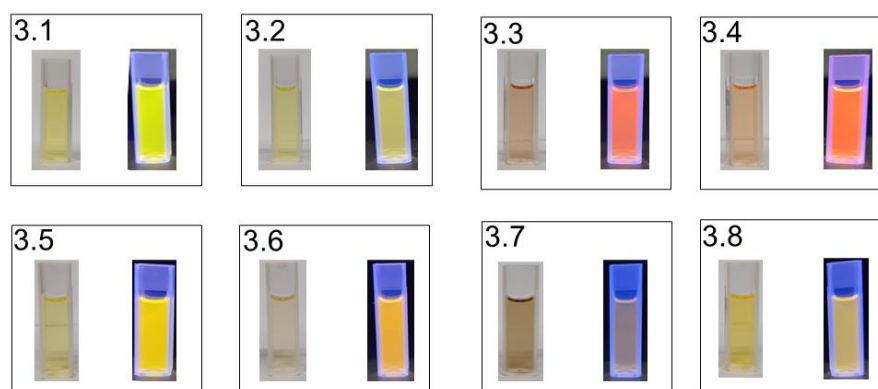
Figure 1. 10 µM solutions of compounds **3.1-3.8** in acetonitrile under visible (left) and UV -365 nm-(right) light.
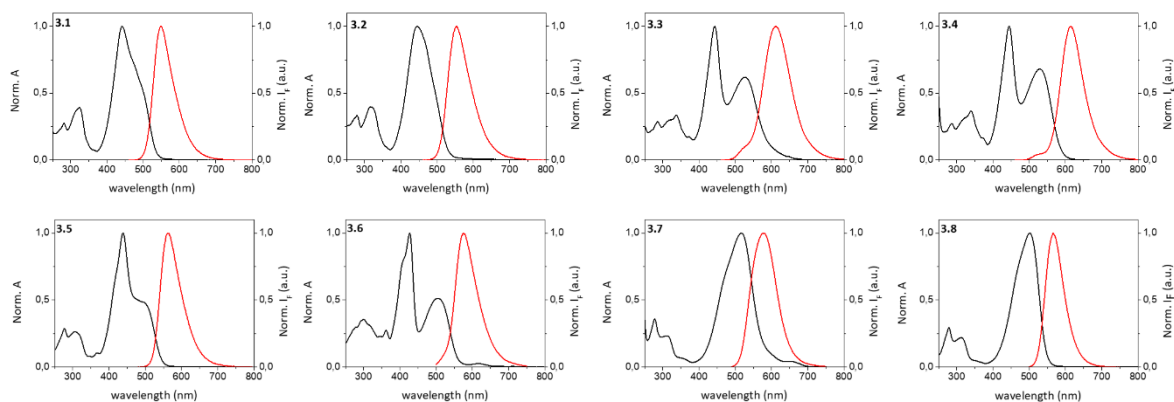
Figure 2. Normalized absorption (black) and emission (red) spectra of compounds **3.1-3.8** in DCM. λ_{exc} was set at the absorption maximum of each compound.
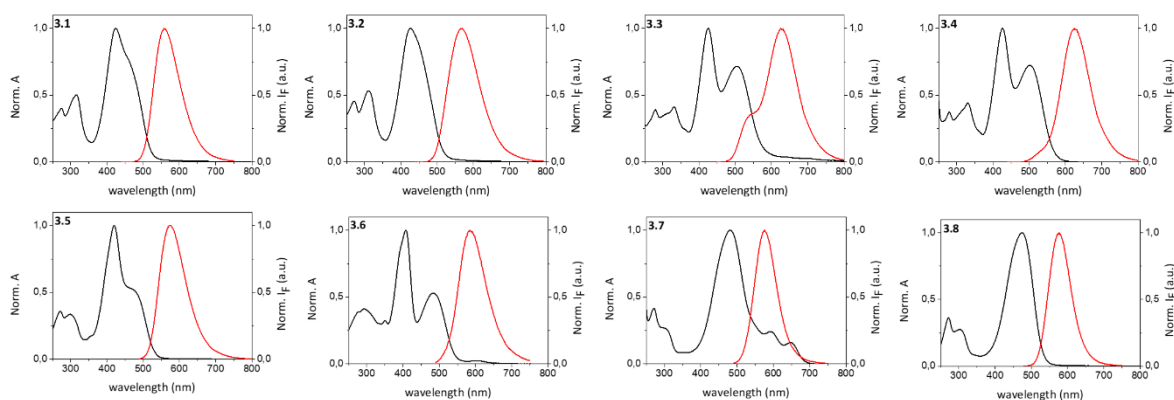
Figure 3. Normalized absorption (black) and emission (red) spectra of compounds **3.1-3.8** in ACN. λ_{exc} was set at the absorption maximum of each compound.
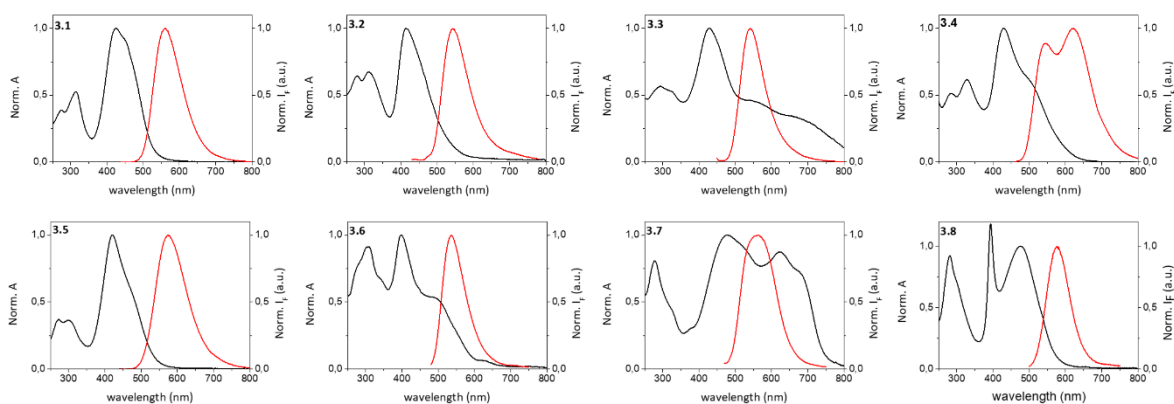
Figure 4. Normalized absorption (black) and emission (red) spectra of compounds **3.1-3.8** in PBS (10 mM, pH 7.4). λ_{exc} was set at the absorption maximum of each compound.

Table 1. Photophysical parameters for different solutions of compounds **3.1-3.8**.

Compd.	Sv.	λabs (log ε) (nm)	λem (nm)	φF	τF (ns)
3.1	ACN	424 (4.64)	557	0.49	τ1 ≤ 1.0 (11 %) τ2 = 3.5 (89 %)
	DCM	442 (4.75)	548	0.95	4.6
	PBS 10 mM pH = 7.4	425 (4.53)	561	0.10	τ1 ≤ 1.0 (82%) τ2 = 3.4 (18 %)
3.2	ACN	426 (4.57)	568	0.13	τ1 = 1.1 (75 %) τ2 = 5.2 (25 %)
	DCM	446 (4.67)	553	0.72	4.7
	PBS 10 mM pH = 7.4	415 (4.30)	542	0.01	τ1 ≤ 1.0 (25 %) τ2 = 3.8 (75 %)
3.3	ACN	425 (4.63) 504 (4.49)	535 -s- 625	0.17	τ1 ≤ 1.0 (43 %) τ2 = 2.2 (57 %)
	DCM	443 (4.71) 527 (4.50)	505 -s- 613	0.38	τ1 = 1.1 (15 %) τ2 = 3.2 (85 %)
	PBS 10 mM pH = 7.4	427 (4.37)	541	0.01	τ1 ≤ 1.0 (9 %) τ2 = 3.7 (91 %)
3.4	ACN	426 (4.66) 501 (4.49)	625	0.38	τ1 ≤ 1.0 (8 %) τ2 = 3.5 (92 %)
	DCM	445 (4.77) 529 (4.60)	525 614	0.59	4.0
	PBS 10 mM pH = 7.4	430 (4.43) 500 -s-	546 623	0.03	τ1 ≤ 1.0 (83 %) τ2 = 3.3 (17 %)
3.5	ACN	420 (4.65) 475 -s-	575	0.39	3.6
	DCM	439 (4.78) 490 -s-	562	0.61	4.1
	PBS 10 mM pH = 7.4	421 (4.54)	573	0.06	τ1 ≤ 1.0 (87 %) τ2 = 3.5 (13 %)
3.6	ACN	408 (4.61) 483 (4.33)	584	0.22	2.1
	DCM	427 (4.68) 504 (4.39)	575	0.45	4.2
	PBS 10 mM pH = 7.4	398 (4.38) 500 -s-	536	0.005	τ1 ≤ 1.0 (46 %) τ2 = 4.0 (54 %)
3.7	ACN	481 (4.72) 593 (4.10) 647 (3.92)	576	0.09	≤ 1.0
	DCM	517 (4.82) 653 (3.46)	577	0.37	1.3
	PBS 10 mM pH = 7.4	478 (4.33) 621 (4.27) 680 -s-	566	0.007	τ1 ≤ 1.0 (89 %) τ2 = 3.8 (11%)
3.8	ACN	474 (4.77)	578	0.28	≤ 1.0
	DCM	501 (4.87)	567	0.54	1.2
	PBS 10 mM pH = 7.4	474 (4.25)	577	0.01	≤ 1.0

s = shoulder

The pyrylium salts here studied show one or two intense absorption bands above 400 nm (see spectra in **Figures 2**-**4** and data in **Table 1**). According to the literature, pyrylium dyes can be considered as two-dimensional chromophoric systems displaying *x* and *y* absorption bands.[38] In the case of styrylpyrylium salts characterized in this chapter,[42,43] the electronic transition that

originates the band at shorter wavelengths (chromophore *y*, around 400 nm) can be assumed to be strongly localized on the pyrylium core and, on the other hand, the transition with the lowest energy (chromophore *x*, around 450-500 nm) can be associated to the whole conjugated system. Sometimes, depending on the solvent, but particularly on the substitution pattern, these two bands overlap and only one transition can be seen. The case of compounds **3.3** and **3.7** is special since, in PBS, the absorption spectra are extended towards very low energies, beyond 700 nm. This behaviour in PBS can be ascribed to the formation of a new band due to the acid-base equilibrium established between the pyrylium cation and the quinoidal base formed after deprotonation of the free OH, as can be seen in **Figure 5**:
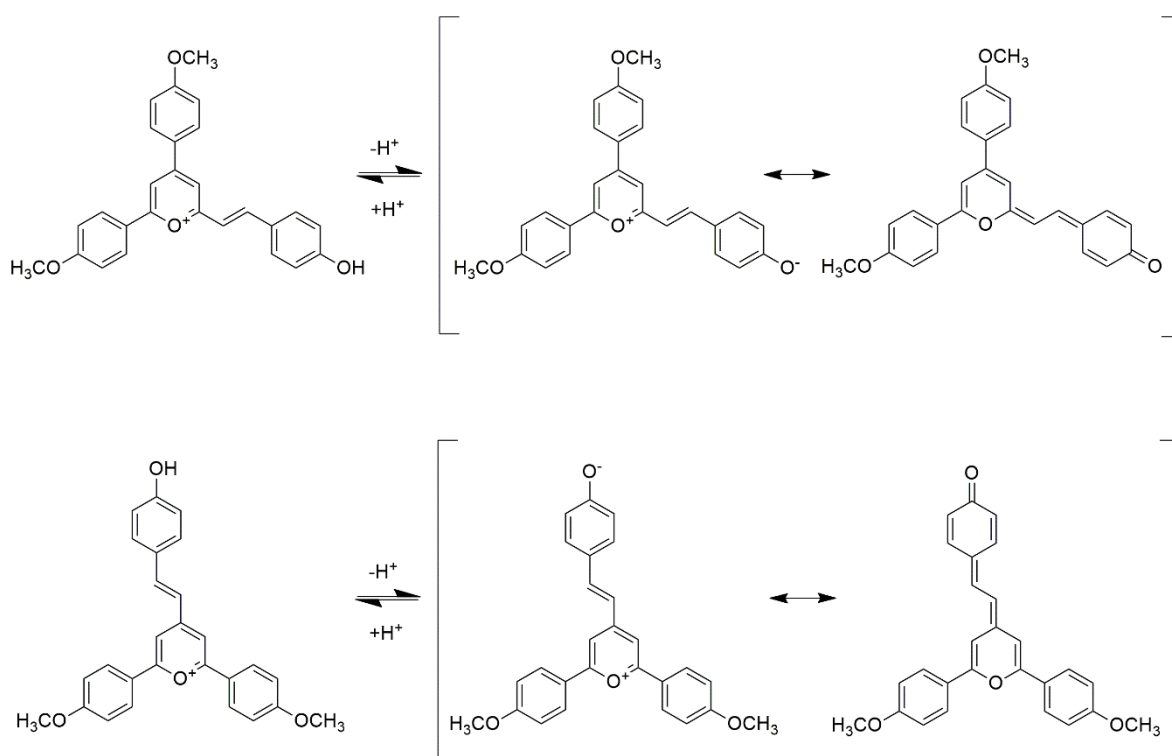
Figure 5. Equilibria between pyrylium cations and the quinoidal bases upon deprotonation of the hydroxyl group (top: **3.3**; bottom: **3.7**).

Related compounds, like flavylium salts, have also shown this acid-base behaviour.[44] And recently, a pyrylium dye with hydroxyl groups has been reported to show a similar shift in the absorption spectrum, from 460 nm to 570 nm, upon deprotonation.[45] Regarding the fluorescence properties of the studied dyes, mainly one emission band is observed, except for particular situations like compound **3.4** in PBS and compound **3.3** in ACN, which show dual fluorescence (very clear for **3.4** and in the form of a shoulder for **3.3**). Nikolov and Vauthey have demonstrated that related compounds (6-styryl-substituted-2,4-diphenyl pyrylium cations) display *non-Kasha* fluorescence behaviour, with two emission bands, one localized in the pyrylium core (L band) and other delocalized throughout the whole dye (D band). Besides, those L and D bands do not exhibit a precursor-successor relationship.[42,43] In the set of molecules here studied, such double fluorescence is not a common pattern, but, as mentioned early, an exception. Likely, the D band (S_2-S_0 transition) is not observable for most of the molecules, but only the lower S_1-S_0 one. Probably, the fact that aryl rings in positions 2 and 4 are substituted with a methoxy substituent implies the formation of a less stabilized charge-transfer (CT) state than for the compounds studied by Nikolov and Vauthey, lacking such methoxy substituent. As a matter of fact, the early reported dyes displayed D emissions more bathochromically shifted (up to 630 - 645 nm depending on the solvent) than any of the studied here. Although it would be desirable to have dual emission features in systems aimed for biological imaging, in the case of the pyrylium dyes aqueous stability is a matter of the utmost importance, and the presence of methoxy groups is mandatory to avoid aqueous hydrolysis, since the donating MeO- groups stabilize the central pyrylium core, thus hampering the opening of the central ring (and loss of colour and emission).[33] Finally, regarding the fluorescence quantum yields, it must be noted that higher values have been recorded in nonpolar dichloromethane than in polar acetonitrile and

PBS (**Table 1**). This fact reflects the CT character of the emissive state, in accordance with previous descriptions of analogous styrylpyrylium cations.[38,42,43] Emission lifetimes are complex and cannot be explained by a single model. Likely, as reported earlier,[42] the presence of several conformers could explain the lifetime distributions.

An important feature of molecules **3.1-3.8** is the large SS observed. This parameter is of great importance to obtain information from biological samples without interference from the excitation source. The absorption and emission spectra of many probes described in the literature, and many of the ones currently commercialized, are separated by scarcely a few nanometers, which causes cross-talk between excitation and fluorescence, implying normally a poor signal-to-noise ratio.[46] The SS of **3.1-3.8** has been collected in **Table 2** (only in PBS since the biological imaging is the ultimate objective of this chapter):

Table 2. Stokes shifts of various commercial dyes, and those corresponding to the compounds synthesized in the present chapter.

Dye	Stokes shift (nm)	Source
Rhodamine 123	22	a
Nile Red	80	a
Nile Blue	32	a
Cy3	14	a
Cy5	18	a
Cy7	25	a
BCEF	43	a
DAPI	97	a
Bodipy 500/510	10	a
Bodipy FL	10	a
Alexa Fluor 488	19	a
Dansyl	190	a
Calcium Green	22	a
DCF	20	a
Syto 11	18	a
TAMRA	24	a
Texas Red	20	a
Mag-Fura-2	166	a
Oregon Green	25	a
GFP	21	a
Cascade Yellow	146	a
Calcain AM	21	a
Lysosensor Green	60	a
Lysosensor Yellow/Blue	155	a
Mitotracker Red	16	a
Mitotracker Orange	28	a
3.1	136	This chapter
3.2	127	This chapter
3.3	114	This chapter
3.4	116 (L)[b] 193 (D) [b]	This chapter
3.5	152	This chapter
3.6	36	This chapter
3.7	88	This chapter
3.8	103	This chapter

a: data from ThermoFisher Scientific Inc. webpage
b: considering emission band L or D

As it can be seen, the following molecules stand out for their SS, higher than 100 nm (SS value in parenthesis): **3.1** (136 nm), **3.2** (127nm), **3.3** (114 nm), **3.4** (193 nm), **3.5** (152 nm) and **3.8** (103 nm). For comparison purposes, common biological fluorescent stains are included in the same table. It must be noted that an approach to achieve larger SS normally described in the literature consists of the combination of two optically active moieties in the same molecule, communicated via Förster Resonance Energy Transfer (FRET) mechanism.[47,48] However, this strategy requires a considerable synthetic effort, leading to complex molecules in very low chemical yields. On the contrary, the approach reported in this chapter affords notable amounts of dyes in few synthetic steps, and the purification is carried out avoiding chromatographic techniques, only by the precipitation method (typically 200-300 mg of each dye were produced, and the synthesis can be easily escalated).

3.2.2. *CELLULAR IMAGING*

3.2.2.1. CELLULAR UPTAKE IN HEP3B CELL LINE

Before carrying out biological assays, a stability test towards hydrolysis over long periods was conducted with all the synthesized compounds. Since pyrylium core is susceptible to nucleophilic attacks due to its electron deficiency, especially at positions 2 and 6, compounds with electron-donating substituents were expected to be more stable to hydrolysis in an aqueous environment. Measurement of the absorbance spectrum of each compound in PBS over time showed that **3.1, 3.2** and **3.5, 3.6** suffered a fast hydrolytic process making these dyes less suitable for bioimaging assays. Hence, live-cell imaging assays were conducted with probes **3.3, 3.4** and **3.7, 3.8**, stable over periods of hours. It must be recalled that the search for pyrylium dyes with enhanced aqueous stability is a relevant objective, not only for bioimaging but for other optical applications. In this regard, the group of L. Yuan and L. Shi investigated in detail

synthetic strategies to develop rigidized alkylamino derivatives of pyrylium cations displaying enhanced stability in an aqueous environment.[33]

The cellular uptake and subcellular localization of the four probes were studied by confocal laser scanning microscopy (CLSM) using the human hepatoblastoma cell line Hep3B. The choice of this line is justified both considering that hepatocytes possess many mitochondria compared to other cell types and regarding the interest of search for drugs with cytotoxic properties in the context of hepatocellular carcinoma (HCC). Visualization of the four dyes within the cells was performed after 30 min of incubation (1 µM of each dye) as shown in **Figure 6A**. Cells were also stained with Hoechst 33342 to mark nuclei. The intensity of the fluorescent signal displayed by **3.4** and **3.7** was comparable and significantly higher than the intensity displayed by **3.3** and **3.8** (**Figures 6A-7A**). When cells were exposed to a higher concentration (5 µM) for 30 min, **3.4** revealed the highest fluorescence intensity, with saturation of the signal, whereas the rest of the molecules afforded well-resolved images (**Figures 6B-7B**). Thus, since **3.4** was the probe rendering the highest fluorescence intensity and cellular internalization, its ability to stain mitochondria was also confirmed with a lower concentration (0.5 µM) as shown in **Figure 6C**. Similar or higher concentrations of pyrylium dyes have been employed for intracellular assays reported in the literature. For instance, 1 µM for dye C2,[32] 5 µM for TPPF-NTF[33] and 20 µM for pentacyclic pyrylium PS-OH.[45]
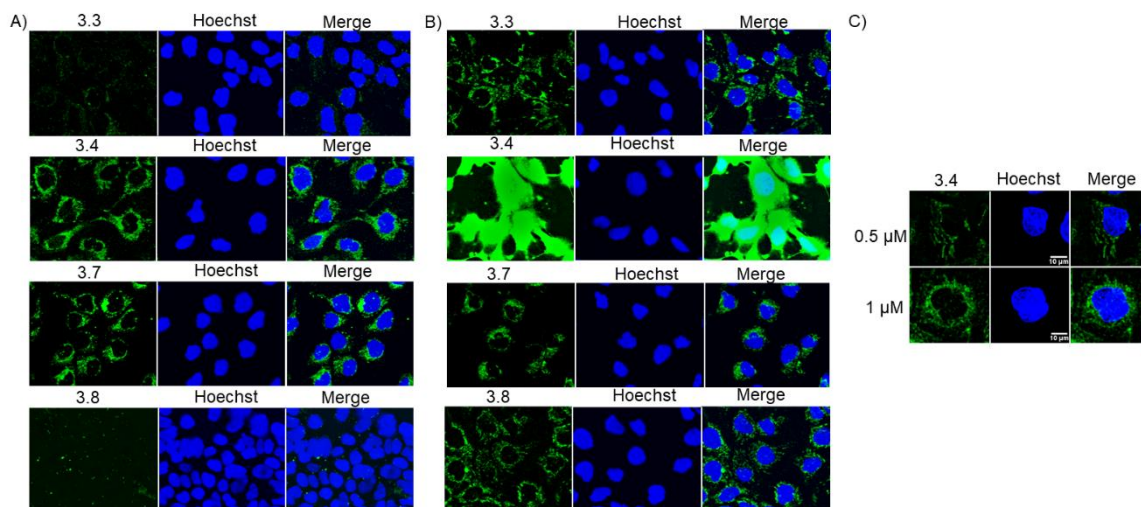
Figure 6. Nuclei were stained with Hoechst 33342 (blue) and confocal microscope images were obtained after exposure to (A) 1 µM of **3.3**, **3.4**, **3.7** or **3.8**; (B) 5 µM of **3.3**, **3.4**, **3.7** or **3.8**; and (C) 0.5 µM or 1 µM of **3.4**.
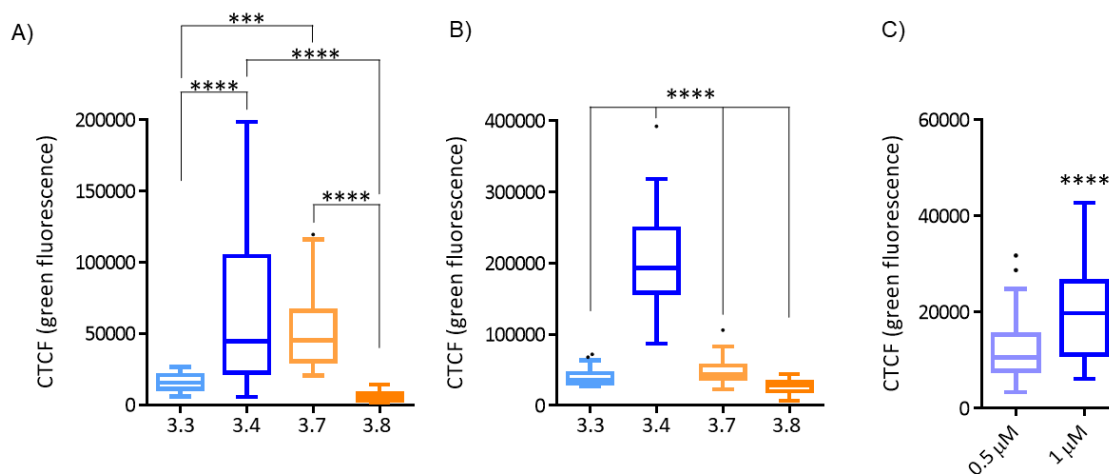
Figure 7, Quantification of the green fluorescent signal (CTCF, corrected total cell fluorescence) of images from Figure 6 is displayed. Data are shown as median ± (inter-quartile range) IQR, n=3. Statistical analysis was performed by one-way ANOVA followed by Tukey's multiple comparisons tests (*** indicates a p-value ≤ 0.001 and **** indicates a p-value ≤ 0.0001) for A and B, and unpaired t-test (**** indicates a p-value ≤ 0.0001) for C.

3.2.2.2.   COLOCALIZATION STUDIES

The morphology of the marked subcellular structures, filamentous and interconnected, and their perinuclear location, strongly suggested mitochondrial staining. The pattern of subcellular localization was very similar for the four tested compounds (**Figure 6**). To assess

the specificity of the assayed fluorogenic dyes to stain mitochondria, colocalization experiments with the mitochondria-specific far-red fluorescent dye MitoView 633 were performed. To this purpose, pyrylium dyes **3.4** (1µM) and **3.8** (5µM) were co-incubated with MitoView 633 (100 nM). A clear correlation of each of the fluorochromes with MitoView 633 can be observed in **Figure 8**, indicating the mitochondrial location of the tested compounds, with Pearson´s correlation coefficients of 0.78 and 0.81, respectively. Of note, despite being an excellent mitochondrial marker, MitoView 633 has been reported to have some photosensitization effects, leading to mitophagy, resulting from the generation of reactive oxygen species (ROS), like singlet oxygen ($^1O_2$), upon irradiation.[49] This process is very unlikely to occur with pyrylium dyes due to their low efficiency generating ROS.[50]
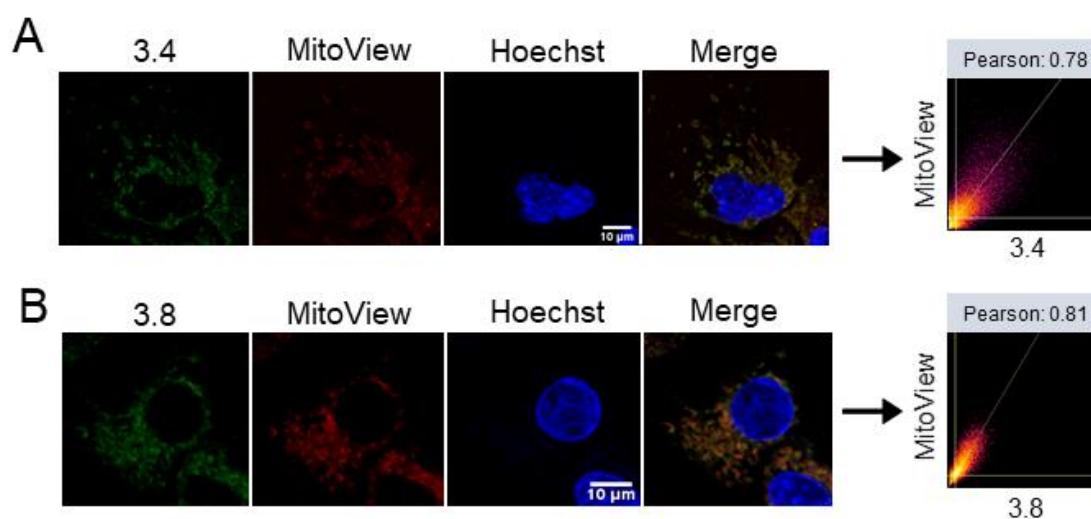
Figure 8. Assessment of fluorescence in cells co-stained with the mitochondrial dye MitoView. Nuclei were stained with Hoechst 33342 (blue), MitoView 633 (red) were added, and confocal fluorescence microscope images were obtained after 30-min-exposure to 1 µM **3.4** (A) or 5 µM **3.8** (B). Representative images and correlation between the green and the red fluorescent signal are displayed (Pearson´s coefficient).

3.2.2.3.   TREATMENT WITH CCCP

To confirm the mitochondrial localization of the probes, cells were exposed to carbonyl cyanide m-chlorophenyl hydrazone (CCCP), a lipid-soluble weak acid and a potent

mitochondrial uncoupling agent that causes acidification of the mitochondrial matrix, thus dissipating the transmembrane potential and depolarizing this organelle.[51] Incubation with CCCP, and then with pyrylium dyes, led to only residual staining of the mitochondria, both with **3.4** and with **3.8** (**Figure 9**). Considering the hydrophobic and cationic nature of the tested compounds, the observed location and the effect of CCCP, it can be concluded that pyrylium dyes **3.3, 3.4** and **3.7, 3.8** are electrostatically directed to mitochondria (likely accumulating in the mitochondrial membrane, a hydrophobic environment that enhances their emission and protect them against hydrolysis).
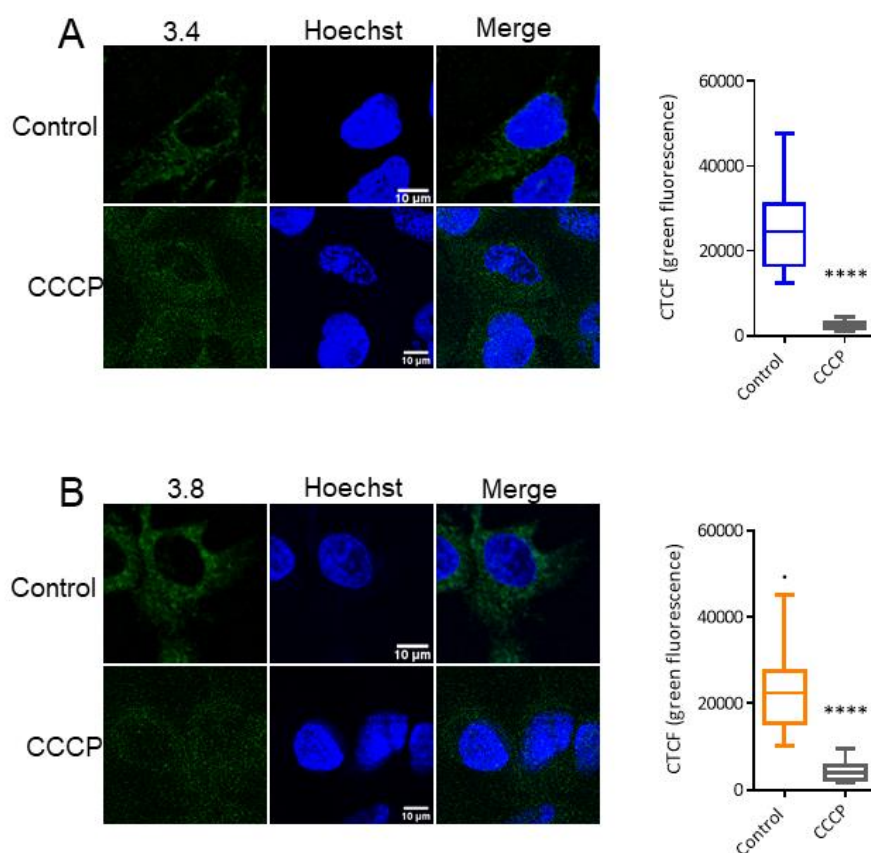
Figure 9. Assessment of fluorescence in cells treated with the mitochondrial membrane uncoupler CCCP. Cells were exposed to or not to CCCP (50 µM, 30 min). Nuclei were stained with Hoechst 33342 (blue) and confocal microscope images were obtained after 30-min-exposure to 1 µM **3.4** (A) or 5 µM **3.8** (B). Representative images and quantification of the green fluorescent signal (CTCF) are displayed. Data are shown as median±IQR, n=3. Statistical analysis was performed by unpaired t-test (**** indicates a p-value ≤ 0.0001).

3.2.2.4.   TOXICITY ASSAYS

Taking advantage of the efficient uptake by hepatocarcinoma cells of the four tested dyes, the possibility of using some of these compounds as anticancer drugs was also explored. In a classical and pioneering example, rhodamine 123 was first reported by the group of L. B. Chen as an efficient mitochondrial dye,[10] and later confirmed by the same group as a selective anticancer drug against pancreatic carcinoma line CRL 1420 and breast carcinoma line MCF-7.[52] In this case, toxicity assays were conducted to estimate at which order or magnitude molecules **3.3, 3.4** and **3.7, 3.8** showed promising activity in this regard against Hep3B cells. To assess the toxicity, acid phosphatase activity in culture was measured. Incubation of Hep3B cells with all the compounds (24 h - 0, 1, 3, 10, 30, 100, 300 µM) allowed to obtain the dose-response curves as shown in **Figure 10**. The following IC_{50} values were found: 4.2 µM (**3.8**), 5.8 µM (**3.4**), 6.5 µM (**3.7**) and 11.5 µM (**3.3**). These values are in line with the reported IC_{50} data for anticancer drugs against Hep3B cells. For instance, the IC_{50} of a series of drugs for Hep3B has been found in the micromolar range:[53] doxorubicin (4.5 µM), sorafenib (9.4 µM) and OSU-2S (2.8 µM). In another example with Hep3B cells, α-mangostin was found to have an IC_{50} of 13.1 µM, whereas two derivatives of it have higher IC_{50} values (25 µM for Man-3DG and 12.5 for Man-6DG).[54] At the present stage it is not possible to point out to the mechanism explaining the toxicity of **3.3, 3.4** and **3.7, 3.8**, but considering their cationic and lipophilic nature, it may be suggested that the accumulation of dye in the mitochondria elicits mitochondrial-dependent cell death, as occurs for similar DLCs.[52] The possibility of using pyrylium dyes as anticancer agents is well supported by the reported example of triarylpyrylium dye AA1, with an estimated IC_{50} of 6 µM against carcinoma cells CX-1[35] and even prolonging

the survival of mice on *in vivo* assays. In that case, the inhibition of ATPase activity was found as the cause of the anticancer effect. The description of theranostic activities (imaging and antiproliferative) is not uncommon, as exemplifies the set of mitochondria-targeted F16 derivatives[5] or the family of isoquinolinum dyes[55] recently described.
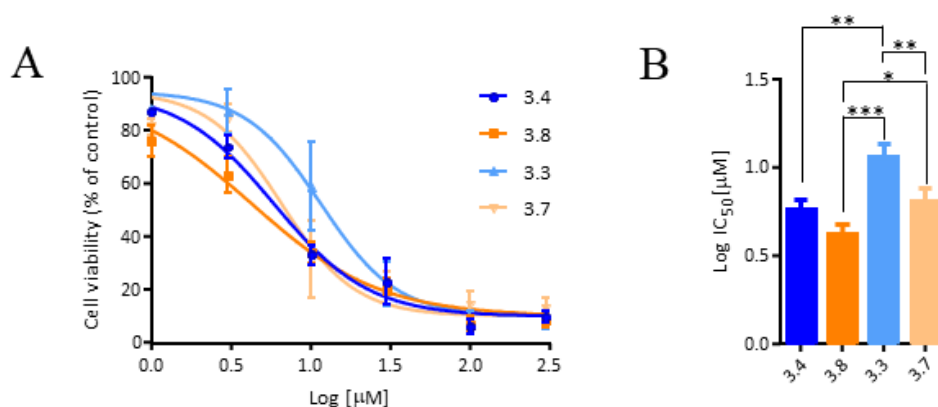
Figure 10. Assessment of cell viability after 24h-treatment with **3.3**, **3.4**, **3.7** and **3.8**. Cells were exposed to the mitochondrial probes in the concentration range (0, 1, 3, 10, 30, 100 and 300 µM). (A) Concentration-effect curves. (B) IC_{50} of each compound. Data are shown as mean±SD, n=3. Statistical analysis was performed by one-way ANOVA followed by Tukey's multiple comparisons tests (* indicates a p-value ≤ 0.05, ** indicates a p-value ≤ 0.01 and *** indicates a p-value ≤ 0.001).

3.3. CONCLUSIONS

In summary, a family of eight styrylpyrylium dyes with different architectures (4 or 6-styryl) and substituents in the peripheral aromatic rings (R = -H, -CF$_3$, -OH and -OMe) have been synthesized and characterized both chemically (^{1}H/^{13}C NMR, HRMS) and optically (UV-vis absorption and fluorescence steady-state / time-resolved spectroscopies). All the synthesized molecules have fluorescence in the yellow-orange range, and some of them display dual emission, arising from localized and delocalized excited states. The Stokes shift of six of the dyes exceeds 100 nm, reaching 193 nm in one case (**3.4**). The biological studies have been carried out with the most stable dyes in an aqueous medium (**3.3, 3.4** and **3.7, 3.8**) using a human

hepatoma cell line (Hep3B) and CLSM. It has been demonstrated that all the molecules stain the mitochondria of Hep3B cells, by means of colocalization experiments (MitoView as reference probe) and by studying depolarization of the mitochondrial membrane with CCCP. Notably, the cytotoxic concentrations of the tested probes found to be in the micromolar range (from 4.2 µM to 11.5 µM), like other know cytotoxic agents against this cancer cell line. Although the toxicity studies are preliminary, the dual activity of the presented dyes as imaging agents and potential anticancer molecules open the way to further studies with optimized styrylpyrylium analogues as theranostic agents.

3.4. EXPERIMENTAL SECTION

3.4.1. *Reagents and instruments*

All commercially available reagents and solvents were used as received. ^{1}H and ^{13}C NMR spectra were recorded at 25 °C with a 400 MHz Bruker Advance III HD spectrometer (101 MHz for ^{13}C-NMR). High-resolution mass spectra were obtained using a Waters Q-Tof Premier mass spectrometer with an electrospray source. UV-vis spectra were recorded using a 1 cm path length quartz cuvette on a Cary 60 UV-vis spectrophotometer. Steady-state emission was recorded with an Agilent Cary-Eclipse spectrofluorometer. Time-resolved fluorescence experiments were performed with an IBH5000U apparatus by using 464 nm (fwhm 1.4 ns) nanoLED as the excitation source.

3.4.2. *Synthesis of compounds 3.1-3.4*

Synthesis of 2,4-bis(4-methoxyphenyl)-6-methylpyrylium tetrafluoroborate

To a solution of *para*-methoxyacetophenone (6.5 g, 0.043 mol) in acetic anhydride (8.1 ml, 0.086 mol), BF_3 diethyl etherate (3.8 ml, 0.030 mol) was added dropwise under continuous stirring at room temperature. Then, the solution was heated to reflux at 138 °C for 2 hours. After cooling down to room temperature, the reaction mixture was poured into 200 ml of diethyl ether, and the red precipitate was recovered by filtration, washed with diethyl ether, and dried under vacuum (red solid, 3.0 g, yield 35 %).

^{1}H NMR (400 MHz, CD$_3$CN) δ 8.38 (d, *J* = 1.8 Hz, 1H), 8.29 – 8.24 (m, 2H), 8.22 – 8.17 (m, 2H), 7.93 (d, *J* = 1.8 Hz, 1H), 7.25 – 7.17 (m, 4H), 3.95 (s, 3H), 3.95 (s, 3H), 2.86 (s, 3H). ^{13}C NMR (101 MHz, CD$_3$CN) δ 175.30, 171.90, 167.20, 166.64, 164.66, 133.03, 131.73, 125.26,

122.20, 116.80, 116.54, 116.48, 113.02, 57.01, 56.94, 21.42. HRMS (ESI-TOF)$^+$ calculated for C$_{20}$H$_{19}$O$_3^+$ (M$^+$) (m/z): 307.1334; experimental (M$^+$) (m/z): 307.1334.

Synthesis of styrylpyrylium dyes **3.1-3.4**

To a suspension of 2,4-bis(4-methoxyphenyl)-6-methylpyrylium tetrafluoroborate (0.25 g, 0.64 mmol) in acetic acid (10 ml), the corresponding *para*-substituted aldehyde (5 or 10 equivalents), was added at room temperature. Then, the mixture was heated to reflux at 138 °C (a dark solution was formed) for 24 hours. After cooling down to room temperature, the crude reaction mixture was poured into 150 ml of diethyl ether, and the formed precipitate was recovered by filtration, washed with diethyl ether, and dried under vacuum before use.

3.1. *(E)-2,4-bis(4-methoxyphenyl)-6-styrylpyrylium tetrafluoroborate* (red solid, 0.23 g, yield 75 %). ^{1}H NMR (400 MHz, CD$_3$CN) δ 8.28 – 8.23 (m, 2H), 8.20 (d, *J* = 1.8 Hz, 1H), 8.16 – 8.10 (m, 2H), 7.99 (d, *J* = 16.2 Hz, 1H), 7.95 (d, *J* = 1.7 Hz, 1H), 7.81 – 7.70 (m, 2H), 7.55 – 7.45 (m, 3H), 7.30 (d, *J* = 16.2 Hz, 1H), 7.18 – 7.12 (m, 4H), 3.92 (s, 3H), 3.92 (s, 3H). ^{13}C NMR (101 MHz, CD$_3$CN) δ 169.76, 168.32, 166.97, 166.48, 163.18, 144.94, 135.29, 132.80, 132.69, 131.76, 130.30, 129.86, 125.24, 122.05, 118.82, 116.64, 116.42, 115.32, 112.21, 56.89, 56.81. HRMS (ESI-TOF)$^+$ calculated for C$_{27}$H$_{23}$O$_3^+$ (M$^+$) (m/z): 395.1647; experimental (M$^+$) (m/z): 395.1645.

3.2. *(E)-2,4-bis(4-methoxyphenyl)-6-(4-(trifluoromethyl)styryl)pyrylium tetrafluoroborate* (orange solid, 0.29 g, yield 84 %). ^{1}H NMR (400 MHz, CD$_3$CN) δ 8.41 – 8.34 (m, 3H), 8.26 – 8.20 (m, 2H), 8.14 (d, *J* = 16.3 Hz, 1H), 8.10 (d, *J* = 1.7 Hz, 1H), 7.98 (d, *J* = 8.4 Hz, 2H), 7.84 (d, *J* = 8.3 Hz, 2H), 7.49 (d, *J* = 16.3 Hz, 1H), 7.28 – 7.21 (m, 4H), 3.98 (s, 3H), 3.97 (s, 3H). ^{13}C NMR (101 MHz, CD$_3$CN) δ 170.26, 167.24, 166.81, 166.39, 163.53, 142.11, 132.49,

131.72, 129.76, 126.75, 125.08, 121.86, 121.21, 116.41, 116.15, 115.85, 112.97, 56.61, 56.56. HRMS (ESI-TOF)$^+$ calculated for $C_{28}H_{22}F_3O_3^+$ (M$^+$) (m/z): 463.1521; experimental (M$^+$) (m/z): 463.1514.

3.3. *(E)-2-(4-hydroxystyryl)-4,6-bis(4-methoxyphenyl)pyrylium tetrafluoroborate* (dark brown solid, 0.27 g, yield 87 %). ^{1}H NMR (400 MHz, CD$_3$CN) δ 8.33 – 8.29 (m, 2H), 8.23 (d, *J* = 1.7 Hz, 1H), 8.21 – 8.14 (m, 2H), 8.09 (d, *J* = 16.1 Hz, 1H), 7.96 (d, *J* = 1.6 Hz, 1H), 7.73 (d, *J* = 8.7 Hz, 2H), 7.25 – 7.18 (m, 5H), 6.97 (d, *J* = 8.7 Hz, 2H), 3.96 (s, 3H), 3.96 (s, 3H). ^{13}C NMR (101 MHz, CD$_3$CN) δ 169.23, 168.97, 166.29, 165.84, 162.55, 161.64, 145.49, 132.11, 132.06, 131.17, 127.15, 125.34, 122.10, 117.01, 116.23, 115.99, 115.38, 114.66, 111.57, 56.50, 56.45. HRMS (ESI-TOF)$^+$ calculated for $C_{27}H_{23}O_4^+$ (M$^+$) (m/z): 411.1596; experimental (M$^+$) (m/z): 411.1594.

3.4. *(E)-2,4-bis(4-methoxyphenyl)-6-(4-methoxystyryl)pyrylium tetrafluoroborate* (brown solid, 0.24 g, yield 74 %). ^{1}H NMR (400 MHz, DMSO-d$_6$) δ 8.67 (d, *J* = 1.5 Hz, 1H), 8.54 – 8.46 (m, 2H), 8.45 – 8.37 (m, 3H), 8.22 (d, *J* = 16.2 Hz, 1H), 7.85 (d, *J* = 8.8 Hz, 2H), 7.44 (d, *J* = 16.2 Hz, 1H), 7.29 – 7.21 (m, 4H), 7.12 (d, *J* = 8.9 Hz, 2H), 3.95 (s, 3H), 3.94 (s, 3H), 3.87 (s, 3H). ^{13}C NMR (101 MHz, DMSO-d$_6$) δ 168.27, 167.72, 165.10, 164.50, 162.44, 161.00, 143.93, 131.88, 131.14, 130.80, 127.23, 124.55, 121.54, 116.05, 115.51, 115.25, 115.00, 113.70, 56.11, 56.01, 55.63. HRMS (ESI-TOF)$^+$ calculated for $C_{28}H_{25}O_4^+$ (M$^+$) (m/z): 425.1753; experimental (M$^+$) (m/z): 425.1747.

3.4.3.   Synthesis of compounds 3.5-3.8

Synthesis of 2,6-bis(4-methoxyphenyl)-4-methylpyrylium tetrafluoroborate

2,6-bis(4-methoxyphenyl)pyrylium hydrogen sulfate (orange solid, 2.4 g, yield 28 %). To a solution of *para*-methoxyacetophenone (6.5 g, 0.043 mol) in triethyl orthoformate (14.4 ml, 0.086 mol), H_2SO_4 (1.2 ml, 0.020 mol) was added dropwise under continuous stirring at room temperature. Then, the solution was heated to reflux at 100 °C for 2 hours. After cooling down to room temperature, the reaction mixture was poured into 200 ml of ethyl acetate, and the orange precipitate was recovered by filtration, washed with ethyl acetate, and dried under vacuum.

^{1}H NMR (400 MHz, CD_3CN) δ 8.68 (t, *J* = 8.4 Hz, 1H), 8.34 – 8.27 (m, 4H), 8.21 (d, *J* = 8.4 Hz, 2H), 7.32 – 7.23 (m, 4H), 4.01 (s, 6H). ^{13}C NMR (101 MHz, CD_3CN) δ 171.85, 166.95, 155.61, 132.04, 121.85, 117.55, 116.76, 56.96. HRMS (ESI-TOF)$^+$ calculated for $C_{19}H_{17}O_3^+$ (M$^+$) (m/z): 293.1178; experimental (M$^+$) (m/z): 293.1171.

2,6-bis(4-methoxyphenyl)-4-methyl-4H-pyran (brown oil, 1.65 g, quantitative). To a suspension of *2,6-bis(4-methoxyphenyl)pyrylium hydrogen sulfate* (2.1 g, 5.4 mmol) in anhydrous diethyl ether (50 ml), 3 M solution of CH_3MgI in diethyl ether (26.9 ml, 80.7 mmol) was added dropwise under nitrogen atmosphere. Then, the mixture was allowed to react overnight under continuous stirring at room temperature. After that, the crude reaction mixture was poured into 20 ml of distilled water and extracted 3 x 40 ml with NH_4Cl (ss) and 3 x 40 ml with water. The organic phase was dried over Na_2SO_4 and the solvent was evaporated under vacuum, to give a dark sticky residue, used without purification.

^{1}H NMR (400 MHz, CD$_3$CN) δ 7.65 – 7.60 (m, 4H), 6.97 – 6.93 (m, 4H), 5.36 (d, J = 3.7 Hz, 2H), 3.81 (s, 6H), 3.22 – 3.13 (m, 1H), 1.21 (d, J = 6.8 Hz, 3H). ^{13}C NMR (101 MHz, CD$_3$CN) δ 160.83, 148.48, 129.06, 128.09, 126.64, 119.21, 118.26, 114.93, 114.72, 101.93, 55.96, 27.53, 25.20.

2,6-bis(4-methoxyphenyl)-4-methylpyrylium tetrafluoroborate (light brown solid, 0.95 g, yield 45 %). To a solution of *2,6-bis(4-methoxyphenyl)-4-methyl-4H-pyran* (1.65 g, 5.4 mmol) in anhydrous acetonitrile (50 ml), Ph$_3$CBF$_4$ (1.95 g, 5.9 mmol) was added under nitrogen atmosphere. Then, the mixture was allowed to react for 3 hours under continuous stirring at room temperature. After that, the solvent was evaporated under vacuum and the residue was dissolved in the minimum volume of acetone and poured into 200 ml of ethyl acetate. The brown precipitate was recovered by filtration, washed with ethyl acetate, and dried under vacuum.

^{1}H NMR (400 MHz, CD$_3$CN) δ 8.26 – 8.21 (m, 4H), 8.09 (d, J = 0.5 Hz, 2H), 7.26 – 7.21 (m, 4H), 3.96 (s, 6H), 2.72 (s, 3H). ^{13}C NMR (101 MHz, CD$_3$CN) δ 171.91, 170.03, 166.55, 131.68, 121.75, 118.36, 116.64, 56.88, 23.78. HRMS (ESI-TOF)$^+$ calculated for C$_{20}$H$_{19}$O$_3^+$ (M$^+$) (m/z): 307.1334; experimental (M$^+$) (m/z): 307.1332.

Synthesis of styrylpyrylium dyes **3.5-3.8**

To a suspension of *2,6-bis(4-methoxyphenyl)-4-methylpyrylium tetrafluoroborate* (0.25 g, 0.64 mmol) in acetic acid (10 ml), the correspondent *para*-substituted aldehyde (5 or 10 equivalents), was added at room temperature. Then, the mixture was heated to reflux at 138 °C (a dark solution was formed) for 24 hours. After cooling down to room temperature, the reaction mixture was poured into 150 ml of diethyl ether, and the formed precipitate was recovered by filtration, washed with diethyl ether, and dried under vacuum before use.

3.5. *(E)-2,6-bis(4-methoxyphenyl)-4-styrylpyrylium tetrafluoroborate* (brown solid, 0.19 g, yield 63 %). ^{1}H NMR (400 MHz, CD$_3$CN) δ 8.26 – 8.17 (m, 5H), 8.15 (s, 2H), 7.84 – 7.74 (m, 2H), 7.59 – 7.49 (m, 3H), 7.38 (d, *J* = 16.2 Hz, 1H), 7.24 – 7.16 (m, 4H), 3.94 (s, 6H). ^{13}C NMR (101 MHz, CD$_3$CN) δ 169.54, 166.32, 162.63, 148.26, 135.68, 133.24, 131.36, 130.45, 130.21, 124.01, 122.20, 116.56, 113.17, 56.83. HRMS (ESI-TOF)$^+$ calculated for C$_{27}$H$_{23}$O$_3^+$ (M$^+$) (m/z): 395.1647; experimental (M$^+$) (m/z): 395.1645.

3.6. *(E)-2,6-bis(4-methoxyphenyl)-4-(4-(trifluoromethyl)styryl)pyrylium tetrafluoroborate* (brown solid, 0.30 g, yield 86%). ^{1}H NMR (300 MHz, CD$_3$CN) δ 8.31 – 8.15 (m, 7H), 7.93 (d, *J* = 8.3 Hz, 2H), 7.82 (d, *J* = 8.3 Hz, 2H), 7.48 (d, *J* = 16.3 Hz, 1H), 7.26 – 7.18 (m, 4H), 3.95 (s, 6H). ^{13}C NMR (75 MHz, CD$_3$CN) δ 169.79, 166.11, 145.09, 131.16, 129.98, 126.85, 126.79, 121.82, 116.24, 113.39, 56.50. HRMS (ESI-TOF)$^+$ calculated for C$_{28}$H$_{22}$F$_3$O$_3^+$ (M$^+$) (m/z): 463.1521; experimental (M$^+$) (m/z): 463.1515.

3.7. *(E)-4-(4-hydroxystyryl)-2,6-bis(4-methoxyphenyl)pyrylium tetrafluoroborate* (brown solid, 0.22 g, yield 71 %). ^{1}H NMR (400 MHz, DMSO-d$_6$) δ 10.68 (s, 1H), 8.50 – 8.41 (m, 3H), 8.30 – 8.23 (m, 4H), 7.68 (d, *J* = 8.8 Hz, 2H), 7.27 (d, *J* = 16.1 Hz, 1H), 7.26 – 7.20 (m, 4H), 6.96 (d, *J* = 8.7 Hz, 2H), 3.92 (s, 6H). ^{13}C NMR (101 MHz, DMSO-d$_6$) δ 166.90, 164.27, 162.25, 161.54, 148.43, 132.03, 130.14, 126.22, 121.61, 120.11, 116.76, 115.44, 111.56, 56.00. HRMS (ESI-TOF)$^+$ calculated for C$_{27}$H$_{23}$O$_4^+$ (M$^+$) (m/z): 411.1596; experimental (M$^+$) (m/z): 411.1599.

3.8. *(E)-2,6-bis(4-methoxyphenyl)-4-(4-methoxystyryl)pyrylium tetrafluoroborate* (dark red solid, 0.19 g, yield 58 %). ^{1}H NMR (400 MHz, CD$_3$CN) δ 8.24 – 8.16 (m, 5H), 8.06 (s, 2H), 7.79 – 7.72 (m, 2H), 7.26 – 7.17 (m, 5H), 7.10 – 7.03 (m, 2H), 3.95 (s, 6H), 3.89 (s, 3H). ^{13}C

NMR (101 MHz, CD$_3$CN) δ 168.67, 165.90, 164.46, 162.57, 148.71, 132.56, 130.96, 128.35, 122.22, 121.29, 116.30, 115.94, 112.31, 56.63, 56.33. HRMS (ESI-TOF)$^+$ calculated for C$_{28}$H$_{25}$O$_4^+$ (M$^+$) (m/z): 425.1753; experimental (M$^+$) (m/z): 425.1747.

3.4.4. Photophysical characterisation of the compounds

1 mM stock solutions of compounds **3.1-3.8** were prepared in acetonitrile (in dimethyl sulfoxide for compound **3.4**). For UV-vis spectra measurements, the corresponding stock solution for each compound was diluted to reach a final concentration of 10 µM, in dichloromethane (DCM), acetonitrile (ACN) and phosphate-buffered saline (PBS, 10 mM, pH 7.4). For fluorescence spectra acquisition, concentration was adjusted to reach a value of 0.1 in absorbance, in order to minimize the primary inner filter effect. λ$_{exc}$ was set at the absorption maximum of each compound.

Fluorescence Quantum Yield Measurements (ϕ$_F$). The fluorescence quantum yields of all compounds were determined in DCM, ACN, and PBS (10 mM, pH 7.4), under an N$_2$ atmosphere. *(E)-2-(4-methoxystyryl)-4,6-diphenylpyrylium tetrafluoroborate* was used as a reference since its fluorescence quantum yield was described in DCM (ϕ$_F$ = 0.38).[38,39]

The concentration of the reference and the studied compounds were adjusted to obtain the same absorption at the excitation wavelength. Fluorescence quantum yields were calculated by using [Equation (1)]:

$$\phi_F = \phi_R \cdot (A_R \cdot F_S / A_S \cdot F_R) \cdot (n_S^2 / n_R^2) \qquad (1)$$

where ϕ$_F$ is the fluorescence quantum yield, F is the integral of the emission spectrum, A is the absorption intensity, and n is the refractive index. The sub-index R refers to the reference compound and S to the studied pyrylium salt.

Fluorescence Lifetime Measurements (τ_F). The fluorescence lifetimes of all compounds were determined in DCM, ACN, and PBS (10 mM, pH 7.4) under an N_2 atmosphere. Solutions were prepared similarly to those used to obtain the emission spectra. Fluorescence lifetimes were determined by using the technique of time-correlated single-photon counting (TCSPC). Data obtained from the experiments were adjusted to a single or double exponential model by using the software IBH DAS6.

3.4.5. Cell culture and treatments

Hep3B (ATCC HB-8064), a human hepatoblastoma cell line was employed to test the fluorescent dyes in an *in vitro* setting. Cell cultures were maintained in MEM supplemented with 10 % inactivated fetal bovine serum, 2 mM L-glutamine, non-essential amino acids, and 1 mM sodium pyruvate at 37^0C, in a cell culture incubator (MCO-19AICUV-PE, Panasonic Healthcare Co. Ltd., Tokyo, Japan) with a humidified 5 % CO_2/95 % air atmosphere (AirLiquide Medical, Valencia, Spain). Cell cultures were maintained in the presence of penicillin (50 units/mL) and streptomycin (50 µg/mL) and used for experiments at a passage number lower than 25. Reagents employed in cell culture were purchased from ThermoFisher Scientific (Walthman, MA, USA).

3.4.6. Cell viability assay

Cell viability was assessed by means of acid phosphatase assay, based on the conversion of *p*-NPP to *para*-nitrophenol by cytosolic acid phosphatase.[56] Cells were seeded in a 96-well-plate (15×10^4 cells/well) and treated with increasing concentrations of the mitochondrial fluorescent dyes (1, 3, 10, 30, 100 and 300 µM) in complete cell culture medium. After 24 h, the medium was removed and each well was washed once with 100 µl PBS, 100 µl of assay

buffer (0.1 M sodium acetate at pH 5.0, 0.1% Triton X-100), and 7.25 mM p-NNP was then added. Plates were incubated at 37°C for 2 h. The reaction was stopped with the addition of 50 µl of 1 M NaOH and color development was evaluated at 405 nm using a Multiskan® EX plate reader (ThermoFisher Scientific). The non-enzymatic hydrolysis of the pNPP substrate was determined by including wells that contained the assay solution without cells.

3.4.7. Live cell imaging

Cells were seeded (15×10^4/well) in a sterile µ-Slide 8-well-chamber slide (Ibidi, Inycom, Madrid, Spain) and let to adhere overnight. The next day, cells were incubated with 0.5, 1 or 5 µM of the mitochondrial fluorescent dyes in Krebs-HEPES buffer (140 mM NaCl, 5.9 mM KCl, 1.2 mM MgCl$_2$, 15 mM HEPES) supplemented with 2.5 mM CaCl$_2$, and 5 mM D-glucose. 100 nM Hoechst 33342 (Merck KGaA, Darmstadt, Germany) was added to stain nuclei. In some experiments, 100 nM MitoView™ 633 (Biotyum, Hayward, CA, USA) was also added - a far-red fluorescent mitochondrial dye with absorbance/emission at 622/648 nm. For treatment with CCCP (carbonyl cyanide m-chlorophenyl hydrazone), a protonophore that uncouples the proton gradient established by the electron transport chain,[57] cells were treated with 50 µM of this compound for 30 minutes before staining with the mitochondrial probes. The plate was then transferred to a heated stage above a 40x magnification with HCxPL APO CS2 40.0 x 1.30 oil UV objective on an inverted confocal laser-scanning microscope (Leica DMI8-CS) equipped with a white light laser and a diode laser. Measurements were carried out using excitation at 488 nm with a pixel dwell time of 1.5 µs; two to three FOV (field of view) were recorded for each condition/probe. The detection range was set to 500-625 nm for the mitochondrial dyes, with pinholes set to 1 Airy unit.

3.4.8. Image processing and analysis

Images were processed with ImageJ2 (National Institutes of Health, Bethesda, MD, USA); a subtract background function was employed with a sliding paraboloid function of 50 pixels followed by a median filtering function used with a radius of 1 pixel. Single cells were selected with the ROI manager using the polygon selection and the area of selected cells, the mean fluorescence and the integrated density measured. Corrected total cell fluorescence (CTCF) was calculated by subtracting the integrated density to the product of the area and mean fluorescence of the background. For colocalization, colocalization threshold plugin in ImageJ2 was employed. Data were then represented using Graphpad Prism.

3.5. SPECTROSCOPIC DATA OF COMPOUNDS

2,4-bis(4-methoxyphenyl)-6-methylpyrylium tetrafluoroborate
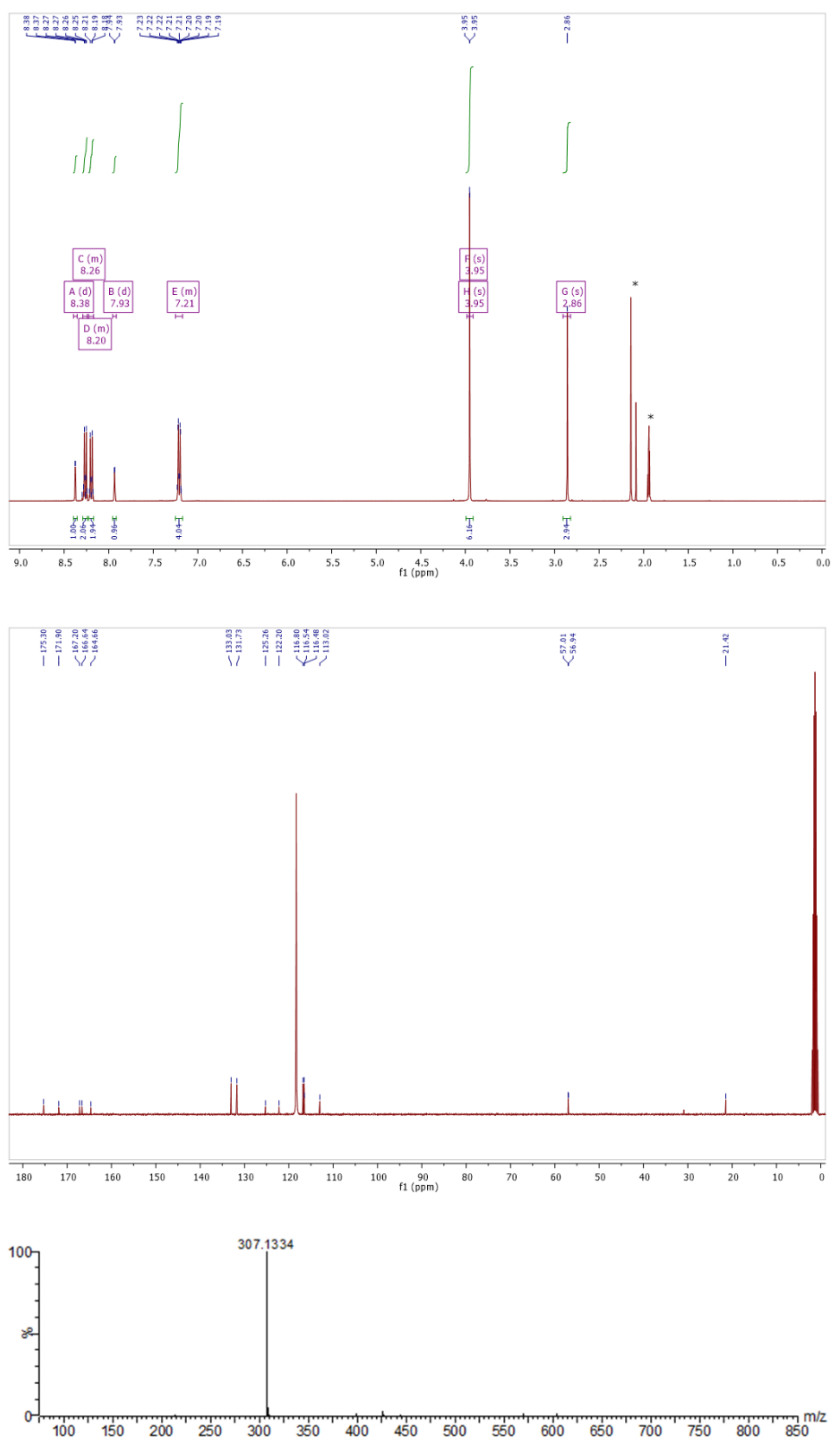
Figure 11. ^{1}H NMR, ^{13}C NMR (CD$_3$CN) and HRMS spectra of the precursor *2,4-bis(4-methoxyphenyl)-6-methylpyrylium tetrafluoroborate*.

Compound 3.1
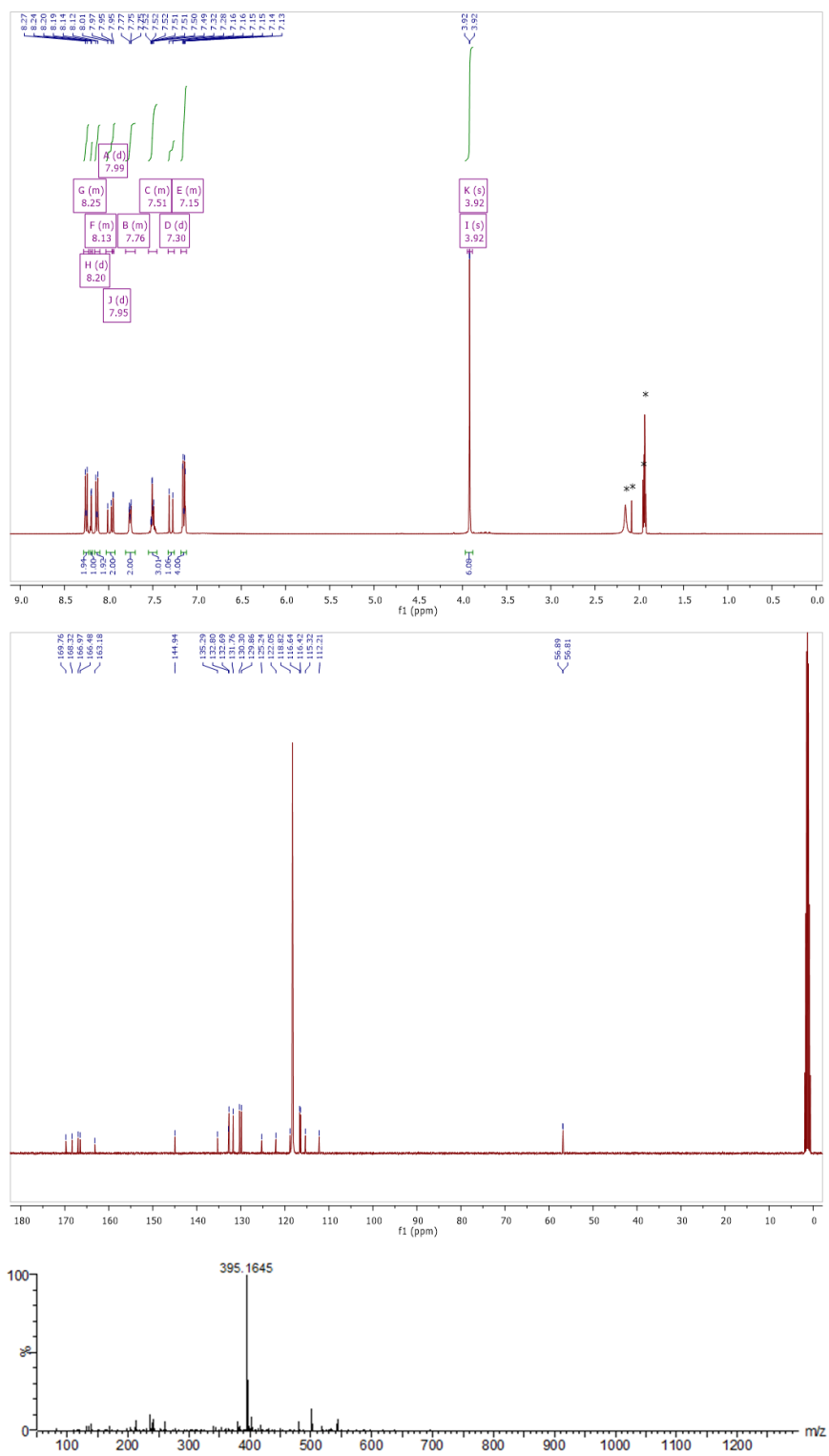
Figure 12. ^{1}H NMR, ^{13}C NMR (CD$_3$CN) and HRMS spectra of compound **3.1**.

Compound 3.2
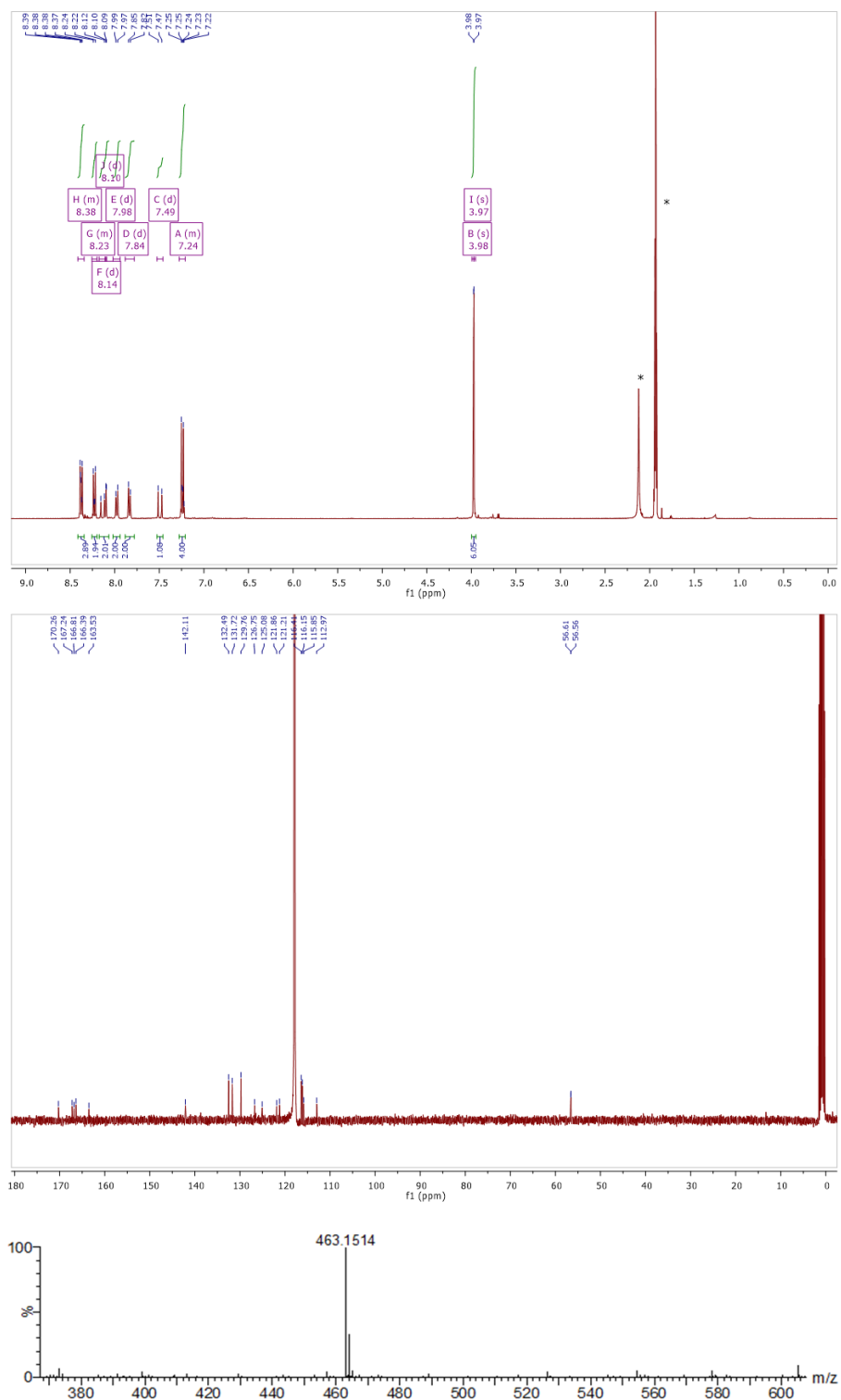
Figure 13. ^{1}H NMR, ^{13}C NMR (CD$_3$CN) and HRMS spectra of compound **3.2**.

Compound 3.3
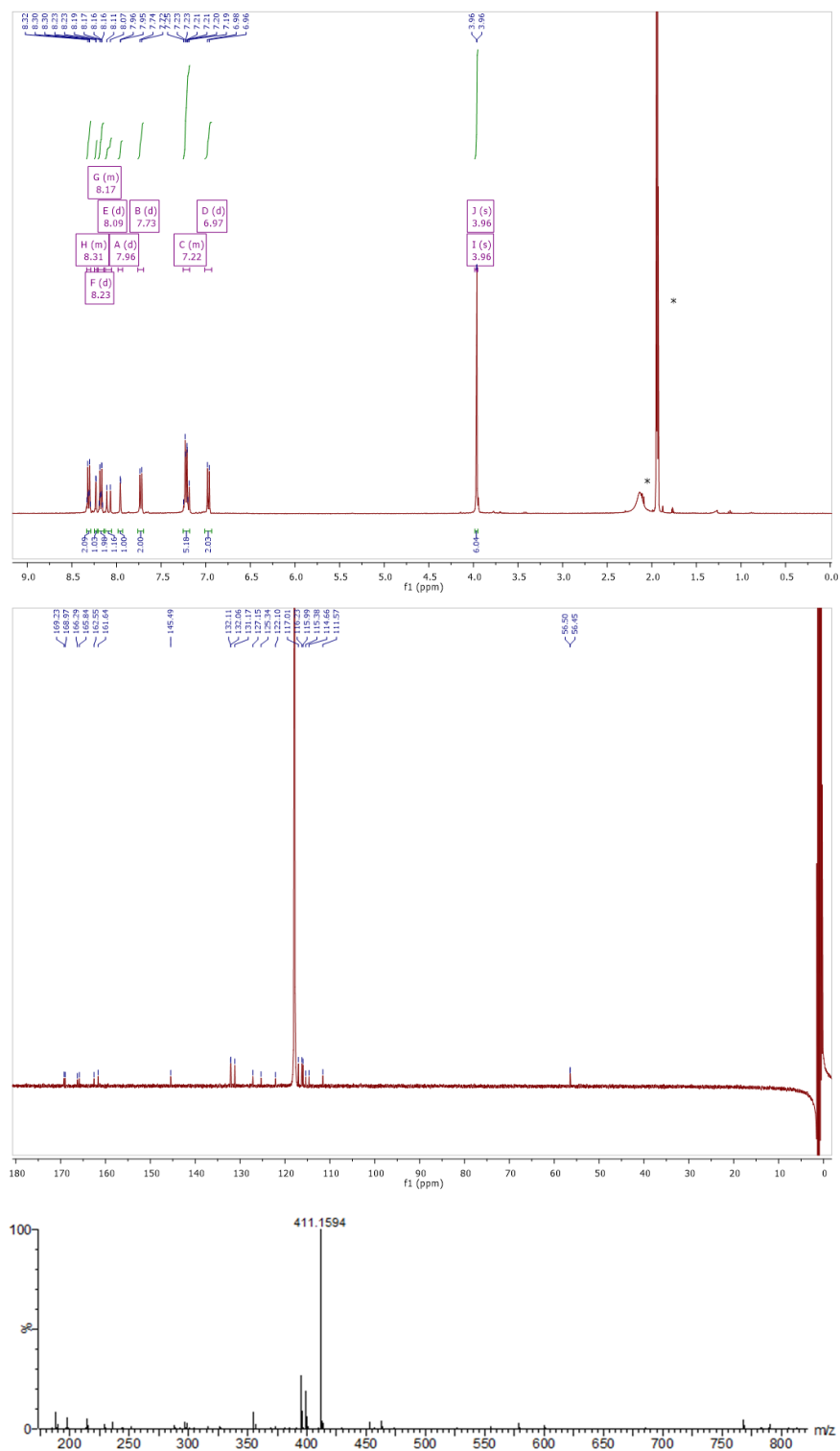
Figure 14. ^{1}H NMR, ^{13}C NMR (CD$_3$CN) and HRMS spectra of compound **3.3**.

Compound 3.4
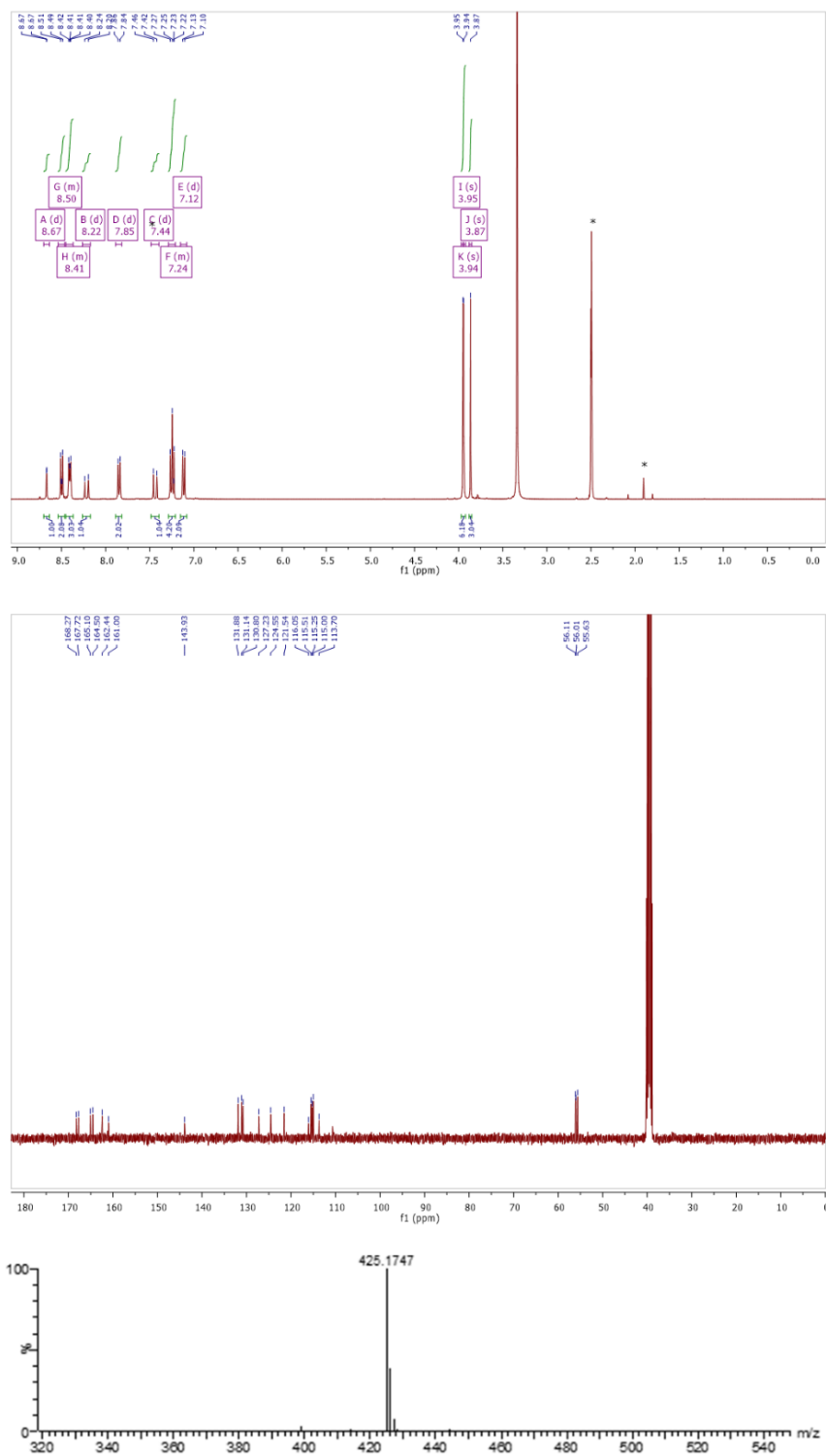
Figure 15. ^{1}H NMR, ^{13}C NMR (DMSO-d$_6$) and HRMS spectra of compound **3.4**.

2,6-bis(4-methoxyphenyl) hydrogen sulfate
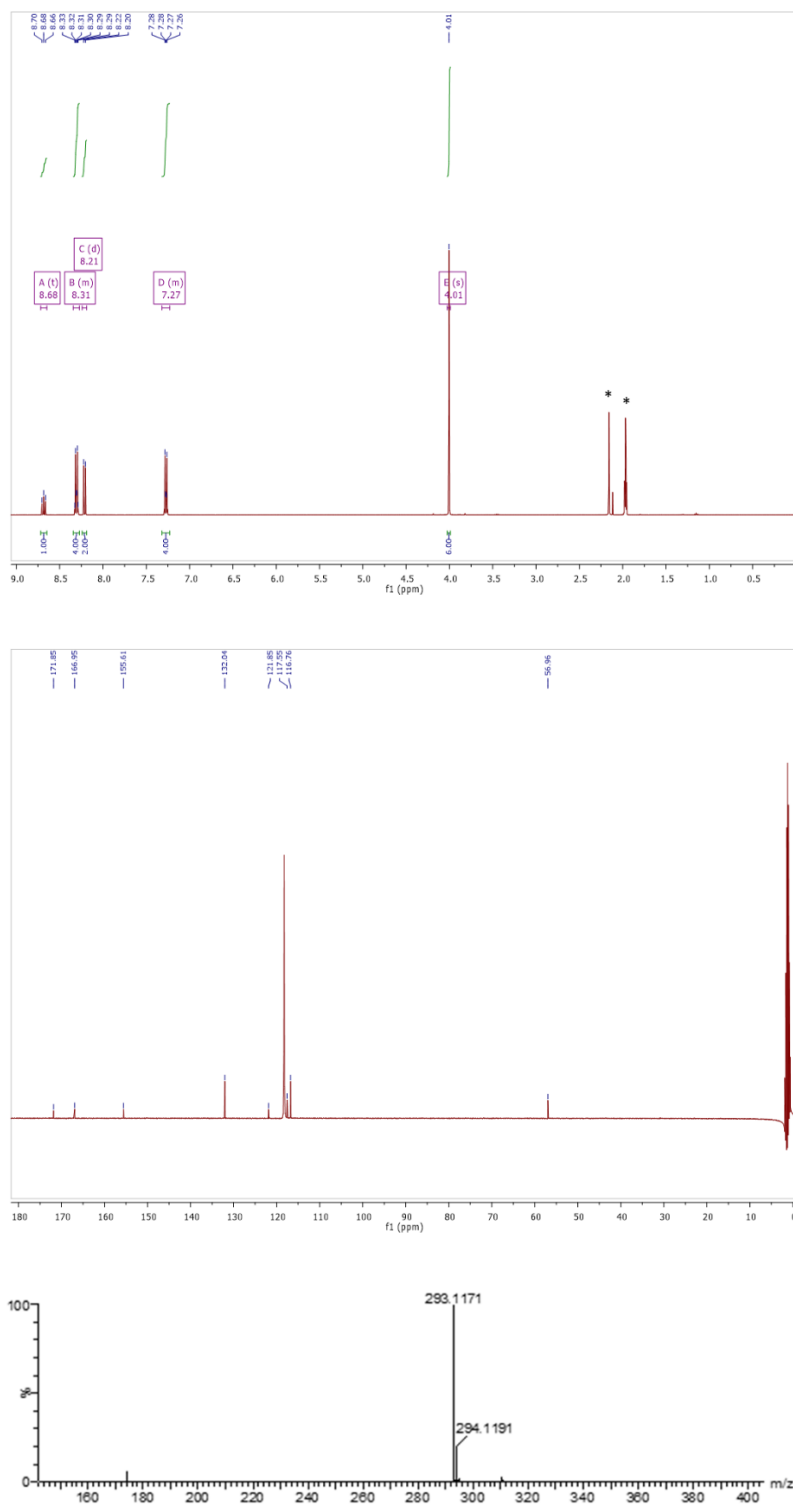
Figure 16. ^{1}H NMR, ^{13}C NMR (CD$_3$CN) and HRMS spectra of the precursor *2,6-bis(4-methoxyphenyl) hydrogen sulfate*.

2,6-bis(4-methoxyphenyl)-4-methyl-4H-pyran
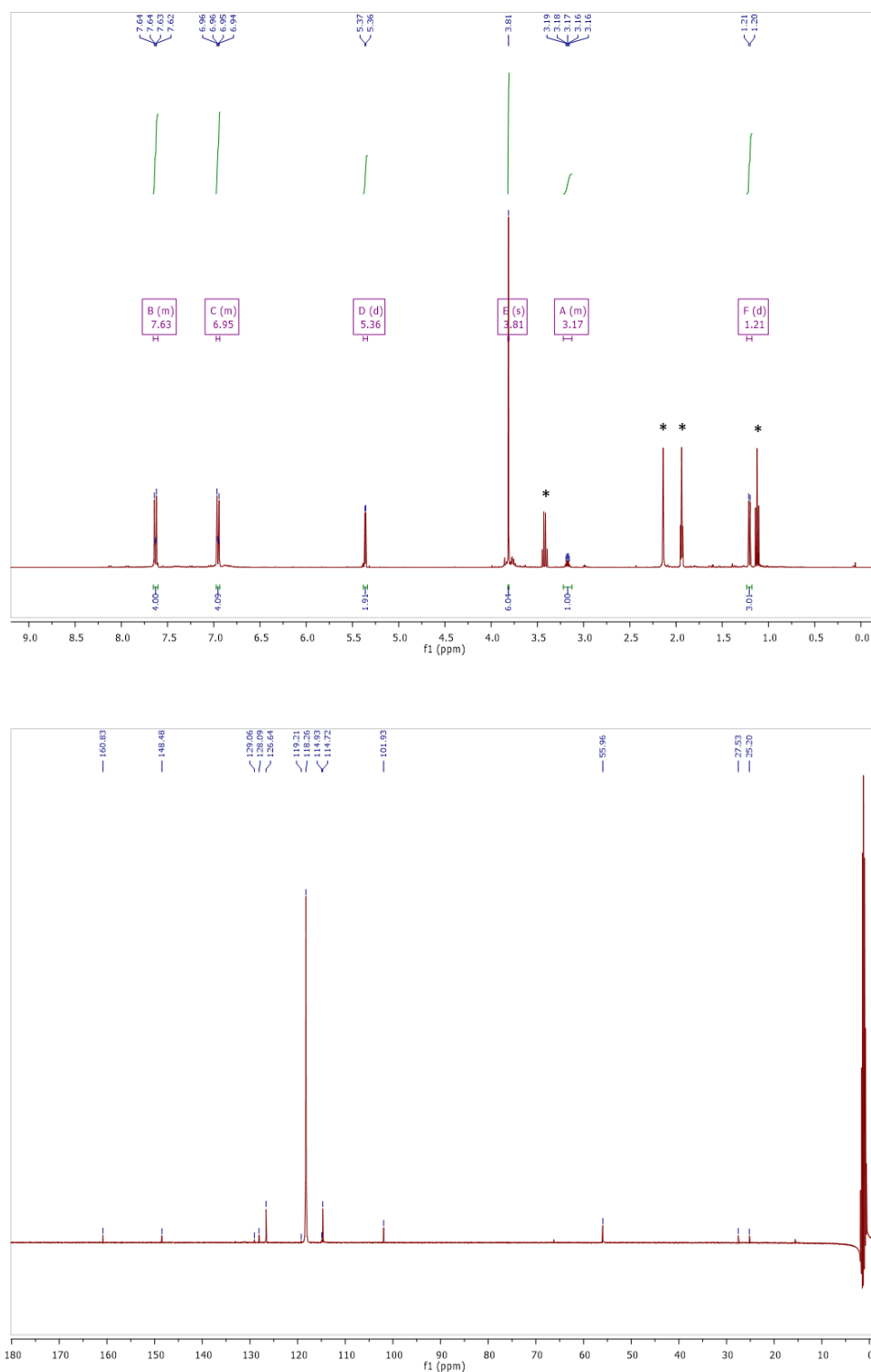
Figure 17. ^{1}H NMR and[13]C NMR (CD$_3$CN) spectra of the precursor *2,6-bis(4-methoxyphenyl)-4-methyl-4H-pyran*.

2,6-bis(4-methoxyphenyl)-4-methylpyrylium tetrafluoroborate
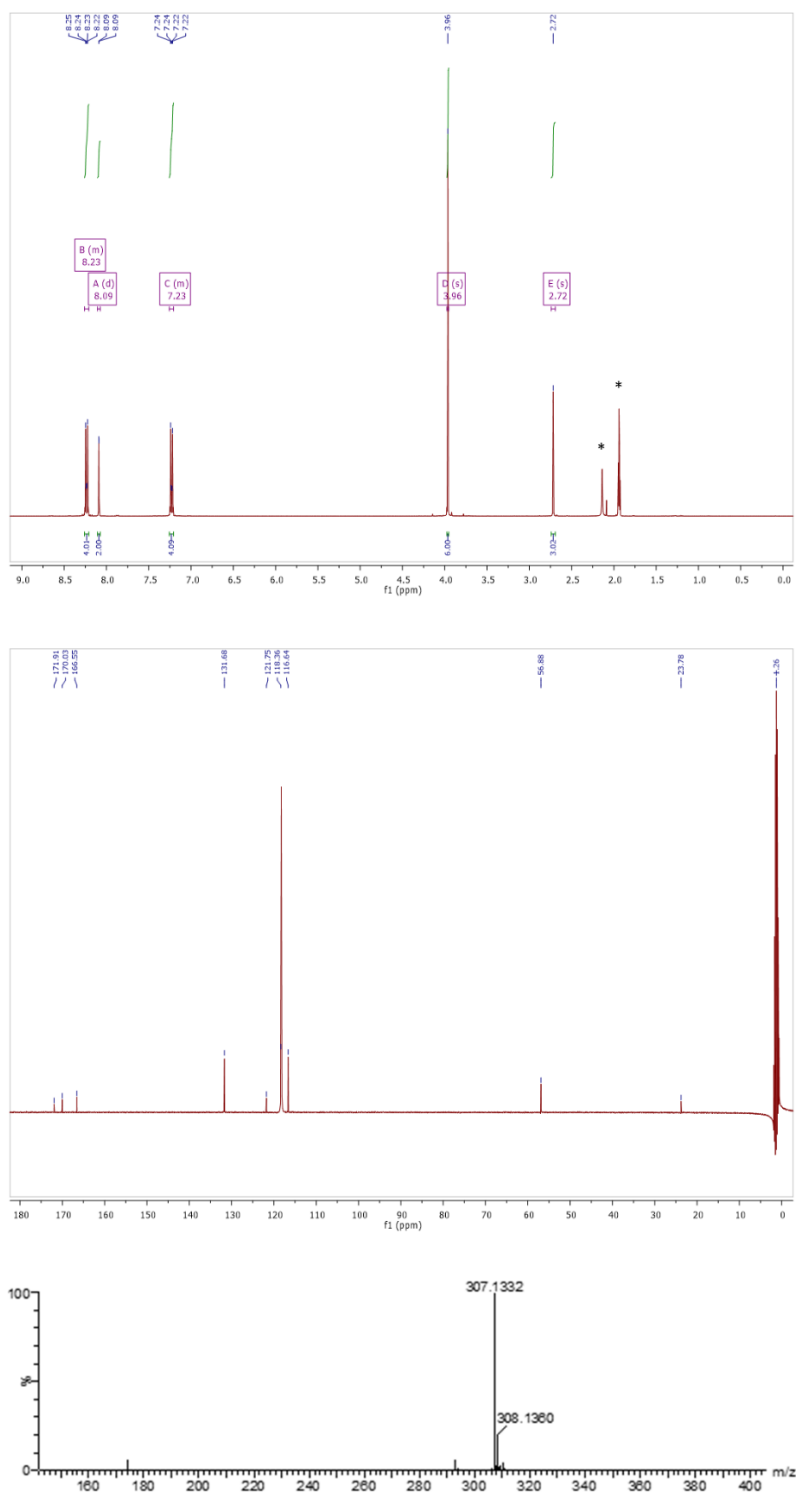
Figure 18. ^{1}H NMR, ^{13}C NMR (CD$_3$CN) and HRMS spectra of the precursor *2,6-bis(4-methoxyphenyl)-4-methylpyrylium tetrafluoroborate*.

Compound 3.5
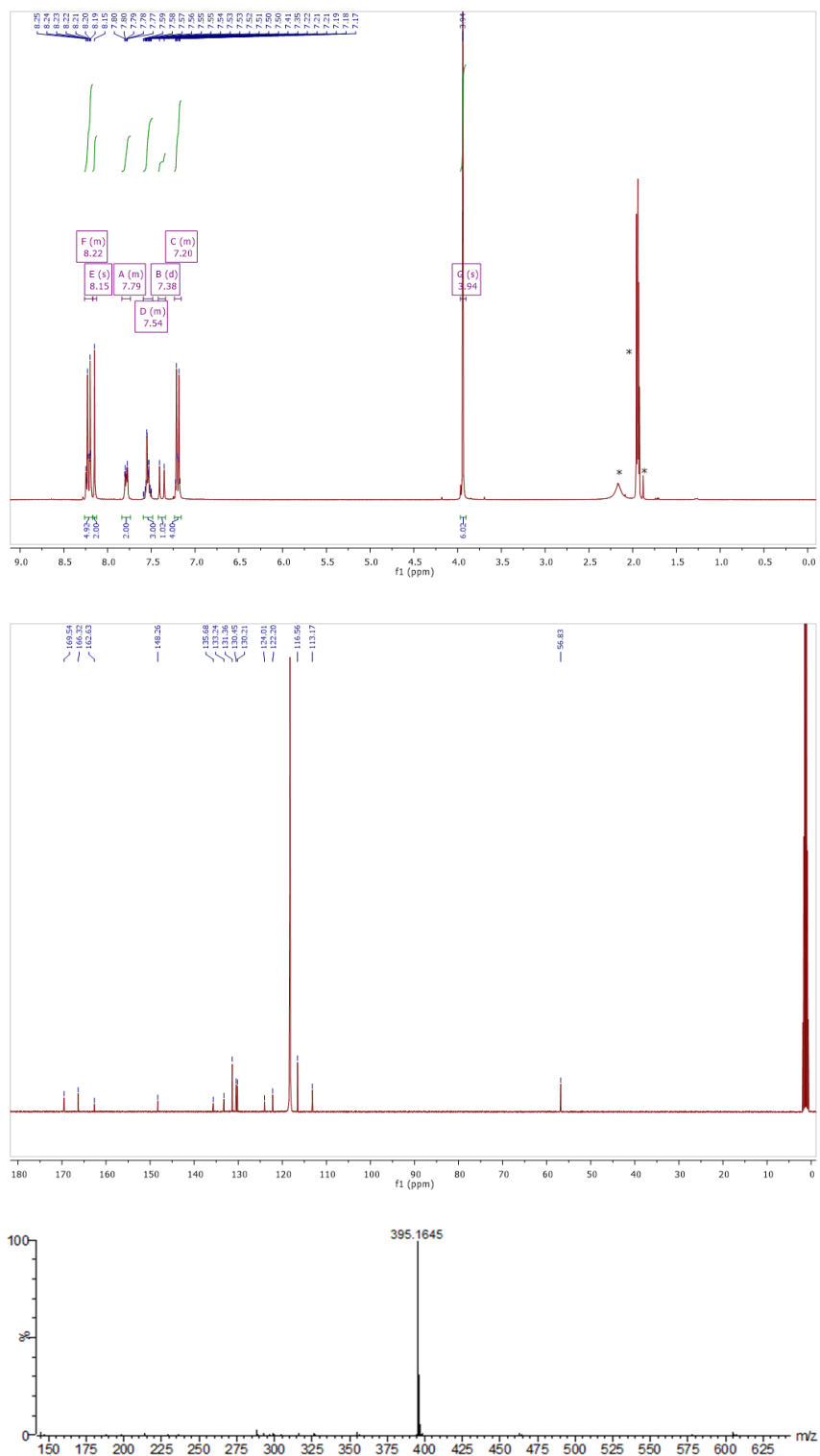
Figure 19. ^{1}H NMR, ^{13}C NMR (CD$_3$CN) and HRMS spectra of compound **3.5**.

Compound 3.6
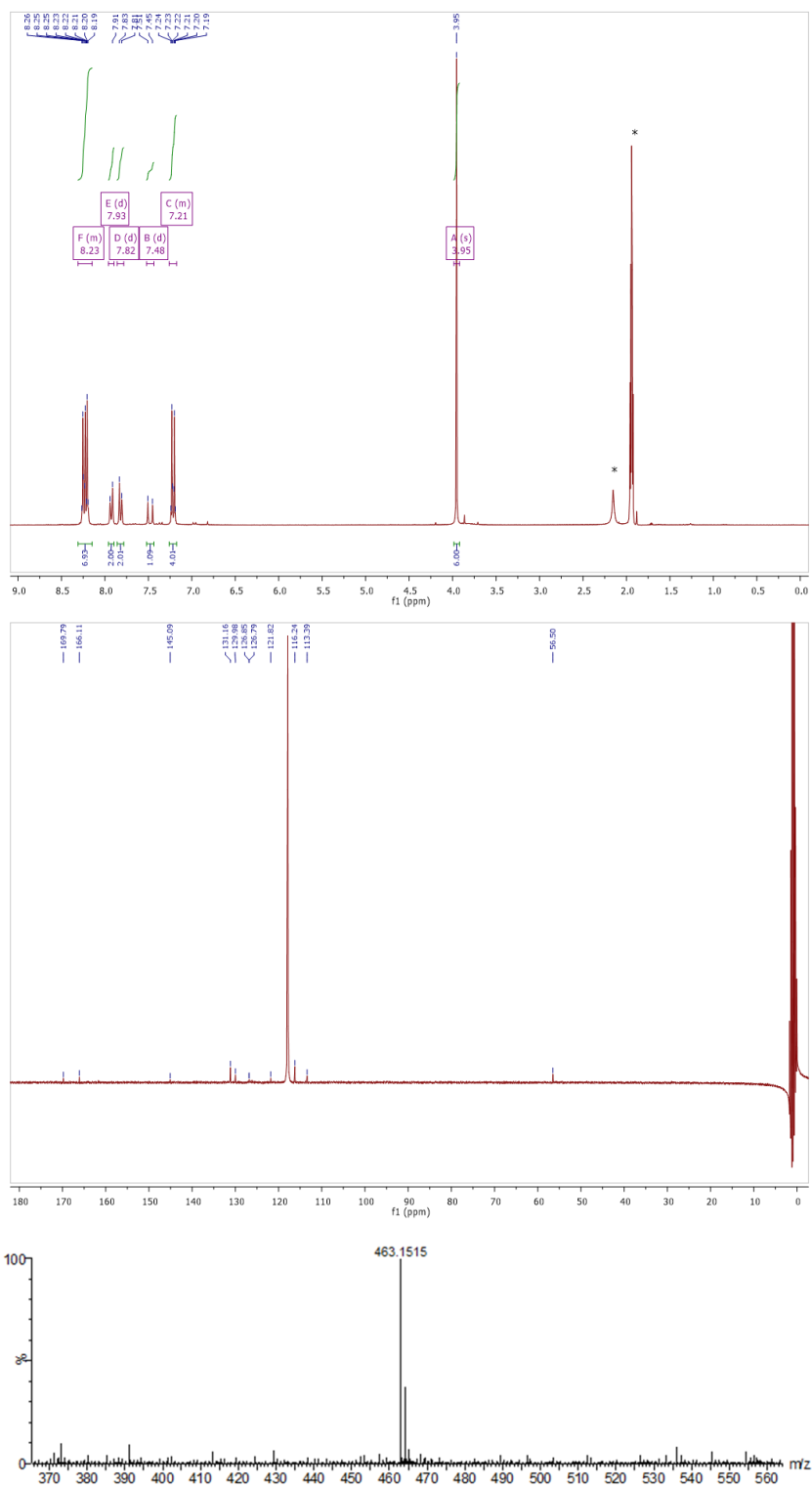
Figure 20. ^{1}H NMR, ^{13}C NMR (CD$_3$CN) and HRMS spectra of compound **3.6**.

Compound 3.7
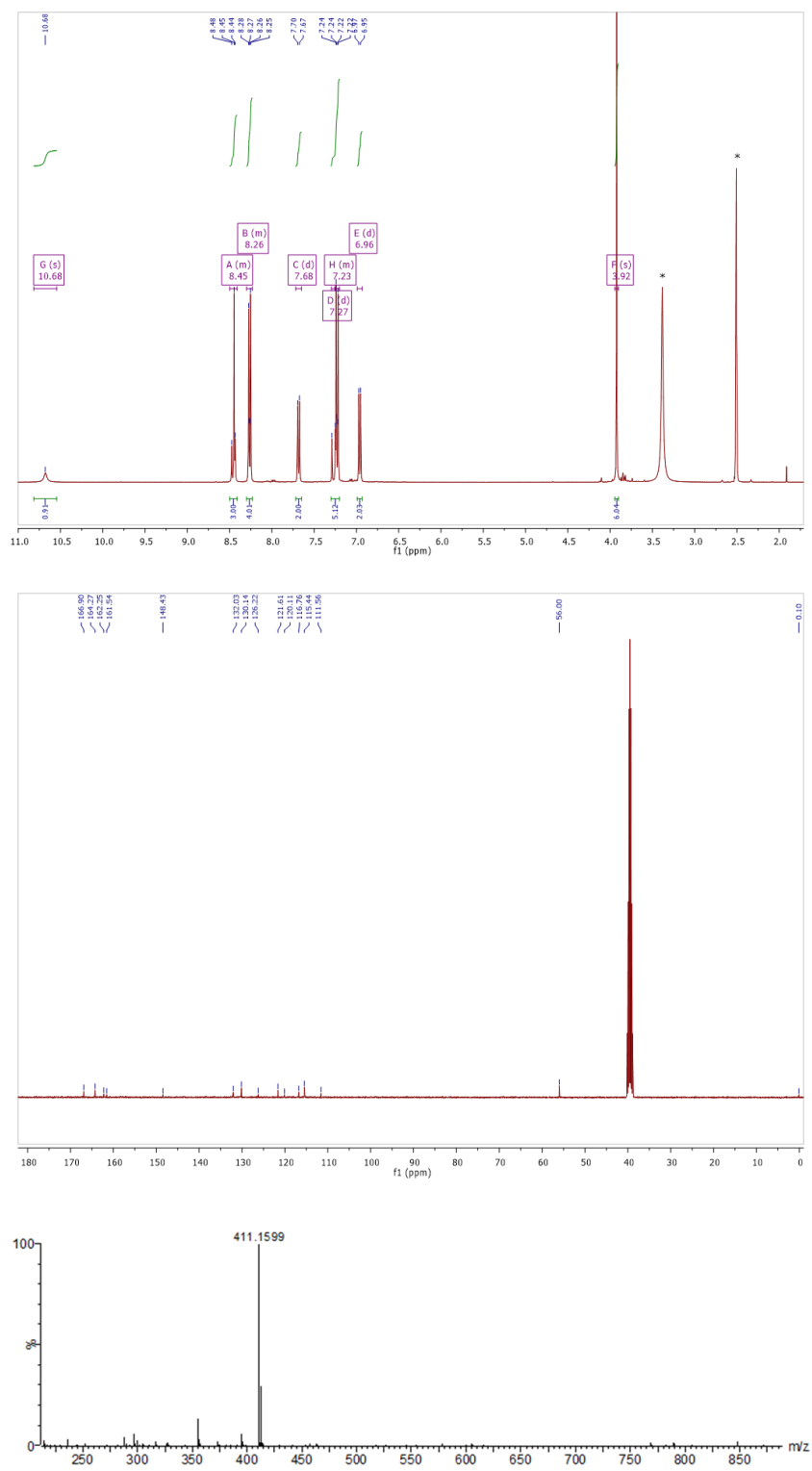
Figure 21. ^{1}H NMR, ^{13}C NMR (CD$_3$CN) and HRMS spectra of compound **3.7**.

Compound 3.8
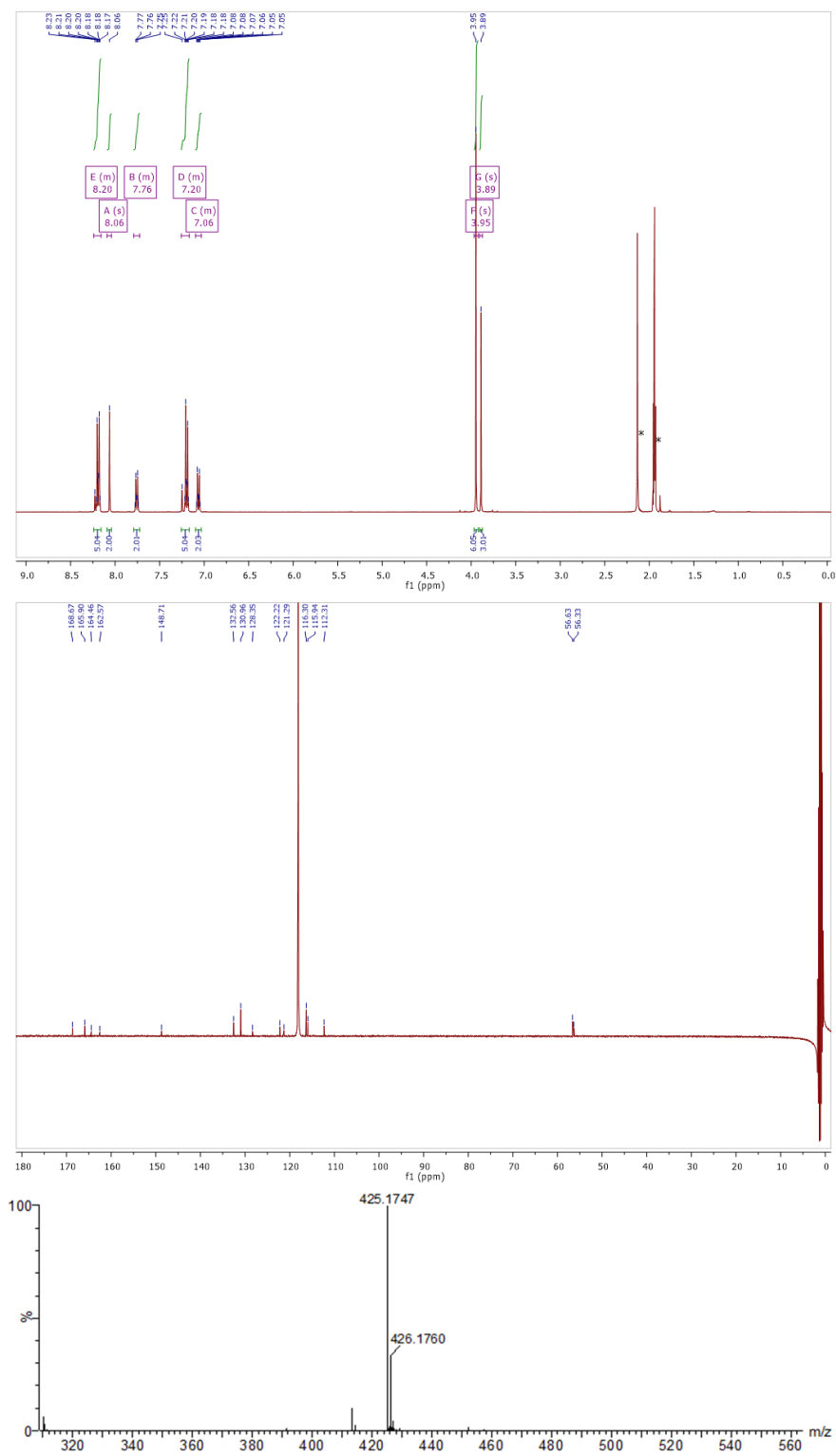
Figure 22. ^{1}H NMR, ^{13}C NMR (CD$_3$CN) and HRMS spectra of compound **3.8**.

Measurements of the fluorescence lifetime
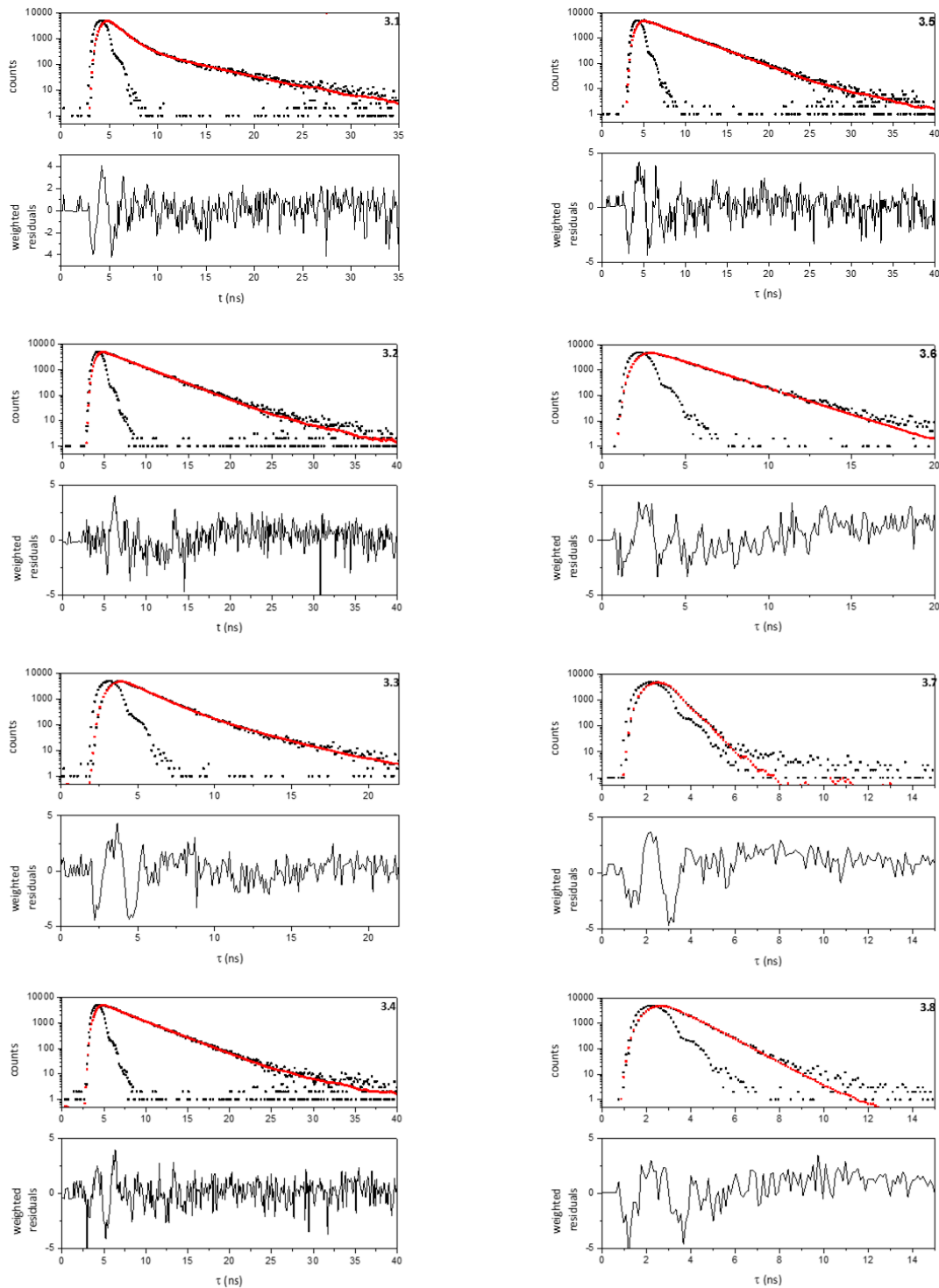
Figure 23. Fluorescence decay curves for compounds **3.1-3.8** in dichloromethane at 295 K. λ_{exc} was set at 464 nm. λ_{em} was set at the emission maximum for each compound. The incident light pulse and the residuals are also shown.
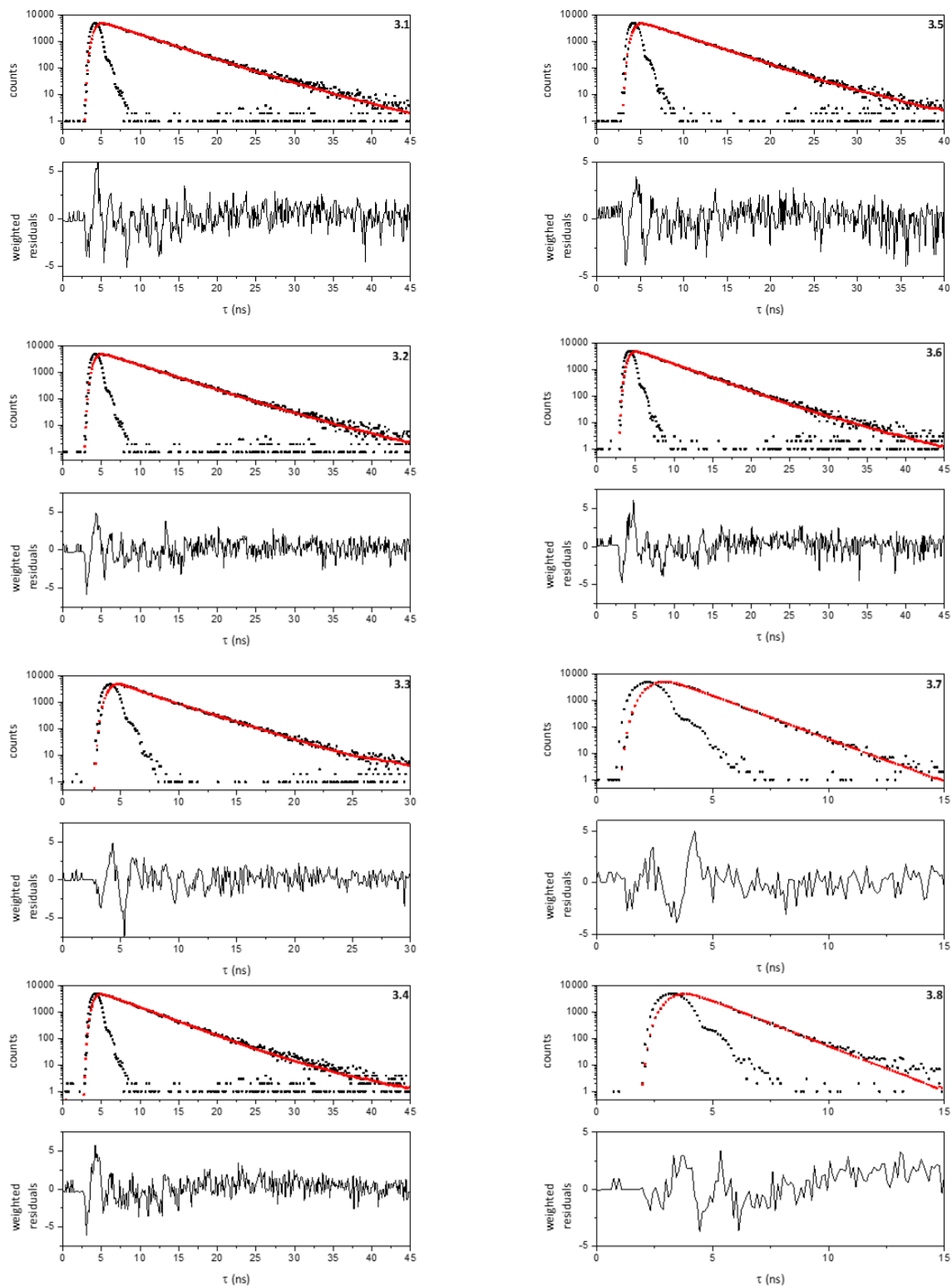
Figure 24. Fluorescence decay curves for compounds **3.1-3.8** in acetonitrile at 295 K. λ_{exc} was set at 464 nm. λ_{em} was set at the emission maximum for each compound. The incident light pulse and the residuals are also shown.
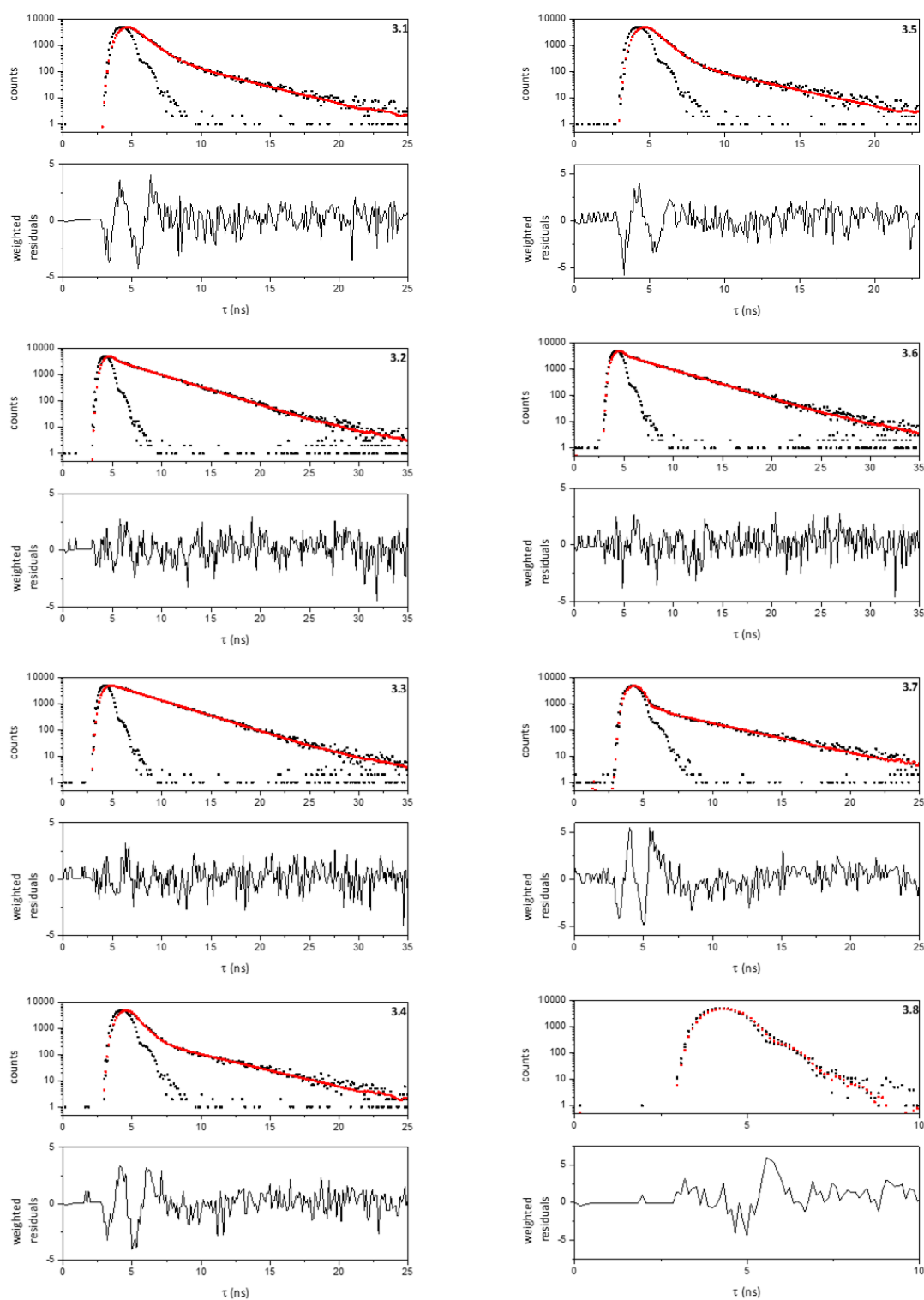
Figure 25. Fluorescence decay curves for compounds **3.1-3.8** in PBS (10 mM, pH 7.4) at 295 K. λ_{exc} was set at 464 nm. λ_{em} was set at the emission maximum for each compound. The incident light pulse and the residuals are also shown.

3.6. REFERENCES

1   C. Ma, F. Xia and S. O. Kelley, Mitochondrial Targeting of Probes and Therapeutics to the Powerhouse of the Cell, *Bioconjug. Chem.*, 2020, **31**, 2650–2667.

2   S. Samanta, Y. He, A. Sharma, J. Kim, W. Pan, Z. Yang, J. Li, W. Yan, L. Liu, J. Qu and J. S. Kim, Fluorescent Probes for Nanoscopic Imaging of Mitochondria, *Chem*, 2019, **5**, 1697–1726.

3   J. S. Modica-Napolitano and J. R. Aprille, Delocalized lipophilic cations selectively target the mitochondria of carcinoma cells, *Adv. Drug Deliv. Rev.*, 2001, **49**, 63–70.

4   J. Zielonka, J. Joseph, A. Sikora, M. Hardy, O. Ouari, J. Vasquez-Vivar, G. Cheng, M. Lopez and B. Kalyanaraman, Mitochondria-Targeted Triphenylphosphonium-Based Compounds: Syntheses, Mechanisms of Action, and Therapeutic and Diagnostic Applications, *Chem. Rev.*, 2017, **117**, 10043–10120.

5   H. Chen, J. Wang, X. Feng, M. Zhu, S. Hoffmann, A. Hsu, K. Qian, D. Huang, F. Zhao, W. Liu, H. Zhang and Z. Cheng, Mitochondria-targeting fluorescent molecules for high efficiency cancer growth inhibition and imaging, *Chem. Sci.*, 2019, **10**, 7946–7951.

6   W. Xu, Z. Zeng, J. H. Jiang, Y. T. Chang and L. Yuan, Discerning the Chemistry in Individual Organelles with Small-Molecule Fluorescent Probes, *Angew. Chemie - Int. Ed.*, 2016, **55**, 13658–13699.

7   M. C. Harwig, M. P. Viana, J. M. Egner, J. J. Harwig, M. E. Widlansky, S. M. Rafelski and R. B. Hill, Methods for imaging mammalian mitochondrial morphology: A prospective on MitoGraph, *Anal. Biochem.*, 2018, **552**, 81–99.

8   P. Gao, W. Pan, N. Li and B. Tang, Fluorescent probes for organelle-targeted bioactive species imaging, *Chem. Sci.*, 2019, **10**, 6035–6071.

9   K. Yu, J. Pan, E. Husamelden, H. Zhang, Q. He, Y. Wei and M. Tian, Aggregation-induced Emission Based Fluorogens for Mitochondria-targeted Tumor Imaging and Theranostics, *Chem. - An Asian J.*, 2020, **15**, 3942–3960.

10   L. V. Johnson, M. L. Walsh and L. B. Chen, Localization of mitochondria in living cells with rhodamine 123, *Proc. Natl. Acad. Sci. U. S. A.*, 1980, **77**, 990–994.

11   H. He, Z. Ye, Y. Xiao, W. Yang, X. Qian and Y. Yang, Super-Resolution Monitoring of Mitochondrial Dynamics upon Time-Gated Photo-Triggered Release of Nitric Oxide, *Anal. Chem.*, 2018, **90**, 2164–2169.

12   X. Zhou, Y. Fang, L. Lesiak and C. I. Stains, A Phosphinate-Containing Fluorophore Capable of Selectively Inducing Apoptosis in Cancer Cells, *ChemBioChem*, 2019, **20**, 1712–1716.

13   M. I. Sánchez, J. Martínez-Costas, J. L. Mascareñas and M. E. Vázquez, MitoBlue: A nontoxic and photostable blue-emitting dye that selectively labels functional mitochondria, *ACS Chem. Biol.*, 2014, **9**, 2742–2747.

14   M. I. Sánchez, Y. Vida, E. Pérez-Inestrosa, J. L. Mascareñas, M. E. Vázquez, A. Sugiura and J. Martínez-Costas, MitoBlue as a tool to analyze the mitochondria-lysosome communication, *Sci. Rep.*, 2020, **10**, 1–12.

15   A. Gandioso, R. Bresolí-Obach, A. Nin-Hill, M. Bosch, M. Palau, A. Galindo, S. Contreras, A. Rovira, C. Rovira, S. Nonell and V. Marchán, Redesigning the Coumarin Scaffold into Small Bright Fluorophores with Far-Red to Near-Infrared Emission and Large Stokes Shifts Useful for Cell Imaging, *J. Org. Chem.*, 2018, **83**, 1185–1195.

16   A. Gandioso, M. Palau, R. Bresolí-Obach, A. Galindo, A. Rovira, M. Bosch, S. Nonell and V. Marchán, High Photostability in Nonconventional Coumarins with Far-Red/NIR

Emission through Azetidinyl Substitution, *J. Org. Chem.*, 2018, **83**, 11519–11531.

17   A. Rovira, M. Pujals, A. Gandioso, M. López-Corrales, M. Bosch and V. Marchán, Modulating Photostability and Mitochondria Selectivity in Far-Red/NIR Emitting Coumarin Fluorophores through Replacement of Pyridinium by Pyrimidinium, *J. Org. Chem.*, 2020, **85**, 6086–6097.

18   N. Jiang, J. Fan, F. Xu, X. Peng, H. Mu, J. Wang and X. Xiong, Ratiometric Fluorescence Imaging of Cellular Polarity: Decrease in Mitochondrial Polarity in Cancer Cells, *Angew. Chemie*, 2015, **127**, 2540–2544.

19   H. Wang, J. Hu, G. Yang, X. Zhang, R. Zhang, K. Uvdal, Z. Zhang, X. Wu and Z. Hu, Real-time tracking of mitochondrial dynamics by a dual-sensitive probe, *Sensors Actuators, B Chem.*, 2020, **320**, 128418.

20   L. Krčová, S. Rimpelová, M. Havlík, B. Dolenský, F. Vellieux, T. Ruml, P. Martásek, V. Král and T. Bříza, Highly selective mitochondrial probes based on fluorinated pentamethinium salts: On two-photon properties and microscopic applications, *Dye. Pigment.*, 2020, **172**, 107802.

21   E. Hase, H. Takanari, K. Hoshi, M. Okamoto, A. Tabata, H. Nagamune, T. Minamikawa, T. Yasui, Y. Yoshida, K. Minagawa, Y. Kawamura, Y. Imada and F. Yagishita, Two-And three-photon excitable quaternized imidazo[1,2-a]pyridines as mitochondrial imaging and potent cancer therapy agents, *Org. Biomol. Chem.*, 2020, **18**, 7571–7576.

22   J. Yang, R. Zhang, Y. Zhao, J. Tian, S. Wang, C. P. Gros and H. Xu, Red/NIR neutral BODIPY-based fluorescent probes for lighting up mitochondria, *Spectrochim. Acta - Part A Mol. Biomol. Spectrosc.*, 2021, **248**, 119199.

23   C. W. T. Leung, Y. Hong, S. Chen, E. Zhao, J. W. Y. Lam and B. Z. Tang, A photostable

AIE luminogen for specific mitochondrial imaging and tracking, *J. Am. Chem. Soc.*, 2013, **135**, 62–65.

24   J. Li, N. Kwon, Y. Jeong, S. Lee, G. Kim and J. Yoon, Aggregation-Induced Fluorescence Probe for Monitoring Membrane Potential Changes in Mitochondria, *ACS Appl. Mater. Interfaces*, 2018, **10**, 12150–12154.

25   Z. Yang, L. Li, J. Ling, T. Liu, X. Huang, Y. Ying, Y. Zhao, Y. Zhao, K. Lei, L. Chen and Z. Chen, Cyclooctatetraene-conjugated cyanine mitochondrial probes minimize phototoxicity in fluorescence and nanoscopic imaging, *Chem. Sci.*, 2020, **11**, 8506–8516.

26   X. Mu, Y. Liu, S. Liu, Y. Sun, N. Lu, Y. Lu, W. Li, X. Zhou, B. Liu and Z. Li, A cyanine-derived near-infrared molecular rotor for ratiometric imaging of mitochondrial viscosity in cells, *Sensors Actuators, B Chem.*, 2019, **298**, 126831.

27   P. Herrero-Foncubierta, M. del C. González-García, S. Resa, J. M. Paredes, C. Ripoll, M. D. Girón, R. Salto, J. M. Cuerva, A. Orte and D. Miguel, Simple and non-charged long-lived fluorescent intracellular organelle trackers, *Dye. Pigment.*, 2020, **183**, 108649.

28   A. Blázquez-Moraleja, I. Sáenz-De-Santa María, M. D. Chiara, D. Álvarez-Fernández, I. García-Moreno, R. Prieto-Montero, V. Martínez-Martínez, I. López Arbeloa and J. L. Chiara, Shedding light on the mitochondrial matrix through a functional membrane transporter, *Chem. Sci.*, 2020, **11**, 1052–1065.

29   M. P. Murphy and R. C. Hartley, Mitochondria as a therapeutic target for common pathologies, *Nat. Rev. Drug Discov.*, 2018, **17**, 865–886.

30   Y. Yamada, Satrialdi, M. Hibino, D. Sasaki, J. Abe and H. Harashima, Power of mitochondrial drug delivery systems to produce innovative nanomedicines, *Adv. Drug Deliv. Rev.*, 2020, **154**–**155**, 187–209.

31   P. L. Toogood, Mitochondrial drugs, *Curr. Opin. Chem. Biol.*, 2008, **12**, 457–463.

32   E. Molnár, S. Kuntam, P. K. R. Cingaram, B. Peksel, B. Suresh, G. Fábián, L. Z. Fehér, A. Bokros, Á. Medgyesi, F. Ayaydin and L. G. Puskás, Combination of small molecule microarray and confocal microscopy techniques for live cell staining fluorescent dye discovery, *Molecules*, 2013, **18**, 9999–10013.

33   S. Y. Wen, W. Zhang, T. B. Ren, Q. L. Zhang, Y. P. Liu, L. Shi, R. Hu, X. B. Zhang and L. Yuan, Donor and Ring-Fusing Engineering for Far-Red to Near-Infrared Triphenylpyrylium Fluorophores with Enhanced Fluorescence Performance for Sensing and Imaging, *Chem. - A Eur. J.*, 2019, **25**, 6973–6979.

34   X. Chen, L. Yan, Y. Liu, Y. Yang and J. You, Switchable cascade C–H annulation to polycyclic pyryliums and pyridiniums: discovering mitochondria-targeting fluorescent probes, *Chem. Commun.*, 2020, 15080–15083.

35   X. Sun, K. Song, J. Hu and K. D. Garlid, AA1, A Newly Synthesized Monovalent Lipophilic Cation, Expresses Potent in Vivo Antitumor Activity, *Cancer Res.*, 1994, **54**, 1465–1471.

36   N. K. Brennan, J. P. Hall, S. R. Davies, S. O. Gollnick, A. R. Oseroff, S. L. Gibson, R. Hilf and M. R. Detty, In vitro photodynamic properties of chalcogenopyrylium analogues of the thiopyrylium antitumor agent AA1, *J. Med. Chem.*, 2002, **45**, 5123–5135.

37   A. Dinculescu, T. S. Balaban, C. Popescu, D. Toader and A. T. Balaban, Synthesis of Pyrylium Salts with Various Anions, *Bull. des Sociétés Chim. Belges*, 1991, **100**, 665–672.

38   F. Haucke, Gunter; Czerney, Peter; Cebulla, Absorption and fluorescence of pyrilium salts, *Berichte der Bunsengesellschaft für Phys. Chemie*, 1992, **96**, 880–886.

39 A. Beltrán, M. I. Burguete, S. V. Luis and F. Galindo, Styrylpyrylium Dyes as Solvent-Sensitive Molecules Displaying Dual Fluorescence, *European J. Org. Chem.*, 2017, 4864–4870.

40 I. Muñoz Resta, J. F. Miravet, M. Yamaji and F. Galindo, Solid-state white-light emission from a pyrylium dye obtained in one synthetic step, *J. Mater. Chem. C*, 2020, **8**, 14348–14352.

41 S. Elsayed, A. Agostini, L. E. Santos-Figueroa, R. Martínez-Máñez and F. Sancenón, An instantaneous and highly selective chromofluorogenic chemodosimeter for fluoride anion detection in pure water, *ChemistryOpen*, 2013, **2**, 58–62.

42 P. Nikolov and S. Metzov, Peculiarities in the photophysical properties of some 6-styryl-2,4-disubstituted pyrylium salts, *J. Photochem. Photobiol. A Chem.*, 2000, **135**, 13–25.

43 A. Pigliucci, P. Nikolov, A. Rehaman, L. Gagliardi, C. J. Cramer and E. Vauthey, Early excited state dynamics of 6-styryl-substituted pyrylium salts exhibiting dual fluorescence, *J. Phys. Chem. A*, 2006, **110**, 9988–9994.

44 F. Pina, M. J. Melo, C. A. T. Laia, A. J. Parola and J. C. Lima, Chemistry and applications of flavylium compounds: A handful of colours, *Chem. Soc. Rev.*, 2012, **41**, 869–908.

45 S. Chakraborty, M. M. Joseph, S. Varughese, S. Ghosh, K. K. Maiti, A. Samanta and A. Ajayaghosh, A new pentacyclic pyrylium fluorescent probe that responds to pH imbalance during apoptosis, *Chem. Sci.*, 2020, 12695–12700.

46 T. B. Ren, W. Xu, W. Zhang, X. X. Zhang, Z. Y. Wang, Z. Xiang, L. Yuan and X. B. Zhang, A General Method to Increase Stokes Shift by Introducing Alternating Vibronic Structures, *J. Am. Chem. Soc.*, 2018, **140**, 7716–7722.

47 A. V. Saura, M. J. Marín, M. I. Burguete, D. A. Russell, F. Galindo and S. V. Luis, The

synthesis of new fluorescent bichromophoric compounds as ratiometric pH probes for intracellular measurements, *Org. Biomol. Chem.*, 2015, **13**, 7736–7749.

48   A. Vanessa Saura, M. Isabel Burguete, F. Galindo and S. V. Luis, Novel fluorescent anthracene-bodipy dyads displaying sensitivity to pH and turn-on behaviour towards Cu(II) ions, *Org. Biomol. Chem.*, 2017, **15**, 3013–3024.

49   C. W. Hsieh, C. H. Chu, H. M. Lee and W. Yuan Yang, Triggering mitophagy with far-red fluorescent photosensitizers, *Sci. Rep.*, 2015, **5**, 1–13.

50   M. A. Miranda and H. García, 2,4,6-Triphenylpyrylium Tetrafluoroborate as an Electron-Transfer Photosensitizer, *Chem. Rev.*, 1994, **94**, 1063–1089.

51   P. G. Heytler and W. W. Prichard, A new class of uncoupling agents-carbonyl cyanide phenylhydrazones, *Biochem. Biophys. Res. Commun.*, 1962, **7**, 272–275.

52   T. J. Lampidis, S. D. Bernal, I. C. Summerhayes and L. B. Chen, Selective Toxicity of Rhodamine 123 in Carcinoma Cells in Vitro, *Cancer Res.*, 1983, **43**, 716–720.

53   H. A. Omar, D. M. Zaher, V. Srinivasulu, F. Hersi, H. Tarazi and T. H. Al-Tel, Design, synthesis and biological evaluation of new pyrrolidine carboxamide analogues as potential chemotherapeutic agents for hepatocellular carcinoma, *Eur. J. Med. Chem.*, 2017, **139**, 804–814.

54   S. M. Kim, J. M. Han, T. T. Le, J. K. Sohng and H. J. Jung, Anticancer and antiangiogenic activities of novel α-mangostin glycosides in human hepatocellular carcinoma cells via downregulation of c-met and HIF-1α, *Int. J. Mol. Sci.*, 2020, **21**, 1–19.

55   M. Y. Wu, L. Liu, Q. Zou, J. K. Leung, J. L. Wang, T. Y. Chou and S. Feng, Simple synthesis of multifunctional photosensitizers for mitochondrial and bacterial imaging and photodynamic anticancer and antibacterial therapy, *J. Mater. Chem. B*, 2020, **8**, 9035–

9042.

56   T. T. Yang, P. Sinai and S. R. Kain, An acid phosphatase assay for quantifying the growth of adherent and nonadherent cells, *Anal. Biochem.*, 1996, **241**, 103–108.

57   E. Gottlieb, S. M. Armour, M. H. Harris and C. B. Thompson, Mitochondrial membrane potential regulates matrix configuration and cytochrome c release during apoptosis, *Cell Death Differ.*, 2003, **10**, 709–717.

Chapter 4

Pyrylium probes for nitric oxide sensing

The results presented in this chapter are based on the following article:

Detection of subcellular nitric oxide in the mitochondria by a pyrylium probe: assays in cell cultures and peripheral blood. Muñoz Resta, I.; Bedrina, B.; Martínez-Planes, E.; Minguela, A.; Galindo, F. **2021**. *Submitted*.

Assays in peripheral blood samples were done in collaboration with Dr. Alfredo Minguela and Elena Martínez Planes from the Department of Immunology, Hospital Universitario Virgen de la Arrixaca (Murcia, Spain).

4.1. INTRODUCTION

Fluorescence imaging of intracellular species is now possible due to the great number of available molecular and nanoscopic probes.[1–5] From the first developed dyes based on a common set of core scaffolds, like coumarins, fluoresceins or rhodamines, to the more recent quantum dots and metal nanoparticles, a vast library of fluorescent compounds has been used during the last years in fields as diverse as chemical analysis, biosensing and disease diagnosis.

Within the enormous variety of species of biological relevance, nitric oxide (NO) stands out as one of the three vital signal gasotransmitters. Endogenously produced by inducible and constitutive nitric oxide synthases from the amino acid L-arginine, it performs a pivotal role in functions like vasodilatation, signal transduction, hormone secretion and immune system regulation.[6–8] However, a misregulation of its physiological concentration is associated with several pathologies like cardiac disorders, neurodegeneration, Parkinson's, and Alzheimer's. Therefore, it is mandatory to develop fluorescent probes that allow intracellular imaging and quantification of NO with high selectivity and sensitivity.

For this purpose, several strategies have been followed. From the o-diamino aromatics designed by Nagano's group[9,10] in the last ´90s to the metal-complex based probes first introduced by Lippard's group,[11] a big number of dyes have been synthesized, comprising different approaches for nitric oxide detection: formation of fluorescent triazoles[12–17] or diazo ring compounds,[18–20] deamination of aromatic primary amines,[21,22] N-nitrosation of aromatic secondary amines,[23–26] conversion of Hantzsch esters into pyridines,[27,28] etc. Although the o-phenylenediamine is the most widely used functionality for NO detection, it has some limitations, like reacting with other competitive biological species such as ascorbic or

dehydroascorbic acid. So, a great effort has been made during the last 20 years to improve nitric oxide detection, but even now is not clear if any of the NO trapping groups highlights among the others. These recent advances have been documented in numerous reviews.[29–37]

Despite the great number of NO sensors described so far, only a limited number of them target the mitochondria of living cells.[28,38–43] Mitochondrial NO and other reactive nitrogen/oxygen species are key in the understanding of, for instance, cancer,[44,45] bacterial[46] and viral[47] infections, pharmacological treatments[48] and to track inflammatory cells.[49,50] Several delocalized lipophilic cations -DLC- have been used in the past to track the mitochondria in response to their negative inside transmembrane potential.[51] In Chapter 3, it was described that minimalistic styrylpyrylium dyes, delocalized lipophilic cations (DLC) obtained in three synthetic steps, can reach the mitochondria of Hep3B hepatocarcinoma cells very efficiently, without the need of a directing group, like the triphenylphosphonium cation (TPP). A paradigmatic example of them is molecule **3.8**, which, on the contrary to TPP, is intrinsically fluorescent. So, it was reasoned that simple modification of **3.8** with appropriate reactive groups would lead to molecules with the potential to generate fluorescence inside mitochondria of live cells upon the correct stimulus. Pyrylium cations have been used for several applications but scarcely for intracellular analysis.[52–55]

So, it was decided to synthesize an analogue with the proper trapping group that allows the reaction with NO. For that purpose, an amino group in *ortho* to the methoxy in **3.8** was introduced, yielding compound **4.1** (**Chart 1**). The presence of this group not only would impart the desired reactivity to the indicator but also would quench the emission of the probe (mandatory for a turn-on response upon reaction). Also, model compounds with a different

position of the methoxy group (**4.2**) or without this functionality (**4.3**) were synthesized. In this chapter, the ability of **4.1** to respond to nitrosative stimulus producing a positive fluorescence response in the mitochondria of HT29 and RAW 264.7 cells and peripheral blood leukocytes is reported.
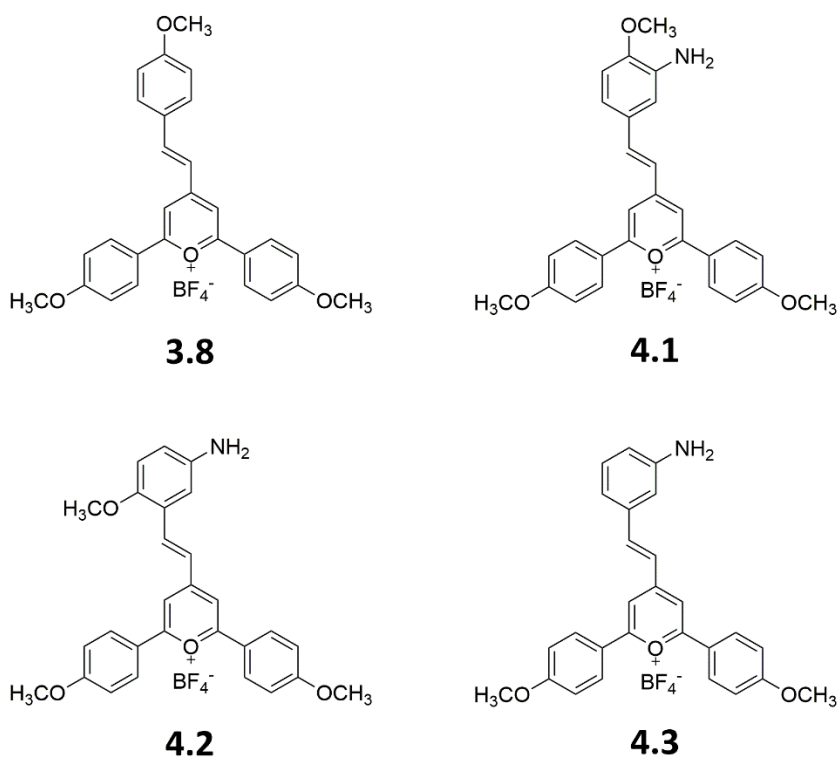
Chart 1. Mitochondrial marker **3.8**, its analogue **4.1** designed to sense nitric oxide in the mitochondria and model compounds **4.2** and **4.3**.

4.2. RESULTS AND DISCUSSION

4.2.1. SYNTHESIS AND CHARACTERISATION

For the synthesis of compounds **4.1-4.3,** a two step-reaction has been followed: a condensation between the 4-methylsubstituted pyrylium precursor and the corresponding substituted nitro-benzaldehydes in acetic acid, attended by a reduction with $SnCl_2$ in acidic media (**Scheme 1**). All the products were easily purified just by precipitation, avoiding

chromatographic techniques and, for that, providing a relative advantage over the synthetic procedures of other probes. The dyes were characterized by ^{1}H-NMR, ^{13}C-NMR and, HRMS.
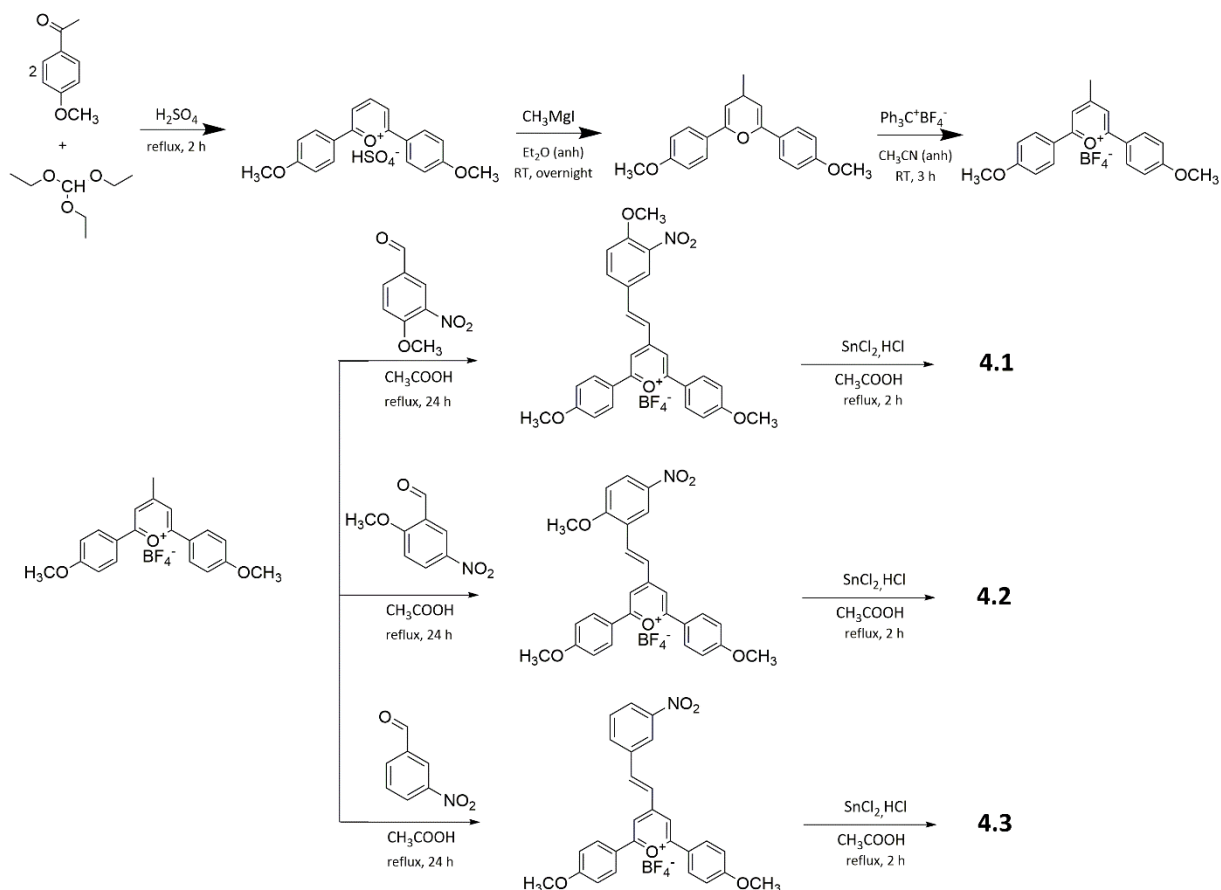
Scheme 1. Synthetic route for compounds **4.1-4.3**.

4.2.2. STUDIES IN CUVETTE

The spectroscopic response of probe **4.1** to nitric oxide was studied in phosphate-buffered saline -PBS- 10 mM at pH = 7.4 (using a 20 % of dimethylformamide -DMF- as a cosolvent). For that, UV-vis absorption and emission spectra were recorded over time, after the reaction with an excess of NO (in an aerated medium to generate the surrogate reactive nitrosating species N_2O_3) released by the commercial donor diethylamine NONOate sodium salt -DEA NONOate- (50 equivalents). As shown in **Figure 1**, upon reaction with NO, a new

absorption peak appears at 420 nm and gradually increases. But the more significant changes are observed in the emission spectra: a 120-fold enhancement at 585 nm is noticed after 20 minutes.
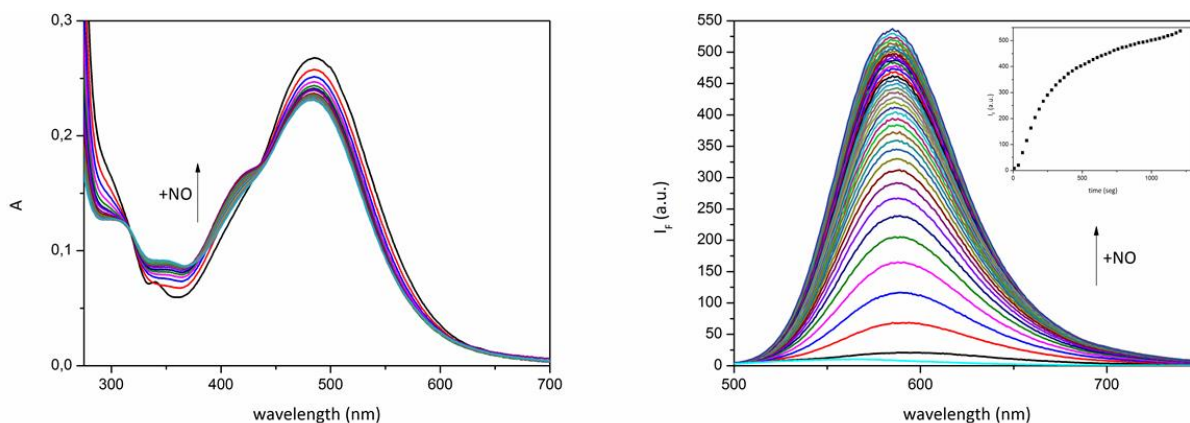
Figure 1. Evolution over time of the absorption (left) and emission (right) spectra of 10 µM solutions of **4.1** in PBS 10 mM (pH 7.4, 20 % DMF as a cosolvent) with 50 equivalents of DEA NONOate. λ_{exc} was set at 480 nm.

The fluorescence enhancement can be attributed to the formation of the correspondent deamination product and the consequent suppression of the photoinduced electron transfer process from the -NH$_2$ group to the pyrylium core. To verify this response mechanism, a water solution of **4.1** (with DMF as a cosolvent) was bubbled with an excess of gaseous NO and further analysed by HRMS. As it can be seen in **Figure 2**, the molecular peak corresponding to **4.1** is absent, and a new peak at m/z = 425.1752 appears, which could be assigned to the deamination product, i.e, [**3.8**] $^+$. Also, the emission of reacted **4.1** matches the fluorescence spectrum of **3.8** (585 nm) (**Figure 3**).
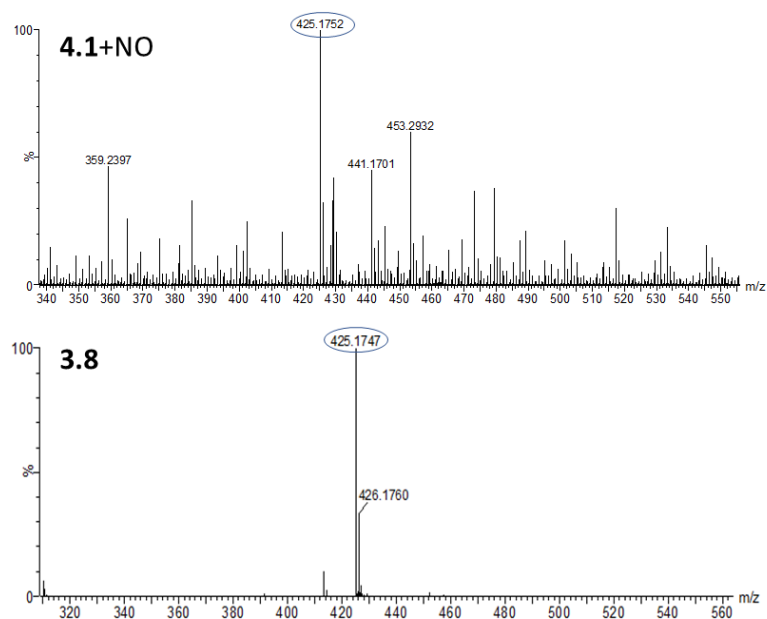
Figure 2. High-resolution mass spectra of **4.1** after the reaction with an excess of gaseous NO (top) and HR-MS of its deamination product, compound **3.8** (bottom).
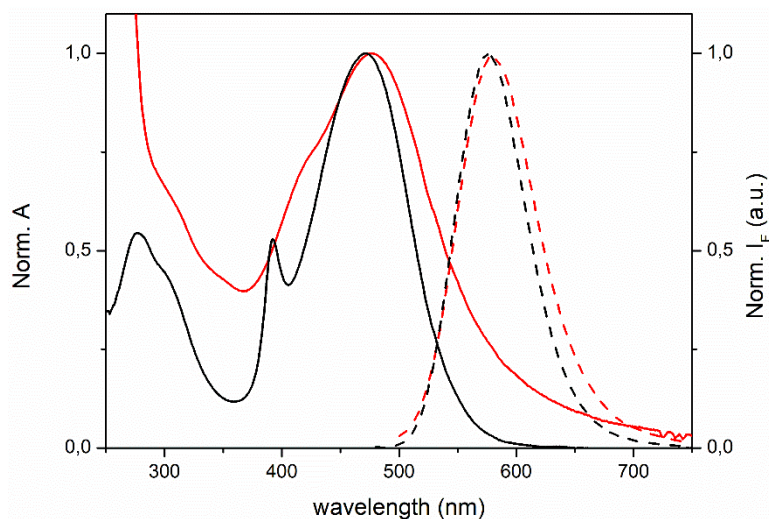
Figure 3. Normalized absorption (straight line) and emission (dashed line) spectra of compound **4.1**+NO (red) and compound **3.8** (black) in PBS (10 mM, pH 7.4, 20 % DMF as a cosolvent). λ_{exc} was set at 480 nm.

To study the concentration dependence of **4.1** reacting with NO, 10 µM solutions of the probe in PBS (20 % DMF as a cosolvent) were allowed to react for 20 minutes with increasing amounts of NO, from 0 to 1000 µM, and the emission spectra were recorded. As shown in

Figure 4, a good linear correlation between fluorescence intensity at 585 nm and NO concentration between 0-80 µM is observed (R^2 = 0.9958). The limit of detection for NO, calculated as 3σ/k (where σ is the standard deviation of the blank measurements and k is the slope of the calibration curve), is 88 nM, making **4.1** a potential probe to visualize endogenous NO in living cells with high sensitivity.
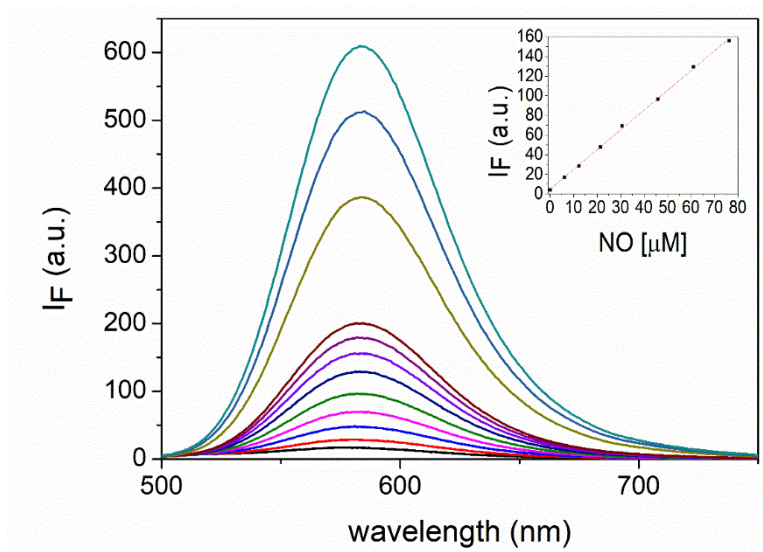
Figure 4. Changes in emission spectra of 10 µM solutions of **4.1** after the addition of different amounts of NO (from 0 to 1000 µM) in PBS 10 mM (pH 7.4, 20 % DMF as a cosolvent). λ_{exc} was set at 480 nm. Inset: fluorescence intensity at 585 nm vs NO concentration from 0 to 80 µM. Spectra were recorded 20 minutes after the addition of NO.

To analyse the time dependence of the reaction between **4.1** and nitric oxide, the fluorescence intensity at 585 of 10 µM solutions of the probe in PBS (20 % DMF as a cosolvent) was measured over time, after the reaction with different equivalents of NO (**Figure 5**). As it can be seen, the fluorescence intensities increase with time with a regular pattern, reaching a plateau in 20 minutes. This time may seem high relative to the short lifetime of NO at physiological conditions, but it must be noticed that the major increment of the signal occurs during the first minutes.
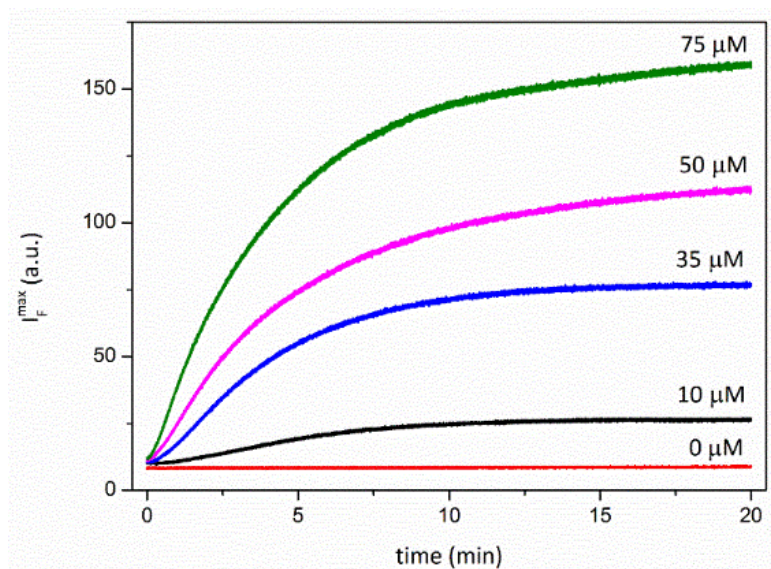
Figure 5. Evolution over time of the fluorescence intensity at 585 nm of 10 µM solutions of **4.1** in PBS 10 mM (pH 7.4, 20 % DMF as a cosolvent) after the addition of different equivalents of NO. λ_{exc} was set at 480 nm.

Considering that a high selectivity is required in the design of useful probes for the imaging and quantification of intracellular species, the fluorescence of **4.1** in the presence of a great excess (50 equivalents) of other relevant biological compounds, such as reactive oxygen species (O_2^-, H_2O_2, $OH^.$, $^1O_2$), reactive nitrogen species (NO, NO_2^-, NO_3^-, $ONOO^-$), ClO^-, ascorbic acid -AA- and dehydroascorbic acid -DHA-, was evaluated. As shown in **Figure 6**, a negligible response is observed for all these analytes, with the obvious exception of NO. These results indicate that **4.1** exhibits a great selectivity to NO over other potential competitive analytes.
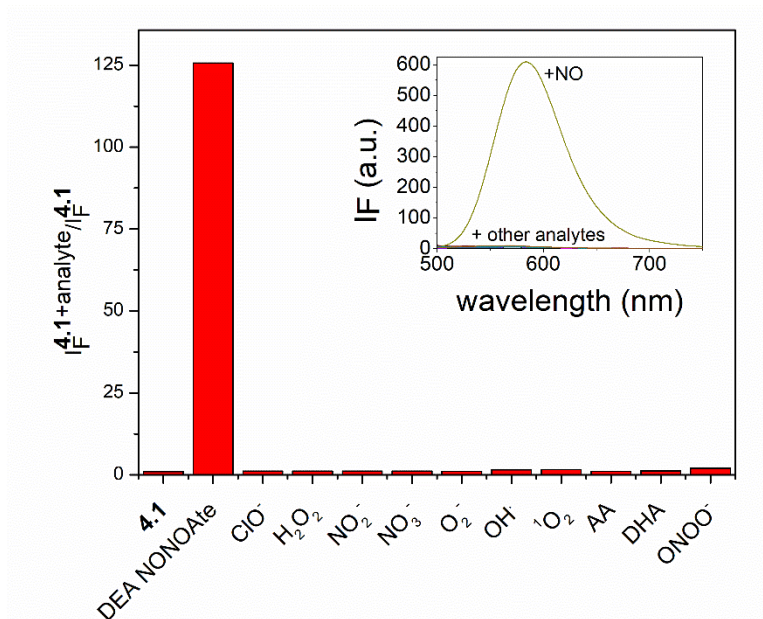
Figure 6. Changes in the fluorescence intensity at 585 nm of 10 µM solutions of **4.1** after the addition of 50 equivalents of different reactive nitrogen, oxygen species, ClO⁻, AA and DHA in PBS 10 mM (pH 7.4, 20 % DMF as a cosolvent). λ_{exc} was set at 480 nm. Spectra were recorded 20 minutes after the addition of the analytes. Inset: emission spectra.

The stability of **4.1** and its deamination product **3.8** was evaluated under different and relevant biological pH values (from 4.5, the pH of the lysosomes, to 8, the pH of the mitochondrial matrix). For this, the fluorescence response of both compounds was studied. While **4.1** shows insignificant emission from pH 5 and above, **4.1** + DEA NONOate (50 equivalents) is highly fluorescent in the same range, and its emission remains almost invariant (**Figure 7**). Consequently, **4.1** can be applied in the imaging of nitric oxide in physiological conditions with low background emission.
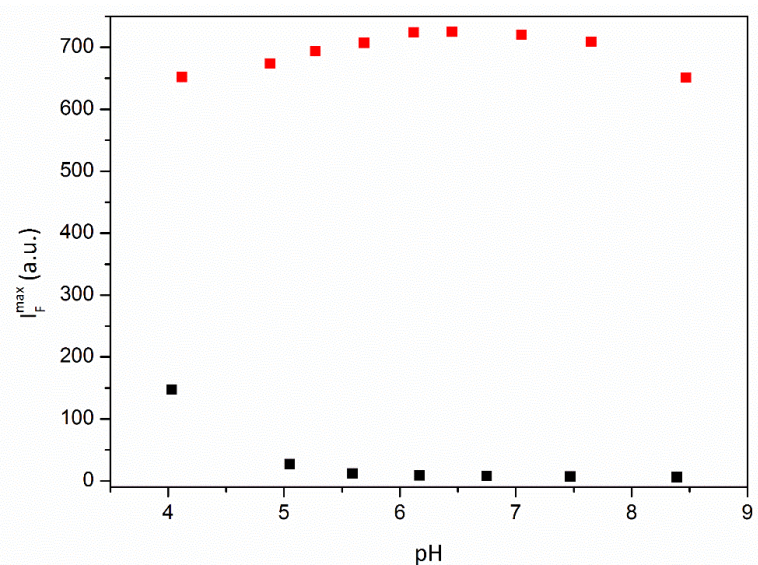
Figure 7. pH response of **4.1** + NO (50 equivalents, red dots) and **4.1** (black dots).

Some structural analogues of **4.1** were synthesized to demonstrate that the *ortho-*methoxyamino substitution in the styryl chain aligned with the y-axis is adequate for the observed reactivity (**Chart 1**). In the case of molecule **4.2**, having the MeO- group in *para* position relative to the -NH$_2$ group, the reactivity is faster than for **4.1**, although with a higher limit of detection (LOD$_{4.2}$ = 0.41 µM). For compound **4.3**, lacking the methoxy group, the response to NO (aerated medium) is very weak (**Figure 8**), which demonstrates that the aryl ring must be activated with an electron-donating group.
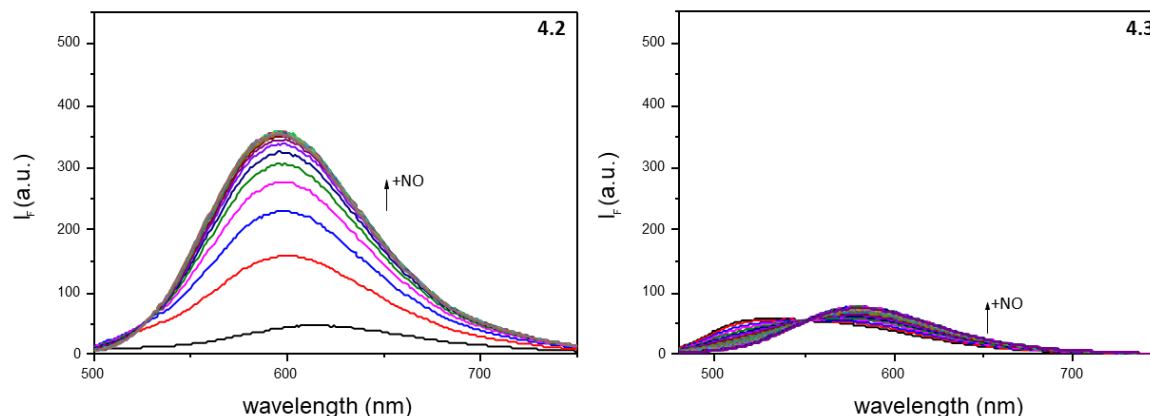
Figure 8. Evolution over time of the emission spectrum of 10 µM solutions of compounds **4.2** and **4.3** in PBS 10 mM (pH 7.4, 20 % DMF as a cosolvent) with 50 equivalents of DEA NONOate. λ_{exc} was set at the absorption maximum for each compound.

4.2.3. STUDIES IN CELL LINES BY CONFOCAL MICROSCOPY AND FLOW CYTOMETRY

As **4.1** could be used successfully for NO sensing in *cuvette* with high sensitivity and selectivity, the next step was its evaluation in biological systems. To assess the cytotoxicity of **4.1**, a standard MTT assay was performed (**Figure 9**). A cell survival rate of 100 % is observed after 48 hours, when incubated probe **4.1** in RAW 264.7 cells from 0-10 µM, and a significant decrease is observed from concentrations above 15 µM.
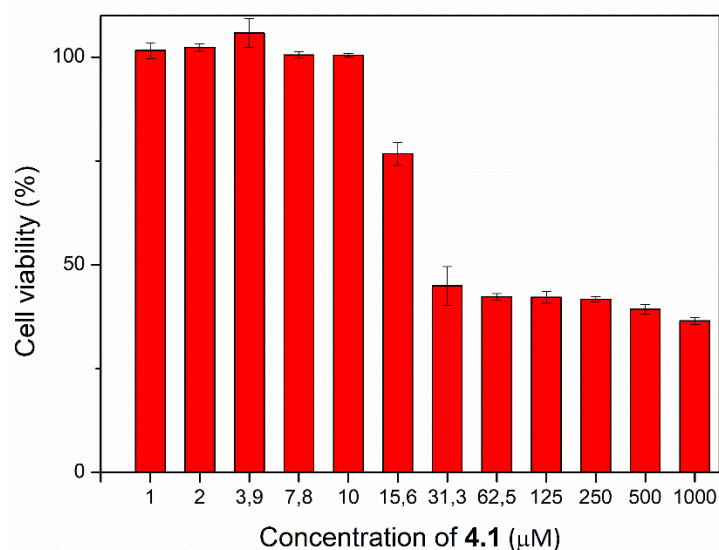
Figure 9. Viability of RAW 264.7 cells after incubation with different concentrations of probe **4.1** for 48 hours. Data are shown as mean±SD, n=3.

For imaging of exogenous NO, HT29 cells were incubated with 10 µM of **4.1** for 30 minutes and then treated with 10 equivalents of S-nitroso-N-acetylpenicillamine -SNAP- (a commercial and well-known NO release agent) for 60 minutes. As shown in **Figure 10A**, negligible fluorescence is observed for **4.1**-stained HT29 cells. As expected, a remarkable increment of fluorescence occurs after incubation with NO, making **4.1** suitable for intracellular detection of nitric oxide (**Figure 10B**). These results were confirmed with the calculation of the corrected total cell fluorescence (CFCT), as shown in **Figure 10C**. Also, flow cytometric analysis was performed in the same conditions, and a 4.5-fold increment of the emission in the treated cells with both the probe and the commercial NO donor is observed (**Figure 11**).
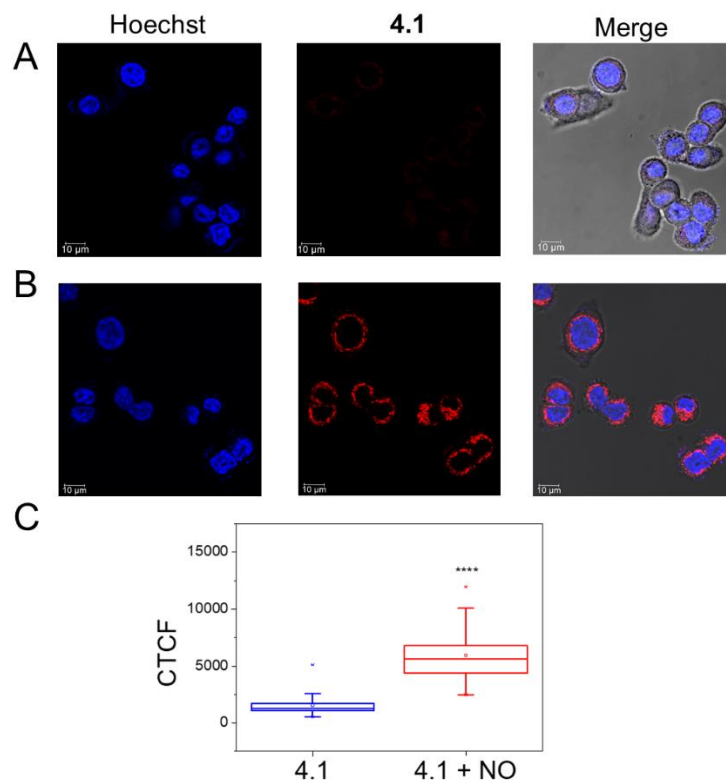
Figure 10. A) HT29 cells stained by **4.1** (10 μM, 30 min) B) HT29 cells stained by **4.1** (10 μM, 30 min) and then treated with SNAP (100 μM, 60 min). In all cases, Hoechst (0.1 mg/ml, 5 min) was added to mark nuclei. C) Corrected total cell fluorescence (CFCT) calculated from A and B (red fluorescence). Data are shown as median ± (inter-quartile range) IQR, n=20. Statistical analysis was performed by unpaired t-test (**** indicates a p-value ≤ 0.0001).
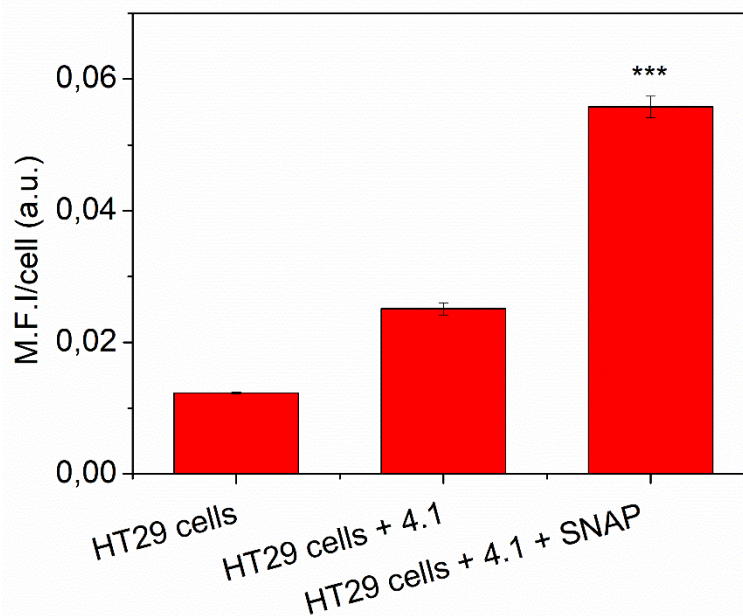
Figure 11. Mean fluorescence intensity obtained by flow cytometry of **4.1**-stained (10 µM, 30 min) HT29 cells exposed to SNAP (100 µM, 60 min). Excitation and emission were set at 488 nm and 585 nm, respectively. Data are shown as mean±SD, n=3. Statistical analysis was performed by one-way ANOVA followed by Tukey's multiple comparisons tests (*** indicates a p-value ≤ 0.001).

The perinuclear distribution and the filamentous morphology of the fluorescent subcellular structures suggest a mitochondrial internalization, as confirmed for compound **3.8** in Chapter 3. To ensure this, colocalization analysis with commercial Mitotracker Green FM was performed. HT29 cells were coincubated with **4.1** (10 uM) and Mitotracker Green FM (75 nM), followed by further incubation with SNAP. As shown in **Figure 12**, there is a great correlation between the fluorescent signal of **4.1** (**Figure 12A**) and the commercial mitochondrial dye (**Figure 12B**), with a calculated Person correlation coefficient of 0.94.
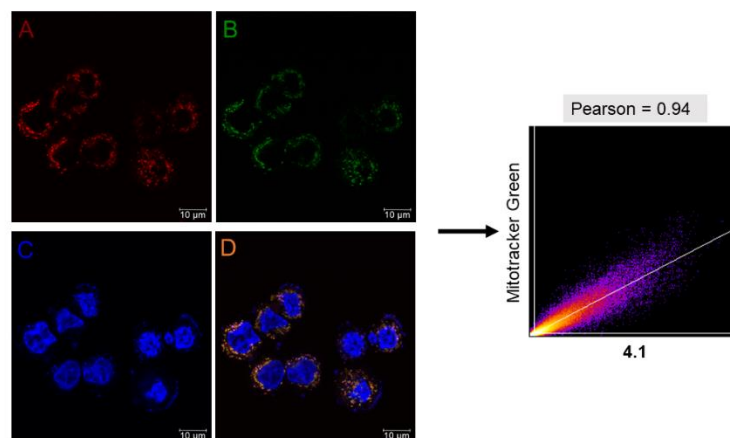
Figure 12. Fluorescence images of HT29 cells coincubated with **4.1** (10 µM) and Mitotracker Green FM (75 nM) for 30 minutes and then treated with SNAP (100 µM, 60 min). Hoechst (0.1 mg/ml, 5 min) was added to mark nuclei. A) Fluorescent signal of **4.1**. B) Fluorescent signal of Mitotracker Green FM. C) Fluorescent signal of Hoechst. D) Merged channels.

For imaging of endogenous NO, RAW 264.7 macrophage cells were treated with lipopolysaccharide -LPS- overnight, and further incubated with **4.1** for 30 minutes. As shown in **Figure 13**, a very weak fluorescent signal is observed when cells were incubated with **4.1**, without stimulation (**Figure 13A**). Treatment with LPS induces an increment in fluorescence (**Figure 13B**), because of the i-NOS activation and, consequently, the boosted NO liberation. As expected, the addition of L-N^G-monomethyl arginine acetate (L-NMMA), an i-NOS inhibitor, results in a negligible response to LPS (**Figure 13C**). Results were confirmed by flow cytometry (**Figure 14**).
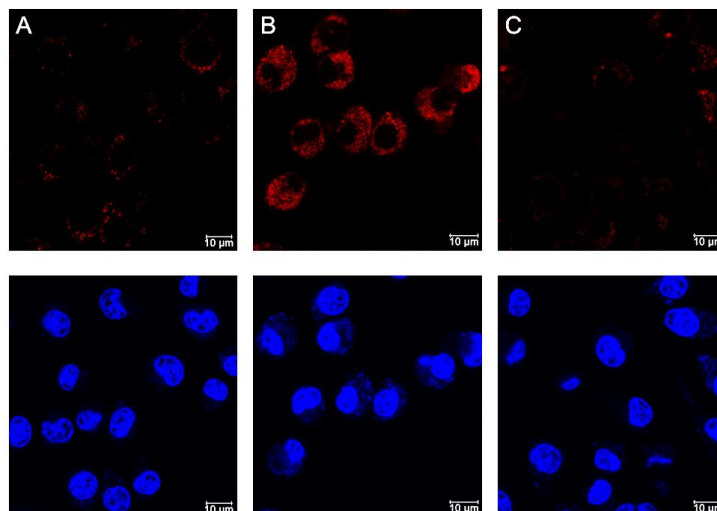
Figure 13. A) RAW 264.7 cells stained by **4.1** (10 µM, 30 min) B) RAW 264.7 cells stained by **4.1** (10 µM, 30 min) after the treatment with LPS (20 µg/ml, overnight) C) RAW 264.7 cells stained by **4.1** (10 µM, 30 min) after the treatment with LPS (20 µg/ml, overnight) and L-NMMA (50 µM, overnight). In all cases, Hoechst (0.1 mg/ml, 5 min) was added to mark nuclei. Top: fluorescent signal of **4.1**; bottom: fluorescent signal of Hoechst.
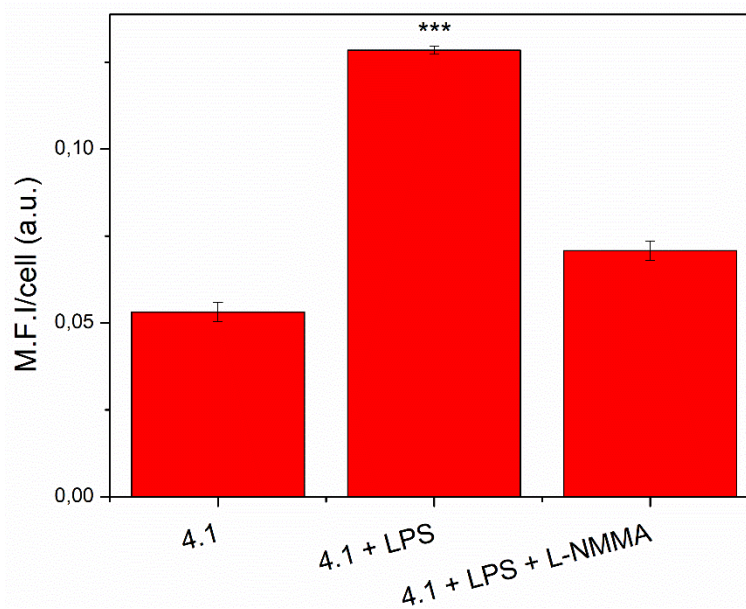
Figure 14. Mean fluorescence intensity obtained by flow cytometry of **4.1**-stained (10 µM, 30 min) RAW 264.7 cells exposed to LPS (20 µg/ml, overnight) and LPS+L-NMMA (20 µg/ml and 50 µM, overnight). Excitation and emission were set at 488 nm and 585 nm, respectively. Data are shown as mean±SD, n=3. Statistical analysis was performed by one-way ANOVA followed by Tukey's multiple comparisons tests (*** indicates a p-value ≤ 0.001).

A nonspecific phagocytosis assay with zymosan particles was also performed. It is well known that zymosan induces an inflammatory response in macrophages, and for that, it was used as a model for the recognition of pathogens for years. As shown in **Figure 15**, an increment of the fluorescent signal is observed by flow cytometry in cells treated with zymosan (3 mg/ml) after 1-hour stimulation, relative to a control group (without stimulus), thus suggesting an increment in the NO production and, consequently, in the fluorescent signal of **4.1**-stained RAW 264.7 cells.
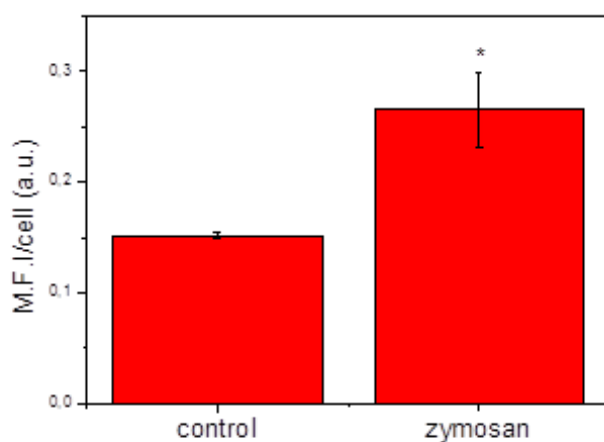
Figure 15. Mean fluorescence intensity of **4.1**-stained (10 µM) RAW 264.7 cells exposed to zymosan particles (3 mg/ml, 60 min). Excitation and emission were set at 488 nm and 585 nm, respectively. Data are shown as mean±SD, n=3. Statistical analysis was performed by unpaired t-test (* indicates a p-value ≤ 0.05).

4.2.4. *STUDIES IN PERIPHERAL BLOOD BY FLOW CYTOMETRY*

Finally, the probe was assayed in a much more complex environment, whole peripheral blood, and using flow cytometry as a bioanalytical tool. This type of test is original within the field of NO-probes since biological assays in this area are normally limited to controlled conditions such as cellular cultures. The aim of this new assay was carried out to demonstrate that **4.1** could extract information from a sample containing leukocytes of different nature (neutrophils, monocytes, NK, B and T cells). Thus, **4.1** was incubated with human peripheral

blood samples extracted from healthy donors, and the fluorescence of leukocyte subsets analysed by flow cytometry using two different lasers as excitation sources of **4.1** (405 nm and 488 nm). The samples were stimulated with LPS to trigger an inflammatory response and monitored over time. As it can be seen in **Figure 16A**, the response of phagocytes (neutrophils and monocytes) is notable, with relative fluorescence signals about one order of magnitude higher than that of lymphocytes (NK, B and T cells). In neutrophils NO levels were similar ex-vivo (MFI = 186) and after 24 hours (MFI = 208) of LPS stimulation, but they were higher after 48 hours of stimulation (MFI = 404). However, in monocytes the level of NO progressively increased from ex-vivo (MFI = 113) to 24 (MFI = 344) and 48 (MFI = 719) hours of LPS stimulation. On lymphocytes, only CD8$^+$ T cells showed increasing values of NO levels after 0 (MFI = 10), 24 (MFI = 51) and 48 (MFI = 66) hours of LPS stimulation. Similar results were observed in the PE (586/42 nm) and the V500 (528/45nm) channels. In the kinetic analysis of the NO levels (**Figure 16B**), compared to cells maintained in RPMI medium, 48 hours of LPS stimulation induced clear increases in the MFI of **4.1** in neutrophils (maximum reached at 15 minutes), monocytes (maximum reached at 12 minutes) and non-classical CD16$^+$ monocytes (maximum reached at 18 minutes). Very low increases were observed for NK and CD8$^+$ T cells. Overall, the higher response of the neutrophils and monocytes is the expected one since these cells are efficient producers of NO upon stimulation, due to their phagocytic function.[56,57]
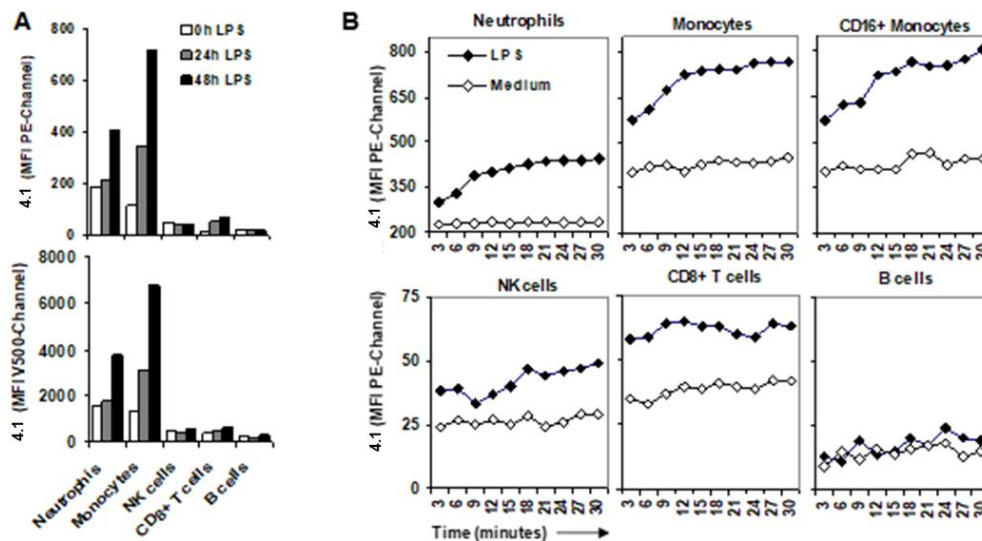
Figure 16. A) Mean fluorescence intensity (MFI) of 10 µM solutions of **4.1** in leukocyte and lymphocyte subsets assayed by incubating whole peripheral blood diluted 1:1 in RPMI-1640 in a culture incubator for 30 minutes. Blood cells were previously stimulated with 1 µM LPS during the 30 minutes, 24h or 48h. Fluorescence of **4.1** was evaluated in the PE-channel (586/42 nm) excited by the blue laser (488nm) and in the V510-channel (528/45) excited by the violet laser (405nm). B) MFI kinetic analysis of **4.1** in the 30 minutes acquisition time for leukocyte and lymphocyte subsets after 48 h incubation at 37 °C with medium (RPMI) or LPS 1 µg/ml. Results of one representative experiment out of three.

4.3. CONCLUSIONS

In summary, molecules **4.1-4.3** have been synthesized and characterized. Fluorescence from **4.1** has been found to be responsive (turn-on) to nitric oxide (aerated medium) with a limit of detection of 88 nM and showing no interference with other RNS, ROS and AA and DHA. The reaction takes place via a deamination process as demonstrated by HRMS. The responsiveness to exogenous (SNAP) and endogenous (LPS induced) NO has been demonstrated in cultured cells (HT-29 and RAW 264.7) and mitochondria have been found as the site of location of this probe (colocalization with Mitotracker Green FM). This is remarkable since most of the reported probes to measure NO at the mitochondria use the triphenylphosphonium cation as a vector. Biological measurements were also carried out in a real sample of peripheral blood, in which **4.1** has been able to discriminate those cells known

for producing high levels of NO (neutrophils and monocytes) from those cells with lower activity in this regard (NK, B and T cells). Beyond the specific performance of **4.1** as a probe for mitochondrial NO, the relevance of this chapter lies in the fact that simple modifications of pyrylium dyes could potentially lead to mitochondrial fluorescent sensors for other mitochondrial species (for instance, using boronate groups for hydrogen peroxide or thiol-reactive groups for glutathione), without using TPP as directing group. Apart from expanding the basic knowledge on mitochondria, styrylpyrylium dyes like the one here reported could be potentially useful for the molecular tracking and imaging of inflammatory cells[49] and hence could orient decision-making processes affecting therapeutic treatments.[50]

4.4. EXPERIMENTAL SECTION

4.4.1. Reagents and instruments

All commercially available reagents and solvents were used as received. ^{1}H and ^{13}C NMR spectra were measured with a Bruker Advance III HD spectrometer (400 MHz for ^{1}H and 101 MHz for ^{13}C). High-resolution mass spectra were performed on a Waters Q-Tof Premier mass spectrometer with an electrospray source. UV-vis spectra were obtained with a Cary 60 UV-vis spectrophotometer, using quartz cuvettes with 1 cm path length and 3 mL volume. Steady-state emission was recorded with an Agilent Cary-Eclipse spectrofluorometer. Cellular images were obtained using a Leica TCS SP8 inverted confocal laser-scanning microscope. Images were processed with Fiji; a subtract background function was employed with a sliding paraboloid function of 50 pixels followed by a median filtering function used with a radius of 1 pixel. Flow cytometric analysis was recorded on BD Accuri^{TM} C6 flow cytometer.

4.4.2. Synthesis of compounds **4.1-4.3**

2,6-bis(4-methoxyphenyl)-4-methylpyrylium tetrafluoroborate was synthesized following the procedure described in Chapter 3.

(E)-4-(4-methoxy-3-nitrostyryl)-2,6-bis(4-methoxyphenyl)pyrylium tetrafluoroborate. (red solid, 0.22 g, 63 % yield). A suspension of 2,6-bis(4-methoxyphenyl)-4-methylpyrylium tetrafluoroborate (0.25 g, 0.63 mmol) and 4-methoxy-3-nitrobenzaldehyde (0.17 g, 0.95 mmol) in acetic acid (10 ml) was heated to reflux (a dark solution was formed) for 24 hours. After cooling down to room temperature, the crude reaction was poured into 200 ml of diethyl ether, and the red precipitate was recovered by filtration, washed, and dried under vacuum.

^{1}H NMR (400 MHz, CD$_3$CN) δ 8.28 – 8.15 (m, 6 H), 8.14 (s, 2H), 8.01 (dd, J = 8.9, 2.2 Hz, 1H), 7.39 (d, J = 9.2 Hz, 1H), 7.35 (d, J = 16.7 Hz, 1H), 7.27 – 7.19 (m, 4H), 4.04 (s, 3H), 3.97 (s, 3H). ^{13}C NMR (101 MHz, CD$_3$CN) δ 169.84, 166.42, 156.25, 145.49, 135.84, 131.44, 131.44, 122.38, 116.63, 116.18, 113.31, 57.97, 56.90, 56.90. HRMS (ESI-TOF)$^+$ calculated for C$_{28}$H$_{24}$NO$_6$$^+$ (M$^+$) (m/z): 470.1598; experimental (M$^+$) (m/z): 470.1595.

Compound 4.1. *(E)-4-(3-amino-4-methoxystyryl)-2,6-bis(4-methoxyphenyl)pyrylium tetrafluoroborate* (dark red solid, 0.16 g, 97 % yield). In a two-neck round-bottom flask, SnCl$_2$.2H$_2$O (0.43 g, 1.89 mmol) was dissolved in acetic acid (10 ml) with HCl (0.29 ml, 9.42 mmol) under continuous stirring and N$_2$ atmosphere. (E)-4-(4-methoxy-3-nitrostyryl)-2,6-bis(4-methoxyphenyl)pyrylium tetrafluoroborate (0. 18 g, 0.31 mmol) was then added, and the reaction was heated to reflux for 2 hours. After cooling down to room temperature, the formed precipitate was recovered by filtration, washed with acetic acid, and dried under vacuum.

^{1}H NMR (400 MHz, DMSO-d$_6$) δ 8.57 (s, 2H), 8.47 (d, J = 15.9 Hz, 1H), 8.34 (d, J = 8.9 Hz, 4H), 7.30 – 7.22 (m, 5H), 7.20 – 7.12 (m, 2H), 7.04 (d, J = 8.2 Hz, 1H), 3.94 (s, 6H), 3.90 (s, 3H). ^{13}C NMR (101 MHz, DMSO-d$_6$) δ 166.80, 164.24, 161.37, 151.30, 149.05, 130.15, 128.00, 121.62, 115.42, 111.62, 55.99, 55.82. HRMS (ESI-TOF)$^+$ calculated for C$_{28}$H$_{26}$NO$_4$$^+$ (M$^+$) (m/z): 440.1856; experimental (M$^+$) (m/z): 440.1858.

(E)-4-(2-methoxy-5-nitrostyryl)-2,6-bis(4-methoxyphenyl)pyrylium tetrafluoroborate (red solid, 0.27 g, yield 76 %). A suspension of 2,6-bis(4-methoxyphenyl)-4-methylpyrylium tetrafluoroborate (0.25 g, 0.63 mmol) and 2-methoxy-5-nitrobenzaldehyde (0.17 g, 0.95 mmol) in acetic acid (10 ml) was heated to reflux (a dark solution was formed) for 24 hours. After

cooling down to room temperature, the crude reaction was poured into 200 ml of diethyl ether, and the red precipitate was recovered by filtration, washed, and dried under vacuum.

^{1}H NMR (400 MHz, CD$_3$CN) δ 8.63 (d, J = 2.8 Hz, 1H), 8.42 – 8.34 (m, 2H), 8.31 – 8.25 (m, 4H), 8.23 (s, 2H), 7.69 (d, J = 16.4 Hz, 1H), 7.29 (d, J = 9.3 Hz, 1H), 7.27 – 7.22 (m, 4H), 4.13 (s, 3H), 3.98 (s, 6H). ^{13}C NMR (101 MHz, CD$_3$CN) δ 170.05, 166.50, 164.79, 162.68, 142.67, 141.07, 131.56, 129.31, 127.43, 126.63, 124.89, 122.33, 116.64, 113.69, 113.63, 57.87, 56.92. HRMS (ESI-TOF)$^+$ calculated for C$_{28}$H$_{24}$NO$_6^+$ (M$^+$) (m/z): 470.1598; experimental (M$^+$) (m/z): 470.1615.

Compound 4.2. *(E)-4-(5-amino-2-methoxystyryl)-2,6-bis(4-methoxyphenyl)pyrylium tetrafluoroborate* (red solid, 0.17 g, 90 % yield). In a two-neck round-bottom flask, SnCl$_2$.2H$_2$O (0.49 g, 2.15 mmol) was dissolved in acetic acid (10 ml) with HCl (0.33 ml, 10.8 mmol) under continuous stirring and N$_2$ atmosphere. (E)-4-(2-methoxy-5-nitrostyryl)-2,6-bis(4-methoxyphenyl)pyrylium tetrafluoroborate (0.2 g, 0.36 mmol) was then added, and the reaction was heated to reflux for 2 hours. After cooling down to room temperature, the formed precipitate was recovered by filtration, washed with acetic acid, and dried under vacuum.

^{1}H NMR (400 MHz, MeOD) δ 8.57 (d, J = 16.4 Hz, 1H), 8.54 (s, 2H), 8.46 – 8.40 (m, 4H), 7.95 (d, J = 2.7 Hz, 1H), 7.79 (d, J = 16.3 Hz, 1H), 7.59 (dd, J = 8.9, 2.7 Hz, 1H), 7.38 (d, J = 9.0 Hz, 1H), 7.35 – 7.29 (m, 4H), 4.14 (s, 3H), 4.03 (s, 6H). ^{13}C NMR (101 MHz, MeOD) δ 170.47, 166.98, 163.49, 160.82, 142.00, 131.71, 128.53, 127.37, 126.33, 125.64, 125.28, 122.78, 116.80, 114.52, 113.51, 57.05, 56.60. HRMS (ESI-TOF)$^+$ calculated for C$_{28}$H$_{26}$NO$_4^+$ (M$^+$) (m/z): 440.1856; experimental (M$^+$) (m/z): 440.1854.

(E)-2,6-bis(4-methoxyphenyl)-4-(3-nitrostyryl)pyrylium tetrafluoroborate. (dark brown solid, 0.21 g, 79 % yield) A suspension of 2,6-bis(4-methoxyphenyl)-4-methylpyrylium tetrafluoroborate (0.20 g, 0.51 mmol) and 3-nitrobenzaldehyde (0.12 g, 0.76 mmol) in acetic acid (10 ml) was heated to reflux (a dark solution was formed) for 24 hours. After cooling down to room temperature, the crude reaction was poured into 200 ml of diethyl ether, and the red precipitate was recovered by filtration, washed, and dried under vacuum.

^{1}H NMR (400 MHz, CD$_3$CN) δ 8.61 (t, J = 2.0 Hz, 1H), 8.35 (ddd, J = 8.2, 2.2, 0.9 Hz, 1H), 8.33 – 8.24 (m, 7H), 8.15 (d, J = 7.8 Hz, 1H), 7.78 (t, J = 8.0 Hz, 1H), 7.57 (d, J = 16.3 Hz, 1H), 7.29 – 7.23 (m, 4H), 3.98 (s, 6H). ^{13}C NMR (101 MHz, CD$_3$CN) δ 170.37, 166.62, 162.07, 144.71, 135.66, 131.79, 131.62, 126.76, 124.07, 122.28, 116.71, 113.87, 56.94. HRMS (ESI-TOF)$^+$ calculated for C$_{27}$H$_{22}$NO$_5^+$ (M$^+$) (m/z): 440.1492; experimental (M$^+$) (m/z): 440.1491.

Compound 4.3. *(E)-4-(3-aminostyryl)-2,6-bis(4-methoxyphenyl)pyrylium tetrafluoroborate* (red solid, 0.09 g, 95 % yield). In a two-neck round-bottom flask, SnCl$_2$.2H$_2$O (0.26 g, 1.12 mmol) was dissolved in acetic acid (10 ml) with HCl (0.18 ml, 5.87 mmol) under continuous stirring and N$_2$ atmosphere. (E)-2,6-bis(4-methoxyphenyl)-4-(3-nitrostyryl)pyrylium tetrafluoroborate (0.10 g, 0.19 mmol) was then added, and the reaction was heated to reflux for 2 hours. After cooling down to room temperature, the formed precipitate was recovered by filtration, washed with acetic acid, and dried under vacuum.

^{1}H NMR (400 MHz, DMSO-d$_6$) δ 8.69 (s, 2H), 8.47 (d, J = 16.1 Hz, 1H), 8.39 (d, J = 8.8 Hz, 4H), 7.43 (d, J = 16.1 Hz, 1H), 7.31 (d, J = 9.0 Hz, 4H), 7.26 (d, J = 7.8 Hz, 1H), 7.11 – 7.00 (m, 2H), 6.84 (d, J = 8.0 Hz, 1H), 3.96 (s, 6H). ^{13}C NMR (101 MHz, DMSO-d$_6$) δ 168.53,

164.86, 129.49, 120.61, 114.60, 111.39, 54.40. HRMS (ESI-TOF)$^+$ calculated for $C_{27}H_{24}NO_3^+$ (M$^+$) (m/z): 410.1751; experimental (M$^+$) (m/z): 410.1750.

4.4.3. Fluorescence measurements

10 µM solutions of **4.1-4.3** in PBS 10 mM, pH 7.4 (20 % DMF as a cosolvent) were prepared. For the kinetic analysis, different equivalents of DEA NONOate were added, and the absorption spectra/emission spectra/maximum fluorescence intensity was measured over time. DEA NONOate is a commercial NO donor with a half-life of 16 minutes at 22-25 °C in 0.1 M phosphate buffer (pH 7.4). It liberates 1.5 moles of NO per mole of the parent compound. For the concentration dependence study, different aliquots (3 ml each) of 10 µM solutions of **4.1** were titrated by adding increasing volumes of 12.25 mM DEA NONOate stock solution (in NaOH 10 mM). The fluorescence spectra were measured after 20 minutes of reaction at the corresponding excitation wavelength (480 nm).

4.4.4. Preparation of gaseous NO

Gaseous nitric oxide (NO) was synthesized by a reaction between KI (1 M) and $NaNO_2$ (1 M) catalyzed by acid, according to the following reaction:

$$2 \, NO_2^- \, (aq) + 2 \, I^- \, (aq) + 4 \, H^+(aq) \rightarrow 2 \, NO \, (g) + I_2 \, (s) + 2 \, H_2O \, (l)$$
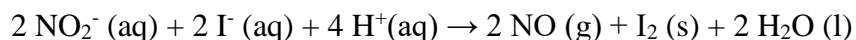
4.4.5. Selectivity test

Different analytes (final concentration: 500 µM): NO, ClO$^-$, H_2O_2, NO_2^- NO_3^-, O_2^-, HO$^-$, $^1O_2$, ascorbic acid (AA), dehydroascorbic acid (DHA), and ONOO$^-$ were added to 10 µM solutions of **4.1** in PBS 10 mM, pH 7.4 (20 % DMF as a cosolvent). The resulting solutions were kept at ambient temperature for 20 min and then the emission spectra were recorded (λ_{exc} = 480 nm). Aqueous solutions of $NaNO_2$, $NaNO_3$, AA and NaClO were prepared freshly and

used as sources of NO_2^-, NO_3^-, AA and ClO^-, respectively. Dimethyl sulfoxide solutions of KO_2 and DHA were used as sources of O_2^- and DHA. H_2O_2 was diluted promptly from 35 % wt solution. Hydroxyl radicals were generated by the reaction of Fe^{2+} with H_2O_2 (molar ratio of Fe^{2+} to H_2O_2 is 1:10).[58] Nitric oxide (NO) was generated from DEA/NONOate (stock solution 12.25 mM in 10 mM NaOH). Singlet oxygen ($^1O_2$) was generated from ClO^- and H_2O_2.[59] $ONOO^-$ was prepared by reaction of NO_2^- and H_2O_2.[60]

4.4.6. Cell cultures and treatments

HT29 human colon cancer cell line and RAW 264.7 (ATCC® TIB-71™) murine macrophage cell line were employed to test probe **4.1** in an *in vitro* setting. Cell cultures were maintained in DMEM high glucose supplemented with 10 % inactivated fetal bovine serum, 2 mM L-glutamine, 1% P/E (penicillin and streptomycin) at 37 ⁰C, in a cell culture incubator with a humidified 5 % CO_2/95 % air atmosphere. Cell cultures were used for experiments at passage numbers lower than 20.

4.4.7. Effects on Cell Growth/Viability

The cytotoxic effects of probe **4.1** were assessed using the MTT assay in RAW 264.7 cells. Briefly, cells were grown in microplates (tissue culture grade, 96 wells, flat bottom) in a final volume of 100 μL culture medium per well in a humidified atmosphere (37 °C, 5 % CO_2/95 % air), before the incubation with different concentrations of **4.1**, from 0 to 1000 μM (n = 3). After the incubation period (48 h), 10 μl of the MTT labeling reagent (final concentration 0.5 mg/ml) was added to each well and incubated for 3 h in a humidified atmosphere (37 °C, 5% CO_2). The purple formazan crystals formed were then dissolved by the addition of 100 μL of DMSO into each well. Using a microplate reader (Multiskan FC, Termo Scientific), the absorbance of the samples at 550 nm was measured.

4.4.8. Visualization of Exogenous NO in HT29 living cells

10 mM stock solution of **4.1** in DMSO was prepared. HT29 cells were seeded (5×10^4 cells/mL) in sterile µ-Slide 4-well-chamber slide (Ibidi, Inycom, Madrid, Spain). After 24 h incubation (37 °C in a 5 % CO_2/95 % air), the culture medium was removed and freshly prepared serum-free medium with **4.1** (10 µM, 0.1% DMSO as the cosolvent) was added. Cells were then incubated at 37 °C for 30 minutes (5 minutes before this time end, 0.01 mg/ml Hoechst 33342 was added to stain nuclei). For the positive control group, **4.1**-loaded cells were then supplied with NO (100 µM SNAP as the donor) in PBS for another 60 min. In all experiments, the cells were washed with PBS (3×0.5 mL/well) before the fluorescence imaging using a confocal microscope. In colocalization analysis, **4.1** was coincubated with Mitotracker Green FM (ThermoFisher M7514, 75 nM).

4.4.9. Flow Cytometry Analysis of NO in HT29 cells

HT29 cells were seeded into a six-well plate at the density of 1×10^5 cells/ml. After 24 h incubation (37 °C in a 5 % CO_2/95 % air), the culture medium was removed and freshly prepared serum-free medium with **4.1** (10 µM, 0.1% DMSO as the cosolvent) was added. Cells were then incubated at 37 °C for 30 minutes, washed with PBS (3×1 mL/well), and further incubated with SNAP (100 µM), for 1 hour. The well-containing cells only was used as the blank group, and the group of **4.1**-loaded cells was employed as control. Before flow cytometry analysis, cells were collected and washed with PBS (3×1 mL/tube or Eppendorf). All the measurements were performed three times.

4.4.10. Visualization of Endogenous NO in Raw 264.7 macrophage cells

10 mM stock solution of **4.1** in DMSO was prepared. RAW 264.7 macrophage cells were seeded (5×10^4 cells/ mL) in sterile μ-Slide 4-well-chamber slide (Ibidi, Inycom, Madrid, Spain). After 24 h incubation (37 °C in a 5% CO_2/95% air), the culture medium was removed and fresh serum-free medium containing 20 µg/mL of LPS was added. After incubation at 37 °C overnight, LPS activated RAW 264.7 cells were incubated with fresh serum-free culture medium containing **4.1** (10 μM, 0.1% DMSO as the cosolvent) for another 30 minutes (5 minutes before this time end, 0.01 mg/ml Hoechst 33342 was added to stain nuclei). The cells were washed with PBS (3×0.5 mL/well) before the fluorescence imaging using a confocal microscope. In a control experiment, the cells were treated with 20 µg/mL LPS and 50 μM iNOS inhibitor L-NMMA overnight and then incubated with probe **4.1** (10 μM, 0.1% DMSO as the cosolvent) for 30 min (5 minutes before this time end, 0.01 mg/ml Hoechst 33342 was added to stain nuclei).

4.4.11. Flow Cytometry Analysis of NO in inflamed macrophage cells

RAW 264.7 cells were seeded into a six-well plate at the density of 1×10^5 cells/ml. After 24 h incubation (37 °C in a 5 % CO_2/95 % air), the culture medium was removed and freshly prepared serum-free medium with LPS (20 µg/mL) was added. Cells were then incubated at 37 °C overnight, washed with PBS (3×1 mL/well), and further incubated with **4.1** (10 µM, 0.1% DMSO as the cosolvent), for 30 minutes. **4.1**-stained cells were washed with PBS (3×1 mL/well) and removed from the plate using a cell scraper. The well-containing cells only were used as the blank group, and the group of **4.1**-loaded cells was employed as control. Before flow cytometry analysis, cells were washed with PBS (3×1 mL/tube). In a control experiment, the cells were treated with 20 µg/mL LPS and 50 μM iNOS inhibitor L-NMMA overnight and

then incubated with probe **4.1** (10 µM, 0.1% DMSO as the cosolvent) for 30 min. All the measurements were performed three times.

4.4.12. Intracellular NO analysis by flow cytometry in peripheral blood leukocytes

Whole heparin anti-coagulated peripheral blood diluted 1:1 in 100 µl of RPMI-1640 medium (Gibco, Thermo Fisher Scientific) or RPMI + Lipopolysaccharide 1 µg/ml (LPS, Sigma-Aldrich), were incubated in a U-button 96-well plate for 0 (ex-vivo), 24 or 48 hours in a cell incubator at 37 °C and 5% CO_2. Blood cells were labelled with CD8-BV605 (SK1, Becton-Dickinson, BD), CD16-V450 (3G8, BD), CD45-APC-H7 (2D1, BD), CD56-BV711 (NCAM16.2, BD), CD64-APC (10.1, BD), and HLA-DR-BV786 (L243, Biolegend) monoclonal antibodies during 5 min at 37 °C and then transferred to a flow cytometry tube containing 1.5 ml pre-warmed RPMI with 10 µM **4.1** and immediately acquired during 30 minutes at a low flow rate (time was recorded). During the acquisition, the tube was incubated in a 37 °C water bath protected from light. The level of NO was evaluated as mean fluorescence intensity (MFI) of **4.1** using FACSLyric and DIVA 9.0 software (BD). Photomultiplier voltages were previously adjusted using CS&T beads (BD). Double thresholds in FSC (Forward side scatter) and CD45 APC-H7 were set to differentiate leukocytes (CD45+) from red blood cells and platelets (CD45-). The MFI of **4.1** was evaluated in the PE-channel (586/42 nm) excited by the blue laser (488 nm) and in the V500-channel (528/45) excited by the violet laser (405 nm). Staining with other 488 nm excited fluorochromes was ruled out to avoid compensation with the PE-channel.

4.5. SPECTROSCOPIC DATA OF COMPOUNDS

(E)-4-(4-methoxy-3-nitrostyryl)-2,6-bis(4-methoxyphenyl)pyrylium tetrafluoroborate
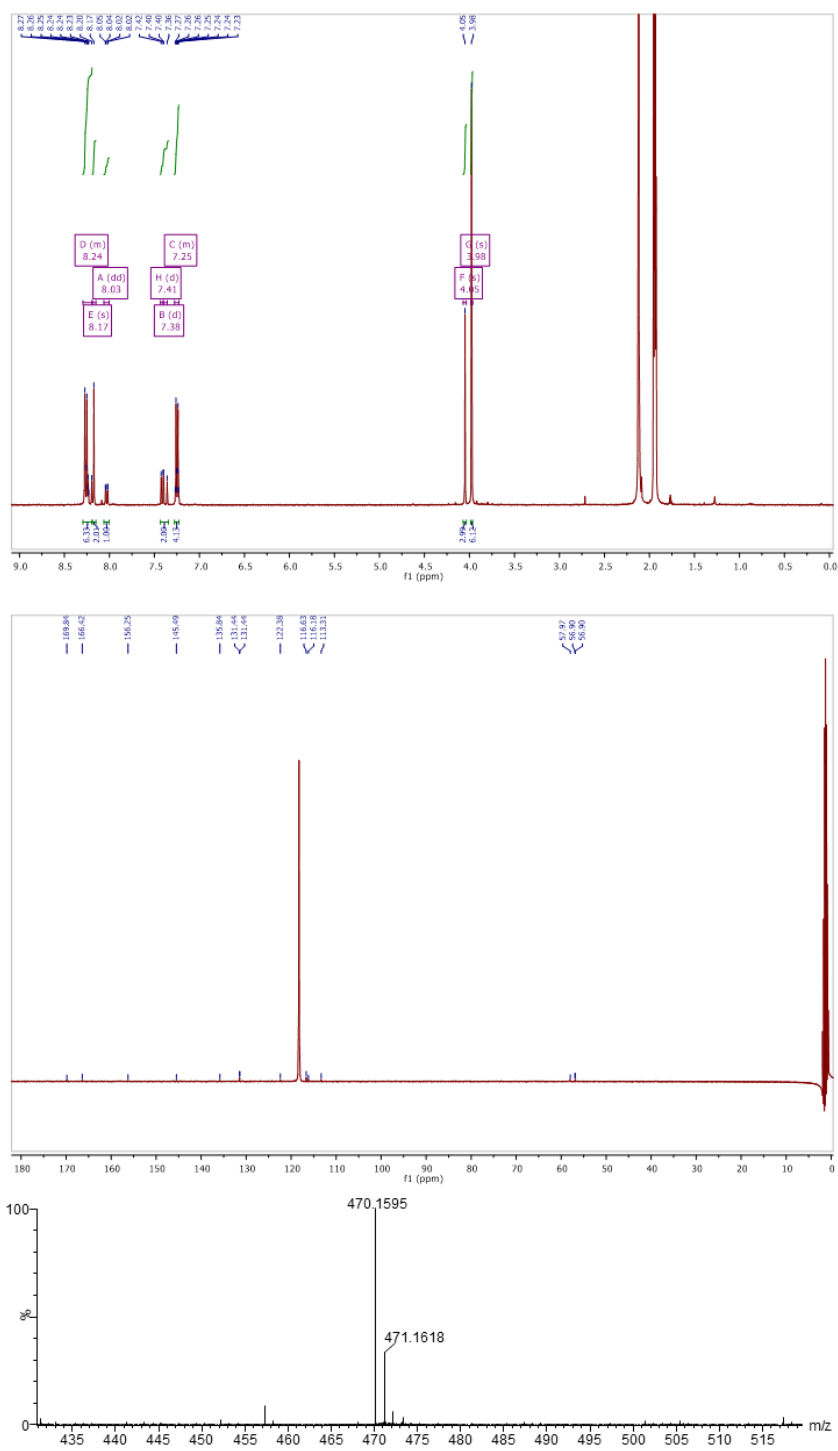
Figure 17. ¹H NMR, ¹³C NMR (CD₃CN) and HRMS spectra of the precursor of compound **4.1**.

Compound 4.1
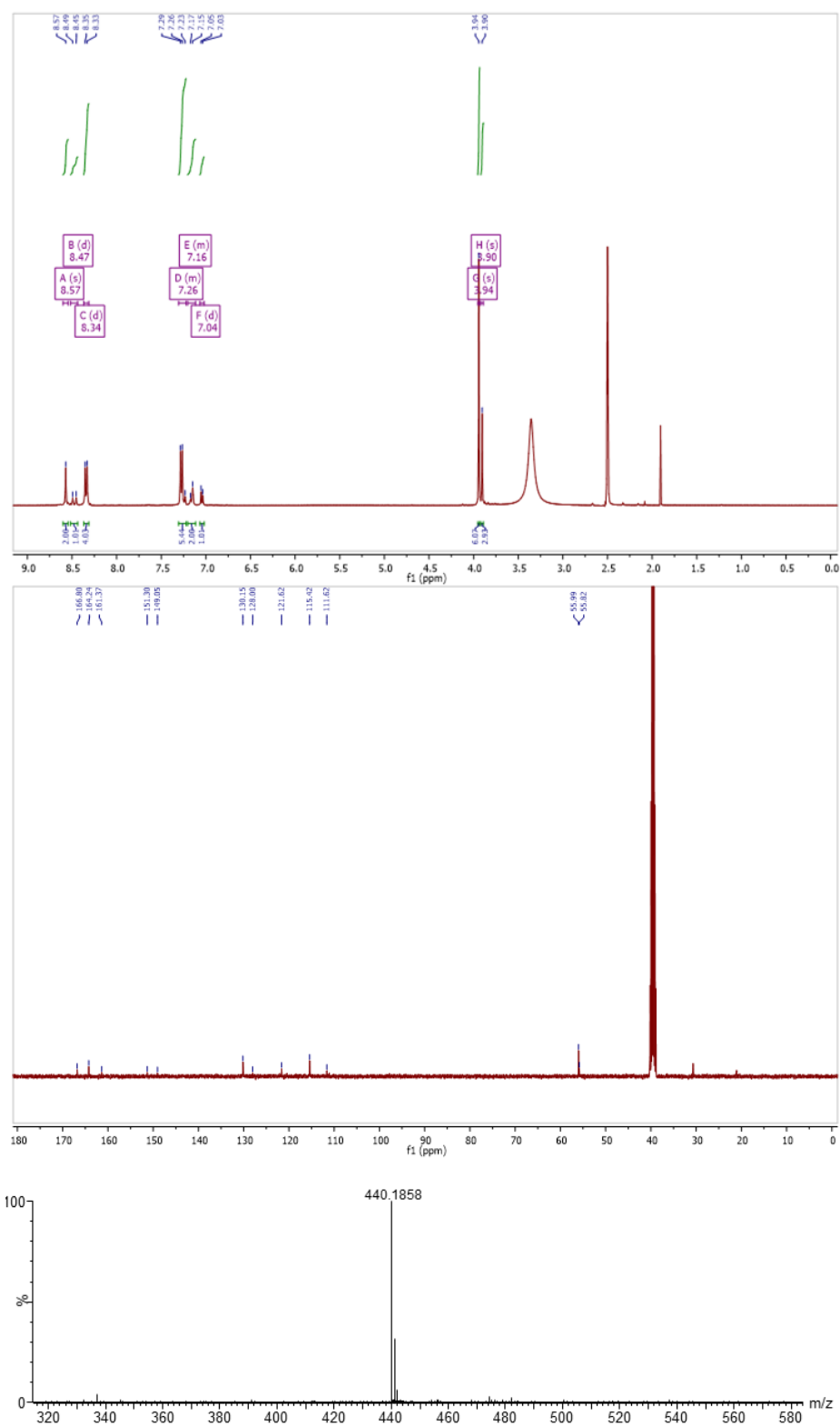
Figure 18. ^{1}H NMR, ^{13}C NMR (DMSO-d$_6$) and HRMS spectra of compound **4.1**.

(E)-4-(2-methoxy-5-nitrostyryl)-2,6-bis(4-methoxyphenyl)pyrylium tetrafluoroborate
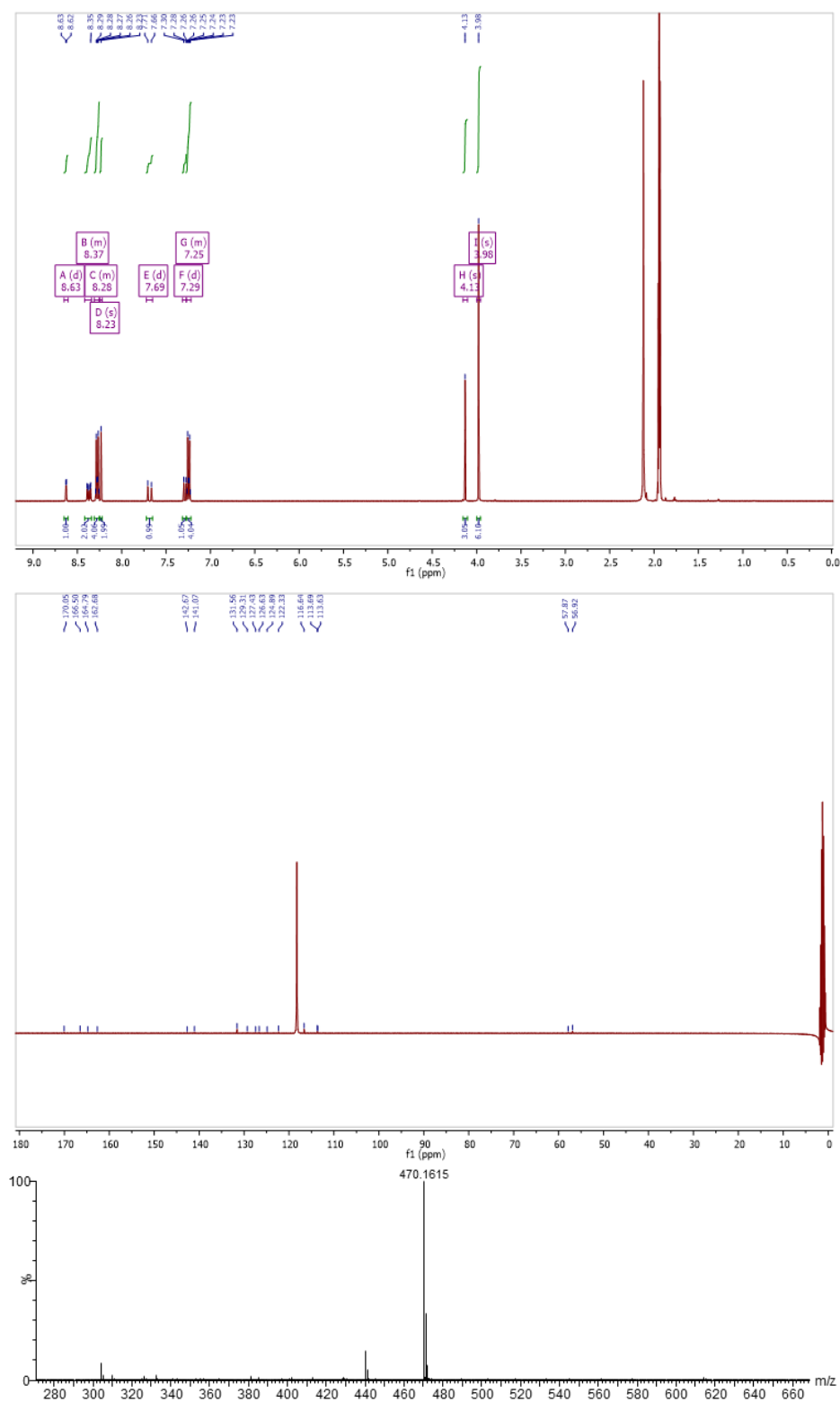
Figure 19. ¹H NMR, ¹³C NMR (CD₃CN) and HRMS spectra of the precursor of compound **4.2**.

Compound 4.2
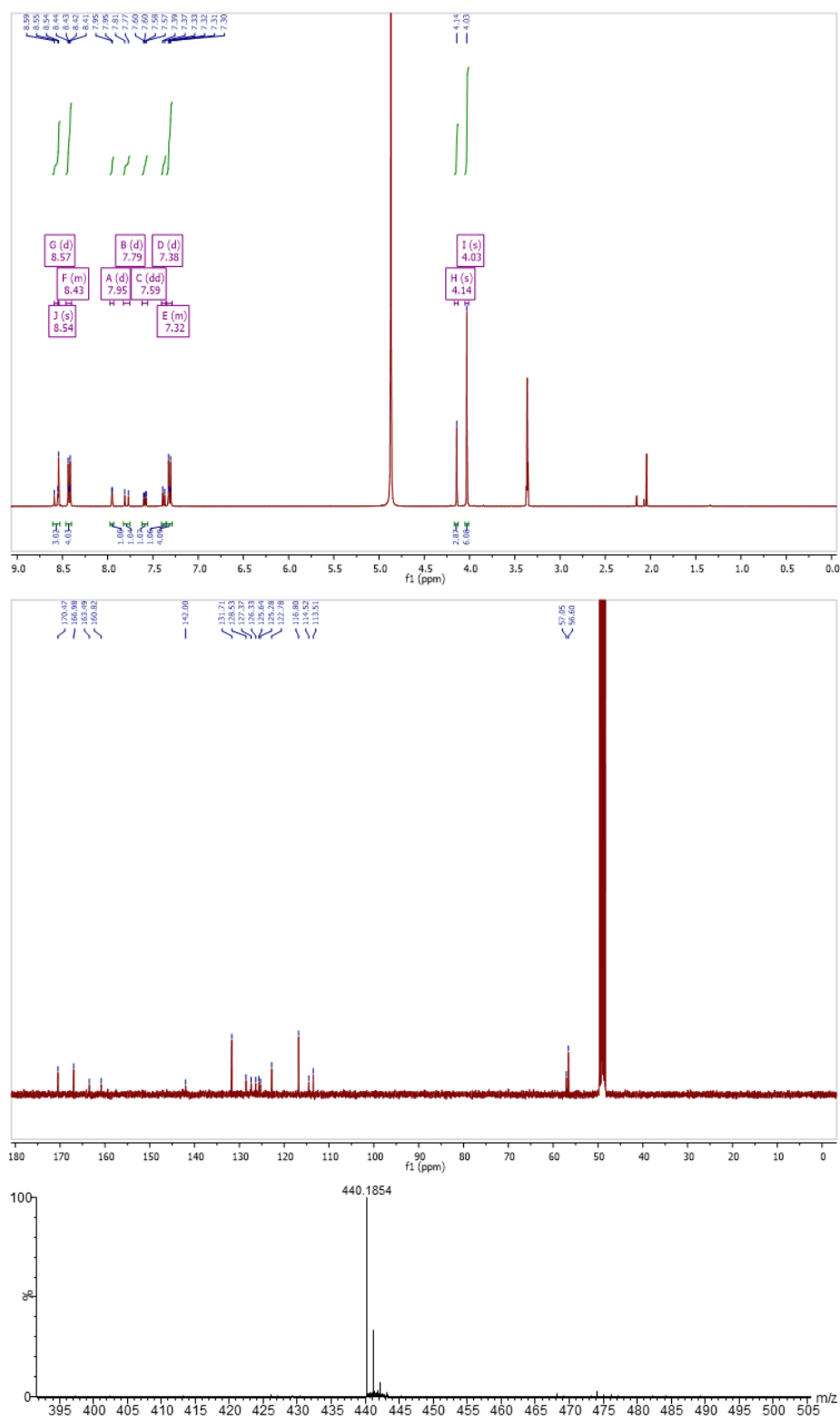
Figure 20. ^{1}H NMR, ^{13}C NMR (CD$_3$OD) and HRMS spectra of compound **4.2**.

(E)-2,6-bis(4-methoxyphenyl)-4-(3-nitrostyryl)pyrylium tetrafluoroborate
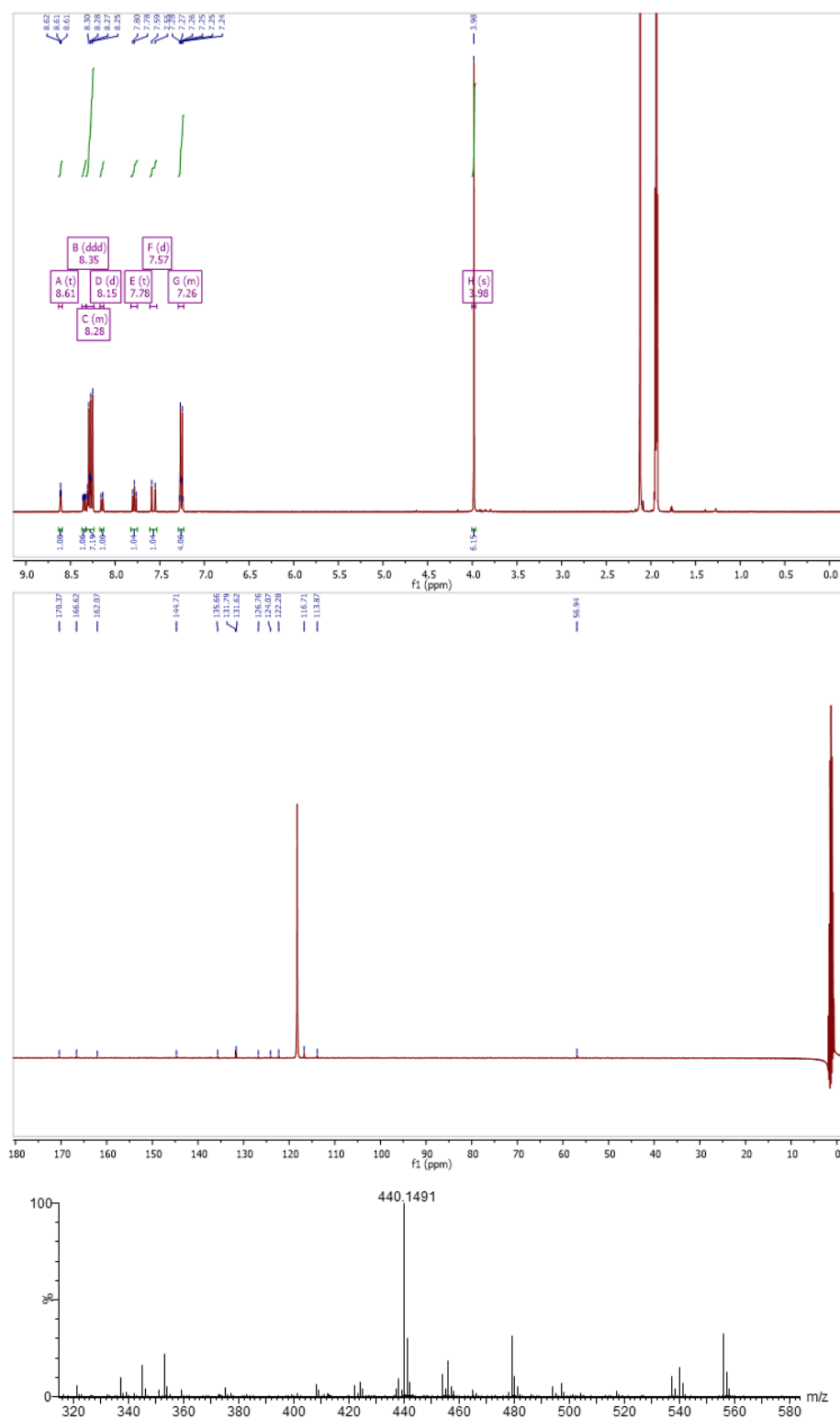
Figure 21. ^{1}H NMR, ^{13}C NMR (CD$_3$CN) and HRMS spectra of the precursor of compound **4.3**.

Compound 4.3
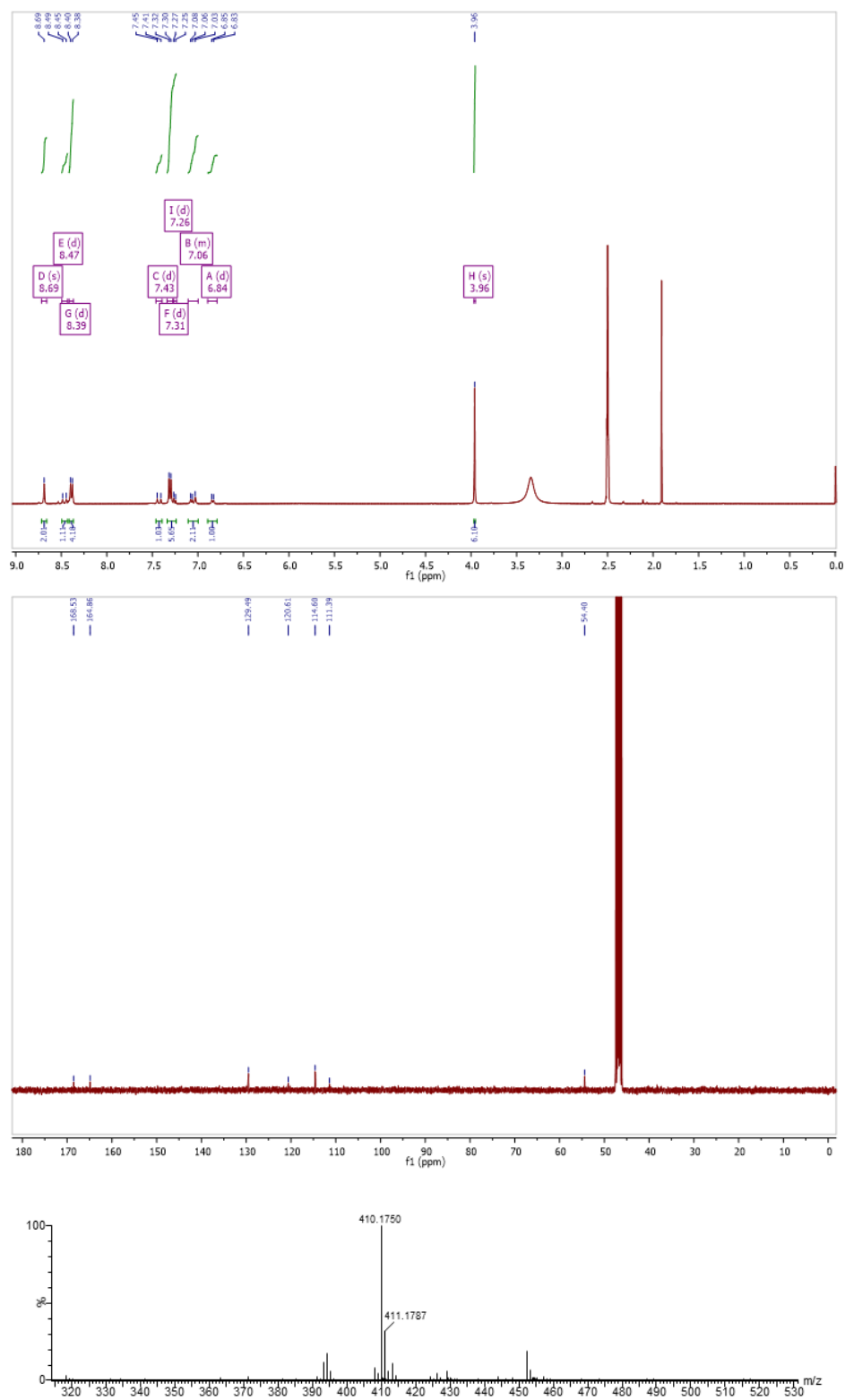
Figure 22. ^{1}H NMR, ^{13}C NMR (CD$_3$CN) and HRMS spectra of compound **4.3**.

4.6. REFERENCES

1   M. J. Ruedas-Rama, J. D. Walters, A. Orte and E. A. H. Hall, Fluorescent nanoparticles for intracellular sensing: A review, *Anal. Chim. Acta*, 2012, **751**, 1–23.

2   L. D. Lavis and R. T. Raines, Bright building blocks for chemical biology, *ACS Chem. Biol.*, 2014, **9**, 855–866.

3   L. D. Lavis, Chemistry Is Dead. Long Live Chemistry!, *Biochemistry*, 2017, **56**, 5165–5170.

4   X. Huang, J. Song, B. C. Yung, X. Huang, Y. Xiong and X. Chen, Ratiometric optical nanoprobes enable accurate molecular detection and imaging, *Chem. Soc. Rev.*, 2018, **47**, 2873–2920.

5   X. Luo, L. Gu, X. Qian and Y. Yang, Molecular probe design via the 'covalent-assembly' principle, *Chem. Commun.*, 2020, **56**, 9067–9078.

6   D. D. Thomas, L. A. Ridnour, J. S. Isenberg, W. Flores-Santana, C. H. Switzer, S. Donzelli, P. Hussain, C. Vecoli, N. Paolocci, S. Ambs, C. A. Colton, C. C. Harris, D. D. Roberts and D. A. Wink, The chemical biology of nitric oxide: Implications in cellular signaling, *Free Radic. Biol. Med.*, 2008, **45**, 18–31.

7   J. C. Toledo and O. Augusto, Connecting the chemical and biological properties of nitric oxide, *Chem. Res. Toxicol.*, 2012, **25**, 975–989.

8   R. Radi, Oxygen radicals, nitric oxide, and peroxynitrite: Redox pathways in molecular medicine, *Proc. Natl. Acad. Sci. U. S. A.*, 2018, **115**, 5839–5848.

9   H. Kojima, N. Nakatsubo, K. Kikuchi, S. Kawahara, Y. Kirino, H. Nagoshi, Y. Hirata

and T. Nagano, Detection and Imaging of Nitric Oxide with Novel Fluorescent Indicators: Diaminofluoresceins, *Anal. Chem.*, 1998, **70**, 2446–2453.

10   H. Kojima and T. Nagano, Fluorescent indicators for nitric oxide, *Angew. Chemie - Int. Ed.*, 1999, **38**, 3209–3212.

11   M. H. Lim, D. Xu and S. J. Lippard, Visualization of nitric oxide in living cells by a copper-based fluorescent probe, *Nat. Chem. Biol.*, 2006, **2**, 375–380.

12   L. Yuan, W. Lin, Y. Xie, B. Chen and J. Song, Development of a ratiometric fluorescent sensor for ratiometric imaging of endogenously produced nitric oxide in macrophage cells, *Chem. Commun.*, 2011, **47**, 9372–9374.

13   L. Yuan, W. Lin, Y. Xie, B. Chen and S. Zhu, Single fluorescent probe responds to H_2O_2, NO, and H_2O_2/NO with three different sets of fluorescence signals, *J. Am. Chem. Soc.*, 2012, **134**, 1305–1315.

14   M. Wang, Z. Xu, X. Wang and J. Cui, A fluorescent and colorimetric chemosensor for nitric oxide based on 1,8-naphthalimide, *Dye. Pigment.*, 2013, **96**, 333–337.

15   Z. Dai, L. Tian, B. Song, X. Liu and J. Yuan, Development of a novel lysosome-targetable time-gated luminescence probe for ratiometric and luminescence lifetime detection of nitric oxide in vivo, *Chem. Sci.*, 2017, **8**, 1969–1976.

16   H. W. Yao, J. B. Chen, X. F. Guo and H. Wang, Simultaneous monitoring of intra- and extracellular nitric oxide in living cells by means of dual-color fluorescence imaging, *Nitric Oxide - Biol. Chem.*, 2017, **67**, 30–38.

17   T. Zhou, J. Wang, J. Xu, C. Zheng, Y. Niu, C. Wang, F. Xu, L. Yuan, X. Zhao, L. Liang

and P. Xu, A Smart Fluorescent Probe for NO Detection and Application in Myocardial Fibrosis Imaging, *Anal. Chem.*, 2020, **92**, 5064–5072.

18   Y. Yang, S. K. Seidlits, M. M. Adams, V. M. Lynch, C. E. Schmidt, E. V. Anslyn and J. B. Shear, A highly selective low-background fluorescent imaging agent for nitric oxide, *J. Am. Chem. Soc.*, 2010, **132**, 13114–13116.

19   L. Chen, D. Wu and J. Yoon, An ESIPT based fluorescence probe for ratiometric monitoring of nitric oxide, *Sensors Actuators, B Chem.*, 2018, **259**, 347–353.

20   P. R. Escamilla, Y. Shen, Q. Zhang, D. S. Hernandez, C. J. Howard, X. Qian, D. Y. Filonov, A. V. Kinev, J. B. Shear, E. V. Anslyn and Y. Yang, 2-Amino-3′-dialkylaminobiphenyl-based fluorescent intracellular probes for nitric oxide surrogate N_2O_3, *Chem. Sci.*, 2020, **11**, 1394–1403.

21   T. W. Shiue, Y. H. Chen, C. M. Wu, G. Singh, H. Y. Chen, C. H. Hung, W. F. Liaw and Y. M. Wang, Nitric oxide turn-on fluorescent probe based on deamination of aromatic primary monoamines, *Inorg. Chem.*, 2012, **51**, 5400–5408.

22   Y. Huo, J. Miao, Y. Li, Y. Shi, H. Shi and W. Guo, Aromatic primary monoamine-based fast-response and highly specific fluorescent probes for imaging the biological signaling molecule nitric oxide in living cells and organisms, *J. Mater. Chem. B*, 2017, **5**, 2483–2490.

23   R. Leggett, P. Thomas, M. J. Marín, J. Gavrilovic and D. A. Russell, Imaging of compartmentalised intracellular nitric oxide, induced during bacterial phagocytosis, using a metalloprotein-gold nanoparticle conjugate, *Analyst*, 2017, **142**, 4099–4105.

24   Y. Huo, J. Miao, J. Fang, H. Shi, J. Wang and W. Guo, Aromatic secondary amine-functionalized fluorescent NO probes: improved detection sensitivity for NO and potential applications in cancer immunotherapy studies, *Chem. Sci.*, 2019, **10**, 145–152.

25   Y. Liu, H. Fan, Y. Wen, T. Jia, Q. Su and F. Li, ICT-based near infrared fluorescent switch-on probe for nitric oxide bioimaging in vivo, *Dye. Pigment.*, 2019, **166**, 211–216.

26   P. Liu, B. Li, J. Zheng, Q. Liang, C. Wu, L. Huang, P. Zhang, Y. Jia and S. Wang, A novel N-nitrosation-based ratiometric fluorescent probe for highly selective imaging endogenous nitric oxide in living cells and zebrafish, *Sensors Actuators, B Chem.*, 2021, **329**, 129147.

27   S. F. Ma, Q. H. Wang, F. T. Liu, H. L. Wang, D. C. Fang, B. Gong, L. He and Z. L. Lu, Dihydropyridine-based fluorescence probe for nitric oxide, *RSC Adv.*, 2016, **6**, 85698–85703.

28   C. Gao, L. Lin, W. Sun, Z. L. Tan, J. R. Huang, L. He and Z. L. Lu, Dihydropyridine-derived BODIPY probe for detecting exogenous and endogenous nitric oxide in mitochondria, *Talanta*, 2018, **176**, 382–388.

29   T. Nagano and T. Yoshimura, Bioimaging of nitric oxide, *Chem. Rev.*, 2002, **102**, 1235–1269.

30   L. E. McQuade and S. J. Lippard, Fluorescent probes to investigate nitric oxide and other reactive nitrogen species in biology (truncated form: fluorescent probes of reactive nitrogen species), *Curr. Opin. Chem. Biol.*, 2010, **14**, 43–49.

31   P. N. Coneski and M. H. Schoenfisch, Nitric oxide release: Part III. Measurement and

reporting, *Chem. Soc. Rev.*, 2012, **41**, 3753–3758.

32   X. Chen, F. Wang, J. Y. Hyun, T. Wei, J. Qiang, X. Ren, I. Shin and J. Yoon, Recent progress in the development of fluorescent, luminescent and colorimetric probes for detection of reactive oxygen and nitrogen species, *Chem. Soc. Rev.*, 2016, **45**, 2976–3016.

33   K. Yang, J. L. Kolanowski and E. J. New, Mitochondrially targeted fluorescent redox sensors, *Interface Focus*, 2017, **7**, 20160105.

34   B. Kalyanaraman and J. Zielonka, Small-molecule luminescent probes for the detection of cellular oxidizing and nitrating species, *Free Radic. Biol. Med.*, 2018, **128**, 3–22.

35   M. N. Möller, N. Rios, M. Trujillo, R. Radi, A. Denicola and B. Alvarez, Detection and quantification of nitric oxide-derived oxidants in biological systems, *J. Biol. Chem.*, 2019, **294**, 14776–14802.

36   Y. Chen, Recent developments of fluorescent probes for detection and bioimaging of nitric oxide, *Nitric Oxide - Biol. Chem.*, 2020, **98**, 1–19.

37   L. Wang, J. Zhang, X. An and H. Duan, Recent progress on the organic and metal complex-based fluorescent probes for monitoring nitric oxide in living biological systems, *Org. Biomol. Chem.*, 2020, **18**, 1522–1549.

38   H. Yu, X. Zhang, Y. Xiao, W. Zou, L. Wang and L. Jin, Targetable fluorescent probe for monitoring exogenous and endogenous NO in mitochondria of living cells, *Anal. Chem.*, 2013, **85**, 7076–7084.

39   Y. Q. Sun, J. Liu, H. Zhang, Y. Huo, X. Lv, Y. Shi and W. Guo, A mitochondria-targetable fluorescent probe for dual-channel no imaging assisted by intracellular

cysteine and glutathione, *J. Am. Chem. Soc.*, 2014, **136**, 12520–12523.

40   C. Wang, X. Song, Z. Han, X. Li, Y. Xu and Y. Xiao, Monitoring Nitric Oxide in Subcellular Compartments by Hybrid Probe Based on Rhodamine Spirolactam and SNAP-tag, *ACS Chem. Biol.*, 2016, **11**, 2033–2040.

41   X. Zhu, J. Q. Chen, C. Ma, X. Liu, X. P. Cao and H. Zhang, A ratiometric mitochondria-Targeting two-photon fluorescent probe for imaging of nitric oxide in vivo, *Analyst*, 2017, **142**, 4623–4628.

42   Z. Yu, J. Zhou, X. Dong, W. Zhao and Z. Chen, Visualizing Nitric oxide in mitochondria and lysosomes of living cells with N-Nitrosation of BODIPY-based fluorescent probes, *Anal. Chim. Acta*, 2019, **1067**, 88–97.

43   X. He, F. Ding, W. Xu, C. Xu, Y. Li, Y. Qian, S. Zhao, H. Chen and J. Shen, FRET-based colorimetric and ratiometric sensor for visualizing pH change and application for bioimaging in living cells, bacteria and zebrafish, *Anal. Chim. Acta*, 2020, **1127**, 29–38.

44   S. S. Sabharwal and P. T. Schumacker, Mitochondrial ROS in cancer: initiators, amplifiers or an Achilles' heel?, *Nat. Rev. Cancer*, 2014, **14**, 709–721.

45   B. Kalyanaraman, G. Cheng, M. Hardy, O. Ouari, B. Bennett and J. Zielonka, Teaching the basics of reactive oxygen species and their relevance to cancer biology: Mitochondrial reactive oxygen species detection, redox signaling, and targeted therapies, *Redox Biol.*, 2018, **15**, 347–362.

46   E. Ramond, A. Jamet, M. Coureuil and A. Charbit, Pivotal role of mitochondria in macrophage response to bacterial pathogens, *Front. Immunol.*, 2019, **10**, 1–11.

47   M. Khan, G. H. Syed, S. J. Kim and A. Siddiqui, Mitochondrial dynamics and viral infections: A close nexus, *Biochim. Biophys. Acta - Mol. Cell Res.*, 2015, **1853**, 2822–2833.

48   N. Apostolova, H. A. Funes, A. Blas-Garcia, F. Alegre, M. Polo and J. V. Esplugues, Involvement of nitric oxide in the mitochondrial action of efavirenz: A differential effect on neurons and glial cells, *J. Infect. Dis.*, 2015, **211**, 1953–1958.

49   A. Fernández and M. Vendrell, Smart fluorescent probes for imaging macrophage activity, *Chem. Soc. Rev.*, 2016, **45**, 1182–1196.

50   G. P. Birch, T. Campbell, M. Bradley and K. Dhaliwal, Optical Molecular Imaging of Inflammatory Cells in Interventional Medicine–An Emerging Strategy, *Front. Oncol.*, 2019, **9**, 882.

51   S. Samanta, Y. He, A. Sharma, J. Kim, W. Pan, Z. Yang, J. Li, W. Yan, L. Liu, J. Qu and J. S. Kim, Fluorescent Probes for Nanoscopic Imaging of Mitochondria, *Chem*, 2019, **5**, 1697–1726.

52   S. Chakraborty, M. M. Joseph, S. Varughese, S. Ghosh, K. K. Maiti, A. Samanta and A. Ajayaghosh, A new pentacyclic pyrylium fluorescent probe that responds to pH imbalance during apoptosis, *Chem. Sci.*, 2020, 12695–12700.

53   E. Molnár, S. Kuntam, P. K. R. Cingaram, B. Peksel, B. Suresh, G. Fábián, L. Z. Fehér, A. Bokros, Á. Medgyesi, F. Ayaydin and L. G. Puskás, Combination of small molecule microarray and confocal microscopy techniques for live cell staining fluorescent dye discovery, *Molecules*, 2013, **18**, 9999–10013.

54   S. Y. Wen, W. Zhang, T. B. Ren, Q. L. Zhang, Y. P. Liu, L. Shi, R. Hu, X. B. Zhang and L. Yuan, Donor and Ring-Fusing Engineering for Far-Red to Near-Infrared Triphenylpyrylium Fluorophores with Enhanced Fluorescence Performance for Sensing and Imaging, *Chem. - A Eur. J.*, 2019, **25**, 6973–6979.

55   X. Chen, L. Yan, Y. Liu, Y. Yang and J. You, Switchable cascade C–H annulation to polycyclic pyryliums and pyridiniums: discovering mitochondria-targeting fluorescent probes, *Chem. Commun.*, 2020, 15080–15083.

56   G. Laffi, M. Foschi, E. Masini, A. Simoni, L. Mugnai, G. La Villa, G. Barletta, P. F. Mannaioni and P. Gentilini, Increased production of nitric oxide by neutrophils and monocytes from cirrhotic patients with ascites and hyperdynamic circulation, *Hepatology*, 1995, **22**, 1666–1673.

57   N. C. C. Schachnik, V. Peruhype-Magalhães, G. M. M. Paula, F. Lucas, V. M. Freitas, O. A. Martins-Filho and L. M. S. Dusse, Intracellular nitric oxide assessment in whole blood leukocytes by flow cytometry: Optimization and applicability to monitor patients with chronic graft nephropathy, *J. Immunol. Methods*, 2009, **343**, 103–111.

58   M. Kim, S. K. Ko, H. Kim, I. Shin and J. Tae, Rhodamine cyclic hydrazide as a fluorescent probe for the detection of hydroxyl radicals, *Chem. Commun.*, 2013, **49**, 7959–7961.

59   A. Maetzke and S. J. Knak Jensen, Reaction paths for production of singlet oxygen from hydrogen peroxide and hypochlorite, *Chem. Phys. Lett.*, 2006, **425**, 40–43.

60   S. Miyamoto, G. R. Martinez, A. P. B. Martins, M. H. G. Medeiros and P. Di Mascio,

Direct evidence of singlet molecular oxygen [$O_2(^1\Delta_g)$] production in the reaction of linoleic acid hydroperoxide with peroxynitrite, *J. Am. Chem. Soc.*, 2003, **125**, 4510–4517.

Chapter 5

Pyrylium compounds as moisture sensors

The results presented in this chapter are based on the following article:

Phenol-based styrylpyrylium dyes for trace water detection via chromogenic and fluorogenic responses. Muñoz Resta, I.; Galindo, F. **2021**. *Submitted*.

5.1. INTRODUCTION

Sensing chemical species by chromogenic and fluorogenic molecules or polymers has attracted the interest of numerous researchers during the last years. In 1997, the review paper published by the group of A. P. De Silva marked a milestone in the field.[1] More than two decades later, the interest has not decreased, and the number of published compilations covering specific aspects of chemosensing is considerable.[2, 3, 4–11, 12–15] Among the species whose detection is important, water stands out in the recent years as an object of attention. Several molecules, complexes, polymers and nanoparticles have been described to detect moisture in organic solvents and daily use items, like drugs and food.[16–18] The nature of those chemosensing systems is very diverse, including mainly metallic complexes[19–26] but also rhodamine derivatives,[27–29] phenothiazines,[30,31] naphthalimides,[32] bodipy-related compounds,[33] off-the-shelf commercial dyes,[34,35] bichromophoric compounds,[36,37] organic polymers,[38] carbon dots,[39–41] metallic nanoclusters[42] and other.[43–47] Among that impressive chemical variety, no example of pyrylium dye has been reported so far, despite the easy synthesis of this class of compounds. Here, the design of two simple styrylpyrylium dyes (**5.1** and **5.4** in **Chart 1**) able to detect trace amounts of water (sub-0.005 % vol.) in organic solvents (acetone and acetonitrile) is reported. As mentioned in the general introduction, pyrylium dyes have been used for numerous applications but not for water sensing purposes**.**

5.1 R = -H
5.4 R = -OCH3

5.2 R = -H
5.5 R = -OCH3

5.3 R = -H
5.6 R = -OCH3
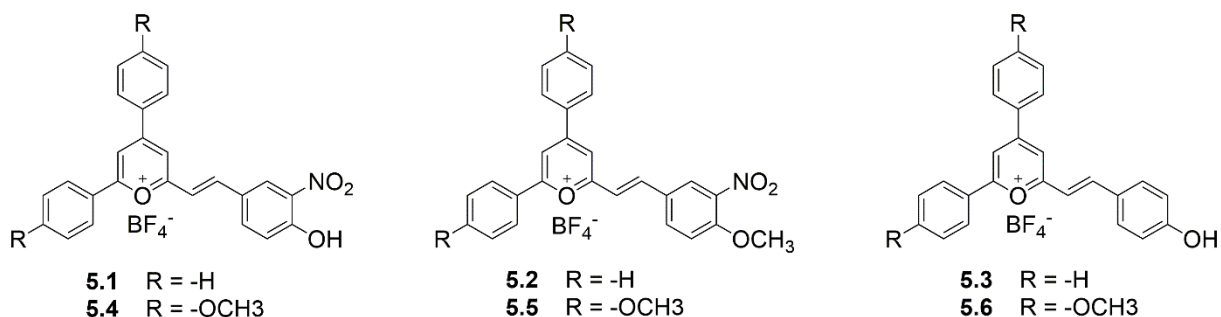
Chart 1. Pyrylium dyes under study.

5.2. RESULTS AND DISCUSSION

5.2.1. Synthesis and characterisation

Synthesis of moisture-sensitive compounds **5.1** and **5.4** along with model compounds **5.2, 5.5** and **5.3, 5.6** was carried out following previous described synthesis of other pyrylium dyes.[48] The synthetic route is summarized in **Scheme 1** and, as can be seen, employs readily available commercial acetophenones and benzaldehydes to give **5.1-5.6** in good yields (50-90 %). It is worth noting that the purification of the intermediates and the final products do not require from chromatographic techniques since it can be carried out by the precipitation method in diethyl ether. The products were characterized by ^{1}H-NMR, ^{13}C-NMR spectroscopy and HRMS spectrometry.
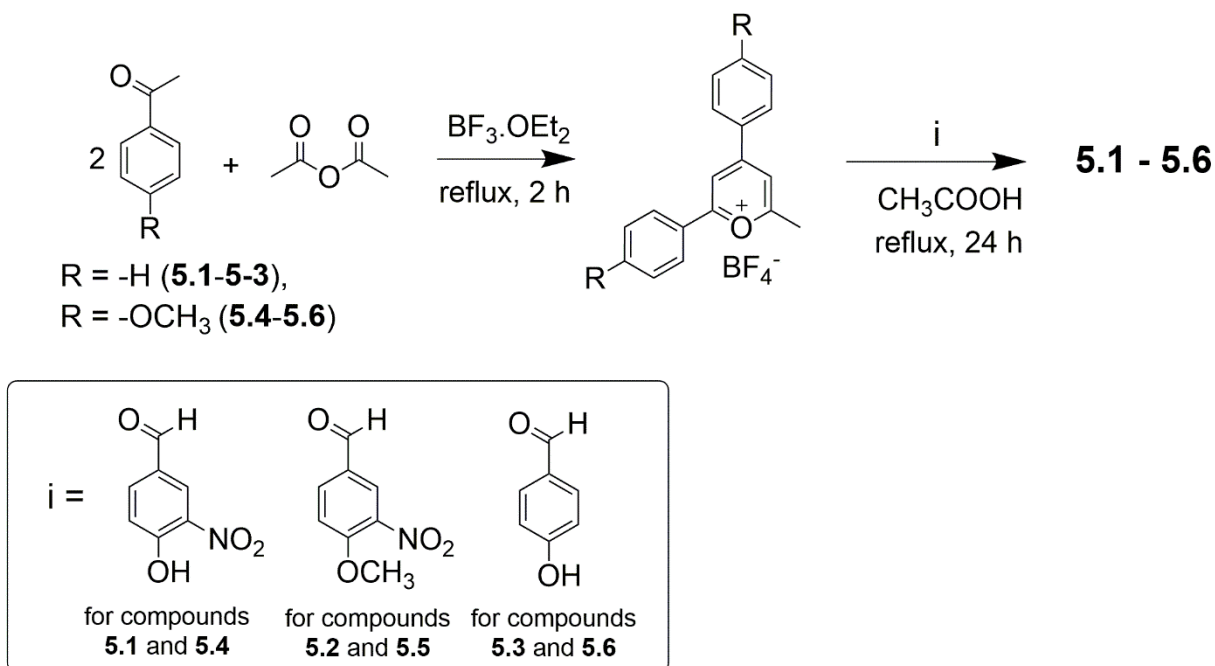
Scheme 1. Synthetic procedures for pyrylium dyes studied in the present chapter.

The absorption spectrum of compound **5.1** in acetonitrile is characterized by three bands, at 370 nm, 460 nm and 667 nm, as can be seen in **Figure 1**. According to the described features for pyrylium dyes, in triarylpyrylium dyes coexists two chromophores with absorptions located at ca. 300-400 nm (aligned with the y-axis) and at ca. 400-500 nm (aligned with the x-axis). The precise position of the peaks depends on the substitution of the peripheral aromatic rings and the solvent. Following this logic, the aforementioned peaks could be assigned to the y (370 nm) and x (460 nm) chromophores. Regarding the other band (667 nm), it could be ascribed to the product resulting after deprotonation of the phenol (quinoidal form, depicted in **Scheme 2**), from now on designated as the Q band. Compound **5.2**, synthesized as a model, with a methoxy group instead of a -OH functionality, displays the typical absorption expected in acetonitrile, with only x and y bands matching the bands of **5.1**, but lacking the one at 665 nm. Additionally, when

compound **5.1** is dissolved in water at pH 2, the same optical features as **5.2** in ACN can be observed, thus confirming the proposed equilibrium between pyrylium and quinoidal form.
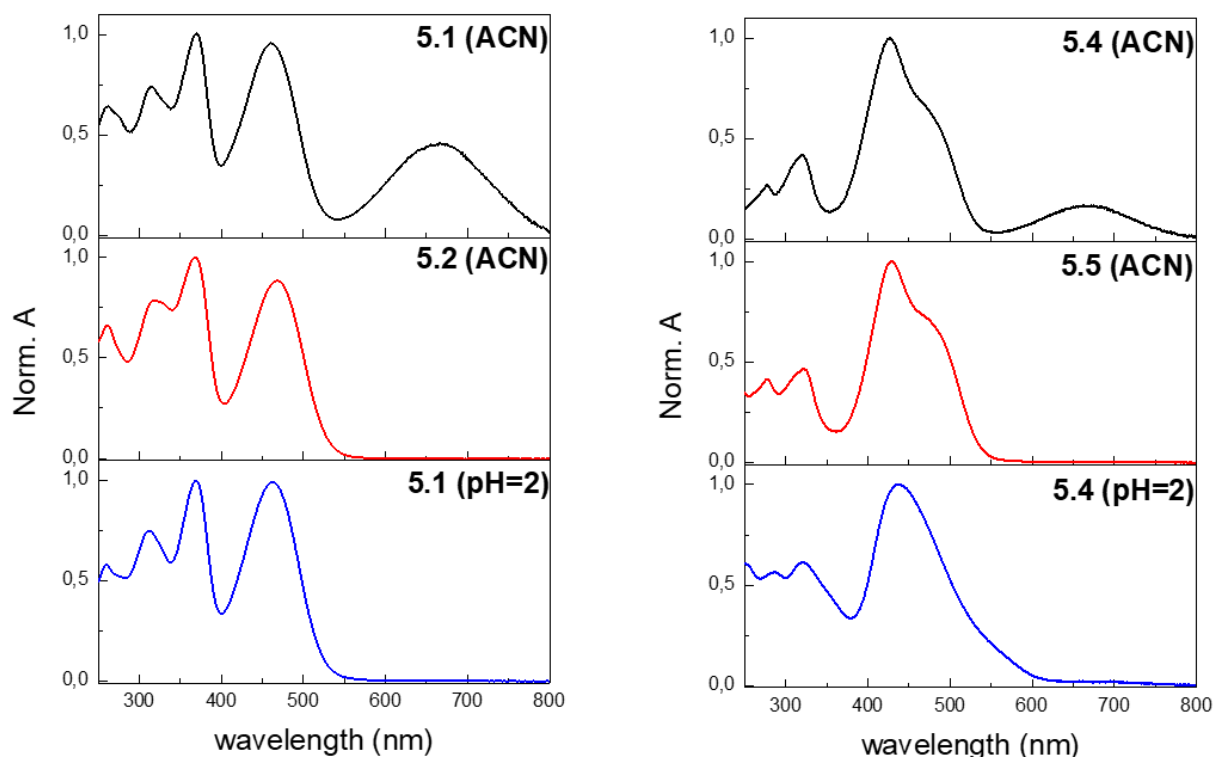
Figure 1. Normalized absorption spectrum of 10 µM solution of compound **5.1** in ACN, model compound **5.2** in ACN and compound **5.1** in water (pH = 2) (left). Normalized absorption spectrum of 10 µM solution of compound **5.4** in ACN, model compound **5.5** in ACN and compound **5.4** in water (pH = 2) (right).

For compound **5.4**, with MeO- groups in the 4 and 6 aryl rings, analogous observations can be made. Thus, in ACN, the *y* and *x* bands are located at ca. 426 nm and 486 nm, respectively, with substantial overlapping, whereas the Q absorption is located at ca. 665 nm and is relatively less intense than in the case of **5.1**. If compared with model compound **5.5** (with MeO- instead of -OH) and with **5.4** at acidic pH (**Figure 1**), the same conclusion can be drawn

as for **5.1**, i.e., the long-wavelength absorption band corresponds to the quinoidal form after deprotonation.
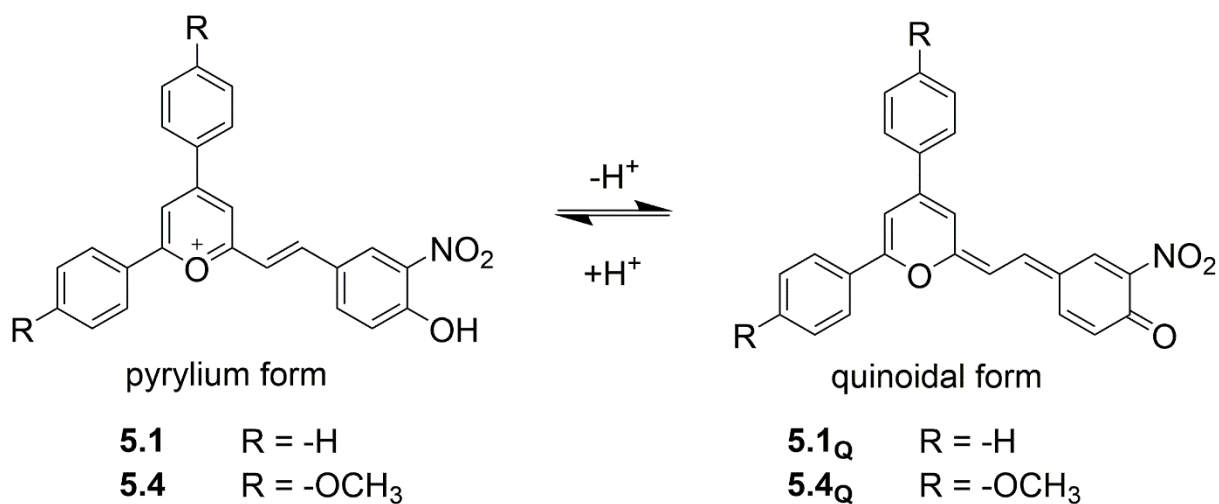
Scheme 2. Acid-base equilibrium between pyrylium and quinoidal forms.

The absorption spectrum of **5.1** and **5.4** in other solvents, like acetone and THF, were recorded, with the observation of the same phenomenon (see **Figure 2**).
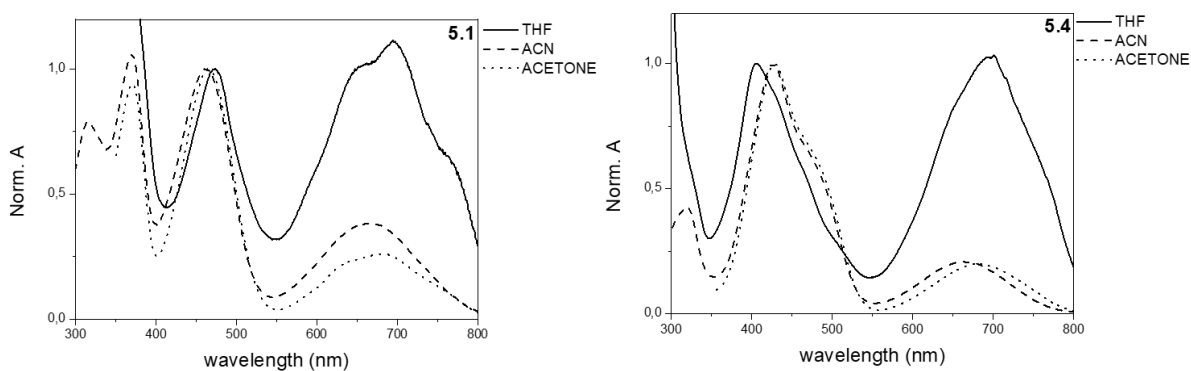
Figure 2. Normalized absorption spectra of 10 µM solutions of compound **5.1** in acetone, ACN and THF (left). Normalized absorption spectra of 10 µM solutions of compound **5.4** in acetone, ACN and THF (right).

5.2.2. Acid-base behaviour

To study deeper the acid-base equilibrium responsible for the formation of the Q band and disappearance of the *x* band, a pH titration with **5.1** was performed (**Figure 3**). A plot of the absorbance at 682 nm (Q band) vs. pH yielded the curve shown in **Figure 3**. The curve was fitted to the model represented by equation 1:[49]

$$A\,(pH) = A_{I-} + \frac{(A_{HI} - A_{I-})}{1 + exp^{pH-pKa}}$$
$\hspace{10cm}$ Equation 1

where A is the absorbance at a certain pH, A_{I-} and A_{HI} are the absorbances of the deprotonated and protonated forms and pK_a is the pH at the inflection point.

The calibration affords a pK_a of 3.79, a value notably low for a phenolic proton (typical pK_a of unsubstituted phenols are around 10; however, substituted phenols with electron-withdrawing groups have a lower pK_a; for instance, *ortho*-nitrophenol has a pK_a of 7.2). The very low value recorded for **5.1** can be rationalized considering that the formation of the quinoidal form is very favoured by the presence of an electron-deficient pyrylium structure. On the other hand, when titration of **5.4** was carried out, a value of pK_a 5.36 was obtained, notably higher than the pK_a of **5.1**, probably because the pyrylium core in **5.4** is less electron-deficient than in **5.1**, because of the presence of the MeO- groups. To evaluate the role of the nitro group in the studied pyrylium salts, it was carried out the pH titration of model compounds **5.3** and **5.6** lacking such nitro functionality. As it can be seen in **Figure 3**, the pK_a recorded was 6.86 for **5.3** and 6.91 for **5.6**, thus confirming that both the nitro and the pyrylium core exert a notable influence on the acidity of the phenolic proton in **5.1** and **5.4**.
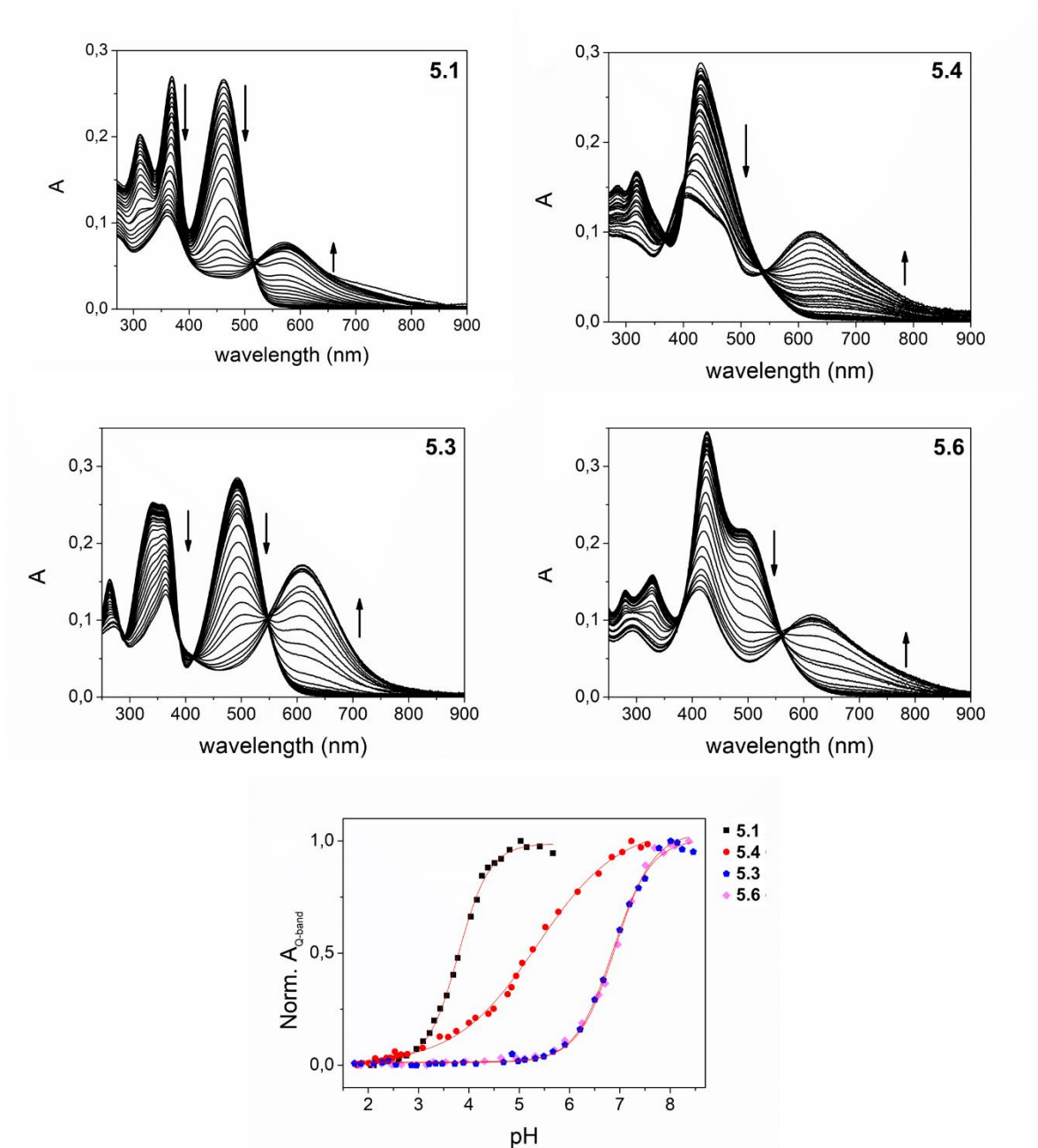
Figure 3. Variation of absorption spectra with pH for 10 µM solutions (in water) of compounds **5.1, 5.4** and **5.3, 5.6** (top and middle). Normalized absorbance of the Q-band vs pH (bottom).

5.2.3. *Photophysical characterisation of the compounds*

Compounds **5.1** and **5.4** display also fluorescence emission, with bands peaking around 567-603 nm (see **Figure 4**), and emission quantum yields (ϕ_F) in the range 0.06-0.17, depending

on the solvent. The complete set of optical properties, including fluorescence lifetimes (τ_F) can be seen in **Table 1**.
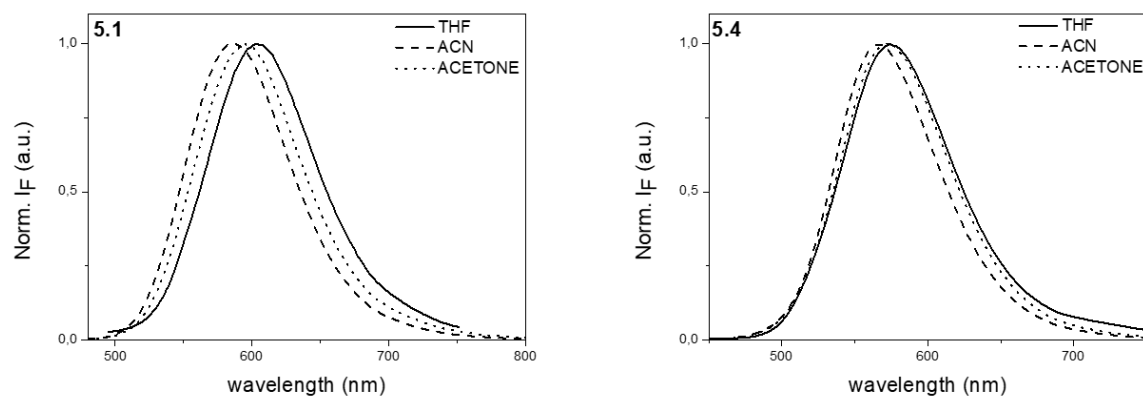
Figure 4. Normalized emission spectra of 10 µM solutions of compound **5.1** in acetone, ACN and THF (left). Normalized emission spectra of 10 µM solutions of compound **5.4** in acetone, ACN and THF (right).

Table 1. Photophysical properties of compounds **5.1** and **5.4** in acetone, ACN and THF.

Compd.	Solvent	λ_{abs} (log ε) (nm)			λ_{em} (nm)	ϕ_F	τ_F (ns)	
5.1	Acetone	371	465	682	595	0.06	$\tau_1 < 1$ (20%)	$\tau_2 = 1.7$ (80%)
	ACN	370	460	667	588	0.08	$\tau_1 < 1$ (18%)	$\tau_2 = 2.3$ (86%)
	THF		473	694	603	0.06	$\tau_1 < 1$ (24%)	$\tau_2 = 1.5$ (76%)
5.4	Acetone	429	486 (s)	684	572	0.10	$\tau_1 < 1$ (39%)	$\tau_2 = 2.8$ (61%)
	ACN	426	486 (s)	665	567	0.08	$\tau_1 = 1.1$ (36%)	$\tau_2 = 3.0$ (64%)
	THF	406	465 (s)	701	574	0.17	$\tau_1 = 1.0$ (34%)	$\tau_2 = 2.9$ (66%)

5.2.4. *Water sensing*

The confirmation of the acid-base behaviour leading to a new Q band and a decrease of the intensity of the *x* band led to the exploration of the potential of **5.1** and **5.4** to detect moisture in organic solvents. It was rationalized that upon the addition of incremental amounts of water,

the balance between the *x* and Q bands would shift, since water would act as a base, leading to the formation of the conjugated quinoidal species, and eventually to a ratiometric optical behaviour. In parallel, the fluorescence of **5.1** and **5.4** in the studied solvents would be also affected by the prototropic equilibrium, thus leading to a potential dual channel chemosensor (colorimetric and fluorometric) for water. The spectral changes induced by the addition of water to 5 µM solutions of **5.1** and **5.4** in acetone and ACN can be seen in **Figures 5** (absorption) and **6** (fluorescence). As shown, the presence of micromolar concentrations of water causes a notable change in the intensities of the Q and *x* bands along with quenching of the fluorescence.
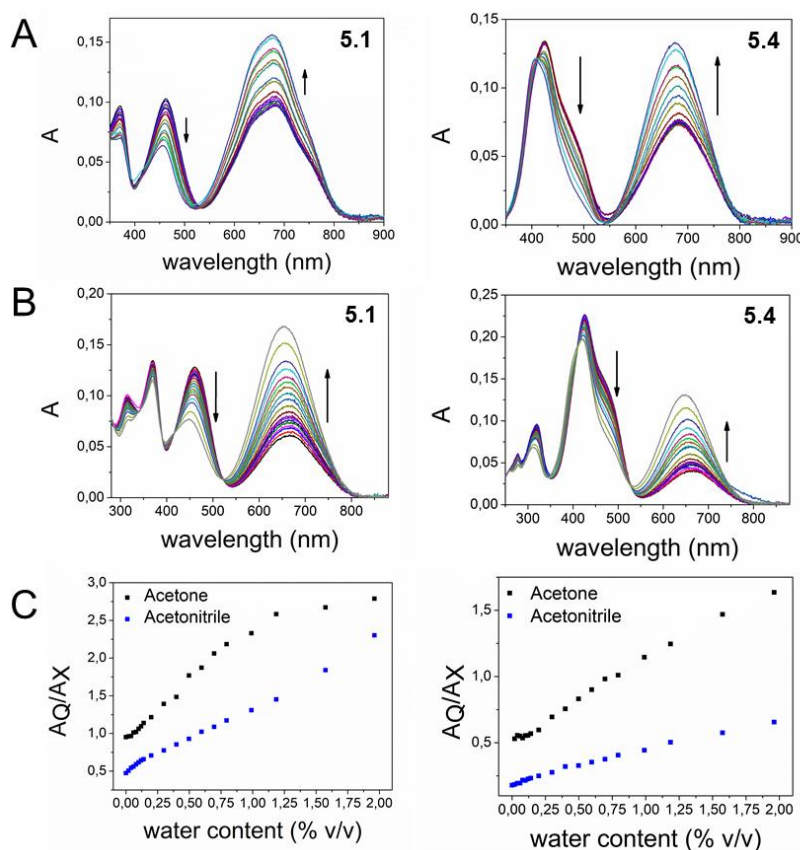
Figure 5. A) Changes in absorption spectra of 5 µM solutions of compounds **5.1** (left) and **5.4** (right) upon the addition of increasing amounts of water in acetone. B) Changes in absorption spectra of 5 µM solutions of compounds **5.1** (left) and **5.4** (right) upon the addition of increasing amounts of water in ACN. C) Changes in absorbance ratio (A_Q/A_X) of 5 µM solutions of compounds **5.1** (left) and **5.4** (right) in acetone and ACN upon the addition of increasing amounts of water.
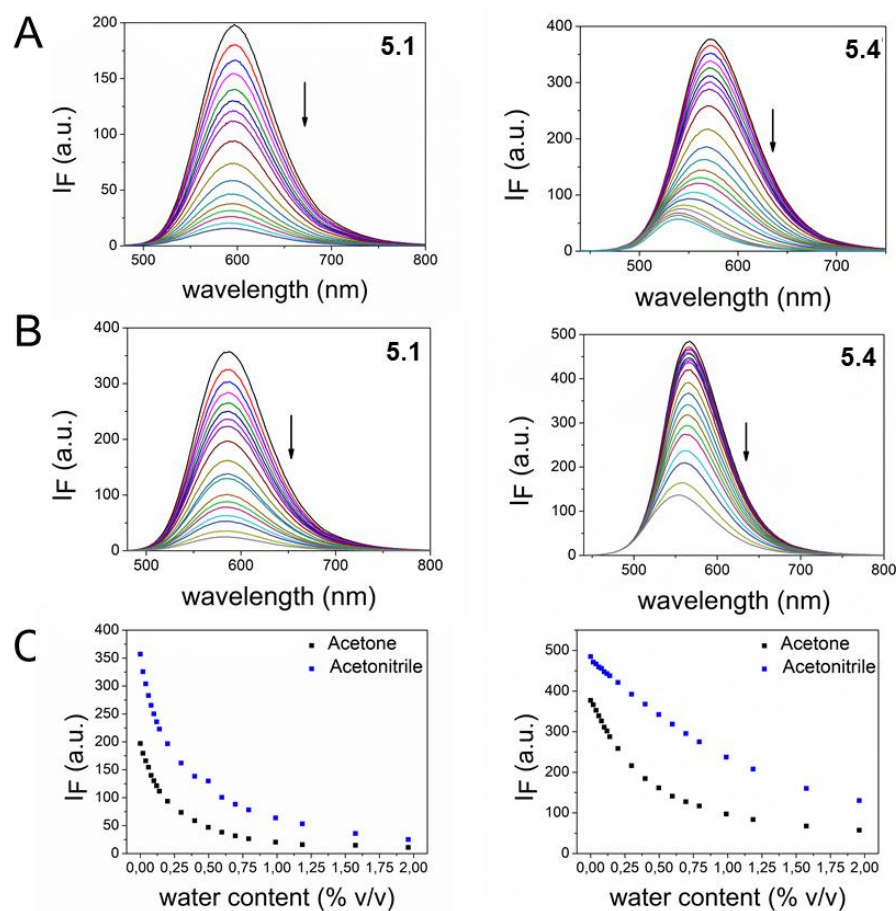
Figure 6. A) Changes in fluorescence spectra of 5 µM solutions of compounds **5.1** (left) and **5.4** (right) upon the addition of increasing amounts of water in acetone. B) Changes in fluorescence spectra of 5 µM solutions of compounds **5.1** (left) and **5.4** (right) upon the addition of increasing amounts of water in ACN. C) Changes in fluorescence intensity of 5 µM solutions of compounds **5.1** (left) and **5.4** (right) in acetone and ACN upon the addition of increasing amounts of water.

The sensors were suited for naked-eye detection, providing their intense optical changes. An example can be seen in **Figure 7**, for compound **5.1** (with increasing amounts of water to 10 µM solutions in dry ACN).
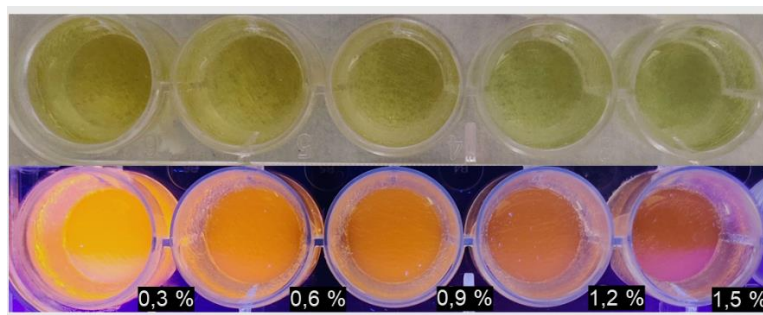
Figure 7. 10 uM solutions of **5.1** in dry ACN with increasing amounts of water under visible (up) and UV 365 nm (down) light.

The limit of detection (LOD) was calculated according to a $3\sigma/|k|$ model (where σ is the standard deviation of the blank measurements and k is the slope of the calibration curve) leading to the values presented in **Table 2**. Also, the limit of quantification is reported ($10\sigma/|k|$).

Table 2. Detection (LOD) and quantification (LOQ) limits in % vol. for water content in dry acetone and ACN using **5.1** and **5.4** as moisture sensors.

	Acetone				Acetonitrile			
	Abs.		Fluo.		Abs.		Fluo.	
Compound	LOD	LOQ	LOD	LOQ	LOD	LOQ	LOD	LOQ
5.1	0.008	0.025	0.003	0.012	0.054	0.180	0.004	0.013
5.4	0.024	0.084	0.011	0.036	0.044	0.145	0.010	0.033

Comparing to values described in the literature, these LOD are within the range of those described earlier, even better than many of them. A careful examination of the recent literature on water sensing using optical methods allow to conclude that most of the reported systems have good to moderate sensitivities (LOD about 0.5% to 0.005% weight or volume, depending on the study) and less than one-quarter of them have LOD $\leq$ 0.005% (wt. or vol.). For compound **5.1**, the LOD determined by fluorescence spectroscopy are within the range 0.003 – 0.004 % vol. In

the case of **5.4**, the LOD are higher than for **5.1**, ranging in the interval 0.010 – 0.011 % vol. The lower LOD for **5.1** as compared to **5.4** could be due to the already mentioned effect of the methoxy groups on the electron-withdrawing ability of the central pyrylium core. To appreciate that the LOD here reported are exceptionally low, the reader is referred to the comprehensive compilation of humidity sensors reported recently.[17]

It must be mentioned that the molecules here described can be used as moisture sensors in organic solvents in a direct way, without the addition of other species. Some effective chemosensors systems have been described using coordinating anions (fluoride) to displace the reaction towards the deprotonated species.[34,35,38,47] Other systems use metallic cations like Cu^{2+} to form a complex which is altered by the addition of water.[19,21] None of such modifications are needed in the case of the sensors here reported. Contrary to the aforementioned cases, where water molecules act as proton donors, for the molecules here described water would be acting as a base, removing the phenolic proton. Similar behaviour was reported for a flavylium salt bearing a –OH group.[43]

Another interesting property of probes **5.1** and **5.4** is the fact that absorption changes upon the addition of water occur in the range 600-800 nm. Comparing to other sensors for humidity reported in the literature it must be indicated that typically reported changes take place below 600 nm. Exceptions to this common trend are the sensing systems comprised of Sudan III[34] or quinizarin[35] plus added fluoride ions (absorption changes at ca. 500-700 nm) and a probe based on the trithienyl-bodipy structure[33] (absorption changes at ca. 600-800 nm).

5.3. CONCLUSIONS

Pyrylium dyes **5.1** and **5.4** have been synthesized (only two steps) and characterized chemically and photophysically. The presence of an *ortho*-hydroxynitro functionality in their structures makes these compounds very sensitive to deprotonation by traces of water in organic solvents. The presence of humidity in solutions of those dyes in acetone, acetonitrile and THF leads to the formation of a new band at long-wavelength (ca. 600-800 nm) attributable to the formation of the quinoidal form, as demonstrated by comparison to a series of model compounds. In addition to the chromogenic change, there is also a fast quenching of the fluorescence emission upon the addition of water. The LOD and LOQ of **5.1** and **5.4** have been estimated, ranging from 0.054 to 0.003 % vol., depending on the solvent and the analytical technique used (absorption or fluorescence). The best sensitivity is displayed by compound **5.1**, which can detect trace water with LOD of 0.003% vol. in acetone, and 0.004% vol. in acetonitrile (fluorescence spectroscopy). The absorption changes take place in the 600-800 nm region and the mechanism of action involves water acting as a base. Due to the simplicity of the synthetic procedures involved in the preparation and purification of the presented dyes, it is envisaged that variations of these dyes will appear in the future, designed for a variety of sensing purposes.

5.4. EXPERIMENTAL SECTION

5.4.1. *Reagents and instruments*

All commercially available reagents and solvents were used as received. ^{1}H and ^{13}C NMR were recorded with a Bruker Advance III HD spectrometer (400 MHz for ^{1}H and 101 MHz for ^{13}C). High-resolution mass spectra (by ESI) were acquired using a Waters Q-Tof Premier mass spectrometer. Absorption spectra were measured on a Cary 60 UV-vis spectrophotometer. Fluorescence spectra were recorded with an Agilent Cary-Eclipse spectrofluorometer. Time-resolved fluorescence experiments were performed with an IBH5000U apparatus using 464 nm nanoLED (fwhm 1.4 ns) as excitation source.

5.4.2. *Synthesis of compounds 5.1-5.3*

2-methyl-4,6-diphenylpyrylium tetrafluoroborate (yellow solid, 1.3 g, yield 32 %). To a solution of acetophenone (3.0 ml, 24.3 mmol) in acetic anhydride (4.6 ml, 48.6 mmol), BF_3 diethyl etherate (2.1 ml, 17.0 mmol) was added dropwise under continuous stirring at room temperature. Then, the solution was heated to reflux in a silicone oil bath (at 138 ºC) for 2 hours. After cooling down to room temperature, the reaction mixture was poured into 200 ml of diethyl ether, and the formed precipitate was recovered by filtration, washed with diethyl ether and dried under vacuum.

^{1}H NMR (400 MHz, CD_3CN) δ 8.67 (d, J = 1.7 Hz, 1H), 8.36 – 8.32 (m, 2H), 8.23 – 8.17 (m, 3H), 7.86 – 7.81 (m, 2H), 7.77 – 7.71 (m, 4H), 3.00 (s, 3H). ^{13}C NMR (101 MHz, CD_3CN) δ 178.78, 173.27, 167.67, 136.58, 133.68, 131.39, 131.20, 130.74, 130.08, 129.73, 120.11, 116.51, 22.12. HRMS (ESI-TOF)[+] calculated for $C_{18}H_{15}O^+$ (M^+) (m/z): 247.1120; experimental (M^+) (m/z): 247.1123.

To a suspension of 2-methyl-4,6-diphenylpyrylium tetrafluoroborate (0.3 g, 0.9 mmol) in acetic acid (10 ml), the corresponding substituted aldehyde (1.5 equivalents), was added at room temperature. Then, the mixture was heated to reflux at 138 °C (a dark solution was formed) for 24 hours. After cooling down to room temperature, the crude reaction mixture was poured into 150 ml of diethyl ether, and the formed precipitate was recovered by filtration, washed with diethyl ether, and dried under vacuum before use.

5.1. (E)-2-(4-hydroxy-3-nitrostyryl)-4,6-diphenylpyrylium tetrafluoroborate (dark red solid, 0.3 g, 77 % yield). ^{1}H NMR (400 MHz, DMSO-d$_6$) δ 8.98 (d, J = 1.1 Hz, 1H), 8.69 (s, 1H), 8.59 (d, J = 7.5 Hz, 2H), 8.53 (d, J = 2.0 Hz, 1H), 8.45 (d, J = 16.3 Hz, 1H), 8.41 (d, J = 7.6 Hz, 2H), 8.10 (dd, J = 8.8, 2.1 Hz, 1H), 7.84 (t, J = 7.3 Hz, 2H), 7.80 – 7.74 (m, 4H), 7.71 (d, J = 16.2 Hz, 1H), 7.30 (d, J = 8.7 Hz, 1H). ^{13}C NMR (101 MHz, DMSO-d$_6$) δ 170.01, 168.84, 163.35, 155.09, 143.84, 137.50, 134.93, 134.83, 134.68, 132.52, 129.96, 129.74, 129.43, 129.12, 128.63, 127.22, 125.77, 120.23, 117.88, 116.86, 113.96. HRMS (ESI-TOF)$^+$ calculated for C$_{25}$H$_{18}$NO$_4$$^+$ (M$^+$) (m/z): 396.1230; experimental (M$^+$) (m/z): 396.1231.

5.2. (E)-2-(4-methoxy-3-nitrostyryl)-4,6-diphenylpyrylium tetrafluoroborate (red solid, 0.2 g, 50 % yield). ^{1}H NMR (400 MHz, CD$_3$CN) δ 8.56 (d, J = 1.7 Hz, 1H), 8.43 – 8.36 (m, 3H), 8.29 – 8.18 (m, 4H), 8.11 (dd, J = 8.9, 2.2 Hz, 1H), 7.89 – 7.80 (m, 2H), 7.80 – 7.72 (m, 4H), 7.49 (d, J = 16.2 Hz, 1H), 7.43 (d, J = 8.9 Hz, 1H), 4.05 (s, 3H). ^{13}C NMR (101 MHz, CD$_3$CN) δ 171.05, 170.82, 166.21, 156.40, 144.82, 136.20, 136.09, 135.81, 133.83, 131.11, 130.93, 130.20, 130.05, 129.63, 127.72, 127.19, 118.86, 118.65, 116.16, 115.87, 58.07. HRMS (ESI-TOF)$^+$ calculated for C$_{26}$H$_{20}$NO$_4$$^+$ (M$^+$) (m/z): 410.1387; experimental (M$^+$) (m/z): 410.1391.

5.3. (E)-2-(4-hydroxystyryl)-4,6-diphenylpyrylium tetrafluoroborate (brown solid, 0.2 g, 49% yield). ^{1}H NMR (400 MHz, CD3CN) δ 8.44 (d, J = 1.7 Hz, 1H), 8.37 (ddd, J = 7.1, 3.2, 1.8 Hz, 2H), 8.28 (d, J = 16.1 Hz, 1H), 8.20 (d, J = 1.7 Hz, 1H), 8.19 – 8.14 (m, 2H), 7.84 – 7.78 (m, 4H), 7.78 – 7.71 (m, 4H), 7.35 (d, J = 16.0 Hz, 1H), 7.04 – 6.97 (m, 2H). ^{13}C NMR (101 MHz, CD3CN) δ 172.16, 169.93, 165.03, 162.79, 148.61, 135.72, 135.66, 133.18, 131.03, 130.85, 130.27, 129.97, 129.29, 118.00, 117.59, 115.57, 114.77. HRMS (ESI-TOF)[+] calculated for $C_{25}H_{19}O_2^+$ (M[+]) (m/z): 351.1380; experimental (M[+]) (m/z): 351.1384.

5.4.3. *Synthesis of compounds 5.4-5.6*

2,4-bis(4-methoxyphenyl)-6-methylpyrylium tetrafluoroborate (red solid, 1.4 g, yield 35 %). To a solution of *para*-methoxyacetophenone (3.0 g, 20.0 mmol) in acetic anhydride (3.8 ml, 40.0 mmol), BF3 diethyl etherate (1.8 ml, 14.0 mmol) was added dropwise under continuous stirring at room temperature. Then, the solution was heated to reflux in a silicone oil bath (at 138 °C) for 2 hours. After cooling down to room temperature, the reaction mixture was poured into 200 ml of diethyl ether, and the formed precipitate was recovered by filtration, washed with diethyl ether, and dried under vacuum.

^{1}H NMR (400 MHz, CD3CN) δ 8.38 (d, *J* = 1.8 Hz, 1H), 8.29 – 8.24 (m, 2H), 8.22 – 8.17 (m, 2H), 7.93 (d, *J* = 1.8 Hz, 1H), 7.25 – 7.17 (m, 4H), 3.95 (s, 3H), 3.95 (s, 3H), 2.86 (s, 3H). ^{13}C NMR (101 MHz, CD3CN) δ 175.30, 171.90, 167.20, 166.64, 164.66, 133.03, 131.73, 125.26, 122.20, 116.80, 116.54, 116.48, 113.02, 57.01, 56.94, 21.42. HRMS (ESI-TOF)[+] calculated for $C_{20}H_{19}O_3^+$ (M[+]) (m/z): 307.1334; experimental (M[+]) (m/z): 307.1334.

To a suspension of 2,4-bis(4-methoxyphenyl)-6-methylpyrylium tetrafluoroborate (0.3 g, 0.9 mmol) in acetic acid (10 ml), the corresponding substituted aldehyde (1.5 equivalents),

was added at room temperature. Then, the mixture was heated to reflux at 138 °C (a dark solution was formed) for 24 hours. After cooling down to room temperature, the crude reaction mixture was poured into 150 ml of diethyl ether, and the formed precipitate was recovered by filtration, washed with diethyl ether, and dried under vacuum before use.

5.4. (E)-2-(4-hydroxy-3-nitrostyryl)-4,6-bis(4-methoxyphenyl)pyrylium tetrafluoroborate (red solid, 0.3 g, 69 % yield). ^{1}H NMR (400 MHz, DMSO-d_6) δ 8.70 (s, 1H), 8.50 (d, J = 9.0 Hz, 2H), 8.45 – 8.33 (m, 4H), 8.18 (d, J = 16.2 Hz, 1H), 8.00 (dd, J = 8.8, 2.0 Hz, 1H), 7.48 (d, J = 16.3 Hz, 1H), 7.29 – 7.17 (m, 5H), 3.95 (s, 3H), 3.94 (s, 3H). ^{13}C NMR (101 MHz, DMSO-d_6) δ 168.06, 167.22, 165.30, 164.69, 161.20, 154.65, 141.30, 137.23, 134.24, 131.96, 130.95, 126.69, 125.87, 124.29, 121.30, 120.10, 117.81, 115.52, 115.23, 114.02, 110.99, 56.12, 56.00. HRMS (ESI-TOF)$^+$ calculated for $C_{27}H_{22}NO_6^+$ (M$^+$) (m/z): 456.1442; experimental (M$^+$) (m/z): 456.1439.

5.5. (E)-2-(4-methoxy-3-nitrostyryl)-4,6-bis(4-methoxyphenyl)pyrylium tetrafluoroborate (red solid, 0.3 g, 70 % yield). ^{1}H NMR (400 MHz, CD$_3$CN) δ 8.36 – 8.32 (m, 2H), 8.30 (dd, J = 5.5, 2.0 Hz, 2H), 8.21 – 8.17 (m, 2H), 8.08 – 8.01 (m, 2H), 7.99 (d, J = 1.7 Hz, 1H), 7.38 (d, J = 8.9 Hz, 1H), 7.32 (d, J = 16.2 Hz, 1H), 7.25 – 7.20 (m, J = 7.0, 4.6, 2.0 Hz, 4H), 4.03 (s, 3H), 3.98 – 3.96 (m, 6H). ^{13}C NMR (101 MHz, CD$_3$CN) δ 170.01, 169.87, 166.67, 166.25, 141.93, 134.97, 132.35, 131.57, 131.57, 127.58, 126.39, 125.22, 121.97, 118.73, 116.38, 116.38, 116.12, 115.69, 115.41, 112.52, 57.62, 56.59, 56.55. HRMS (ESI-TOF)$^+$ calculated for $C_{28}H_{24}NO_6^+$ (M$^+$) (m/z): 470.1598; experimental (M$^+$) (m/z): 470.1602.

5.6. (E)-2-(4-hydroxystyryl)-4,6-bis(4-methoxyphenyl)pyrylium tetrafluoroborate (dark brown solid, 0.3 g, yield 87 %). ^{1}H NMR (400 MHz, CD$_3$CN) δ 8.33 – 8.29 (m, 2H), 8.23 (d, J = 1.7

Hz, 1H), 8.21 – 8.14 (m, 2H), 8.09 (d, J = 16.1 Hz, 1H), 7.96 (d, J = 1.6 Hz, 1H), 7.73 (d, J = 8.7 Hz, 2H), 7.25 – 7.18 (m, 5H), 6.97 (d, J = 8.7 Hz, 2H), 3.96 (s, 3H), 3.96 (s, 3H). ^{13}C NMR (101 MHz, CD$_3$CN) δ 169.23, 168.97, 166.29, 165.84, 162.55, 161.64, 145.49, 132.11, 132.06, 131.17, 127.15, 125.34, 122.10, 117.01, 116.23, 115.99, 115.38, 114.66, 111.57, 56.50, 56.45. HRMS (ESI-TOF)+ calculated for $C_{27}H_{23}O_4^+$ (M$^+$) (m/z): 411.1591; experimental (M$^+$) (m/z): 411.1594.

5.4.4. *Photophysical characterisation of the compounds*

1 mM stock solutions of compounds **5.1-5.6** were prepared in acetonitrile. For UV-vis spectra measurements, the stock solution for each compound was diluted to reach a concentration of 10 µM, in dry acetone, dry acetonitrile (ACN) and dry tetrahydrofuran (THF). For fluorescence spectra acquisition, concentration was adjusted to reach a value of 0.1 in absorbance, to minimize the primary inner filter effect. λ_{exc} was set at the absorption maximum of each compound.

Fluorescence Quantum Yield Measurements (ϕ_F). The fluorescence quantum yields of compounds **5.1** and **5.4** were determined in dry acetone, ACN, and THF (with 1% of H$_2$SO$_4$ (c) in each solvent) under an N$_2$ atmosphere. Coumarin 6 was used as a reference since its fluorescence quantum yield was described in ethanol (ϕ_F = 0.78).[50]

The concentration of the reference and the studied compounds were adjusted to obtain the same absorption at the excitation wavelength. Fluorescence quantum yields were calculated by using Equation (2):

$$\phi_F = \phi_R \cdot (A_R \cdot F_S / A_S \cdot F_R) \cdot (n_S^2 / n_R^2) \qquad (2)$$

where ϕ_F is the fluorescence quantum yield, F is the integral of the emission spectrum, A is the absorption intensity, and n is the refractive index. The sub-index R refers to the reference compound and S to the studied pyrylium salt.

Fluorescence Lifetime Measurements (τ_F). The fluorescence lifetimes of compounds **5.1** and **5.4** were determined in dry acetone, ACN, and THF (with 1% of H_2SO_4 (c) in each solvent) under an N_2 atmosphere. Solutions were prepared similarly to those used to obtain the emission spectra. Fluorescence lifetimes were determined by using the technique of time-correlated single-photon counting (TCSPC). Data obtained from the experiments were adjusted to a double exponential model by using the software IBH DAS6.

5.4.5. *Acid-base titrations*

10 µM solutions of compounds **5.1, 5.4** and **5.3, 5.6** were prepared in water. HCl 10 M was then added to reach a pH value near 2. UV-vis spectra were recorded upon the addition of increasing amounts of NaOH until a plateau in absorbance of the Q-band was observed.

5.4.6. *Water titrations*

5 µM solutions of compounds **5.1** and **5.4** were prepared in dry acetone and ACN. Increasing amounts of water were then added, and the absorption and emission spectra were recorded right after each addition. λ_{exc} was set at the absorption maximum of each compound.

5.5. SPECTROSCOPIC DATA OF COMPOUNDS

2-methyl-4,6-diphenylpyrylium tetrafluoroborate
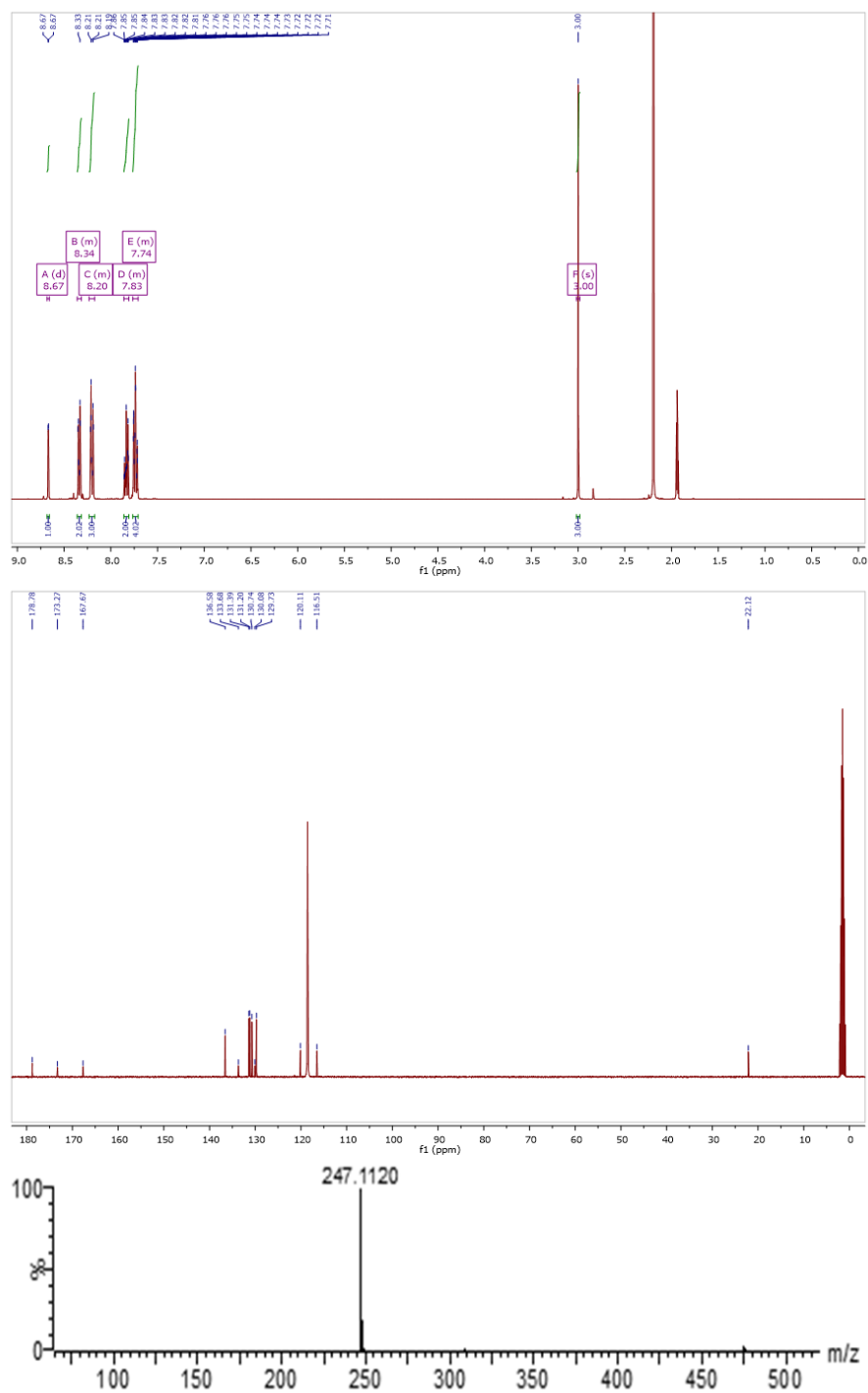
Figure 8. ^{1}H NMR, ^{13}C NMR (CD$_3$CN) and HRMS spectra of the precursor 2-methyl-4,6-diphenylpyrylium tetrafluoroborate.

Compound 5.1
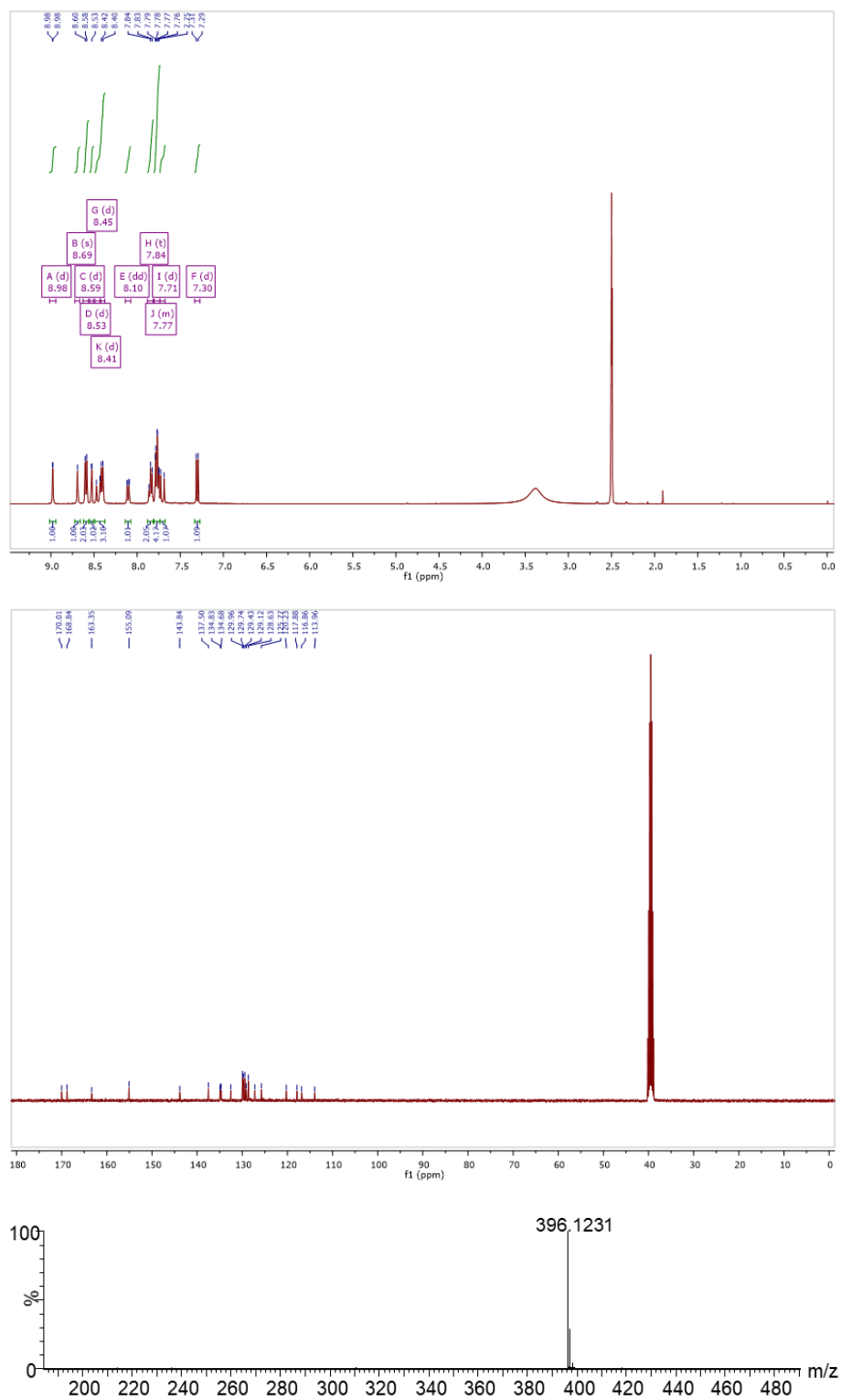
Figure 9. ^{1}H NMR, ^{13}C NMR (DMSO-d$_6$) and HRMS spectra of compound **5.1**.

Compound 5.2
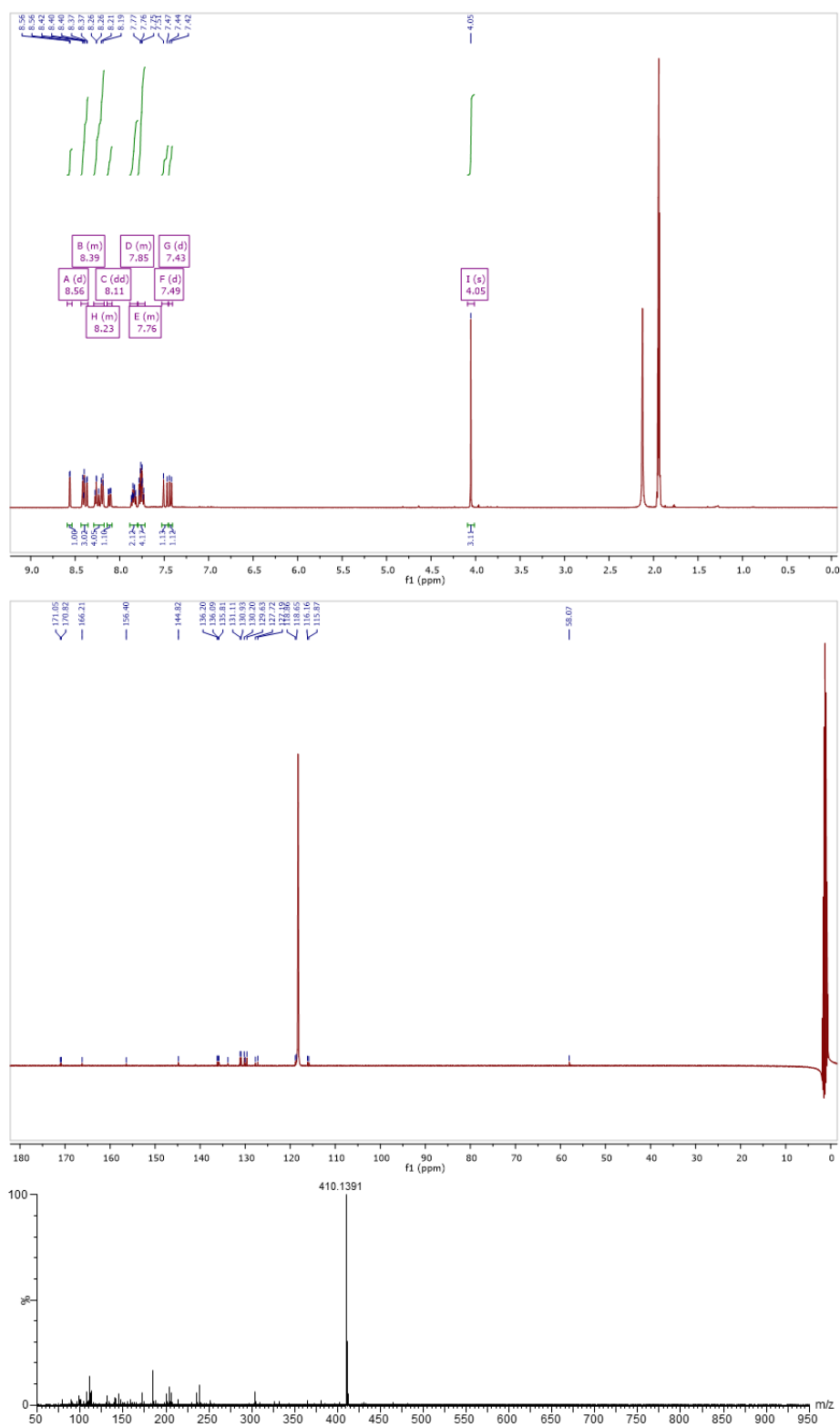
Figure 10. ^{1}H NMR, ^{13}C NMR (CD$_3$CN) and HRMS spectra of compound **5.2**.

Compound 5.3
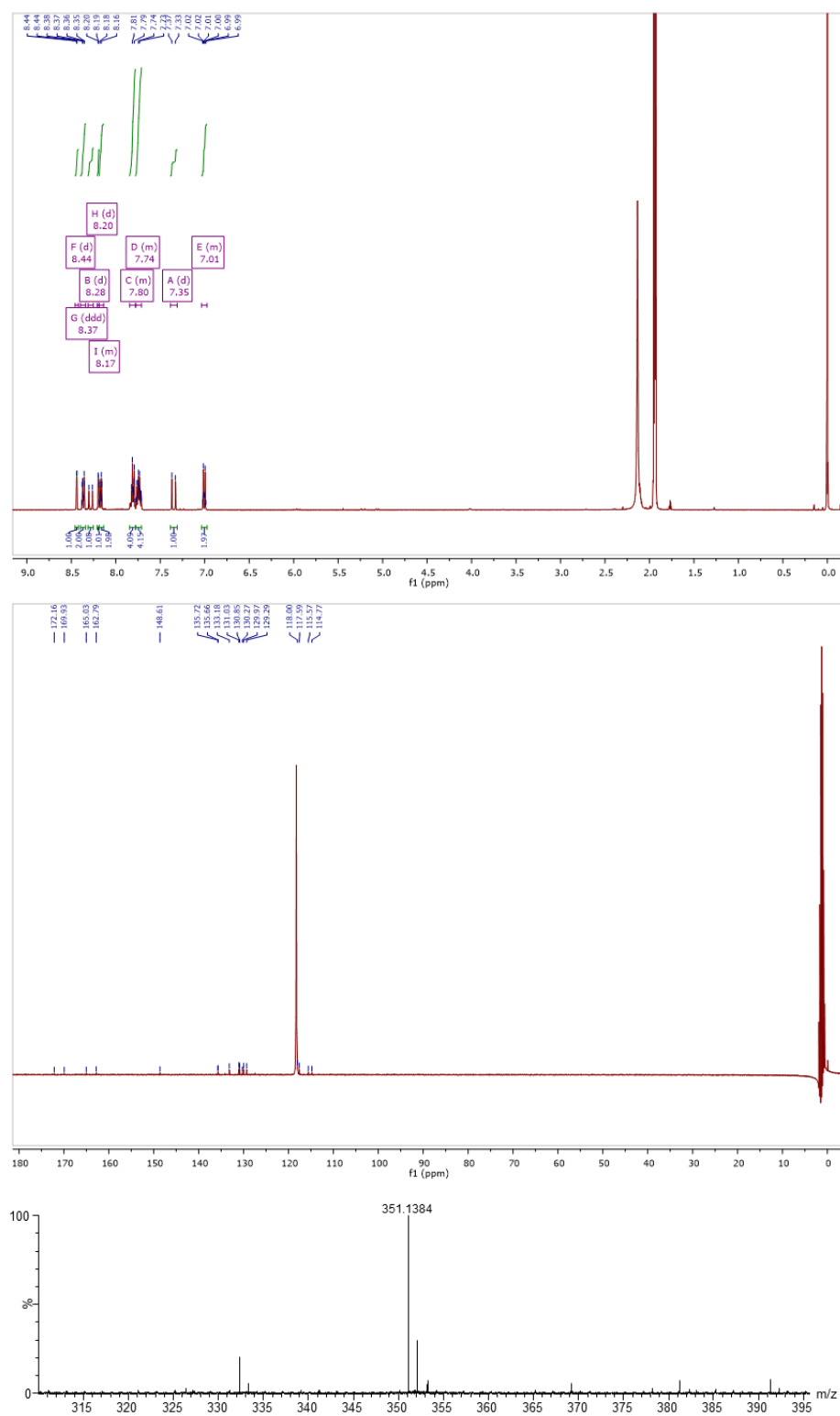
Figure 11. ^{1}H NMR, ^{13}C NMR (CD$_3$CN) and HRMS spectra of compound **5.3**.

2,4-bis(4-methoxyphenyl)-6-methylpyrylium tetrafluoroborate
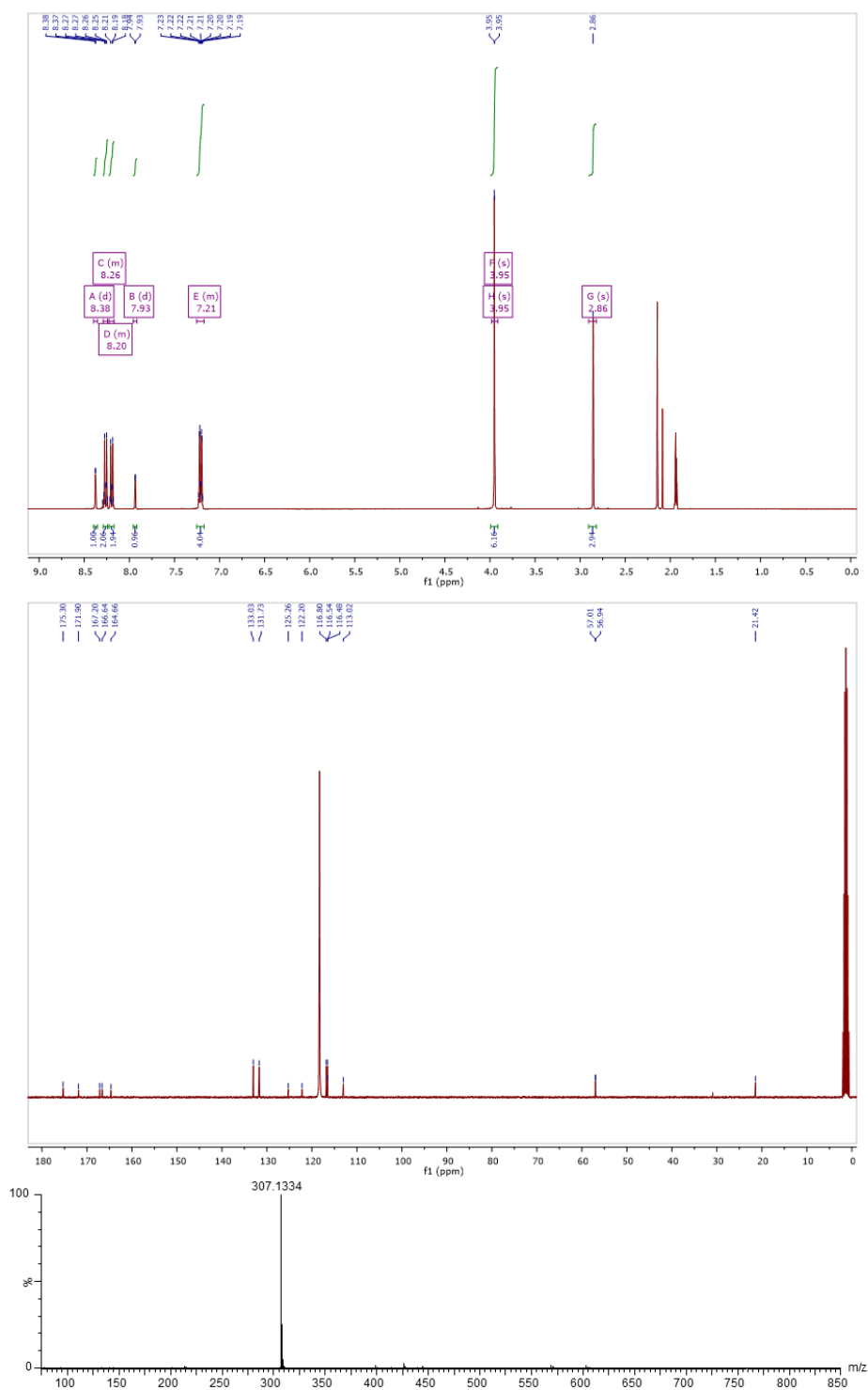
Figure 12. ^{1}H NMR, ^{13}C NMR (CD$_3$CN) and HRMS spectra of the precursor 2,4-bis(4-methoxyphenyl)-6-methylpyrylium tetrafluoroborate.

Compound 5.4
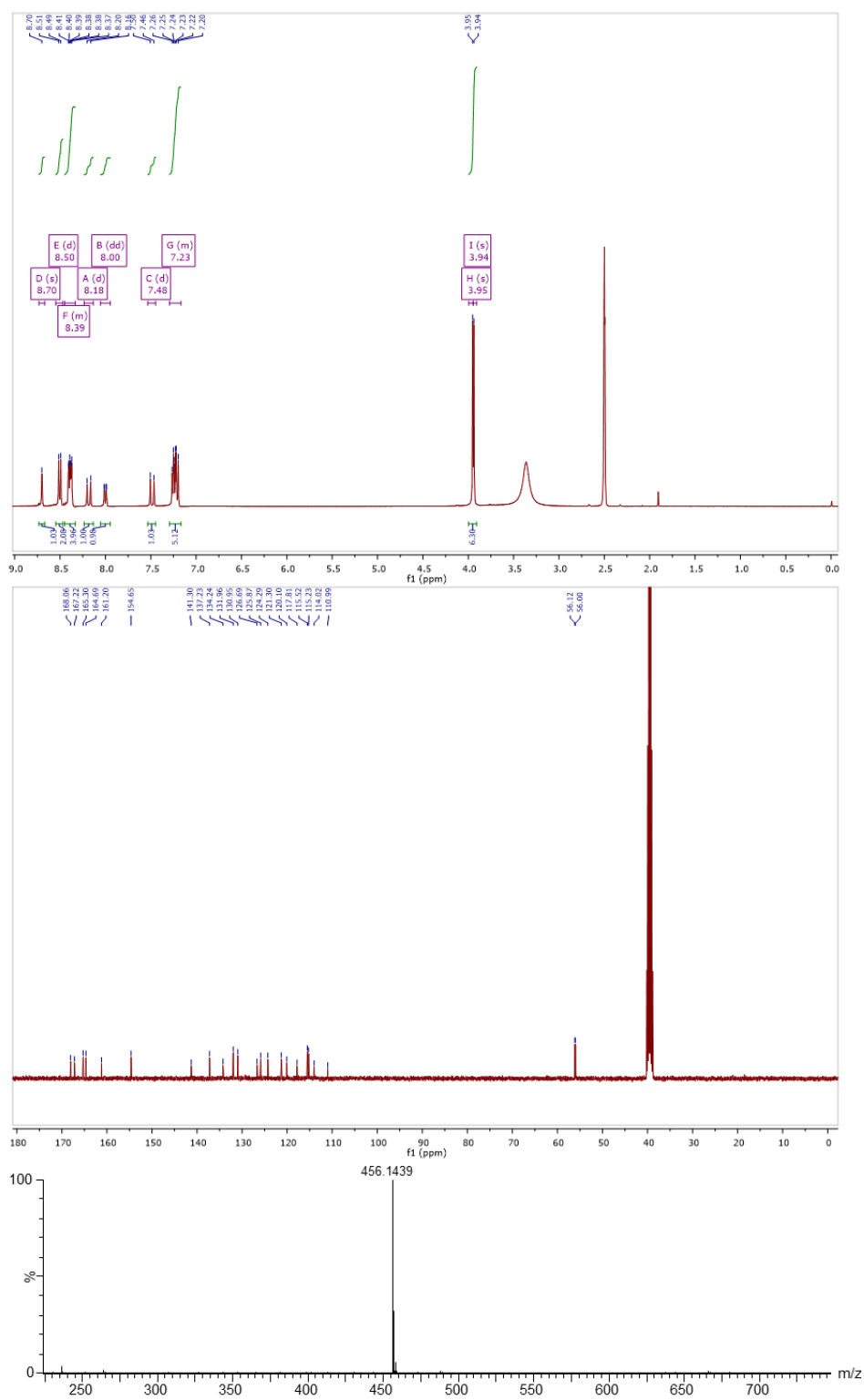
Figure 13. ^{1}H NMR, ^{13}C NMR (DMSO-d$_6$) and HRMS spectra of compound **5.4**.

Compound 5.5
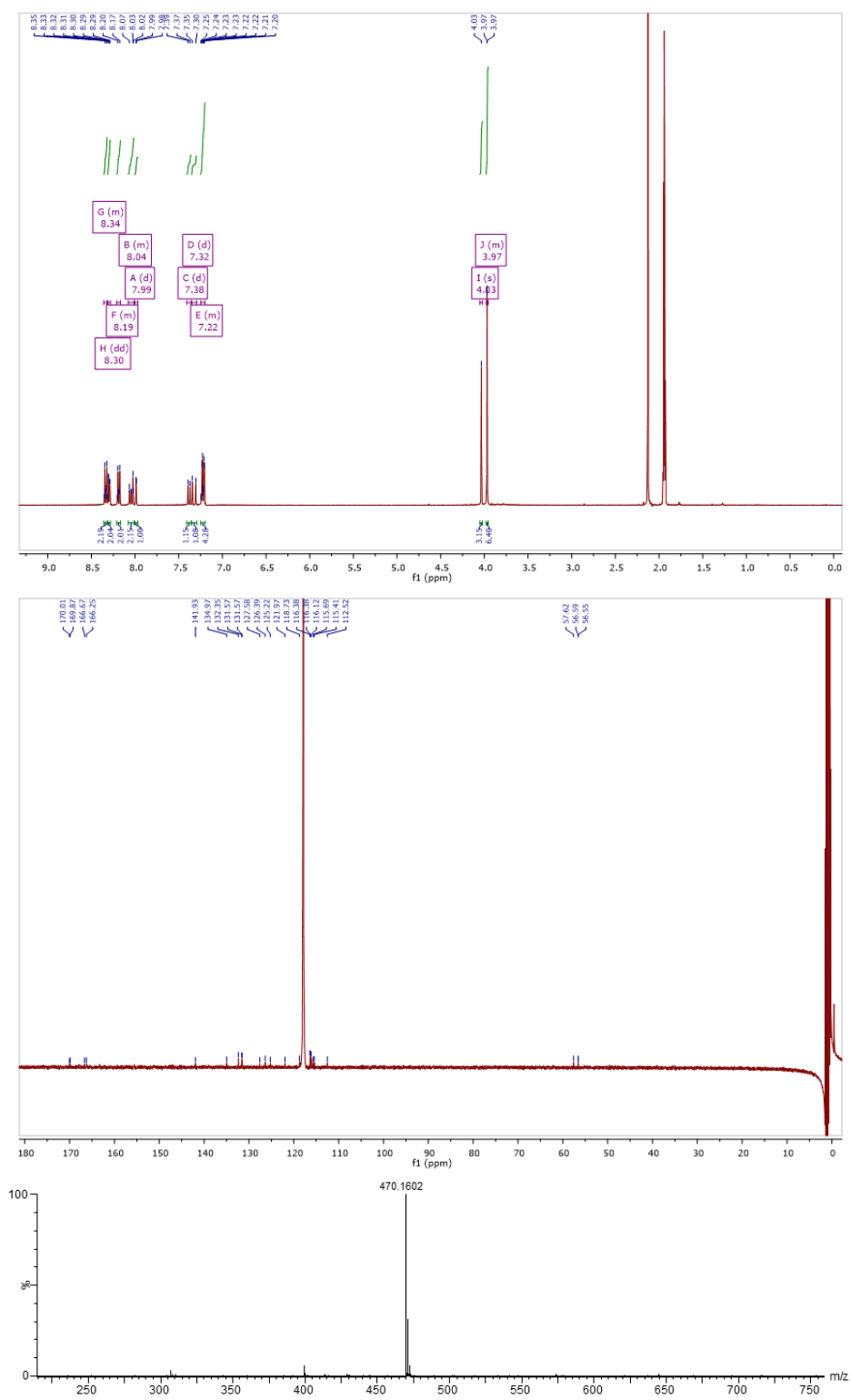
Figure 14. ^{1}H NMR, ^{13}C NMR (CD$_3$CN) and HRMS spectra of compound **5.5**.

Compound 5.6
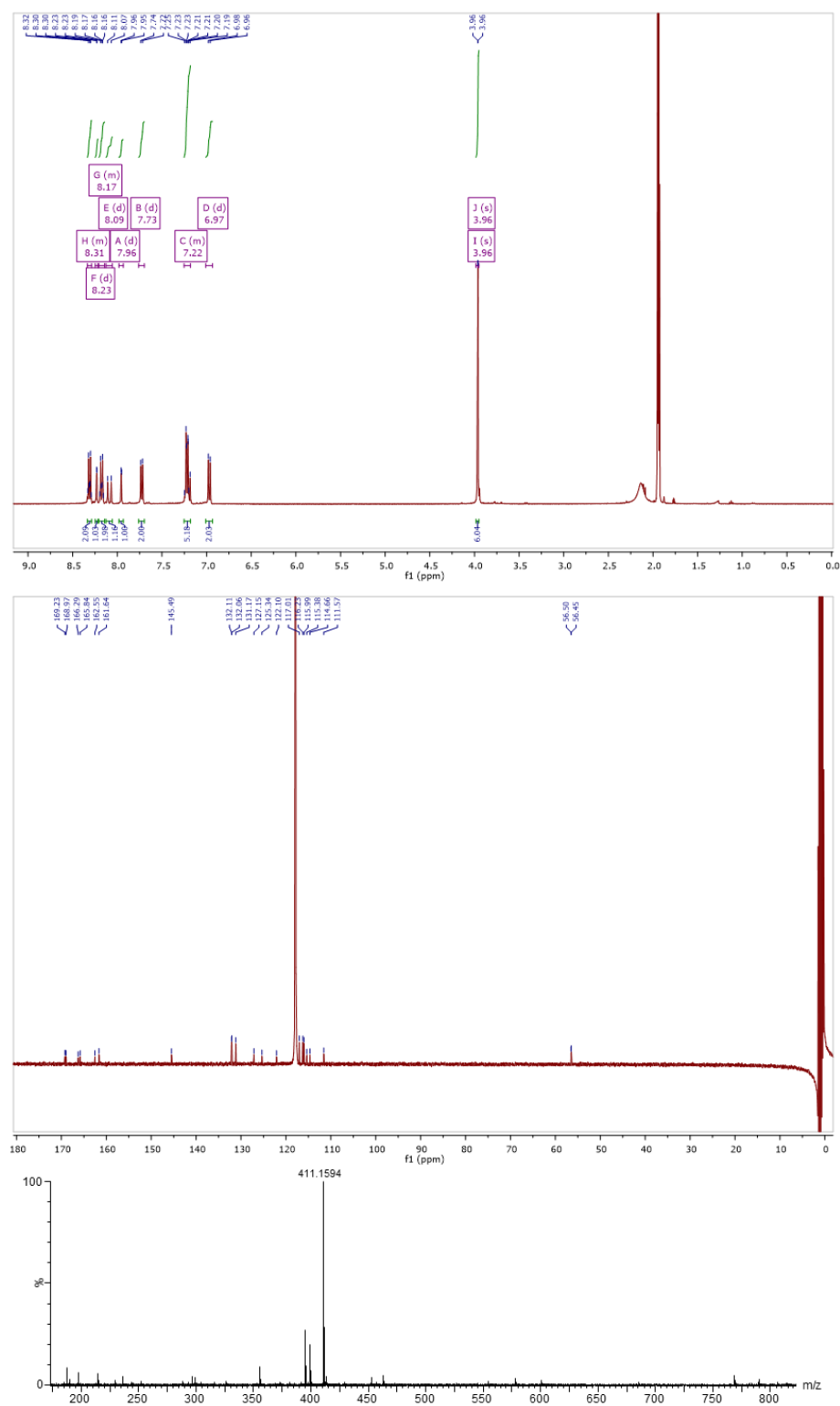
Figure 15. ^{1}H NMR, ^{13}C NMR (CD$_3$CN) and HRMS spectra of compound **5.6**.

Measurements of the fluorescence lifetime
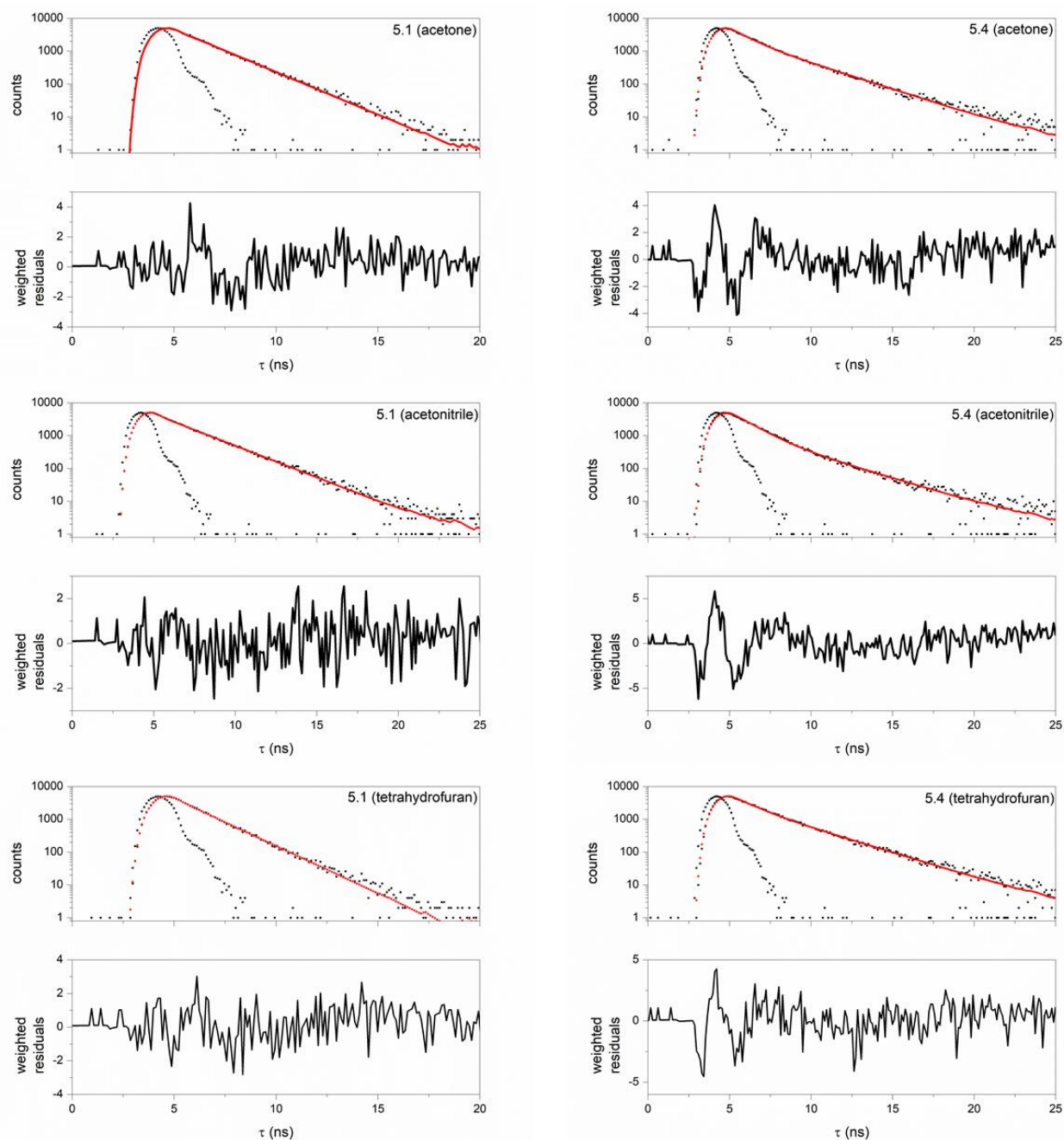
Figure 16. Fluorescence decay curves for compounds **5.1** and **5.4** in acetone, ACN and THF (with 1% of H_2SO_4 (c) in each solvent) at 295 K. λ_{exc} was set at 464 nm. λ_{em} was set at the emission maximum for each compound. The incident light pulse and the residuals are also shown.

5.6. CALIBRATION CURVES

Note: σ is the standard deviation of the blank measurement.
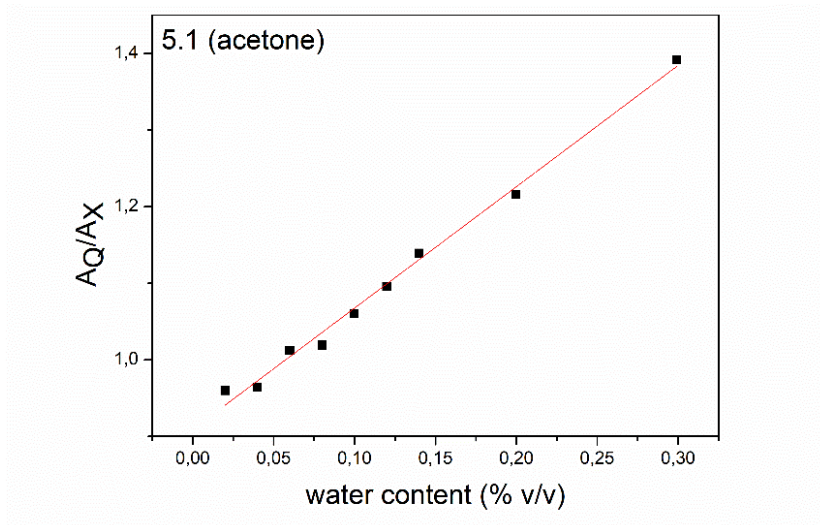
Figure 17. Changes in absorbance ratio (A_Q/A_X) of 5 µM solution of **5.1** in acetone upon the addition of increasing amounts of water.

Linear regression: $A_Q/A_X = 1.584 * (\%v/v) + 0.909$ ($R^2 = 0.9921$) ($\sigma = 0.004$)
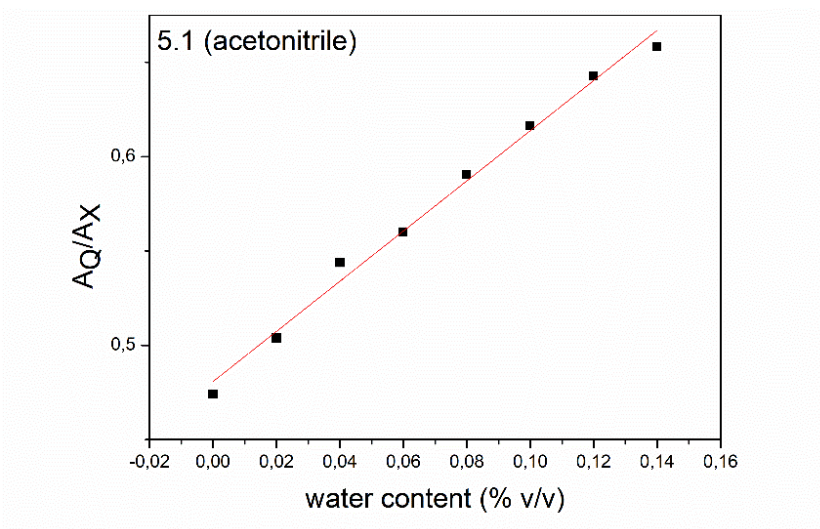
Figure 18. Changes in absorbance ratio (A_Q/A_X) of 5 µM solution of **5.1** in acetonitrile upon the addition of increasing amounts of water.

Linear regression: $A_Q/A_X = 1.330 * (\%v/v) + 0.481$ ($R^2 = 0.9901$) ($\sigma = 0.024$)
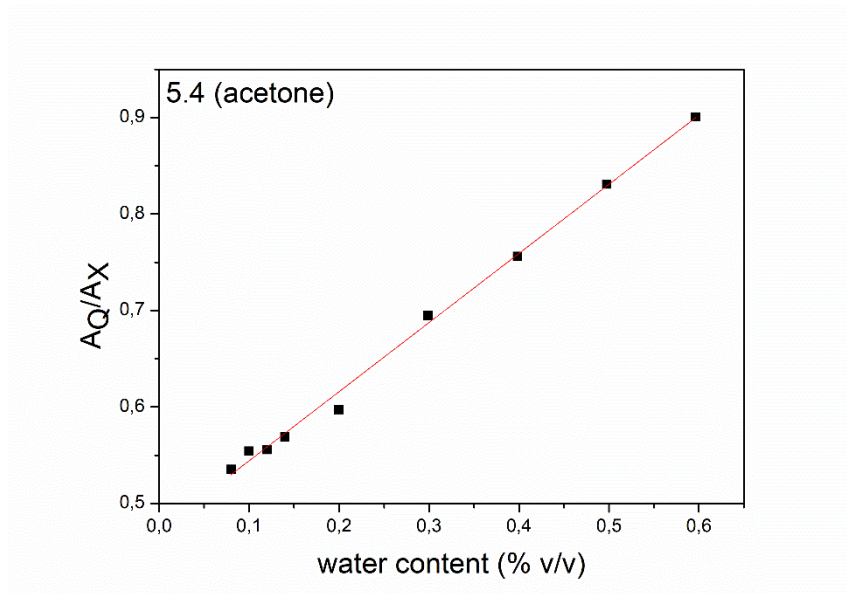
Figure 19. Changes in absorbance ratio (A_Q/A_X) of 5 µM solution of **5.4** in acetone upon the addition of increasing amounts of water.

Linear regression: $A_Q/A_X = 0.717 * (\%v/v) + 0.472$ ($R^2 = 0.9957$) ($\sigma = 0.006$)
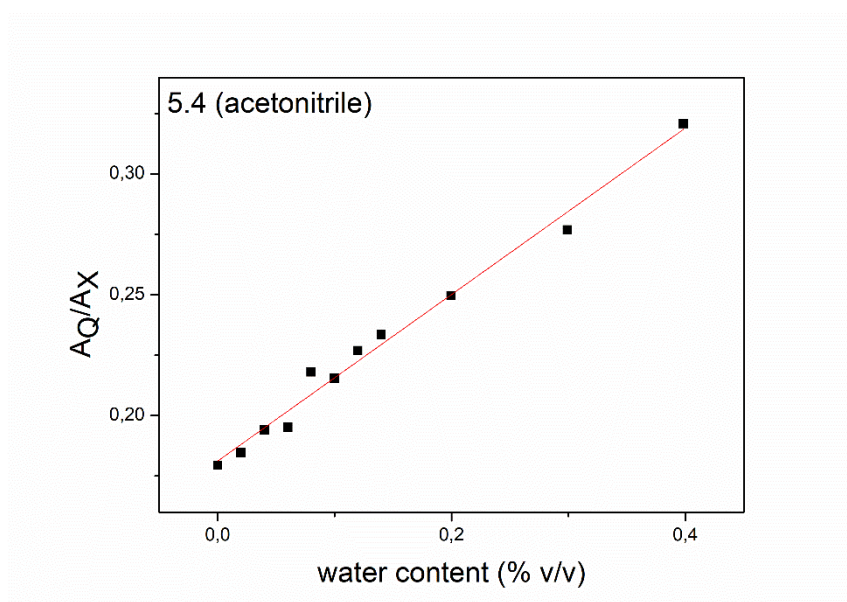
Figure 20. Changes in absorbance ratio (A_Q/A_X) of 5 µM solution of **5.4** in acetonitrile upon the addition of increasing amounts of water.

Linear regression: $A_Q/A_X = 0.345 * (\%v/v) + 0.181$ ($R^2 = 0.9852$) ($\sigma = 0.005$)
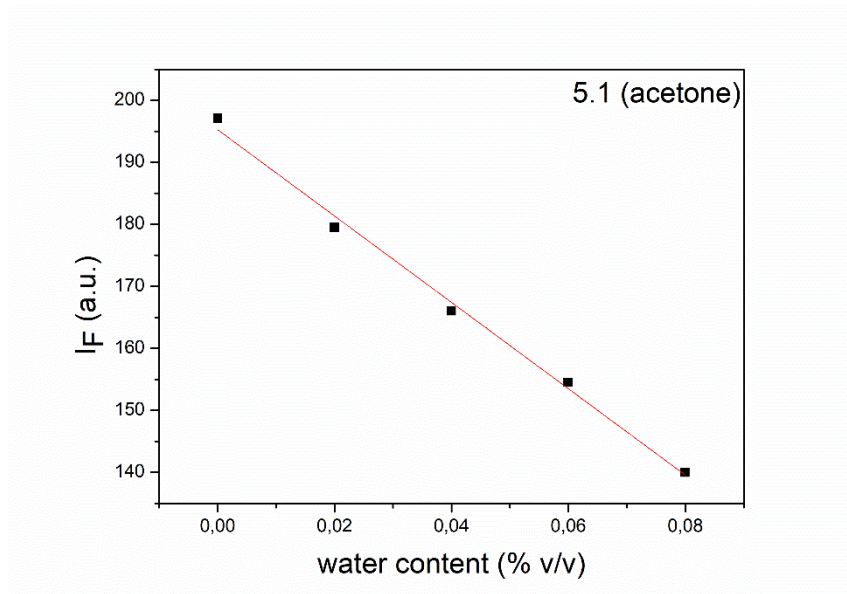
Figure 21. Changes in fluorescence intensity (I_F) of 5 µM solution of **5.1** in acetone upon the addition of increasing amounts of water.

Linear regression: I_F = -696.519 * (%v/v) + 195.281 (R^2 = 0.9932) (σ = 0.805)
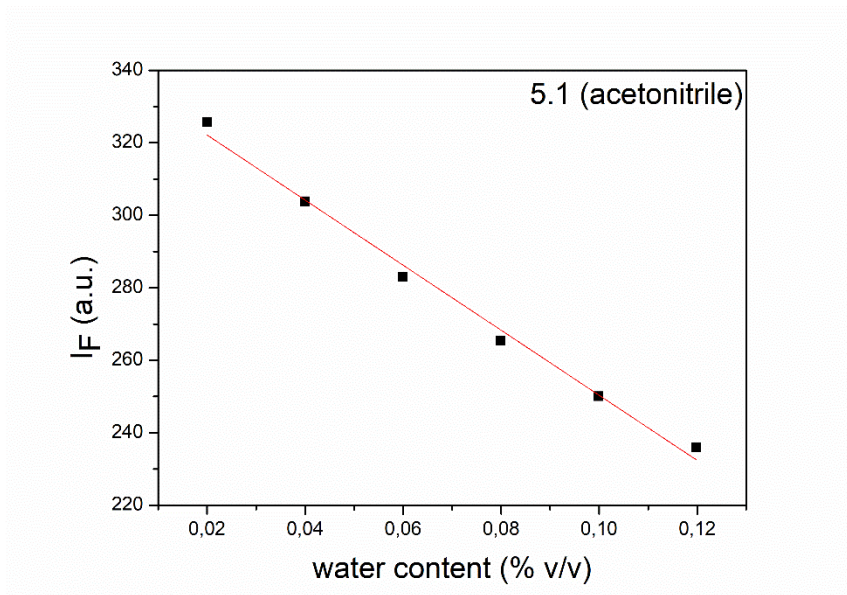
Figure 22. Changes in fluorescence intensity (I_F) of 5 µM solution of **5.1** in acetonitrile upon the addition of increasing amounts of water.

Linear regression: I_F = -897.720 * (%v/v) + 340.125 (R^2 = 0.9905) (σ = 1.156)
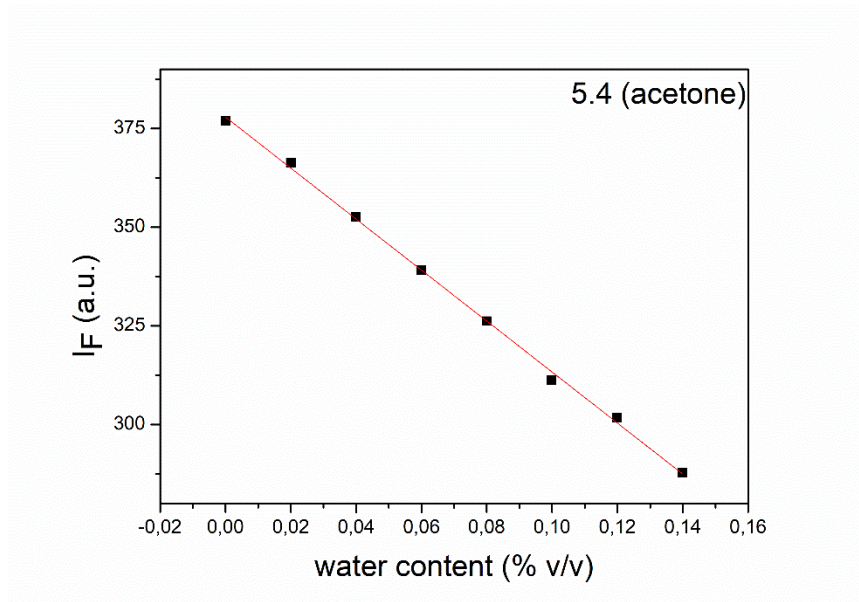
Figure 23. Changes in fluorescence intensity (I_F) of 5 µM solution of **5.4** in acetone upon the addition of increasing amounts of water.

Linear regression: I_F = -646.140 * (%v/v) + 377.905 (R^2 = 0.9985) (σ = 2.344)
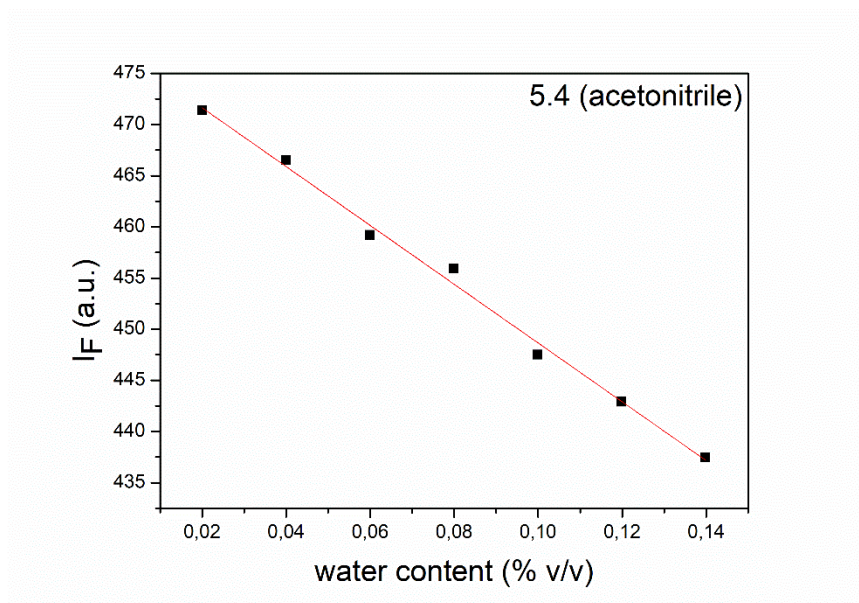
Figure 24. Changes in fluorescence intensity (I_F) of 5 µM solution of **5.4** in acetonitrile upon the addition of increasing amounts of water.

Linear regression: I_F = -287.315 * (%v/v) + 477.388 (R^2 = 0.9935) (σ = 0.941)

5.7. REFERENCES

1   A. P. De Silva, H. Q. N. Gunaratne, T. Gunnlaugsson, A. J. M. Huxley, C. P. McCoy, J. T. Rademacher and T. E. Rice, Signaling recognition events with fluorescent sensors and switches, *Chem. Rev.*, 1997, **97**, 1515–1566.

2   R. Martínez-Máñez and F. Sancenón, Fluorogenic and chromogenic chemosensors and reagents for anions, *Chem. Rev.*, 2003, **103**, 4419–4476.

3   C. Lodeiro and F. Pina, Luminescent and chromogenic molecular probes based on polyamines and related compounds, *Coord. Chem. Rev.*, 2009, **253**, 1353–1383.

4   T. L. Mako, J. M. Racicot and M. Levine, Supramolecular luminescent sensors, *Chem. Rev.*, 2019, **119**, 322–477.

5   G. Fukuhara, Analytical supramolecular chemistry: Colorimetric and fluorimetric chemosensors, *J. Photochem. Photobiol. C Photochem. Rev.*, 2020, **42**, 100340.

6   S. H. Park, N. Kwon, J. H. Lee, J. Yoon and I. Shin, Synthetic ratiometric fluorescent probes for detection of ions, *Chem. Soc. Rev.*, 2020, **49**, 143–179.

7   X. Tian, L. C. Murfin, L. Wu, S. E. Lewis and T. D. James, Fluorescent small organic probes for biosensing, *Chem. Sci.*, 2021, **12**, 3406–3426.

8   H. N. Kim, Z. Guo, W. Zhu, J. Yoon and H. Tian, Recent progress on polymer-based fluorescent and colorimetric chemosensors, *Chem. Soc. Rev.*, 2011, **40**, 79–93.

9   H. Na Kim, W. Xiu Ren, J. Seung Kim and J. Yoon, Fluorescent and colorimetric sensors for detection of lead, cadmium, and mercury ions, *Chem. Soc. Rev.*, 2012, **41**, 3210–3244.

10   X. Li, X. Gao, W. Shi and H. Ma, Design strategies for water-soluble small molecular chromogenic and fluorogenic probes, *Chem. Rev.*, 2014, **114**, 590–659.

11   B. Daly, J. Ling and A. P. De Silva, Current developments in fluorescent PET (photoinduced electron transfer) sensors and switches, *Chem. Soc. Rev.*, 2015, **44**, 4203–4211.

12   J. A. Thomas, Optical imaging probes for biomolecules: An introductory perspective, *Chem. Soc. Rev.*, 2015, **44**, 4494–4500.

13   L. You, D. Zha and E. V. Anslyn, Recent Advances in Supramolecular Analytical Chemistry Using Optical Sensing, *Chem. Rev.*, 2015, **115**, 7840–7892.

14   M. H. Lee, J. S. Kim and J. L. Sessler, Small molecule-based ratiometric fluorescence probes for cations, anions, and biomolecules, *Chem. Soc. Rev.*, 2015, **44**, 4185–4191.

15   D. Wu, A. C. Sedgwick, T. Gunnlaugsson, E. U. Akkaya, J. Yoon and T. D. James, Fluorescent chemosensors: The past, present and future, *Chem. Soc. Rev.*, 2017, **46**, 7105–7123.

16   H. S. Jung, P. Verwilst, W. Y. Kim and J. S. Kim, Fluorescent and colorimetric sensors for the detection of humidity or water content, *Chem. Soc. Rev.*, 2016, **45**, 1242–1256.

17   P. Kumar, A. Ghosh and D. A. Jose, Chemical Sensors for Water Detection in Organic Solvents and their Applications, *ChemistrySelect*, 2021, **6**, 820–842.

18   Y. Guo and W. Zhao, Nanomaterials for luminescent detection of water and humidity, *Analyst*, 2019, **144**, 388–395.

19   P. Kumar, R. Kaushik, A. Ghosh and A. D. Jose, Detection of moisture by fluorescent OFF-ON sensor in organic solvents and raw food products, *Anal. Chem.*, 2016, **88**, 11314–11318.

20   J. Feng, L. X. Duan, Z. Bin Shang, J. Bin Chao, Y. Wang and W. J. Jin, Colorimetric and fluorometric dual sensing of trace water in methanol based on a Schiff Base-Al^{3+} ensemble probe, *Spectrochim. Acta - Part A Mol. Biomol. Spectrosc.*, 2018, **201**, 185– 192.

21   W. Cheng, Y. Xie, Z. Yang, Y. Sun, M. Z. Zhang, Y. Ding and W. Zhang, General Strategy for in Situ Generation of a Coumarin-Cu^{2+} Complex for Fluorescent Water Sensing, *Anal. Chem.*, 2019, **91**, 5817–5823.

22   D. Yang, X. J. Cao, X. T. Wu, Z. X. Yang and B. X. Zhao, A FRET-based ratiometric fluorescent probe for sensing trace water in organic solvents, *Anal. Methods*, 2019, **11**, 3079–3084.

23   K. Zhang, T. T. Chen, Y. J. Shen, L. F. Zhang, S. Ma and Y. Huang, Luminescent macrocyclic Sm(III) complex probe for turn-off fluorescent and colorimetric water detection in organic solvents and liquid fuels, *Sensors Actuators, B Chem.*, 2020, **311**, 127887.

24   P. Kumar, S. Gadiyaram and D. A. Jose, Simple Iron(III) Complex Based Highly Sensitive Fluorescent Off-On Sensor for the Detection of Trace Amount of Water in Organic Solvents and Edible Oilseeds, *ChemistrySelect*, 2020, **5**, 10648–10655.

25   F. Fueyo-González, E. Garcia-Fernandez, D. Martínez, L. Infantes, A. Orte, J. A.

González-Vera and R. Herranz, Smart lanthanide antennas for sensing water, *Chem. Commun.*, 2020, **56**, 5484–5487.

26   P. Kumar and D. A. Jose, Naked eye detection of moisture in organic solvents and development of alginate polymer beads and test cassettes as a portable kit, *Anal. Chim. Acta*, 2020, **1136**, 178–186.

27   P. Yuvaraj, J. Ajantha, S. Easwaramoorthi and J. R. Rao, Low-level detection of water in polar aprotic solvents using an unusually fluorescent spirocyclic rhodamine, *New J. Chem.*, 2020, **44**, 6566–6574.

28   K. C. Behera, B. N. Patra and B. Bag, Dual mode detection of water in an organic solvent with a rhodamine-6G derivative, *Sensors Actuators, B Chem.*, 2021, **338**, 129861.

29   P. Sun, K. Xu, S. Guang and H. Xu, Monodisperse functionalized GO for water detection in wide range through synergistic enhancement effect, *Dye. Pigment.*, 2021, **185**, 108909.

30   H. Song, Y. Zhou, C. Xu, X. Wang, J. Zhang, Y. Wang, X. Liu, M. Guo and X. Peng, A dual-function fluorescent probe: Sensitive detection of water content in commercial products and rapid detection of hypochlorite with a large Stokes shift, *Dye. Pigment.*, 2019, **162**, 160–167.

31   T. Sachdeva and M. D. Milton, Fluorescent dyes for moisture detection in organic solvents: Push-pull based phenothiazine aldehydes with large Stokes shifts, *J. Photochem. Photobiol. A Chem.*, 2020, **402**, 112804.

32   S. A. Yoon, J. H. Oh, S. K. Kim and M. H. Lee, Water-sensitive ratiometric fluorescent probes and application to test strip for rapid and reversible detection of water, *Dye.*

Pigment., 2019, **165**, 421–428.

33   S. Tsumura, K. Ohira, K. Imato and Y. Ooyama, Development of optical sensor for water in acetonitrile based on propeller-structured BODIPY-type pyridine-boron trifluoride complex, *RSC Adv.*, 2020, **10**, 33836–33843.

34   P. Kumar, R. Sakla, A. Ghosh and D. A. Jose, Reversible Colorimetric Sensor for Moisture Detection in Organic Solvents and Application in Inkless Writing, *ACS Appl. Mater. Interfaces*, 2017, **9**, 25600–25605.

35   P. Kumar, A. Ghosh and D. Amilan Jose, A simple colorimetric sensor for the detection of moisture in organic solvents and building materials: Applications in rewritable paper and fingerprint imaging, *Analyst*, 2019, **144**, 594–601.

36   D. Jinbo, K. Ohira, K. Imato and Y. Ooyama, Development of fluorescent sensors based on a combination of PET (photo-induced electron transfer) and FRET (Förster resonance energy transfer) for detection of water, *Mater. Adv.*, 2020, **1**, 354–362.

37   J. Wang, X. Zhang and H. B. Liu, Highly sensitive pyrene–dansyl conjugate-based fluorescent sensor for discriminative detection of water in organic solvents, *Dye. Pigment.*, 2020, **182**, 108685.

38   Y. Wu, J. Ji, Y. Zhou, Z. Chen, S. Liu and J. Zhao, Ratiometric and colorimetric sensors for highly sensitive detection of water in organic solvents based on hydroxyl-containing polyimide-fluoride complexes, *Anal. Chim. Acta*, 2020, **1108**, 37–45.

39   F. Arshad and M. P. Sk, Aggregation-induced red shift in N,S-doped chiral carbon dot emissions for moisture sensing, *New J. Chem.*, 2019, **43**, 13240–13248.

40   J. Wang, J. Wang, W. Xiao, Z. Geng, D. Tan, L. Wei, J. Li, L. Xue, X. Wang and J. Zhu, Lignin-derived red-emitting carbon dots for colorimetric and sensitive fluorometric detection of water in organic solvents, *Anal. Methods*, 2020, **12**, 3218–3224.

41   B. Wang, X. Yuan, X. Lv, Y. Mei, H. Peng, L. Li, Y. Guo, J. Du, B. Zheng and D. Xiao, Carbon dots-based room-temperature phosphorescent test strip: Visual and convenient water detection in organic solvents, *Dye. Pigment.*, 2021, **189**, 1–9.

42   M. Zhao, H. Feng, X. Zhang, H. Ao and Z. Qian, Bonding-induced emission of silyl-protected copper nanoclusters for luminescence turn-on detection of trace water in organic solvents, *Analyst*, 2017, **142**, 4613–4617.

43   F. Galindo, J. C. Lima, S. V. Luis, M. J. Melo, A. Jorge Parola and F. Pina, Water/humidity and ammonia sensor, based on a polymer hydrogel matrix containing a fluorescent flavylium compound, *J. Mater. Chem.*, 2005, **15**, 2840–2847.

44   T. Enoki and Y. Ooyama, Colorimetric and ratiometric fluorescence sensing of water based on 9-methyl pyrido[3,4-b] indole-boron trifluoride complex, *Dalt. Trans.*, 2019, **48**, 2086–2092.

45   J. T. Wang, Y. Y. Pei, S. F. Ren, M. Y. Yan, W. Luo, B. Zhang and Q. F. Li, Two 8-hydroxyquinoline-based fluorescent chemosensors for ultra-fast and sensitive detection of water content in strong polar organic solvents with large Stokes shifts, *Spectrochim. Acta - Part A Mol. Biomol. Spectrosc.*, 2020, **229**, 117956.

46   J. Nootem, C. Sattayanon, S. Namuangruk, P. Rashatasakhon, W. Wattanathana, G. Tumcharern and K. Chansaenpak, Solvatochromic triazaborolopyridinium probes toward

ultra-sensitive trace water detection in organic solvents, *Dye. Pigment.*, 2020, **181**, 108554.

47   K. Santhiya, S. K. Sen, R. Natarajan and B. Murugesapandian, Multifunctional behavior of bis-acylhydrazone: Real-time detection of moisture in organic solvents, halochromism and aggregation induced emission, *Dye. Pigment.*, 2021, **185**, 108891.

48   A. Beltrán, M. I. Burguete, S. V. Luis and F. Galindo, Styrylpyrylium Dyes as Solvent-Sensitive Molecules Displaying Dual Fluorescence, *European J. Org. Chem.*, 2017, 4864–4870.

49   T. P. Silverstein, Fitting imidazole ^{1}H NMR titration data to the Henderson-Hasselbalch equation, *J. Chem. Educ.*, 2012, **89**, 1474–1475.

50   G. A. Reynolds and K. H. Drexhage, New coumarin dyes with rigidized structure for flashlamp-pumped dye lasers, *Opt. Commun.*, 1975, **13**, 222–225.

Chapter 6

Pyrylium salts as solid-state emitters

The results presented in this chapter are based on the following article:

Solid-state white-light emission from a pyrylium dye obtained in one synthetic step. Muñoz Resta, I.; Miravet, J. F.; Yamaji, M.; Galindo, F. *J. Mater. Chem. C* **2020**, 8, 14348.

(reproduced with permission from The Royal Society of Chemistry)

Fluorometric studies in the solid-state and DFT calculations were performed in collaboration with Dr. Minoru Yamaji from the Graduate School of Science and Engineering, Gunma University (Gunma, Japan).

6.1. INTRODUCTION

During the last decades, a great effort has been devoted to the development of new organic materials with appropriate emissive properties in the solid-state. Materials for the manufacture of optoelectronic devices such as organic light-emitting diodes (OLEDs) and organic light-emitting field-effect transistors (OLEFETs) are under a permanent innovation process. The search for systems with higher emission quantum yields (Φ_F) along with simpler production processes is a constant objective for the technological industry. However, most fluorescent molecules in solution become non-emissive in the condensed phase due to processes inhibiting the radiative decay from the excited to the ground state (aggregation-caused quenching, ACQ), typically due to intermolecular interactions, although not limited to this reason.[1]

Molecules able to avoid the quenching process in the solid phase comprise, for instance, unsymmetrical triarylamines,[2] dipiperidinobenzenes,[3] tetraphenylethylenes,[4] siloles,[5] benzoxazole and benzothiazole derivatives,[6] biindenyls[7] and tetrasubstituted benzenes.[8,9] Interestingly, some of these molecules have been implemented in practical devices shortly after the basic development. For instance, Ishow's triarylamines were converted into solid-state lasers[10] whereas Zhang's tetrasubstituted benzenes have been used recently to create optical waveguides.[11]

Within the field of solid-state emitters, there is a growing interest in finding systems capable of attaining a much complex objective like emitting white light. To reach this goal, two strategies have been followed. On the one hand to combine two fluorophores, in a host matrix, one emitting in the blue region of the spectrum and the other in the orange-red part, in such a way that the combination of them yields the desired white luminescence. This is the case, for

instance, of naphthalimide and triazine derivatives contained in silica nanoparticles,[12] or hexanuclear molybdenum clusters embedded in an ureasil matrix.[13] On the other hand, another strategy is the synthesis of organic molecules displaying broad emission bands in the range 400-700 nm. This latter approach is very attractive from the practical point of view and has led recently to interesting molecules that afford white-light emission like, for instance, difunctional 4-pyridone,[14] substituted benzophenones,[15] triazole derivatives,[16] oxazole compounds,[15] o-carborane derivatives,[17] 4-chlorobenzoyldibenzothiophene[18] and 1,2,3,4-tetraphenyloxazolium cations.[19]

Several reviews have covered the field of solid-state emissive materials, including white-light emitters, all showing examples of rational and combinatorial approaches for the discovery of emissive molecular, macromolecular and soft materials.[1,20–23] Currently there is a consensus on the need for simple operational procedures for the synthesis of luminescent materials. As stated by M. Shimizu et al. in 2010: 'High quantum yield is only one of the requirements for versatile emitting materials. Simple, cheap, efficient preparations, effortless purification, are all essential for practical applications'.[20]

In this chapter, the synthesis of seven pyrylium salts **6.1**-**6.7** (**Chart 1**) and their emissive properties, both in solution and in the solid-state, are reported. Among these dyes, compound **6.7** stands out because its luminescence in powder (when evaporated from acetonitrile) meets the criteria of the *Commission Internationale de l'Eclairage* (CIE) for white-light emission. The results presented here can be an opportunity to expand the family of known dyes showing white-light emission to the group of pyrylium compounds. Scarce studies have been published

describing the emission of solid samples of pyrylium salts, most of them from the qualitative viewpoint.[24–27]
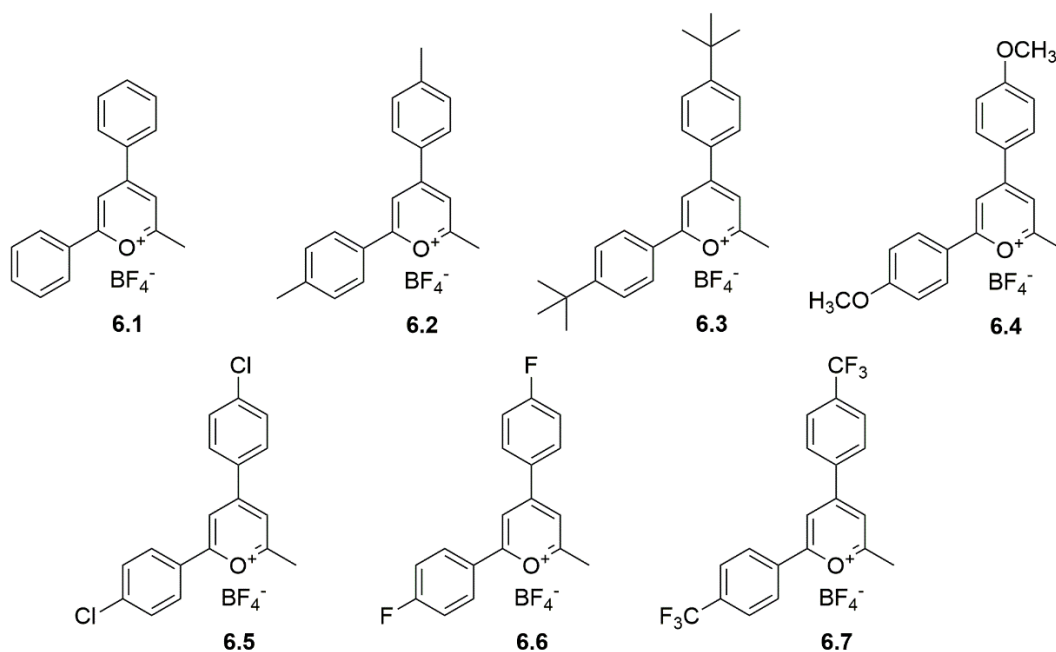
Chart 1. Pyrylium salts synthesized and studied as solid-state emitters.

6.2. RESULTS AND DISCUSSION

6.2.1. SYNTHESIS AND CHARACTERISATION

Synthesis of **6.1-6.7** was accomplished by means of a condensation reaction between acetic anhydride and two molecules of the corresponding p-substituted acetophenone in the presence of BF$_3$-etherate as catalyst (**Scheme 1**).[28] After 2 h of reaction at 138 ºC, the coloured solution was poured into an excess of diethyl ether and the precipitated product was recovered by simple filtration. After washing with abundant ether, multigram samples of the dyes can be obtained (20 - 35 % yields) with excellent purity (checked by ^{1}H / ^{13}C NMR and high-resolution mass spectrometry, HR-MS).
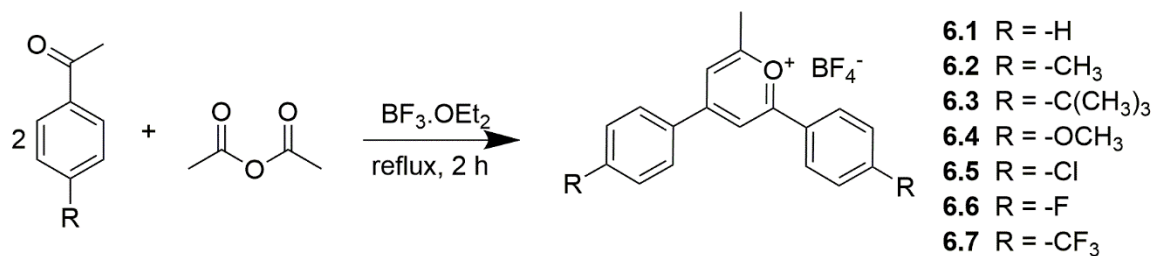
Scheme 1. Synthesis of compounds **6.1**-**6.7.**

Their photophysical properties were determined in two solvents of different polarities: dichloromethane (DCM) and acetonitrile (ACN) (**Figure 1**). The data for all the compounds are collected in **Table 1**.
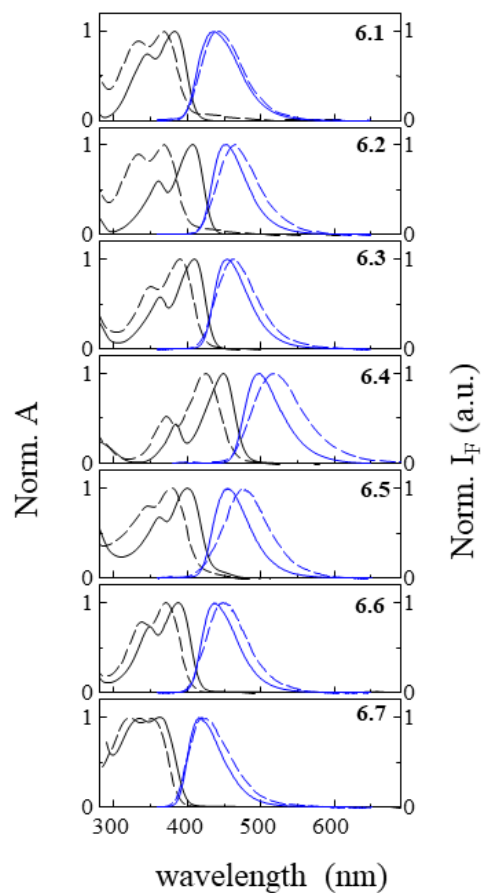
Figure 1. Absorption (black) and fluorescence (blue) spectra of compounds **6.1-6.7** in DCM (full) and ACN (broken). The excitation wavelength for the emission spectra was set at 340 nm (360 nm for compound **6.4**).

Table 1. Photophysical parameters in solution for compounds **6.1-6.7.**

Compd.	Solvent	λabs (log ε) (nm)		λem (nm)	Φ_F	τ (ns)	$k_r/10^8$ (s^{-1})
6.1	DCM	345 (4.36)	383 (4.50)	436	0.38	1.5	2.5
	ACN	333 (4.22)	368 (4.27)	440	0.51	3.4	1.5
6.2	DCM	360 (4.40)	407 (4.62)	453	0.50	2.0	2.5
	ACN	349 (4.31)	388 (4.45)	465	0.63	3.7	1.7
6.3	DCM	363 (4.48)	410 (4.72)	453	0.54	2.0	2.8
	ACN	350 (4.26)	390 (4.37)	461	0.62	3.3	1.9
6.4	DCM	384 (4.42)	448 (4.76)	499	0.82	3.2	2.5
	ACN	371 (4.34)	425 (4.60)	516	0.35	2.3	1.5
6.5	DCM	362 (4.21)	400 (4.38)	455	0.39	1.5	2.5
	ACN	346 (4.35)	378 (4.45)	477	0.51	3.3	1.5
6.6	DCM	349 (4.40)	388 (4.54)	437	0.46	1.8	2.5
	ACN	338 (4.28)	371 (4.36)	447	0.60	3.7	1.6
6.7	DCM	334 (4.40)	362 (4.42)	416	0.25	1.0	2.5
	ACN	321 (4.26)	352 (4.25)	420	0.36	2.3	1.6

In dichloromethane (DCM) and acetonitrile (ACN) solutions, the pyrylium dyes display bluish fluorescence except for **6.4**, with electron-donating methoxy groups, which have the emission displaced to longer wavelengths (**Figure 1**). This band is affected by the polarity of the solvent suggesting the charge-transfer nature of the first singlet excited state (S_1), i.e. occurring the transfer from the external electron-rich aromatic rings to the central electron-poor pyrylium core, in accordance with the observations made for other pyrylium derivatives.[29] Additionally, the shift of the absorption bands towards higher wavelengths in DCM, as compared to ACN, is also compatible with this explanation and matches the behaviour of related pyrylium dyes.[29]

All the studied compounds are strongly emissive, with fluorescence Φ_F ranging from 0.25 to 0.82 (**Table 1**) and with emission lifetimes (τ) ranging from 1.0 to 3.7 ns. Calculated radiative constants using both Φ_F and τ ($k_r = \Phi_F / \tau$) afford two subsets of values: k_r^{DCM} in the range 2.5-2.8 x 10^8 s^{-1} and k_r^{ACN} in the range 1.5-1.9 x 10^8 s^{-1}. Hucke et al. found that the k_r^{ACN}

of triarylpyrylium dyes is about 10-30% lower than the corresponding k_r^{DCM}, which is corroborated in this chapter.[29]

Their thermal properties have been measured by thermogravimetric analysis -TGA- and differential scanning calorimetry -DSC- (**Figure 2**) and it has been found that **6.1**-**6.7** are stable below 240 ºC (**Table 2**), in the same range of temperatures as those reported for other pyrylium salts.[27]

Table 2. Thermal decomposition temperatures (T_{ds}) of **6.1**–**6.7**

Compd.	**6.1**	**6.2**	**6.3**	**6.4**	**6.5**	**6.6**	**6.7**
T_{ds} (ºC)ª	245	253	240	261	241	247	234

(a) 5% weight loss
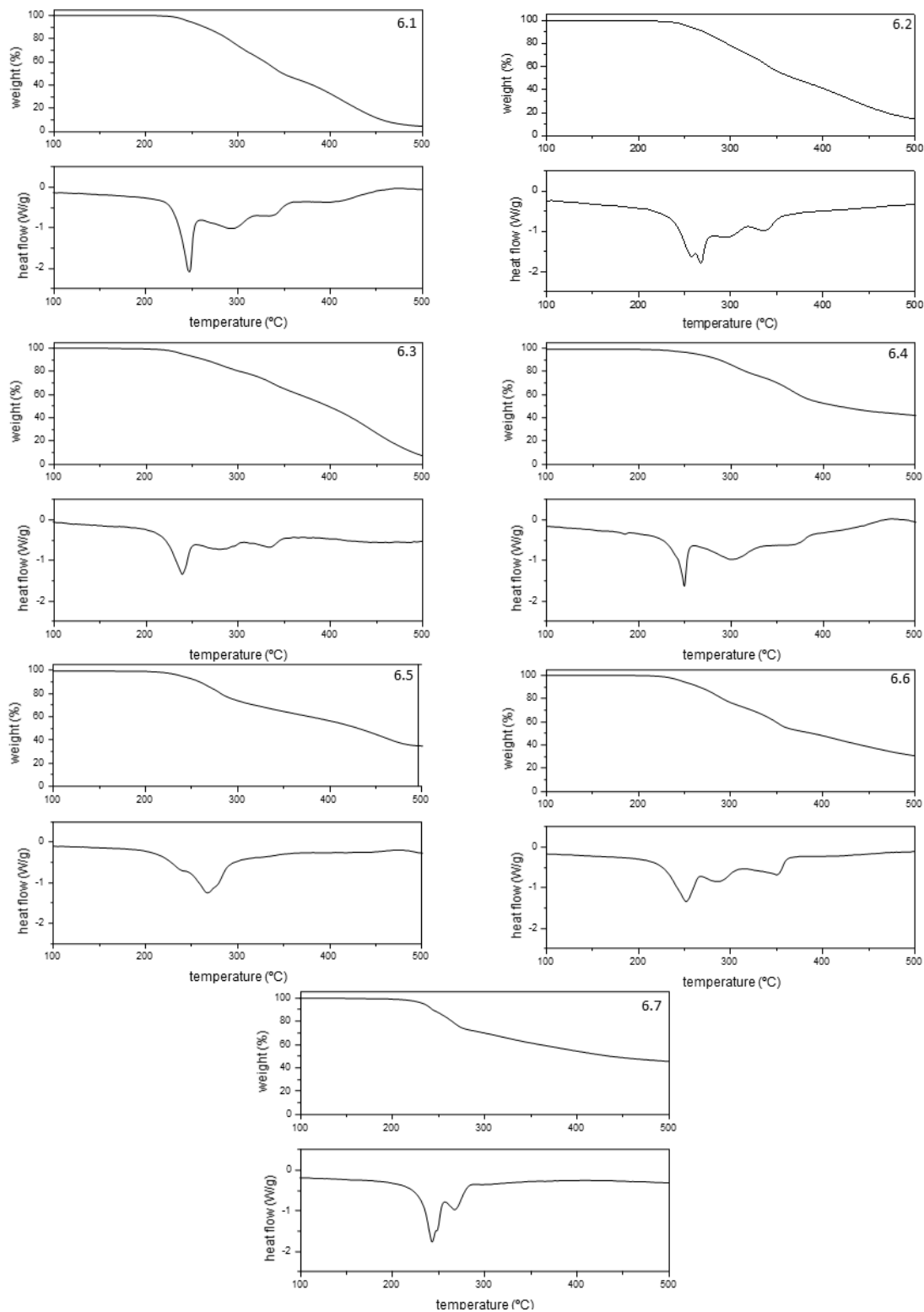
Figure 2. TGA plots and DSC thermograms (exothermic up) for compounds **6.1**-**6.7** obtained at a heating rate of 10ºC/min under N_2 atmosphere.

6.2.2. SOLID-STATE EMISSION

It has been reported that the conditions for the preparation of the solids, either crystalline or amorphous, can have a powerful influence on the emission of the molecules, due to the different polymorphs that can be formed.[30–33] Taking this possibility into account, two samples from each pyrylium salt were prepared, one evaporated from DCM and another from ACN solutions, leading to powders whose spectral features, including solid-state Φ_F, were determined using an integrating sphere (**Table 3**). As it can be seen in **Figure 3**, the emission wavelengths of all the studied compounds are shifted to lower energies, as compared to the fluorescence spectra in solution. This phenomenon is quite commonly observed and reported in the literature, but there is no general explanation for all the described compounds.

Table 3. Photophysical parameters in the solid-state for compounds **6.1-6.7**

Compd.	Evaporated from	λem (nm)			Φ_F	CIE coordinates
6.1	DCM		500		0.43	(0.25, 0.46)
	ACN		500		0.24	(0.25, 0.43)
6.2	DCM	560 (shoulder@500)			0.24	(0.43, 0.51)
	ACN		570		0.27	(0.50, 0.47)
6.3	DCM	495		560	0.26	(0.37, 0.47)
	ACN	550		710	0.10	(0.35, 0.51)
			(broad)			
6.4	DCM		595		0.14	(0.57, 0.42)
	ACN		585		0.19	(0.54, 0.46)
6.5	DCM		480		0.33	(0.16, 0.38)
	ACN	515		680	0.11	(0.28, 0.51)
			(broad)			
6.6	DCM	535 (shoulder@475)			0.21	(0.29, 0.42)
	ACN	450	515	680	0.13	(0.22, 0.33
			(broad)			
6.7	DCM	430		530	0.17	(0.35, 0.46)
	ACN	450		520	0.09	(0.28, 0.36)
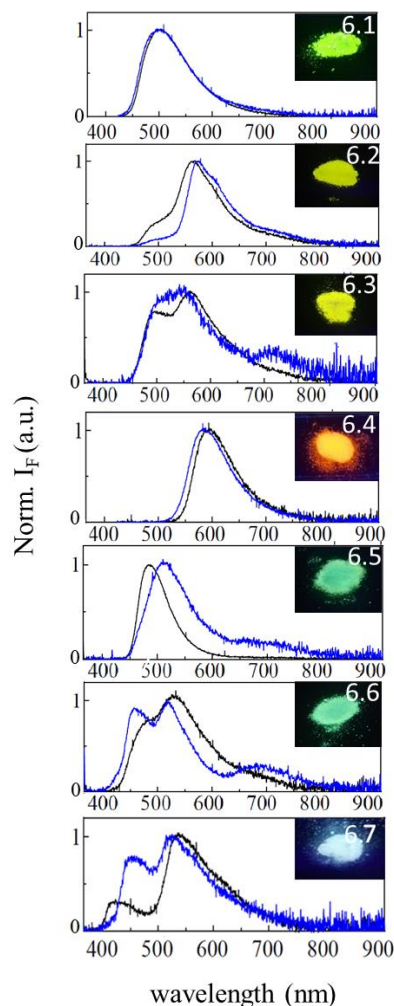
Figure 3. Fluorescence spectra for compounds **6.1**-**6.7** obtained in the solid-state evaporated from DCM (black) and ACN (blue). Inset: emission features in the solid-state (evaporation from ACN) under UV illumination (365 nm).

Emissions from excimers (intermolecular) or exciplexes (normally intramolecular) can account for such low-energy emissions, but also emission from the locally excited S_1 in a constrained molecular organization is possible.[34–38] On other occasions, less common, room temperature phosphorescence is observed. For instance, recently the group of B. Z. Tang has described a molecule displaying white dual phosphorescence (from the triplet excited states T_1 and T_2) at 300 K with a solid-state Φ_F of 7.2 %.[18]

The room-temperature phosphorescence of pyrylium salts have been published, with reported emissions shifted about 40-90 nm to lower energies relative to fluorescence bands (depending on the substitution on the aromatic rings) but always in conditions of restricted movement like in poly(methyl methacrylate) (PMMA) matrices[39] or cucurbiturils as supramolecular hosts.[40] Specifically, there is one report describing the phosphorescence of a compound related to **6.1** (same pyrylium core but ClO_4^- instead of BF_4^- as counterion) in PMMA which situates the emission from T_1 at 525 nm (room temperature).[39] In this case, powders obtained from DCM or ACN display emission at 500 nm at room temperature. However, this occurs in air atmosphere, which makes very unlikely that such an emission comes from a triplet state.

Li and co-workers reported a wide-shape spectrum of a diarylpyrylium salt structurally related to **6.1** but only interpreted the longer wavelength emission as arising from aggregated species.[24] Most likely, excimeric emission or fluorescence from S_1 in a distorted geometry is the most plausible explanation of the emissions observed for **6.1**-**6.7** (**Figure 3**). As a matter of fact, some of the studied compounds show two or even three bands, which points to a combination of emissive processes. Moreover, the existence of solvates or co-crystals could play a key role in the observed emissive properties.

The most remarkable feature of the spectra recorded in the solid-state becomes apparent when the CIE coordinates for such emissions are calculated, and even more clear when looking at pictures of powders of **6.1**-**6.7** (**Figures 3** and **4A**), taken under UV excitation (365 nm). The solid-state emission of compounds **6.1**-**6.3**, **6.5** and **6.6** oscillates within the blue-green-yellow range, whereas the one of compound **6.4** is clearly orange. Notably, the emission of **6.7** is white when evaporated from ACN ($\Phi_F = 9$ %).
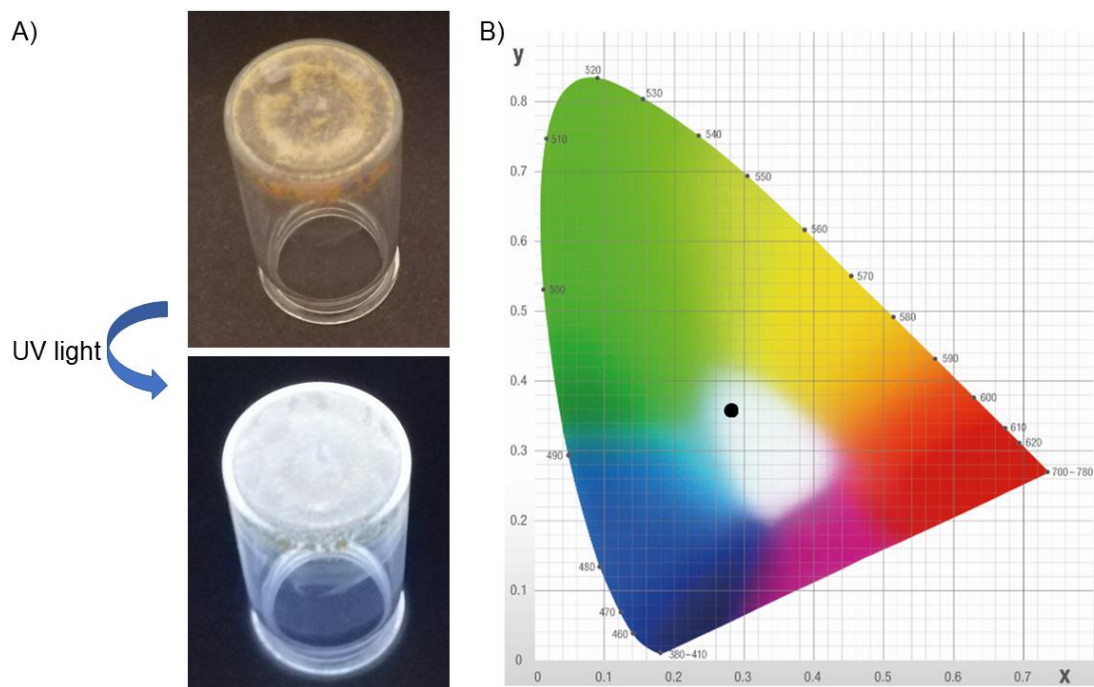
Figure 4. A) Picture of an inverted vial where a solution of **6.7** in ACN has been evaporated under visible (up) and UV light -365 nm- (down) B) Chromatic diagram (from Konica-Minolta) showing the coordinates (0.28, 0.36) for compound **6.7** evaporated from ACN (black dot in the white area).

The recorded chromatic coordinates for **6.7** (from ACN) are (0.28, 0.36), which can be considered as white color according to the published standards (**Figure 4B**).[17,41] This emissive property does not appear when **6.7** is evaporated from DCM. The results here presented highlight the importance of the solvent on the emission properties of the solids resulting after evaporation. Although parameters such as evaporation speed, temperature and initial concentration of emitter are not optimized, it is expected that fine-tuning of those variables would lead, in future studies, to a better adjustment of the emission, until matching the ideal CIE coordinates for white luminescence (0.33, 0.33). In this regard, it is worth mentioning that the counter-anion can have a profound influence on the emission properties of the solids, as it has been recently demonstrated by G. Zhang and co-workers,[42] and consequently, replacing

tetrafluoroborate by other anions, such as chloride, perchlorate, nitrate, etc., could help in the fine tuning of the solid-state emission.

6.2.3. *DFT CALCULATIONS*

To have an insight into the photophysical features of the studied compounds, DFT and TD-DFT calculations were performed at the B3LYP/6-31+G(d) level. In the optimized structures of compounds **6.1-6.7**, the HOMO and LUMO are located over the diphenylpyrylium moiety irrespective of the solvent polarity, as can be seen in **Figures 5** and **6**.
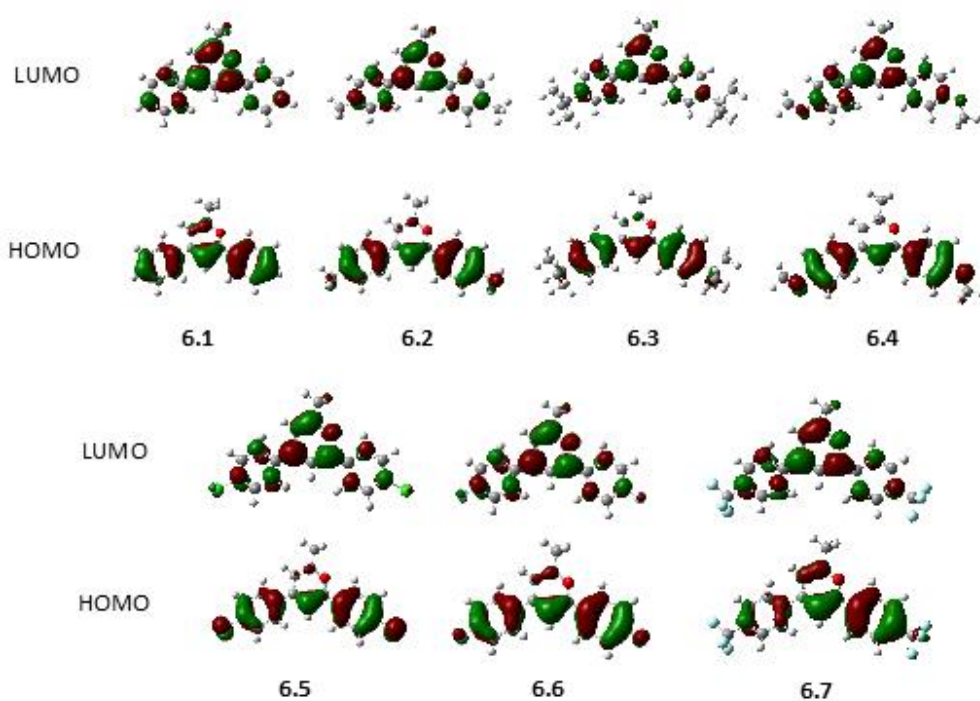
Figure 5. The HOMO and LUMO orbitals of compounds **6.1**-**6.7** in DCM.
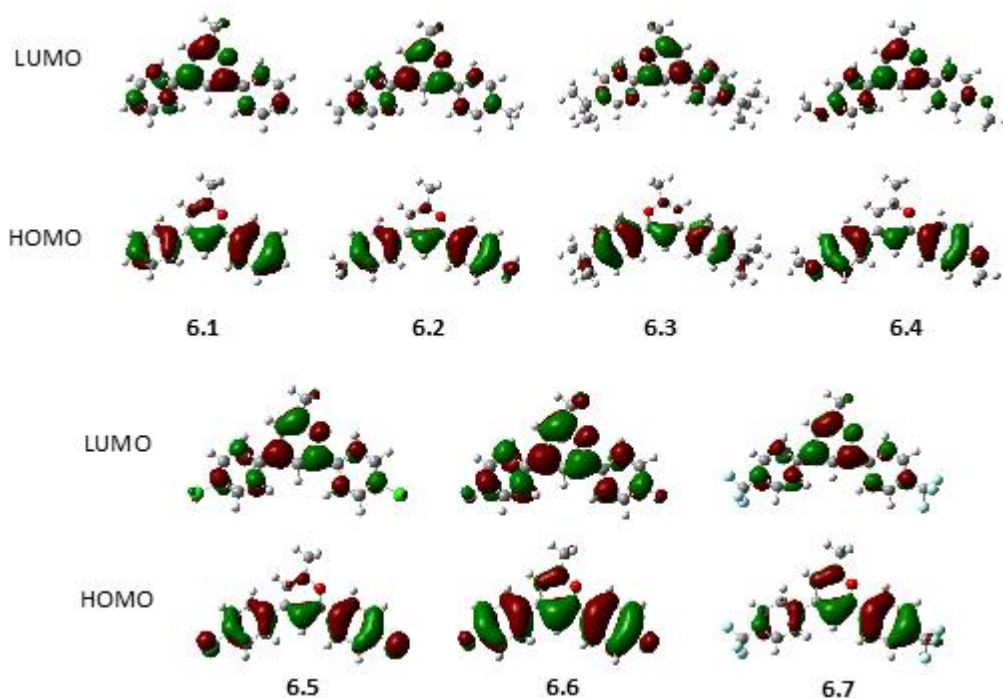
Figure 6. The HOMO and LUMO orbitals of compounds **6.1**-**6.7** in ACN.

The $S_0 \rightarrow S_1$ transitions of compounds **6.1**-**6.7** contributed from the HOMO $\rightarrow$ LUMO configurations can be assigned as a π,π^* transition. The wavelengths (λ_{tr}) estimated from the calculated transition energies are in the 380–450 nm wavelength region and are similar to the experimental λ_{abs} values of the lowest energy absorption bands in DCM (**Table 4**). The magnitude of the calculated oscillator strengths (f) for the $S_0 \rightarrow S_1$ transitions is responsible for the allowed π,π^* transition. The calculated results well agree with those obtained experimentally.

Table 4. Calculation results for compounds **6.1**-**6.7** in DCM.[a]

Compd.	HOMO / eV	LUMO / eV	λ_{tr} [b]/ nm	f [c]	Coefficient[d]
6.1	-7.60	-3.86	383	0.7036	0.70369
	(-7.35)	(-3.59)	(379)	(0.6800)	(0.70526)
6.2	-7.29	-3.75	405	0.8509	0.70191
	(-7.05)	(-3.49)	(400)	(0.8253)	(0.70518)
6.3	-7.28	-3.75	408	0.9282	0.70514
	(-7.06)	(-3.50)	(403)	(0.9050)	(0.70507)
6.4	-6.82	-3.60	442	0.9712	0.70518
	(-6.60)	(-3.35)	(436)	(0.9437)	(0.70507)
6.5	-7.50	-3.98	406	0.8691	0.70539
	(-7.26)	(-3.64)	(400)	(0.8408)	(0.70518)
6.6	-7.57	-3.90	389	0..7352	0.70520
	(-7.32)	(-3.62)	(384)	(0.7101)	(070498)
6.7	-8.05	-4.18	368	0.7256	0.69963
	(-7.77)	(-3.88)	(365)	(0.7052)	(0.69854)

[a] In parentheses, data in ACN.
[b] Wavelength estimated from the HOMO-LUMO energy gap.
[c] Oscillator strength for the $S_0 \rightarrow S_1$ transition.
[d] For the HOMO-LUMO transition.

6.3. CONCLUSIONS

In summary, by means of a straightforward reaction, seven pyrylium salts have been synthesized and characterized employing $^1H/^{13}C$ NMR, HRMS, absorption and emission spectroscopies, including solid-state fluorescence. One of the synthesized dyes displays white-light emission (CIE coordinates 0.28, 0.36) when evaporated from ACN and upon excitation with UV light. Provided the simplicity of the synthetic procedure, compound **6.7** could be of utility for diverse applications in the optoelectronic industry.

6.4. EXPERIMENTAL SECTION

6.4.1. Reagents and instruments

All commercially available reagents and solvents were used as received. ^1H and ^{13}C NMR spectra were recorded with a Bruker Advance III HD spectrometer (400 MHz for ^1H and 101 MHz for ^{13}C). High-resolution mass spectra were obtained with a Waters Q-Tof Premier mass spectrometer with an electrospray source. UV-vis spectra were obtained with a Jasco V-630 UV-vis spectrophotometer. Steady-state emission (solution) was recorded with an Agilent Cary-Eclipse spectrofluorometer. Time-resolved fluorescence experiments (solution) were performed with an IBH5000U apparatus by using 372 nm (fwhm 1.3 ns) and 464 nm (fwhm 1.4 ns) nanoLEDs as excitation sources. Solid-state measurements were recorded in a C13534-01 apparatus from Hamamatsu Photonics K.K. TGA/DSC measurements were performed on a Mettler Toledo TGA/SDTA851e/LF/1600 instrument at a heating rate of 10ºC/min under N_2 atmosphere.

6.4.2. Synthesis of compounds 6.1-6.7

To a solution of the correspondent *para*-substituted acetophenone (10 mmol) in acetic anhydride (20 mmol, 1.89 ml), BF_3 diethyl etherate (7 mmol, 0.88 ml) was added dropwise under continuous stirring at room temperature. Then, the solution was heated to reflux in a silicone oil bath at 138 ºC for 2 hours. After cooling down to room temperature, the reaction mixture was poured into 200 ml of diethyl ether, and the formed precipitate was recovered by filtration and washed with diethyl ether. For compounds **6.3**, **6.4**, **6.5** and **6.7**, further purification by recrystallization in acetic acid was needed. All the obtained solids were dried under vacuum before use.

Compound 6.1. 2-methyl-4,6-diphenylpyrylium tetrafluoroborate (Yellow solid, yield 32%): ^{1}H NMR (400 MHz, CD$_3$CN) δ 8.67 (d, J = 1.7 Hz, 1H), 8.36 – 8.32 (m, 2H), 8.23 – 8.17 (m, 3H), 7.86 – 7.81 (m, 2H), 7.77 – 7.71 (m, 4H), 3.00 (s, 3H). ^{13}C NMR (101 MHz, CD$_3$CN) δ 178.78, 173.27, 167.67, 136.58, 133.68, 131.39, 131.20, 130.74, 130.08, 129.73, 120.11, 116.51, 22.12. HRMS (ESI-TOF)$^+$ calculated for C$_{18}$H$_{15}$O$^+$ (M$^+$) (m/z): 247.1120; experimental (M$^+$) (m/z): 247.1123.

Compound 6.2. 2-methyl-4,6-di-p-tolylpyrylium tetrafluoroborate (Yellow solid, yield 20%): ^{1}H NMR (400 MHz, CD$_3$CN) δ 8.56 (d, J = 1.8 Hz, 1H), 8.25 – 8.17 (m, 2H), 8.14 – 8.06 (m, 3H), 7.55 (dd, J = 8.0, 0.6 Hz, 4H), 2.94 (s, 3H), 2.51 (s, 6H). ^{13}C NMR (101 MHz, CD$_3$CN) δ 177.28, 172.89, 166.62, 148.62, 148.35, 131.91, 131.68, 130.55, 129.45, 127.20, 118.59, 115.03, 22.01, 21.96, 21.71. HRMS (ESI-TOF)$^+$ calculated for C$_{20}$H$_{19}$O$^+$ (M$^+$) (m/z): 275.1436; experimental (M$^+$) (m/z): 247.1438.

Compound 6.3. 2,4-bis(4-(tert-butyl)phenyl)-6-methylpyrylium tetrafluoroborate (Light orange solid, yield 24%): ^{1}H NMR (400 MHz, CD$_3$CN) δ 8.61 (d, J = 1.7 Hz, 1H), 8.31 – 8.22 (m, 2H), 8.20 – 8.11 (m, 3H), 7.86 – 7.71 (m, 4H), 2.95 (s, 3H), 1.40 (s, 18H). ^{13}C NMR (101 MHz, CD$_3$CN) δ 177.38, 177.38, 172.78, 166.47, 161.15, 160.90, 130.59, 130.50, 129.41, 128.34, 128.11, 127.24, 118.75, 115.31, 36.30, 36.28, 31.12, 31.11, 21.73. HRMS (ESI-TOF)$^+$ calculated for C$_{26}$H$_{31}$O$^+$ (M$^+$) (m/z): 359.2375; experimental (M$^+$) (m/z): 359.2383.

Compound 6.4. 2,4-bis(4-methoxyphenyl)-6-methylpyrylium tetrafluoroborate (Red solid, yield 35%): ^{1}H NMR (400 MHz, CD$_3$CN) δ 8.38 (d, J = 1.8 Hz, 1H), 8.29 – 8.24 (m, 2H), 8.22 – 8.17 (m, 2H), 7.93 (d, J = 1.8 Hz, 1H), 7.25 – 7.17 (m, 4H), 3.95 (s, 3H), 3.95 (s, 3H), 2.86 (s, 3H). ^{13}C NMR (101 MHz, CD$_3$CN) δ 175.30, 171.90, 167.20, 166.64, 164.66, 133.03, 131.73,

125.26, 122.20, 116.80, 116.54, 116.48, 113.02, 57.01, 56.94, 21.42. HRMS (ESI-TOF)$^+$ calculated for $C_{20}H_{19}O_3^+$ (M$^+$) (m/z): 307.1334; experimental (M$^+$) (m/z): 307.1332.

Compound 6.5. 2,4-bis(4-chlorophenyl)-6-methylpyrylium tetrafluoroborate (Yellow solid, yield 30%): ^{1}H NMR (400 MHz, CD$_3$CN) δ 8.63 (d, J = 1.7 Hz, 1H), 8.33 – 8.28 (m, 2H), 8.20 (d, J = 1.4 Hz, 1H), 8.19 – 8.14 (m, 2H), 7.78 – 7.73 (m, 4H), 2.99 (s, 3H). ^{13}C NMR (101 MHz, CD3CN) δ 178.92, 171.91, 166.08, 142.55, 142.42, 132.26, 132.07, 131.94, 131.31, 131.27, 131.18, 130.98, 128.42, 119.91, 116.94, 116.32, 21.92. HRMS (ESI-TOF)$^+$ calculated for $C_{18}H_{13}Cl_2O^+$ (M$^+$) (m/z): 315.0343; experimental (M$^+$) (m/z): 315.0347.

Compound 6.6. 2,4-bis(4-fluorophenyl)-6-methylpyrylium tetrafluoroborate (Yellow solid, yield 27%): ^{1}H NMR (400 MHz, CD$_3$CN) δ 8.59 (d, J = 1.3 Hz, 1H), 8.49 – 8.33 (m, 2H), 8.33 – 8.21 (m, 2H), 8.16 (s, 1H), 7.48 (t, J = 8.6 Hz, 4H), 2.98 (s, 3H). ^{13}C NMR (101 MHz, CD$_3$CN) δ 178.19, 171.77, 169.25, 169.03, 166.69, 166.47, 165.85, 133.47, 133.37, 132.42, 132.32, 129.65, 126.22, 119.26, 118.39, 118.28, 115.73, 21.69. HRMS (ESI-TOF)$^+$ calculated for $C_{18}H_{13}F_2O^+$ (M$^+$) (m/z): 283.0934; experimental (M$^+$) (m/z): 283.0934.

Compound 6.7. 2-methyl-4,6-bis(4-(trifluoromethyl)phenyl)pyrylium tetrafluoroborate (Yellow solid, yield 28%): ^{1}H NMR (400 MHz, CD$_3$CN) δ 8.81 (d, J = 1.7 Hz, 1H), 8.51 (dd, J = 8.9, 0.7 Hz, 2H), 8.36 (d, J = 1.5 Hz, 1H), 8.34 (dd, J = 8.9, 0.7 Hz, 2H), 8.09 – 8.03 (m, 4H), 3.08 (s, 3H). ^{13}C NMR (101 MHz, CD$_3$CN) δ 180.92, 171.82, 166.78, 137.11, 136.41, 136.25, 136.09, 135.92, 133.17, 131.33, 130.35, 127.96-127.86 (m), 122.05, 22.36. (ESI-TOF)$^+$ calculated for $C_{20}H_{13}F_6O^+$ (M$^+$) (m/z): 383.0871; experimental (M$^+$) (m/z): 383.0866.

6.4.3. Absorption and Fluorometric studies in solution

1mM stock solutions of compounds **6.1**-**6.7** were prepared in acetonitrile. For the measurements of the absorption spectra, the correspondent stock solution for each compound was diluted to reach a final concentration of 10 µM, both in dichloromethane and acetonitrile. For emission spectra, concentration was adjusted to reach a value of 0.1 in absorbance, to minimize the primary inner filter effect. λ_{exc} was set at 340 nm for all compounds, except for compound **6.4** (360 nm).

Fluorescence Quantum Yield Measurements (ϕ_F). The fluorescence quantum yields of all compounds were determined in dichloromethane and acetonitrile, under an N_2 atmosphere. Quinine sulfate ($\phi_F = 0.55$ in H_2SO_4 0.5 M)[43] was used as a reference for compounds **6.1**-**6.3**, **6.5**-**6.7** and Acridine Orange ($\phi_F = 0.2$ in ethanol -0.01 M KOH-)[44] was used as a reference for compound **6.4**.

The concentration of the reference and the studied compounds were adjusted to obtain the same absorption at the excitation wavelength. Fluorescence quantum yields were calculated by using [Equation (1)]:

$$\phi_F = \phi_R \cdot (A_R \cdot F_S / A_S \cdot F_R) \cdot (n_S^2 / n_R^2) \qquad (1)$$

where ϕ_F is the fluorescence quantum yield, F is the integral of the emission spectrum, A is the absorption intensity, and n is the refractive index. The subindex R refers to the reference compound and S to the studied pyrylium salt.

Fluorescence Lifetime Measurements (τ_F). The fluorescence lifetimes of all compounds were determined in dichloromethane and acetonitrile, under an N_2 atmosphere. For this purpose,

solutions were prepared similarly to those used to obtain the emission spectra. Fluorescence lifetimes were determined by using the technique of time-correlated single-photon counting (TCSPC). Data obtained from the experiments were adjusted to a single exponential model by using the software IBH DAS6.

6.4.4. Fluorometric studies in the solid-state

The fluorescence quantum yields and fluorescence spectra in the solid-state were obtained with an absolute PL quantum yield measurement system (C13534-01) from Hamamatsu Photonics K.K. The 1931 x,y chromaticity diagram was obtained from the Konica-Minolta website.

6.4.5. DFT calculations

The calculation was carried out at the DFT level, using the Gaussian 09 software package. The geometries of the studied compounds **6.1**-**6.7** ignored with the counter anion, BF_4^- were fully optimized by using the 6-31+G(d) base set at the B3LYP method on the CPCM model considering dielectric constants of DCM and ACN. Atom coordinates for the optimized geometries of the compounds are listed in **Tables 5-18**.

6.5. SPECTROSCOPIC DATA OF COMPOUNDS

Compound 6.1
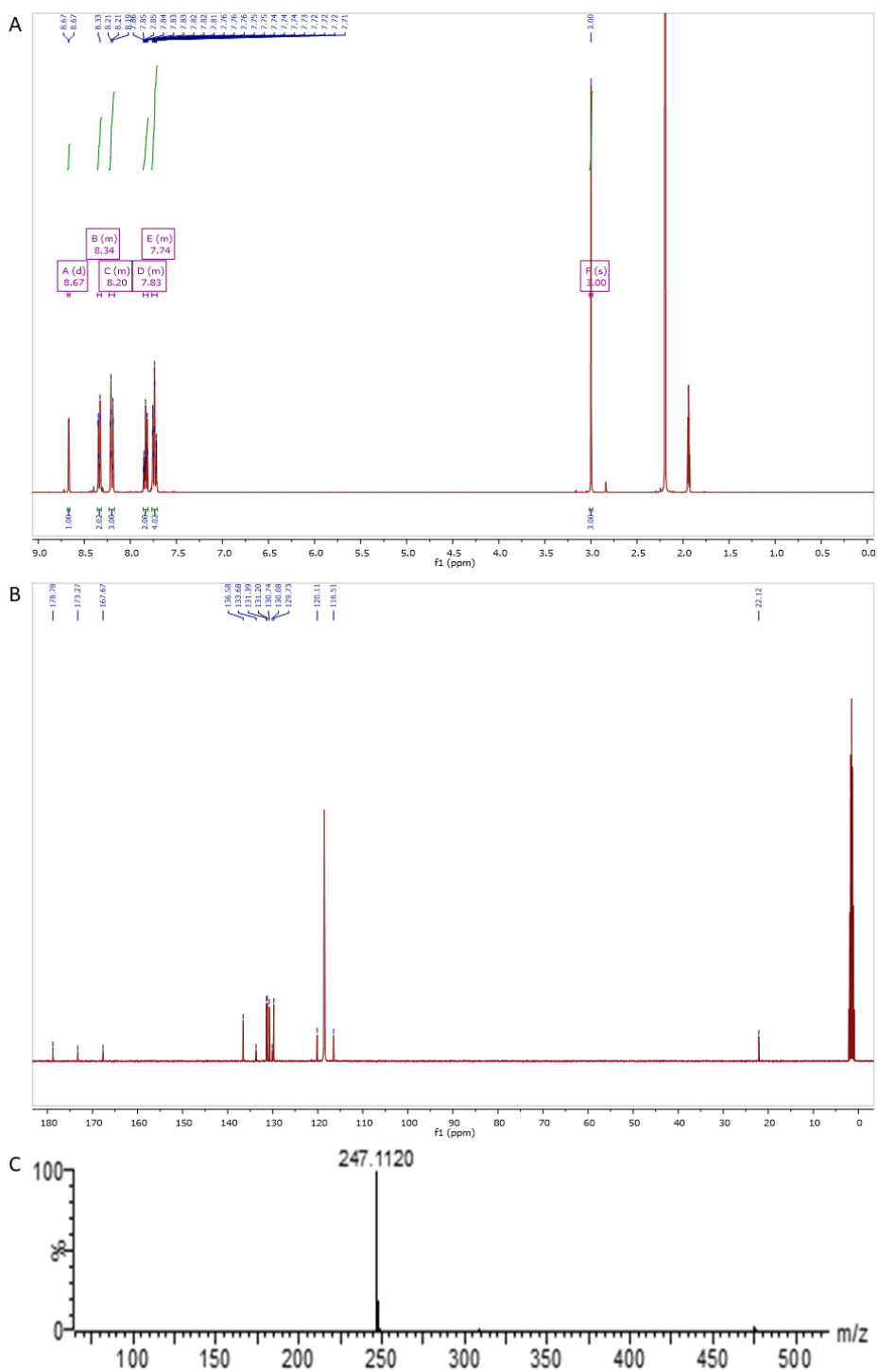
Figure 7. A) ^{1}H NMR (CD$_3$CN) spectrum of compound **6.1** B) ^{13}C NMR (CD$_3$CN) spectrum of compound **6.1** C) HRMS spectrum of compound **6.1**.

Compound 6.2
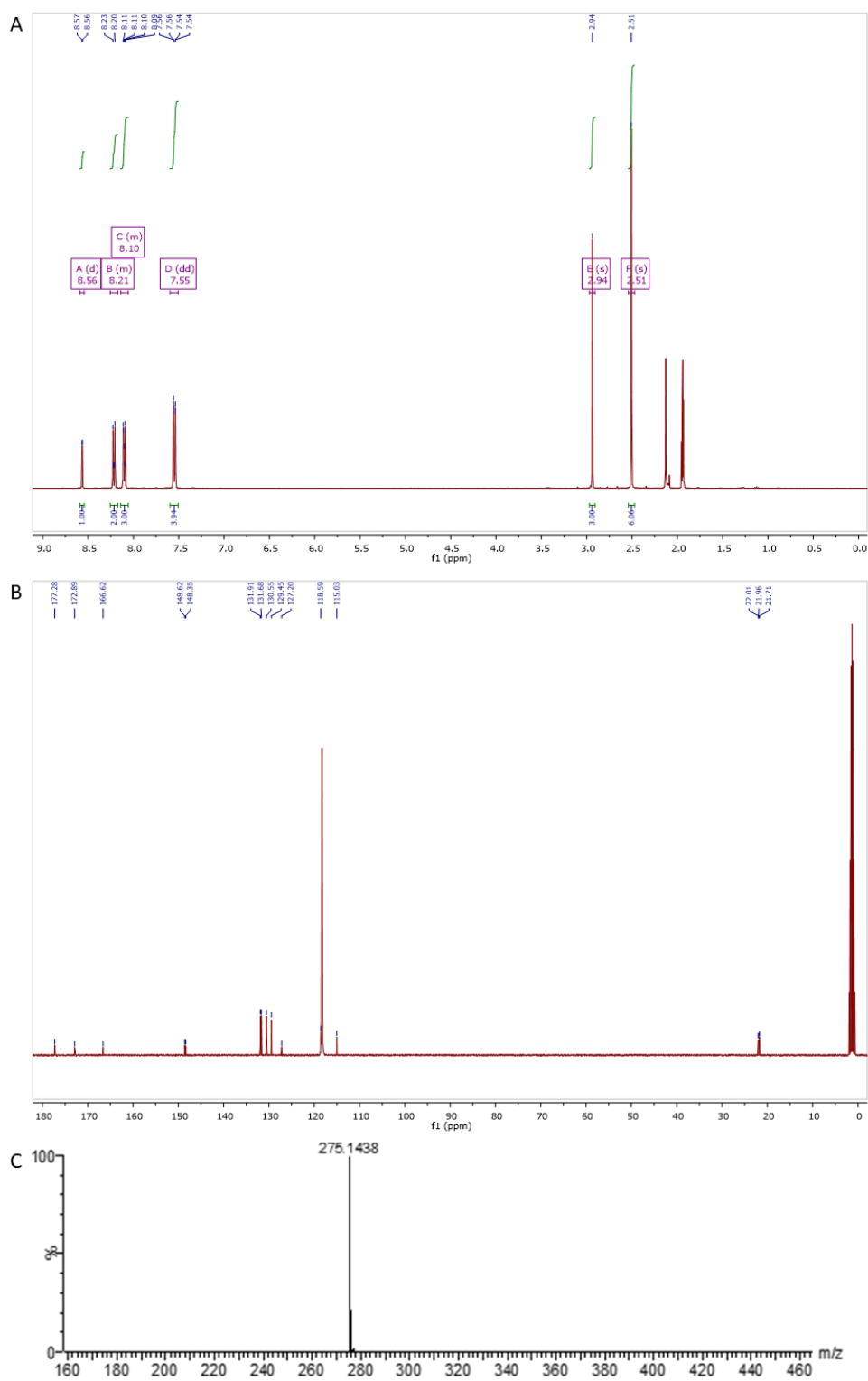
Figure 8. A) ^{1}H NMR (CD$_3$CN) spectrum of compound **6.2** B) ^{13}C NMR (CD$_3$CN) spectrum of compound **6.2** C) HRMS spectrum of compound **6.2**.

Compound 6.3
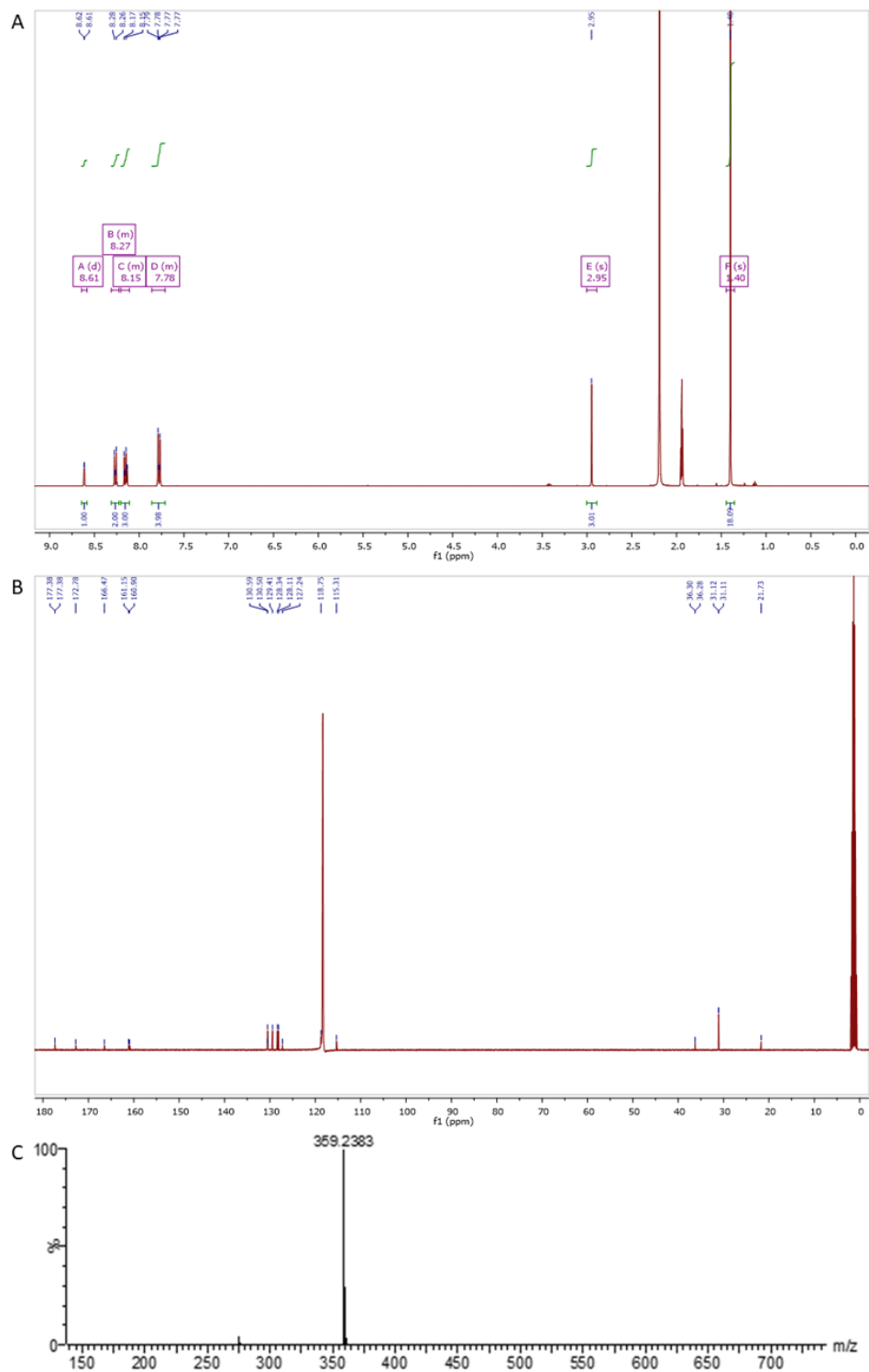
Figure 9. A) ^{1}H NMR (CD$_3$CN) spectrum of compound **6.3** B) ^{13}C NMR (CD$_3$CN) spectrum of compound **6.3** C) HRMS spectrum of compound **6.3**.

Compound 6.4
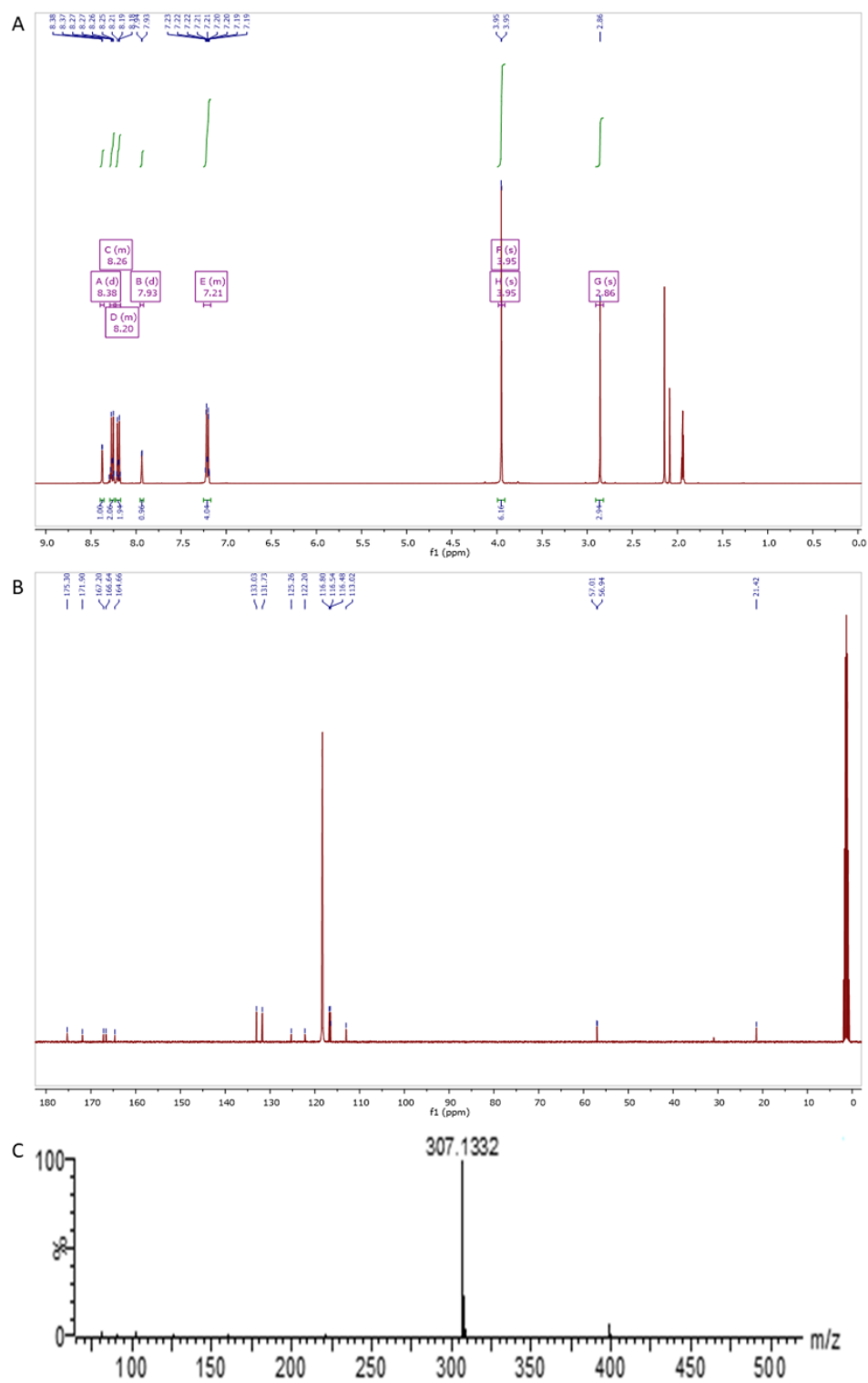
Figure 10. A) ^{1}H NMR (CD$_3$CN) spectrum of compound **6.4** B) ^{13}C NMR (CD$_3$CN) spectrum of compound **6.4** C) HRMS spectrum of compound **6.4**.

Compound 6.5
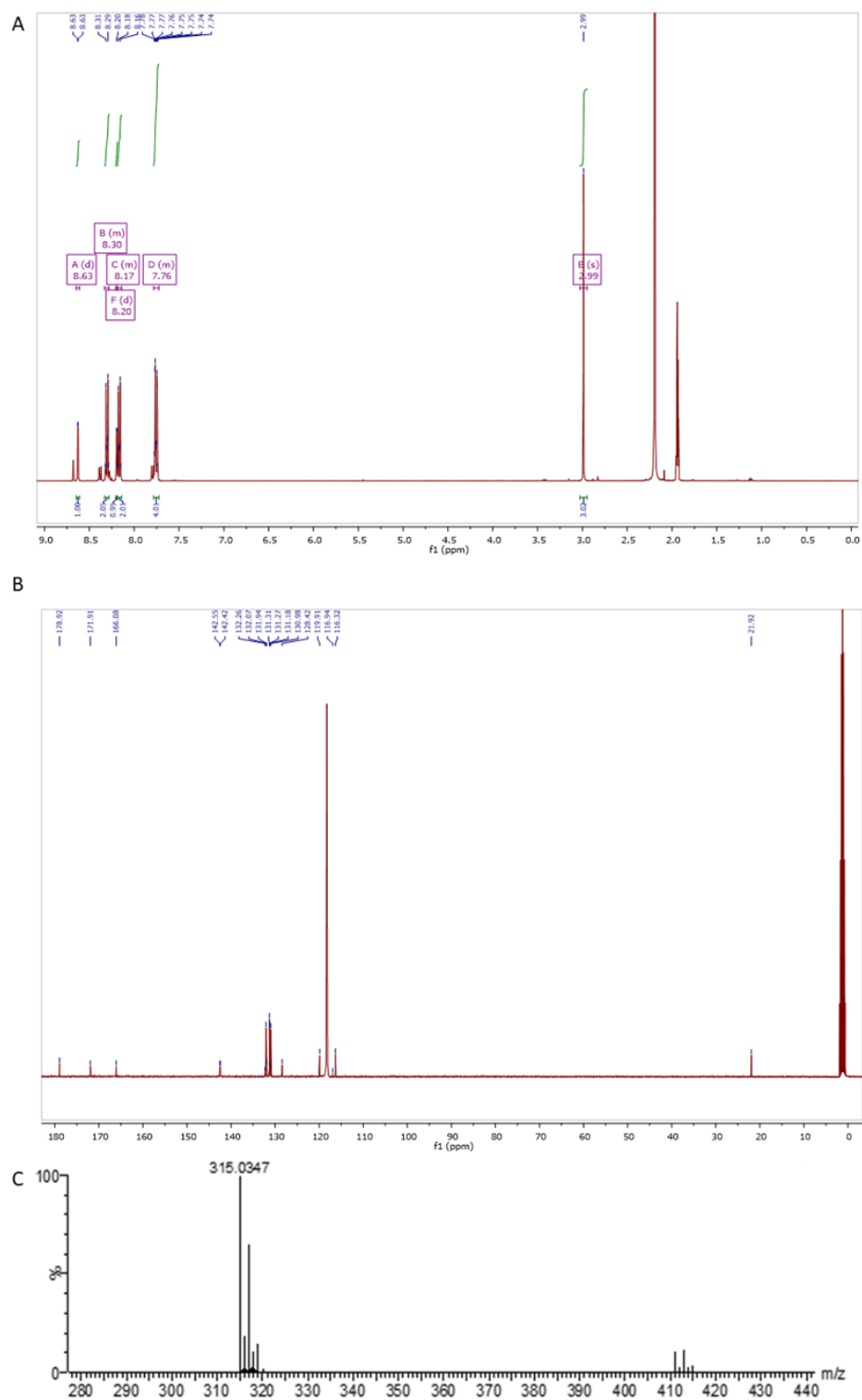
Figure 11. A) ^{1}H NMR (CD$_3$CN) spectrum of compound **6.5** B) ^{13}C NMR (CD$_3$CN) spectrum of compound **6.5** C) HRMS spectrum of compound **6.5**.

Compound 6.6
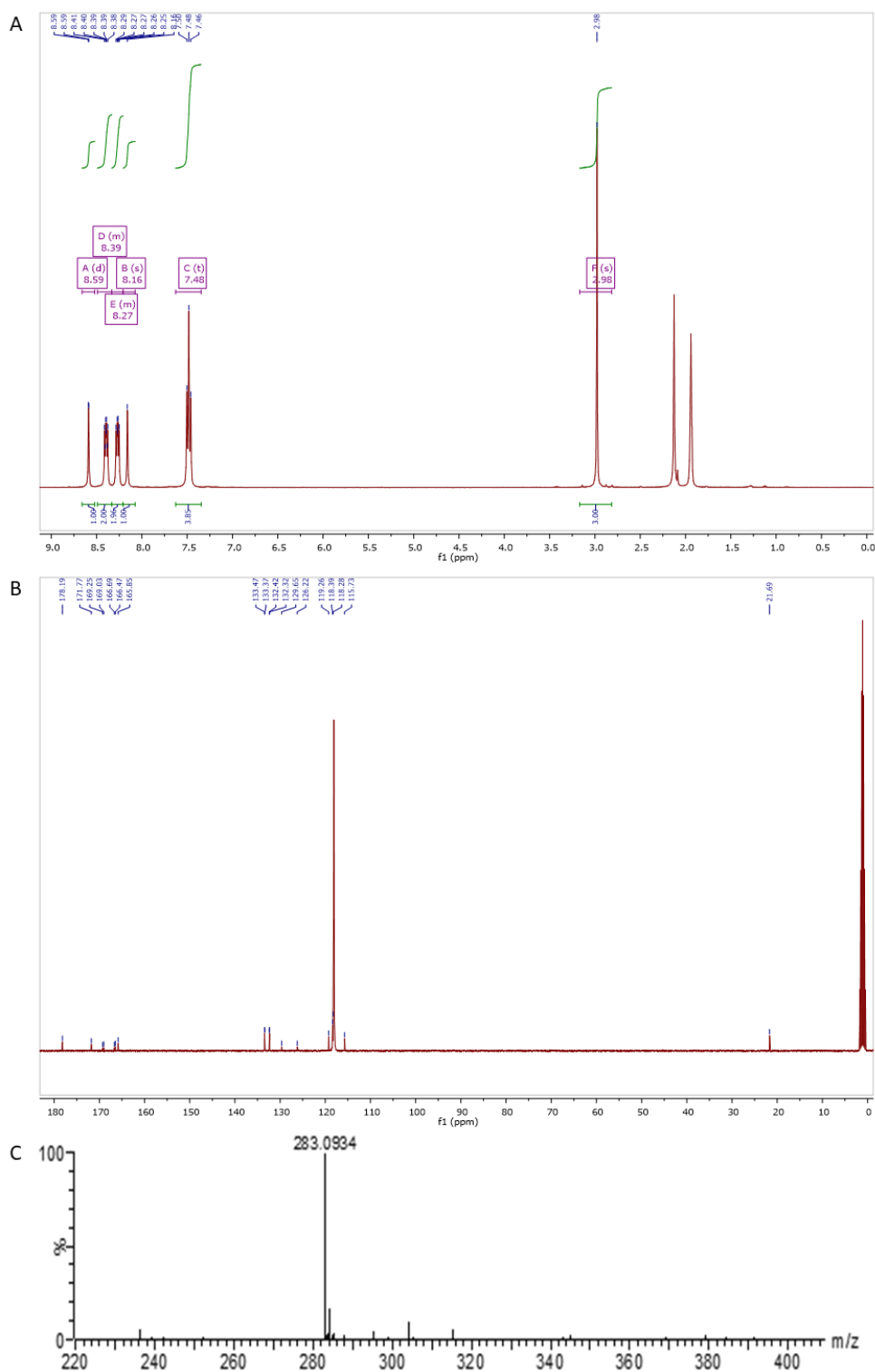
Figure 12. A) ^{1}H NMR (CD$_3$CN) spectrum of compound **6.6** B) ^{13}C NMR (CD$_3$CN) spectrum of compound **6.6** C) HRMS spectrum of compound **6.6**.

Compound 6.7
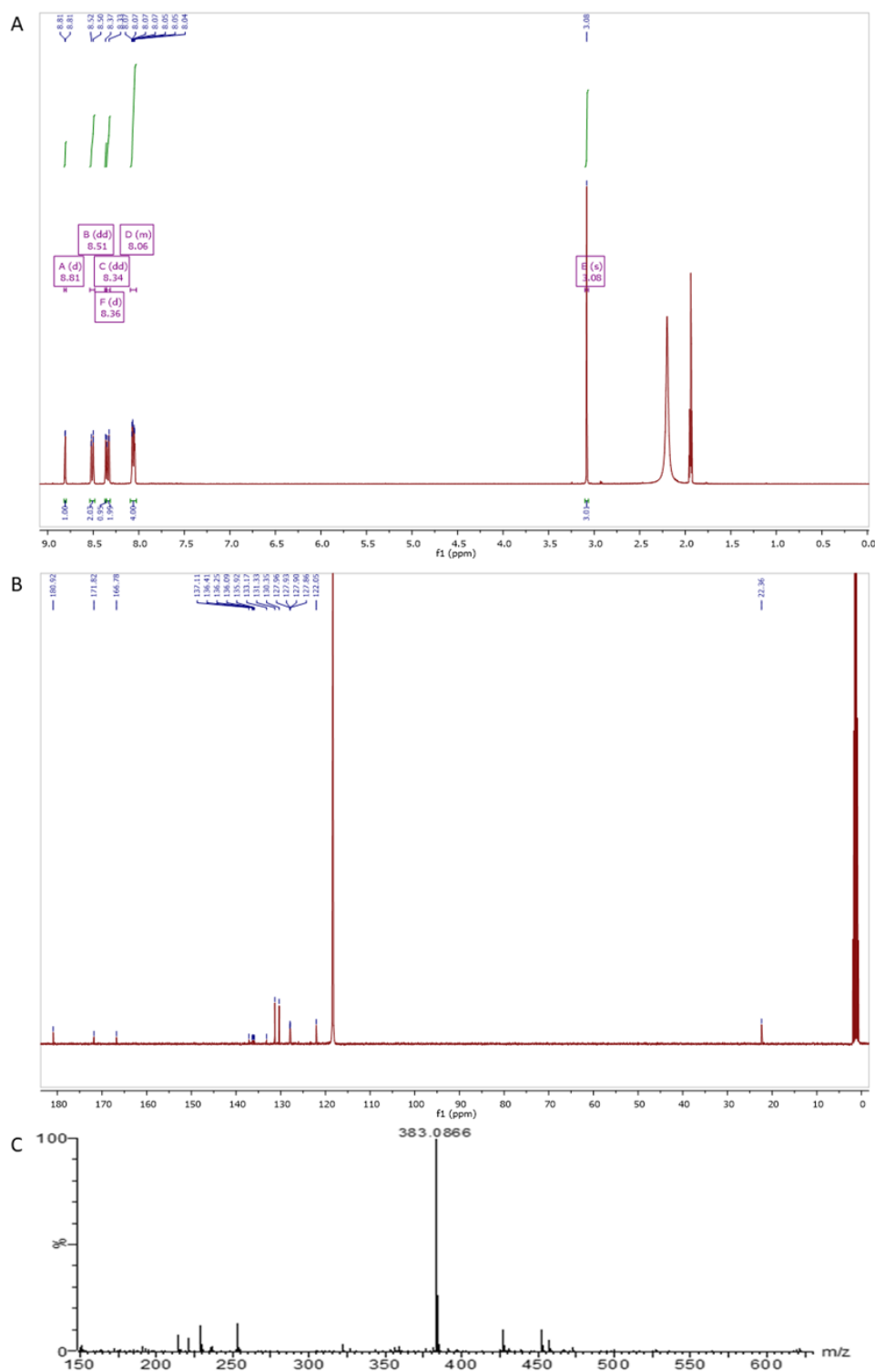
Figure 13. A) ^{1}H NMR (CD$_3$CN) spectrum of compound **6.7** B) ^{13}C NMR (CD$_3$CN) spectrum of compound **6.7** C) HRMS spectrum of compound **6.7**

Measurements of the fluorescence lifetime
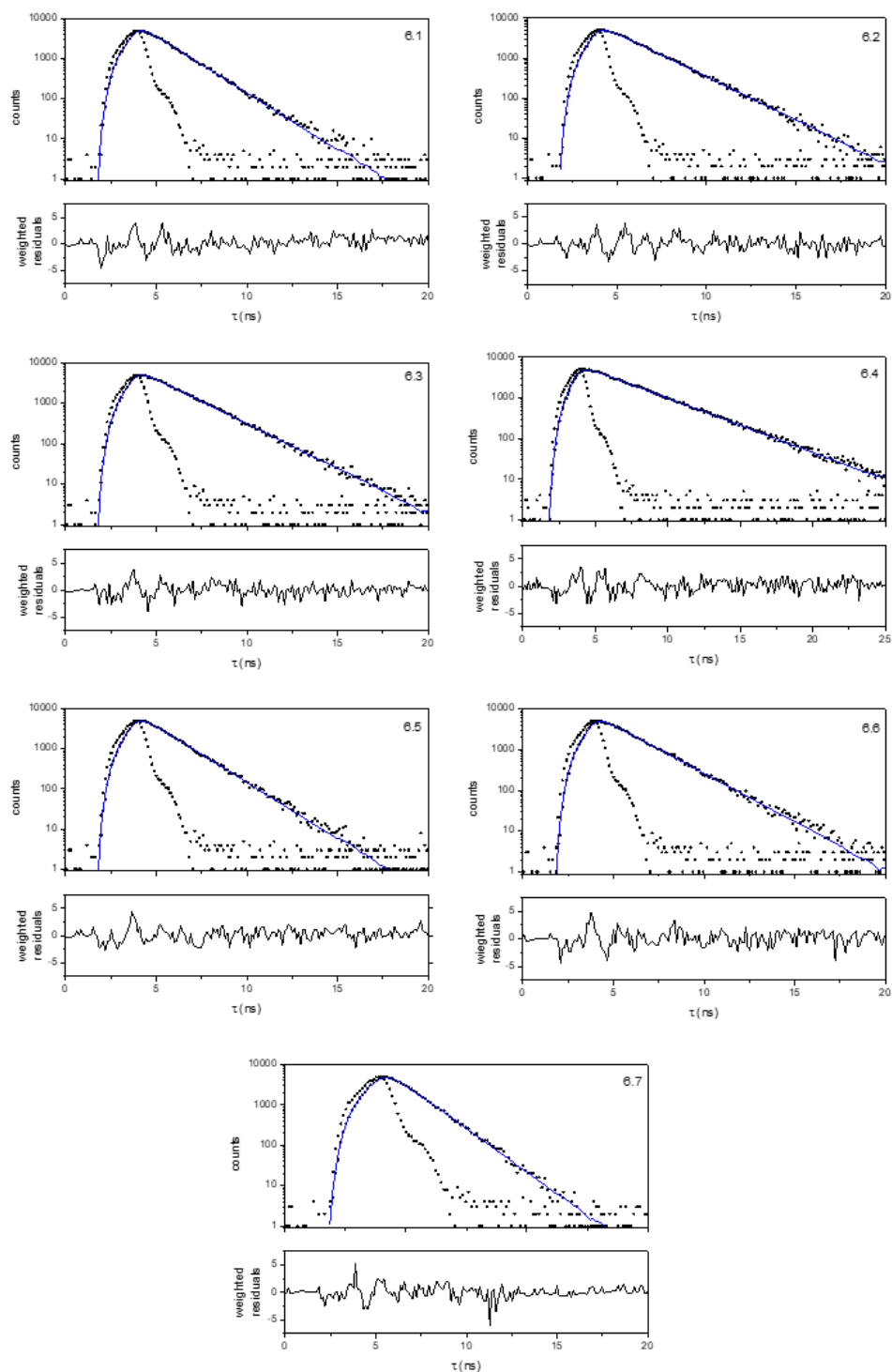
Figure 14. Fluorescence decay curves for compounds **6.1**-**6.7** in dichloromethane at 295 K. λ_{exc} was set at 372 nm (464 nm for compound **6.4**). λ_{em} was set at the emission maximum for each compound. The incident light pulse and the residuals are also shown.
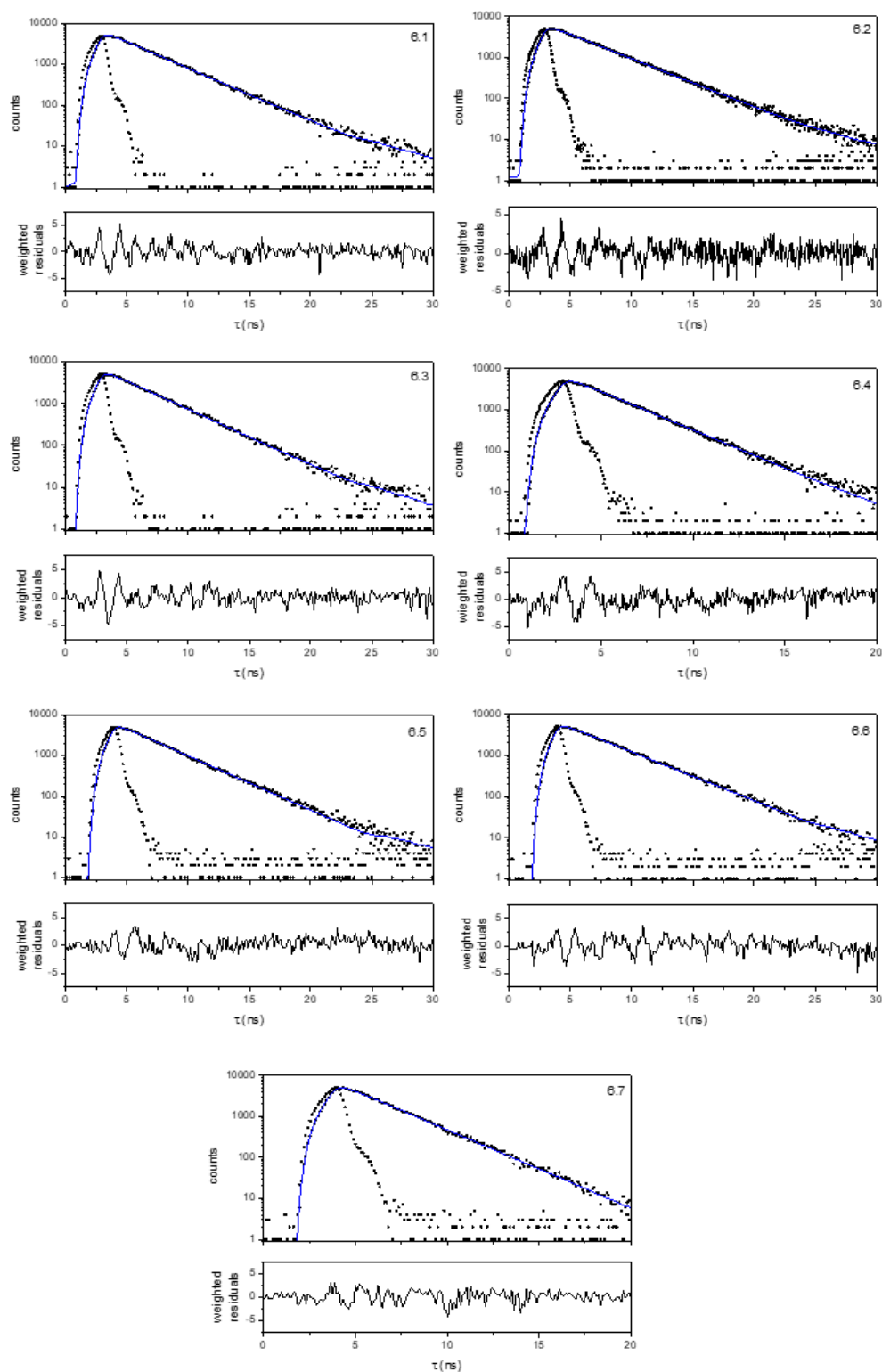
Figure 15. Fluorescence decay curves for compounds **6.1**-**6.7** in acetonitrile at 295 K. λ_{exc} was set at 372 nm (464 nm for compound **6.4**). λ_{em} was set at the emission maximum for each compound. The incident light pulse and the residuals are also shown.

6.6. ATOM COORDINATES

Table 5. Atom coordinates for the optimized geometry of compound **6.1** in DCM.

Atom	X	Y	Z
C	-0.118041	2.397679	-0.196117
C	1.125362	1.823614	-0.152059
C	1.258245	0.416891	-0.047185
C	0.073812	-0.340189	0.012433
C	-1.162776	0.276775	-0.038352
H	1.991924	2.467706	-0.228243
H	0.115926	-1.411781	0.148229
C	-2.472457	-0.368053	0.028690
C	-3.632690	0.397543	0.266933
C	-2.591264	-1.762521	-0.144139
C	-4.877594	-0.222408	0.339462
H	-3.556195	1.470170	0.405576
C	-3.840470	-2.373472	-0.073868
H	-1.718776	-2.372125	-0.353056
C	-4.985835	-1.607311	0.170253
H	-5.763963	0.375017	0.530867
H	-3.920736	-3.447097	-0.214918
H	-5.958603	-2.087410	0.226343
C	2.579636	-0.224229	0.007946
C	2.762493	-1.535600	-0.478438
C	3.688035	0.461555	0.546893
C	4.017897	-2.137671	-0.432876
H	1.933330	-2.073664	-0.927132
C	4.937779	-0.151408	0.606192
H	3.569120	1.460779	0.953775
C	5.107396	-1.449913	0.113243
H	4.147352	-3.141316	-0.827025
H	5.778276	0.382485	1.039648
H	6.084193	-1.923528	0.153606

Atom	X	Y	Z
O	-1.219386	1.621270	-0.141877
C	-0.432980	3.846527	-0.317331
H	-1.021968	4.179118	0.545336
H	0.485419	4.433573	-0.369924
H	-1.029489	4.031045	-1.218134

Sum of electronic and zero-point energies = -770.032536037 Hartree

Table 6. Atom coordinates for the optimized geometry of compound **6.1** in ACN.

Atom	X	Y	Z
C	-0.118041	2.397679	-0.196117
C	1.125362	1.823614	-0.152059
C	1.258245	0.416891	-0.047185
C	0.073812	-0.340189	0.012433
C	-1.162776	0.276775	-0.038352
H	1.991924	2.467706	-0.228243
H	0.115926	-1.411781	0.148229
C	-2.472457	-0.368053	0.028690
C	-3.632690	0.397543	0.266933
C	-2.591264	-1.762521	-0.144139
C	-4.877594	-0.222408	0.339462
H	-3.556195	1.470170	0.405576
C	-3.840470	-2.373472	-0.073868
H	-1.718776	-2.372125	-0.353056
C	-4.985835	-1.607311	0.170253
H	-5.763963	0.375017	0.530867
H	-3.920736	-3.447097	-0.214918
H	-5.958603	-2.087410	0.226343
C	2.579636	-0.224229	0.007946
C	2.762493	-1.535600	-0.478438

C	3.688035	0.461555	0.546893
C	4.017897	-2.137671	-0.432876
H	1.933330	-2.073664	-0.927132
C	4.937779	-0.151408	0.606192
H	3.569120	1.460779	0.953775
C	5.107396	-1.449913	0.113243
H	4.147352	-3.141316	-0.827025
H	5.778276	0.382485	1.039648
H	6.084193	-1.923528	0.153606
O	-1.219386	1.621270	-0.141877
C	-0.432980	3.846527	-0.317331
H	-1.021968	4.179118	0.545336
H	0.485419	4.433573	-0.369924
H	-1.029489	4.031045	-1.218134

Sum of electronic and zero-point energies = -770.038032849Hartree

Table 7. Atom coordinates for the optimized geometry of compound **6.2** in DCM.

Atom	X	Y	Z
C	0.113383	2.652752	0.158875
C	-1.126121	2.073935	0.127576
O	-1.255916	0.662382	0.052746
C	-0.066802	-0.088669	0.009803
C	1.168690	0.533148	0.047248
C	-1.993888	2.717546	0.190380
C	-0.103474	-1.163217	-0.100206
C	2.478050	-0.106223	-0.002628
C	3.644387	0.659188	-0.208284
C	2.606585	-1.502662	0.150716

C	4.889684	0.042691	-0.265587
C	3.573424	1.733626	-0.336105
C	3.857668	-2.104992	0.094921
C	1.735882	-2.124672	0.328664
C	5.024034	-1.347716	-0.113493
C	5.774316	0.650733	-0.435676
C	3.932543	-3.182256	0.218316
C	-2.571910	0.017188	0.012329
C	-2.747896	-1.304521	0.475954
C	-3.699913	0.700810	-0.486916
C	-3.999813	-1.907718	0.445462
H	-1.912522	-1.852556	0.900533
H	-4.945617	0.082211	-0.529018
H	-3.603507	1.709016	-0.877300
H	-5.122694	-1.231186	-0.063507
H	-4.111600	-2.918804	0.828803
H	-5.795315	0.627192	-0.931924
H	1.220435	1.881320	0.121373
H	0.422348	4.105673	0.249014
H	1.010875	4.422515	-0.619857
H	-0.498609	4.689925	0.287767
H	1.016711	4.312666	1.146385
H	-6.469326	-1.905852	-0.125048
H	-6.527905	-2.569557	-0.998241
H	-6.646576	-2.523083	0.762253
H	-7.280160	-1.175937	-0.209543
H	6.378836	-2.007258	-0.146045

H	6.764334	-2.142842	0.873598
H	6.329796	-2.998624	-0.608584
H	7.106254	-1.401308	-0.694944

Sum of electronic and zero-point energies = -848.673120662 Hartree

Table 8. Atom coordinates for the optimized geometry of compound **6.2** in ACN.

Atom	X	Y	Z
C	0.113779	2.652457	0.160769
C	-1.126119	2.073699	0.128907
O	-1.255559	0.662823	0.052939
C	-0.066865	-0.088895	0.009518
C	1.168100	0.533176	0.047845
C	-1.993688	2.717510	0.191682
C	-0.103547	-1.163337	-0.101281
C	2.477962	-0.106335	-0.002381
C	3.643238	0.658582	-0.214384
C	2.607045	-1.501858	0.156955
C	4.888804	0.042130	-0.272128
C	3.571327	1.732391	-0.346973
C	3.858372	-2.104134	0.100623
C	1.736832	-2.122982	0.340132
C	5.023892	-1.347463	-0.114146
C	5.772737	0.649809	-0.447266
C	3.933738	-3.180838	0.228747
C	-2.571966	0.017291	0.011801
C	-2.747974	-1.303855	0.476442
C	-3.699378	0.700538	-0.488808
C	-4.000064	-1.907226	0.445657
H	-1.912619	-1.851629	0.901305

Atom	X	Y	Z
H	-4.945265	0.081849	-0.530933
H	-3.602640	1.708554	-0.879500
H	-5.122554	-1.231113	-0.064426
H	-4.111805	-2.918138	0.829532
H	-5.794731	0.626733	-0.934547
H	1.220191	1.880797	0.122997
H	0.422800	4.105088	0.251927
H	1.012118	4.421841	-0.616383
H	-0.498207	4.689162	0.290278
H	1.016513	4.311022	1.149933
H	-6.469382	-1.905835	-0.126313
H	-6.529030	-2.567437	-1.001040
H	-6.645685	-2.525165	0.759736
H	-7.280179	-1.175502	-0.208291
H	6.378938	-2.006978	-0.147384
H	6.765105	-2.142992	0.871939
H	6.329521	-2.998269	-0.610171
H	7.105895	-1.400765	-0.696675

Sum of electronic and zero-point energies = -848.678306249 Hartree

Table 9. Atom coordinates for the optimized geometry of compound **6.3** in DCM.

Atom	X	Y	Z
C	-0.061905	0.463951	-0.034785
C	1.178078	1.083339	-0.060915
O	1.228220	2.437171	-0.104524
C	0.115802	3.207269	-0.123287
C	-1.120514	2.628206	-0.100076
C	-1.254514	1.210187	-0.055865
C	-2.567179	0.569027	-0.025875

C	2.482524	0.443748	-0.029654
C	2.611702	-0.952402	-0.170889
C	3.862996	-1.557972	-0.140537
C	5.042449	-0.810987	0.033701
C	4.900074	0.585819	0.173547
C	3.660004	1.204930	0.140732
C	-3.699623	1.246883	0.468887
C	-4.946313	0.630092	0.508023
C	-5.135875	-0.682147	0.038968
C	-3.999742	-1.351178	-0.464397
C	-2.749144	-0.752996	-0.490480
C	0.424590	4.663654	-0.186054
C	-6.500006	-1.385427	0.054150
C	-6.892909	-1.757892	-1.398464
C	-7.612083	-0.498518	0.646524
C	-6.397227	-2.675327	0.907283
C	6.436794	-1.450193	0.073844
C	6.388960	-2.980096	-0.105618
C	7.096491	-1.138283	1.441605
C	7.302075	-0.851511	-1.064401
H	-0.096695	-0.613039	0.051349
H	-1.989803	3.271471	-0.149652
H	1.739050	-1.579518	-0.323499
H	3.913256	-2.633723	-0.259791
H	5.779551	1.206018	0.313441
H	3.599134	2.281504	0.255625
H	-3.606992	2.251951	0.869593
H	-5.780635	1.187398	0.917323
H	-4.095752	-2.360456	-0.851805
H	-1.916386	-1.304034	-0.917498
H	1.018431	4.967333	0.684321

H	-0.495709	5.250934	-0.207001
H	1.012267	4.892886	-1.082863
H	-7.867859	-2.258515	-1.401606
H	-6.170384	-2.439043	-1.860651
H	-6.969608	-0.865347	-2.030147
H	-8.559200	-1.048029	0.635363
H	-7.761599	0.419155	0.065492
H	-7.408602	-0.222129	1.687883
H	-7.366817	-3.185793	0.924045
H	-6.118473	-2.445038	1.942066
H	-5.660493	-3.379432	0.506228
H	7.406929	-3.381946	-0.069560
H	5.959928	-3.268987	-1.072454
H	5.817111	-3.471880	0.690213
H	8.094624	-1.588831	1.481797
H	6.506527	-1.548613	2.269287
H	7.212567	-0.062216	1.609032
H	8.300450	-1.303161	-1.046582
H	7.428037	0.231647	-0.962884
H	6.858363	-1.050990	-2.046670

Sum of electronic and zero-point energies = -1084.55255836 Hartree

Table 10. Atom coordinates for the optimized geometry of compound **6.3** in ACN.

Atom	X	Y	Z
C	0.110892	3.229345	0.138035
C	-1.125878	2.643313	0.109884
O	-1.247756	1.230827	0.057866
C	-0.054651	0.485003	0.034670
C	1.176357	1.114552	0.068845
C	-1.997123	3.283565	0.155943
C	-0.083450	-0.591511	-0.056644

C	2.488753	0.479503	0.036452
C	3.650851	1.236613	-0.200328
C	2.627147	-0.908998	0.241514
C	4.901109	0.623542	-0.240542
C	3.578627	2.306051	-0.365504
C	3.880419	-1.504870	0.203342
C	1.761896	-1.529116	0.450735
C	5.052295	-0.759705	-0.041884
C	5.766380	1.246502	-0.434733
C	3.942298	-2.575112	0.373712
C	-2.560219	0.577383	0.021288
C	-2.732255	-0.740917	0.494643
C	-3.691651	1.243685	-0.486074
C	-3.980078	-1.349717	0.466329
C	-1.895966	-1.284715	0.922795
C	-4.935754	0.617120	-0.524971
C	-3.604168	2.247558	-0.889692
C	-5.117069	-0.691706	-0.046005
C	-4.066283	-2.358344	0.858281
C	-5.770469	1.168727	-0.941443
H	1.221659	2.463397	0.120003
H	0.411133	4.685058	0.205730
H	1.009576	4.988928	-0.660878
H	-0.513351	5.264624	0.222112
H	0.992505	4.910768	1.107126
H	-6.478186	-1.404838	-0.059078
H	6.416699	-1.464817	-0.082535

H	6.401955	-2.538032	-1.199861
H	7.371662	-3.048848	-1.237519
H	5.631204	-3.297544	-1.030477
H	6.219624	-2.081969	-2.180172
H	6.678627	-2.148652	1.282897
H	7.648967	-2.659214	1.262949
H	6.698785	-1.411149	2.094020
H	5.913525	-2.894954	1.521584
H	7.575320	-0.488960	-0.365384
H	7.465029	0.007886	-1.336423
H	7.661643	0.282062	0.409299
H	8.519904	-1.044018	-0.384499
H	-6.368435	-2.702678	-0.897874
H	-5.626203	-3.395567	-0.487628
H	-7.335677	-3.219244	-0.911206
H	-6.088265	-2.478324	-1.933915
H	-6.876492	-1.766125	1.394170
H	-6.962358	-0.865620	2.013832
H	-7.847764	-2.275455	1.398246
H	-6.147461	-2.434086	1.865266
H	-7.594169	-0.531126	-0.663854
H	-7.747586	0.392062	-0.092784
H	-7.384837	-0.261837	-1.705822
H	-8.537729	-1.088082	-0.650222

Sum of electronic and zero-point energies = -1084.55765955 Hartree

Table 11. Atom coordinates for the optimized geometry of compound **6.4** in DCM.

Atom	X	Y	Z
C	-0.031120	2.870830	-0.130319
C	1.176586	2.233815	-0.123517
O	1.242089	0.812334	-0.075202
C	0.016391	0.122542	-0.030859
C	-1.189838	0.802922	-0.043956
C	2.071963	2.838177	-0.185832
C	-0.000825	-0.954087	0.059142
C	-2.523876	0.229210	0.005949
C	-3.661154	1.054546	0.179778
C	-2.723395	-1.160449	-0.120625
C	-4.930971	0.510290	0.232121
C	-3.541403	2.127153	0.281496
C	-3.996081	-1.716492	-0.071374
C	-1.883532	-1.828986	-0.275561
C	-5.113891	-0.881862	0.108503
C	-5.802262	1.142378	0.371693
C	-4.108979	-2.788387	-0.178745
C	2.521465	0.107166	-0.065303
C	2.621813	-1.241194	-0.488736
O	3.702594	0.745108	0.367930
C	3.833567	-1.906792	-0.482909
O	1.748664	-1.765396	-0.863106
C	4.925004	0.082834	0.394279
H	3.672486	1.768083	0.728289
H	5.000196	-1.253328	-0.036837
H	3.907235	-2.933519	-0.827398

H	5.803087	0.605745	0.753694
H	-1.178181	2.155463	-0.093596
H	-0.270254	4.338992	-0.191909
H	-0.842336	4.667671	0.683504
H	0.677730	4.879134	-0.220826
H	-0.853932	4.592373	-1.084493
H	6.132680	-1.987322	-0.062261
H	-6.389789	-1.316681	0.172737
H	7.367031	-1.391122	0.364182
H	7.309441	-1.088602	1.415078
H	8.120314	-2.169501	0.245029
H	7.619655	-0.530638	-0.264211
H	-6.660534	-2.722117	0.061715
H	-7.742923	-2.815475	0.146353
H	-6.330048	-3.105535	-0.909320
H	-6.175760	-3.275659	0.872689

Sum of electronic and zero-point energies = -999.097283675 Hartree

Table 12. Atom coordinates for the optimized geometry of compound **6.4** in ACN.

Atom	X	Y	Z
C	-0.031223	2.870419	-0.132851
C	1.176776	2.233178	-0.125855
O	1.241599	0.812434	-0.076070
C	0.016246	0.122088	-0.030660
C	-1.189285	0.802980	-0.044461
C	2.072189	2.837393	-0.188435
C	-0.000993	-0.954438	0.060425
C	-2.524014	0.229358	0.006180
C	-3.660132	1.054434	0.186211

C	-2.724011	-1.159441	-0.125867
C	-4.930298	0.510164	0.239368
C	-3.539538	2.126529	0.292356
C	-3.997054	-1.715338	-0.075900
C	-1.884706	-1.827381	-0.285933
C	-5.113771	-0.881172	0.110302
C	-5.800678	1.142482	0.383923
C	-4.110273	-2.786714	-0.187746
C	2.521415	0.106733	-0.065514
C	2.621790	-1.240799	-0.490562
O	3.701721	0.744252	0.369763
C	3.833961	-1.906419	-0.484359
O	1.748861	-1.764628	-0.865854
C	4.924365	0.081866	0.396308
H	3.671220	1.766878	0.730930
H	4.999816	-1.253442	-0.036480
H	3.907224	-2.932859	-0.829948
H	5.801947	0.604661	0.757047
H	-1.177701	2.154932	-0.095411
H	-0.270161	4.338371	-0.195048
H	-0.839225	4.667507	0.682139
H	0.677949	4.877953	-0.227568
H	-0.856891	4.590606	-1.085884
H	6.133650	-1.987552	-0.061676
H	-6.390590	-1.316705	0.175916
H	7.366516	-1.389713	0.367052
H	7.307114	-1.088125	1.418079

H	8.121469	-2.166583	0.248174
H	7.618541	-0.528021	-0.259862
H	-6.659668	-2.722164	0.059701
H	-7.741742	-2.817652	0.146553
H	-6.330849	-3.101246	-0.913553
H	-6.172012	-3.278498	0.866972

Sum of electronic and zero-point energies = -999.102591885 Hartree

Table 13. Atom coordinates for the optimized geometry of compound **6.5** in DCM.

Atom	X	Y	Z
C	0.113252	2.854160	0.162413
C	-1.126942	2.271680	0.132275
O	-1.251041	0.862288	0.063940
C	-0.062719	0.109742	0.026945
C	1.169533	0.735851	0.063221
C	-1.996853	2.913061	0.191023
C	-0.098735	-0.965310	-0.080114
C	2.482782	0.098777	0.017356
C	3.641586	0.867067	-0.215519
C	2.612872	-1.291812	0.206577
C	4.893545	0.263970	-0.268029
C	3.565413	1.937699	-0.366843
C	3.861802	-1.900995	0.159012
C	1.746622	-1.910986	0.411274
C	4.994255	-1.117430	-0.080677
C	5.780868	0.858799	-0.455104
C	3.955521	-2.970491	0.311995
C	-2.567993	0.212860	0.022719
C	-2.746532	-1.089088	0.533442

216

Cl	-3.681875	0.878755	-0.528000
Cl	-3.993535	-1.705043	0.504195
H	-1.918665	-1.618986	0.993157
H	-4.929794	0.265591	-0.578229
H	-3.575514	1.870061	-0.956159
H	-5.076367	-1.022538	-0.056770
H	-4.124575	-2.699838	0.916001
H	-5.776654	0.779284	-1.020195
H	1.218777	2.082558	0.129993
H	0.419457	4.307137	0.245883
H	1.010429	4.619596	-0.622893
H	-0.502408	4.890053	0.278933
H	1.011071	4.518755	1.144001
H	6.567520	-1.880248	-0.144302
H	-6.646369	-1.795517	-0.105670

Sum of electronic and zero-point energies = -1689.22105919 Hartree

Table 14. Atom coordinates for the optimized geometry of compound **6.5** in ACN.

Atom	X	Y	Z
C	0.113740	2.853584	0.164476
C	-1.126983	2.271163	0.133952
O	-1.250527	0.862627	0.064410
C	-0.062797	0.109211	0.026805
C	1.168801	0.735678	0.063754
C	-1.996746	2.912668	0.192780
C	-0.098961	-0.965763	-0.080732
C	2.482747	0.098518	0.017603
C	3.640327	0.866505	-0.220580
C	2.613226	-1.291015	0.211748

Atom	X	Y	Z
C	4.892689	0.263626	-0.273549
C	3.563217	1.936503	-0.375784
C	3.862486	-1.900205	0.163797
C	1.747472	-1.909361	0.420692
C	4.993397	-1.116747	-0.081255
C	5.779180	0.858361	-0.464753
C	3.956409	-2.969108	0.320653
C	-2.568087	0.212867	0.022556
C	-2.747213	-1.087365	0.536582
Cl	-3.680387	0.877616	-0.531930
Cl	-3.994509	-1.703428	0.506943
H	-1.919929	-1.616263	0.998349
H	-4.928697	0.264621	-0.582354
H	-3.572912	1.867898	-0.962034
H	-5.075544	-1.021725	-0.057515
H	-4.125863	-2.697242	0.920976
H	-5.774558	0.777738	-1.026867
H	1.218380	2.081711	0.131553
H	0.420051	4.306241	0.248655
H	1.010676	4.618554	-0.620351
H	-0.501851	4.888911	0.282487
H	1.012220	4.516698	1.146625
H	6.568638	-1.880175	-0.145534
H	-6.647562	-1.795349	-0.106763

Sum of electronic and zero-point energies = -1689.22719988 Hartree

Table 15. Atom coordinates for the optimized geometry of compound **6.6** in DCM.

Atom	X	Y	Z
C	0.113239	2.854085	0.162284

C	-1.126948	2.271604	0.132137
O	-1.251050	0.862207	0.063833
C	-0.062720	0.109670	0.026839
C	1.169540	0.735785	0.063035
C	-1.996862	2.912984	0.190861
C	-0.098750	-0.965389	-0.080133
C	2.482806	0.098731	0.017251
C	3.641686	0.867162	-0.214802
C	2.612859	-1.291967	0.205700
C	4.893677	0.264121	-0.267212
C	3.565561	1.937880	-0.365521
C	3.861816	-1.901099	0.158252
C	1.746564	-1.911295	0.409727
C	4.994335	-1.117382	-0.080617
C	5.781057	0.859074	-0.453608
C	3.955500	-2.970680	0.310653
C	-2.568010	0.212806	0.022680
C	-2.746576	-1.089144	0.533406
F	-3.681908	0.878757	-0.527939
F	-3.993606	-1.705054	0.504222
H	-1.918714	-1.619078	0.993084
H	-4.929850	0.265642	-0.578107
H	-3.575536	1.870072	-0.956082
H	-5.076442	-1.022491	-0.056663
H	-4.124664	-2.699845	0.916029
H	-5.776720	0.779376	-1.020004
H	1.218768	2.082489	0.129834

Atom	X	Y	Z
H	0.419439	4.307065	0.245693
H	1.010333	4.619520	-0.623139
H	-0.502430	4.889973	0.278804
H	1.011126	4.518713	1.143756
H	6.567642	-1.880147	-0.144121
H	-6.646485	-1.795395	-0.105470

Sum of electronic and zero-point energies = -1689.22105920 Hartree

Table 16. Atom coordinates for the optimized geometry of compound **6.6** in ACN.

Atom	X	Y	Z
C	0.114942	2.628401	0.179585
C	-1.126452	2.049399	0.143108
O	-1.253849	0.641212	0.057411
C	-0.067366	-0.113449	0.009373
C	1.166158	0.509474	0.052875
C	-1.994496	2.692301	0.210822
C	-0.105541	-1.186789	-0.112391
C	2.478090	-0.129712	-0.002339
C	3.636514	0.640025	-0.238764
C	2.604440	-1.522366	0.181586
C	4.888059	0.036513	-0.300128
C	3.558186	1.711000	-0.385473
C	3.851469	-2.135177	0.124930
C	1.736502	-2.137961	0.388890
C	4.967615	-1.340387	-0.117130
C	5.785876	0.615272	-0.488659
C	3.962451	-3.204118	0.271406
C	-2.572260	-0.004800	0.009702
C	-2.750601	-1.313614	0.505720

F	-3.685071	0.672458	-0.532028
F	-3.998323	-1.928365	0.470788
H	-1.921454	-1.848404	0.956839
H	-4.935167	0.063845	-0.588456
H	-3.574535	1.668725	-0.946766
H	-5.064087	-1.224857	-0.080980
H	-4.148647	-2.927305	0.866059
H	-5.792391	0.570121	-1.019220
H	1.218768	1.854798	0.137075
H	0.424865	4.079440	0.280802
H	1.014748	4.401055	-0.585327
H	-0.495637	4.663840	0.323092
H	1.018830	4.277981	1.180284
H	-6.281136	-1.820691	-0.124925
H	6.184702	-1.932904	-0.174241

Sum of electronic and zero-point energies = -968.521466297 Hartree

Table 17. Atom coordinates for the optimized geometry of compound **6.7** in DCM.

Atom	X	Y	Z
C	0.118658	3.193569	0.166044
C	-1.124908	2.610631	0.143812
O	-1.246862	1.204588	0.087114
C	-0.061592	0.446697	0.053592
C	1.169083	1.073524	0.079922
C	-1.995859	3.251397	0.197805
C	-0.101162	-0.629536	-0.042457
C	2.485855	0.433812	0.032033
C	3.635055	1.194298	-0.256186
C	2.615519	-0.947628	0.270958
C	4.884146	0.584002	-0.313852
C	3.553196	2.257755	-0.44812
C	3.865095	-1.555622	0.215809
C	1.752394	-1.555229	0.518054
C	4.998752	-0.790499	-0.080503
C	5.761393	1.177544	-0.546857
C	3.95255	-2.620229	0.404074
C	-2.568012	0.552895	0.051873
C	-2.75599	-0.716955	0.632309
F	-3.661562	1.190568	-0.562213
C	-4.00489	-1.327951	0.604492
F	-1.938149	-1.217395	1.140184
F	-4.908933	0.572401	-0.606938
F	-3.538827	2.157497	-1.038741
C	-5.08054	-0.684202	-0.019417
F	-4.140341	-2.297614	1.072365

F	-5.738771	1.069419	-1.096758
H	1.21913	2.418678	0.135474
H	0.426101	4.64602	0.236582
H	1.015904	4.949775	-0.636066
H	-0.495047	5.229961	0.26683
H	1.020246	4.863633	1.131631
H	-6.41514	-1.383738	-0.080559
H	6.35679	-1.446973	-0.098543
H	6.299427	-2.731518	-0.526486
H	7.23312	-0.797313	-0.900777
H	6.914462	-1.476344	1.143486
H	-6.413739	-2.384073	-1.004378
H	-6.741215	-1.95928	1.104759
H	-7.427645	-0.549587	-0.41035

Sum of electronic and zero-point energies = -1444.14561897 Hartree

Table 18. Atom coordinates for the optimized geometry of compound **6.7** in ACN.

Atom	X	Y	Z
C	0.119138	3.192843	0.167083
C	-1.124905	2.609990	0.144585
O	-1.246384	1.204691	0.087205
C	-0.061675	0.445986	0.053466
C	1.168374	1.073176	0.080242
C	-1.995630	3.250988	0.198369
C	-0.101356	-0.630207	-0.042356
C	2.485749	0.433386	0.032337
C	3.634116	1.193881	-0.258185
C	2.615849	-0.947339	0.273611
C	4.883518	0.584032	-0.315988

C	3.551451	2.256950	-0.451771
C	3.865621	-1.555160	0.218260
C	1.753042	-1.554564	0.522408
C	4.998741	-0.790126	-0.080556
C	5.759982	1.178059	-0.550622
C	3.952909	-2.619424	0.408483
C	-2.568057	0.552790	0.051568
C	-2.756584	-0.715742	0.634159
F	-3.660497	1.189596	-0.564880
C	-4.005616	-1.326704	0.606195
F	-1.939096	-1.215667	1.142952
F	-4.908156	0.571828	-0.609514
F	-3.536917	2.155831	-1.042427
C	-5.080592	-0.683688	-0.019732
F	-4.140919	-2.295715	1.075446
F	-5.737019	1.068780	-1.101005
H	1.218830	2.417709	0.136249
H	0.426794	4.644987	0.237970
H	1.016803	4.948155	-0.634667
H	-0.494342	5.228799	0.268250
H	1.020948	4.861657	1.133181
H	-6.414515	-1.382486	-0.080700
H	6.356052	-1.445907	-0.099016
H	6.300663	-2.731432	-0.526557
H	7.233758	-0.797223	-0.901724
H	6.916948	-1.476214	1.142583
H	-6.415269	-2.385714	-1.002760

H	-6.743666	-1.957028	1.105155
H	-7.428249	-0.549669	-0.412797

Sum of electronic and zero-point energies = -1444.15263283 Hartree

6.7. REFERENCES

1   J. Li, J. Wang, H. Li, N. Song, D. Wang and B. Z. Tang, Supramolecular materials based on AIE luminogens (AIEgens): Construction and applications, *Chem. Soc. Rev.*, 2020, **49**, 1144–1172.

2   E. Ishow, A. Brosseau, G. Clavier, K. Nakatani, P. Tauc, C. Fiorini-Debuisschert, S. Neveu, O. Sandre and A. Léaustic, Multicolor emission of small molecule-based amorphous thin films and nanoparticles with a single excitation wavelength, *Chem. Mater.*, 2008, **20**, 6597–6599.

3   M. Shimizu, Y. Takeda, M. Higashi and T. Hiyama, 1,4-Bis(alkenyl)-2,5-dipiperidinobenzenes: Minimal fluorophores exhibiting highly efficient emission in the solid state, *Angew. Chemie - Int. Ed.*, 2009, **48**, 3653–3656.

4   J. Mei, N. L. C. Leung, R. T. K. Kwok, J. W. Y. Lam and B. Z. Tang, Aggregation-Induced Emission: Together We Shine, United We Soar!, *Chem. Rev.*, 2015, **115**, 11718–11940.

5   Z. Zhao, B. He and B. Z. Tang, Aggregation-induced emission of siloles, *Chem. Sci.*, 2015, **6**, 5347–5365.

6   D. Li, H. Zhang, C. Wang, S. Huang, J. Guo and Y. Wang, Construction of full-color-tunable and strongly emissive materials by functionalizing a boron-chelate four-ring-fused π-conjugated core, *J. Mater. Chem.*, 2012, **22**, 4319–4328.

7   Z. Zhang, B. Xu, J. Su, L. Shen, Y. Xie and H. Tian, Color-tunable solid-state emission of 2,2′-biindenyl-based fluorophores, *Angew. Chemie - Int. Ed.*, 2011, **50**, 11654–11657.

8   B. Tang, C. Wang, Y. Wang and H. Zhang, Efficient Red-Emissive Organic Crystals with Amplified Spontaneous Emissions Based on a Single Benzene Framework, *Angew. Chemie - Int. Ed.*, 2017, **56**, 12543–12547.

9   R. Huang, B. Liu, C. Wang, Y. Wang and H. Zhang, Constructing Full-Color Highly Emissive Organic Solids Based on an X-Shaped Tetrasubstituted Benzene Skeleton, *J. Phys. Chem. C*, 2018, **122**, 10510–10518.

10   H. Rabbani-Haghighi, Ś. Forget, Ś. Ch́nais, A. Siove, M. C. Castex and E. Ishow, Laser operation in nondoped thin films made of a small-molecule organic red-emitter, *Appl. Phys. Lett.*, 2009, **95**, 2007–2010.

11   B. Liu, Q. Di, W. Liu, C. Wang, Y. Wang and H. Zhang, Red-Emissive Organic Crystals of a Single-Benzene Molecule: Elastically Bendable and Flexible Optical Waveguide, *J. Phys. Chem. Lett.*, 2019, **10**, 1437–1442.

12   J. Malinge, C. Allain, A. Brosseau and P. Audebert, White fluorescence from core-shell silica nanoparticles, *Angew. Chemie - Int. Ed.*, 2012, **51**, 8534–8537.

13   E. Ferreira Molina, N. A. Martins de Jesus, S. Paofai, P. Hammer, M. Amela-Cortes, M. Robin, S. Cordier and Y. Molard, When a Red–NIR-Emissive $Cs_2[Mo_6Br_{14}]$ Interacts with an Active Diureasil–PEO Matrix: Design of Tunable and White-Light-Emitting Hybrid Material, *Chem. - A Eur. J.*, 2019, **25**, 15248–15251.

14   Q. Y. Yang and J. M. Lehn, Bright white-light emission from a single organic compound in the solid state, *Angew. Chemie - Int. Ed.*, 2014, **53**, 4572–4577.

15   Z. Xie, C. Chen, S. Xu, J. Li, Y. Zhang, S. Liu, J. Xu and Z. Chi, White-Light Emission

Strategy of a Single Organic Compound with Aggregation-Induced Emission and Delayed Fluorescence Properties, *Angew. Chemie - Int. Ed.*, 2015, **54**, 7181–7184.

16   N. N. Zhang, C. Sun, X. M. Jiang, X. S. Xing, Y. Yan, L. Z. Cai, M. S. Wang and G. C. Guo, Single-component small-molecule white light organic phosphors, *Chem. Commun.*, 2017, **53**, 9269–9272.

17   D. Tu, P. Leong, S. Guo, H. Yan, C. Lu and Q. Zhao, Highly Emissive Organic Single-Molecule White Emitters by Engineering o-Carborane-Based Luminophores, *Angew. Chemie - Int. Ed.*, 2017, **56**, 11370–11374.

18   Z. He, W. Zhao, J. W. Y. Lam, Q. Peng, H. Ma, G. Liang, Z. Shuai and B. Z. Tang, White light emission from a single organic molecule with dual phosphorescence at room temperature, *Nat. Commun.*, 2017, **8**, 1–7.

19   J. Wang, X. Gu, H. Ma, Q. Peng, X. Huang, X. Zheng, S. H. P. Sung, G. Shan, J. W. Y. Lam, Z. Shuai and B. Z. Tang, A facile strategy for realizing room temperature phosphorescence and single molecule white light emission, *Nat. Commun.*, 2018, **9**, 1–9.

20   M. Shimizu and T. Hiyama, Organic fluorophores exhibiting highly efficient photoluminescence in the solid state, *Chem. - An Asian J.*, 2010, **5**, 1516–1531.

21   V. K. Praveen, C. Ranjith and N. Armaroli, White-light-emitting supramolecular gels, *Angew. Chemie - Int. Ed.*, 2014, **53**, 365–368.

22   D. Li, J. Wang and X. Ma, White-Light-Emitting Materials Constructed from Supramolecular Approaches, *Adv. Opt. Mater.*, 2018, **6**, 1–27.

23   M. K. Bera, P. Pal and S. Malik, Solid-state emissive organic chromophores: Design,

strategy and building blocks, *J. Mater. Chem. C*, 2020, **8**, 788–802.

24   D. Li, J. Zhang and M. Anpo, Preparation of organic-inorganic material from MCM-48 and pyrylium salt, *Opt. Mater. (Amst).*, 2005, **27**, 671–673.

25   G.-L. Gong, Wei-Tao; Qian, Xiao-min; Wang, Fu-Rui; Lin, Yuan; Ning, Synthesis and Photophysical Properties of New Highly Conjugated Bispyrylium Compounds, *Heteroat. Chem.*, 2013, **24**, 66–71.

26   L. Yang, J. Ye, Y. Gao, D. Deng, W. Gong, Y. Lin and G. Ning, Highly efficient one-pot synthesis of α-free pyrylium salts with tunable fluorescence emission via ring-expanding reaction of triarylcyclopentadienes, *Tetrahedron Lett.*, 2013, **54**, 2967–2971.

27   P. K. Bhowmik, C. I. Lee, J. J. Koh, H. Han, A. Jubair, V. Kartazaev and S. K. Gayen, Synthesis, optical, and thermal properties of 2,4,6-tris(4-substituted phenyl)pyrylium tosylates and triflimides, *J. Mol. Struct.*, 2020, **1202**, 127325.

28   N. . Markina, T.A.; Boiko, Synthesis of 2-methyl-4,6-diarylpyrylium tetrafluoroborates, *Chem. Heterocycl. Compd.*, 1985, 138–139.

29   F. Haucke, Gunter; Czerney, Peter; Cebulla, Absorption and fluorescence of pyrilium salts, *Berichte der Bunsengesellschaft für Phys. Chemie*, 1992, **96**, 880–886.

30   H. Zhang, Z. Zhang, K. Ye, J. Zhang and Y. Wang, Organic crystals with tunable emission colors based on a single organic molecule and different molecular packing structures, *Adv. Mater.*, 2006, **18**, 2369–2372.

31   N. Oka, F. Ito, Y. Haketa, H. Maeda, T. Miyano, N. Tohnai, S. Ito, H. Miyasaka and S. Ozeki, Dynamic Polymorph Formation during Evaporative Crystallization from

Solution: The Key Role of Liquid-Like Clusters as "Crucible" at Ambient Temperature, *Chem. - A Eur. J.*, 2018, **24**, 4343–4349.

32   Y. Chen, Z. Peng, Y. Tao, Z. Wang, P. Lu and Y. Wang, Polymorphism-dependent emissions of two phenoxazine derivatives, *Dye. Pigment.*, 2019, **161**, 44–50.

33   M. Khorloo, Y. Cheng, H. Zhang, M. Chen, H. H. Y. Sung, I. D. Williams, J. W. Y. Lam and B. Z. Tang, Polymorph selectivity of an AIE luminogen under nano-confinement to visualize polymer microstructures, *Chem. Sci.*, 2020, **11**, 997–1005.

34   H. Sasabe, K. Sasaki, M. Mamiya, Y. Suwa, T. Watanabe, N. Onuma, K. Nakao, M. Yamaji and J. Kido, Unique Solid-State Emission Behavior of Aromatic Difluoroboronated β-Diketones as an Emitter in Organic Light-Emitting Devices, *Chem. - An Asian J.*, 2017, **12**, 2299–2303.

35   M. Yamaji, S. I. Kato, K. Tomonari, M. Mamiya, K. Goto, H. Okamoto, Y. Nakamura and F. Tani, Blue Fluorescence from BF2 Complexes of N,O-Benzamide Ligands: Synthesis, Structure, and Photophysical Properties, *Inorg. Chem.*, 2017, **56**, 12514–12519.

36   M. Yamaji and H. Okamoto, Photophysical features of naphthols having esters, formyl and acetyl groups and the difluoroboronated complex in solution and the solid state, *J. Photochem. Photobiol. A Chem.*, 2018, **360**, 204–209.

37   M. Mamiya, Y. Suwa, H. Okamoto and M. Yamaji, Preparation and photophysical properties of fluorescent difluoroboronated β-diketones having phenanthrene moieties studied by emission and transient absorption measurements, *Photochem. Photobiol. Sci.*,

2016, **15**, 278–286.

38   M. Yamaji, K. Tomonari, K. Ikuma, K. Goto, F. Tani and H. Okamoto, Blue fluorescence from: N,O -coordinated BF$_2$ complexes having aromatic chromophores in solution and the solid state, *Photochem. Photobiol. Sci.*, 2019, **18**, 2884–2892.

39   V. Wintgens, J. Pouliquen, J. Kossanyi, J. L. R. Williams and J. C. Doty, Emission of substituted pyrylium and thiapyrylium salts: Phosphorescence and delayed fluorescence emission in polymeric matrices, *Polym. Photochem.*, 1985, **6**, 1–20.

40   P. Montes-Navajas, L. Teruel, A. Corma and H. Garcia, Specific binding effects for cucurbit[8]uril in 2,4,6-triphenylpyrylium- cucurbit[8]uril host-guest complexes: Observation of room-temperature phosphorescence and their application in electroluminescence, *Chem. - A Eur. J.*, 2008, **14**, 1762–1768.

41   T. Ghosh and E. Prasad, White-light emission from unmodified graphene oxide quantum dots, *J. Phys. Chem. C*, 2015, **119**, 2733–2742.

42   G. Zhang, X. Zhang, L. Kong, S. Wang, Y. Tian, X. Tao and J. Yang, Anion-controlled dimer distance induced unique solid-state fluorescence of cyano substituted styrene pyridinium, *Sci. Rep.*, 2016, **6**, 1–9.

43   A. M. Brouwer, Standards for photoluminescence quantum yield measurements in solution (IUPAC technical report), *Pure Appl. Chem.*, 2011, **83**, 2213–2228.

44   B. Soep, A. Kellmann, M. Martin and L. Lindqvist, Study of triplet quantum yields using a tunable dye laser, *Chem. Phys. Lett.*, 1972, **13**, 241–244.

Chapter 7

Conclusions

Pyrylium salts are versatile and well-known compounds used in a great variety of applications. The present thesis has been focused on the synthesis, characterisation, and applications of novel pyrylium dyes for **cellular bioimaging**, **nitric oxide and moisture sensing** and **solid-state emission**.

In **Chapter 3**, it is concluded that the **mitochondrial internalization** of the synthesized pyrylium compounds is mainly due to their cationic and relatively apolar nature. This represents an advantage from the synthetic point of view since it is not necessary to anchor to the molecule a specific directing group for mitochondria, such as the triphenylphosphonium cation. Thanks to the conjugation and the significant Stokes shifts in solution, the studied salts become highly attractive species for biological imaging applications. Furthermore, by means of a simple study of the structure-activity relationship, the importance of electronically stabilizing the pyrylium core is reinforced, to protect it from the attack by nucleophilic species in aqueous media. The possibility of using these compounds as theranostic agents (diagnosis + treatment) of pathologies associated with mitochondrial disorders is presented.

Different conclusions can be drawn from the study of probes for nitric oxide detection in **Chapter 4**. First, that mitochondrial internalization and the synthetic ease of pyrylium compounds open a world of possibilities regarding the sensing of specific analytes. In this way, by adding the correct functionality ($-NH_2$), it is possible to obtain species that give a **selective turn-on response to nitric oxide**. From a structural point of view, the need for an activated ring with donor substituents becomes mandatory, to enhance this response and make it faster. Working on cell lines expands the application field of pyrylium salts, adding new compounds to the known arsenal of probes for detection and quantification of NO in biological systems.

From the tests on blood samples, it is concluded that the response observed **in the cuvette** and **cell cultures** can be extrapolated to more complex matrices, allowing the differentiation in **peripheral blood samples** between phagocytic cells from other types of leukocytes.

The results obtained in **Chapter 5** allow to conclude, firstly, that a physicochemical study can be extrapolated to a specific application. In this case, to explore the pyrylium-quinone methide equilibrium for the **detection of water in organic solvents**. For this, the synthetic ease of the pyrylium compounds is taken into advantage again. Thus, the selection of a nitro group *ortho* to the hydroxy one increases the acidity of the latter and makes it possible to enhance the response. Furthermore, by developing colorimetric and fluorescent type sensors simultaneously, analytical applicability is strengthened.

From **Chapter 6** it is concluded that, by means of a simple synthetic effort, it is possible to obtain a new family of **solid-state emitters**. In this case, by a one-step reaction and from two commercial compounds, derivatives with different functionalities are obtained, each one of them with distinctive emission characteristics both in solution and in the solid-state. This opens the use of pyrylium salts to the field of optical devices, with the possibility of modulating their characteristics through easily accessible synthetic modifications.

Finally, as a **general conclusion** from this thesis, it can be said that **the use of pyrylium salts could be expanded even further in the future to new applications**, due to their easy synthesis, good photophysical properties and chemical stability. It is hoped that the results here presented contributed positively to the fields of biological imaging, nitric oxide and water sensing and solid-state emission.